

Copyright is owned by the Author of the thesis. Permission is given for a copy to be downloaded by an individual for the purpose of research and private study only. The thesis may not be reproduced elsewhere without the permission of the Author.

# **Carbohydrate-based oil-in-water emulsions for delivery of short-chain fatty acids**

---

Doctor of Philosophy

In Food Technology

at

**Riddet Institute, Massey University,**

**Palmerston North, New Zealand**

---

**Hoang Du Le**

**2020**

---



**MASSEY UNIVERSITY**  
**TE KUNENGA KI PŪREHUROA**  
**UNIVERSITY OF NEW ZEALAND**

## Table of content

List of figures.....	8
List of tables.....	12
Acknowledgement.....	14
Publications and awards.....	17
List of abbreviations and terminology.....	18
Abstract.....	22
<b>Chapter 1 - Introduction.....</b>	<b>25</b>
1.1. General introduction.....	25
1.2. Thesis structure.....	27
<b>Chapter 2 - Literature review.....</b>	<b>31</b>
2.1. SCFAs and their main roles in gut health and the immune system.....	31
2.1.1. Production of SCFAs.....	31
2.1.2. SCFA roles in gut health and the immune system.....	34
2.2. Targeted delivery of SCFAs to the digestive tract.....	41
2.2.1. <i>Supplementation of SCFAs to animals</i> .....	41
2.2.2. <i>Supplementation of SCFAs to human</i> .....	42
2.3. Release of SCFAs from emulsions: dynamics of lipid digestion.....	45
2.4. Conventional O/W emulsions and carbohydrate candidates.....	48
2.4.1. <i>O/W emulsion formation process</i> .....	49
2.4.2. <i>Carbohydrate candidates</i> .....	49
2.5. Pickering emulsions – Cellulose nanocrystals (CNCs).....	58

---

2.5.1. Pickering emulsions .....	58
2.5.2. Cellulose nanocrystals (CNCs) .....	61
2.6. Summary .....	63

### **Chapter 3 – Preparation and *in vitro* digestion of SCFA-supplemented**

#### **emulsions made using various carbohydrate materials: a screening study .... 64**

Abstract .....	64
3.1. Introduction .....	66
3.2. Materials and methods .....	66
3.2.1. Materials .....	66
3.2.2. Preparation of carbohydrate solutions.....	67
3.2.3. Preparation of M-IN.....	68
3.2.4. Preparation of single-layer O/W emulsions .....	68
3.2.5. Preparation of a double-layer O/W emulsion .....	69
3.2.6. Static <i>in vitro</i> GI digestion .....	70
3.2.7. Characterisation of O/W emulsions and digesta .....	72
3.2.8. Quantification of TP .....	73
3.2.9. Quantification of PA .....	74
3.2.10. Nuclear magnetic resonance (NMR) determination of Inulin .....	76
3.2.11. Statistical analysis.....	76
3.3. Results and discussion.....	77
3.3.1. Hydrophobic modification of inulin and its emulsifying capacity .....	77
3.3.2. Single-layer O/W emulsions - emulsification ability of various carbohydrates .....	81
3.3.3. A double-layer O/W emulsion .....	83

---

3.3.4. Performance of various O/W emulsions in <i>in vitro</i> intestinal phase.....	87
3.3.5. Performance of various O/W emulsions in <i>in vitro</i> gastrointestinal phase...	89
3.4. Conclusion .....	94

## **Chapter 4 – Optimisation of PEC-based emulsion system for delivery of SCFAs**

### **- an *in vitro* study ..... 96**

Abstract .....	96
----------------	----

4.1. Introduction .....	98
-------------------------	----

4.2. Materials and methods .....	99
----------------------------------	----

4.2.1. Materials .....	99
------------------------	----

4.2.2. Preparation of emulsions .....	99
---------------------------------------	----

4.2.3. Stability and <i>In vitro</i> gastrointestinal digestion studies .....	100
---	-----

4.2.3.1. Stability study.....	100
-------------------------------	-----

4.2.3.2. <i>In vitro</i> digestion study.....	100
---	-----

4.2.4. <i>In vitro</i> gastrointestinal digestion of emulsions after the removal of free pectin .....	101
--	-----

4.2.5. Kinetics of free fatty acid release .....	102
--	-----

4.2.6. Interactions of adsorbed pectin on the interface with bile salts .....	103
---	-----

4.2.7. Characterisation: droplet size distribution, droplet $\zeta$ -potential and microstructure .....	104
--	-----

4.2.8. Quantification of TP and PA.....	104
---	-----

4.2.9. Determination of pectin coverage .....	104
---	-----

4.2.10. Calculation of pectin coverage on the interface .....	105
---	-----

4.2.11. Statistical analysis.....	105
-----------------------------------	-----

4.3. Results and discussion.....	106
----------------------------------	-----

---

---

4.3.1. Formation and stability of PEC emulsions.....	106
4.3.2. <i>In vitro</i> digestion of pectin-based emulsions .....	112
4.3.2.1. <i>Gastric digestion</i> .....	115
4.3.2.2. <i>Intestinal digestion</i> .....	118
4.3.3. Kinetics of fatty acid release .....	121
4.3.4. Displacement of adsorbed pectin by bile salts .....	124
4.4. Conclusions.....	126
<b>Chapter 5 - Design and <i>In vitro</i> digestion of SCFA-supplemented Pickering emulsions using hydrophobically modified CNCs.....</b>	<b>127</b>
5.1. Introduction .....	129
5.2. Materials and methods .....	130
5.2.1. Materials .....	130
5.2.2. Hydrophobic modification of CNCs .....	130
5.2.3. Structural analysis of MCNCs .....	131
5.2.4. Preparation of Pickering O/W emulsions.....	133
5.2.5. Stability of MCNC-based emulsions under different stresses .....	133
5.2.6. <i>In vitro</i> digestion study .....	134
5.2.7. Kinetics of free fatty acid release .....	134
5.2.8. Characterisation of the Pickering O/W emulsion and digesta .....	135
5.2.8. Quantification of TP, TB and SCFAs.....	135
5.2.9. Statistical analysis.....	135
5.3. Results and discussion.....	136
5.3.1. Hydrophobic modification of CNCs .....	136

---

---

5.3.2. Responsiveness of modified CNCs-based emulsions to various pH and ionic strengths .....	146
5.3.3. <i>In vitro</i> digestion of modified CNCs-based emulsions .....	158
5.3.3.1. <i>Microstructural fate of the emulsions – gastric digestion</i> .....	158
5.3.3.2. <i>Microstructural fate of the emulsions – intestinal digestion</i> .....	162
5.3.3.3. <i>Kinetics of fatty acid release and short-chain triglyceride hydrolysis</i> ..	169
5.4. Conclusions.....	174

## **Chapter 6 - *In vivo* digestion of SCFA-supplemented emulsions using**

<b>cannulated pigs .....</b>	<b>176</b>
Abstract .....	176
6.1. Introduction .....	178
6.2. Materials and methods .....	180
6.2.1. Materials .....	180
6.2.2. Preparation of the emulsion .....	180
6.2.3. Static <i>in vitro</i> GI digestion and fermentation.....	181
6.2.4. <i>In vivo</i> assay using ileal-cannulated pigs .....	181
6.2.5. Characterisation of the O/W emulsions and digesta .....	185
6.2.6. Quantification of TP, TB, BA and PA .....	185
6.2.7. Quantification of TiO <sub>2</sub> .....	186
6.2.8. Statistical analysis.....	186
6.3. Results and discussion.....	187
6.3.1. <i>In vitro</i> digestion of the PEC-based emulsions.....	187
6.3.2. <i>In vivo</i> digestion and fermentation of the PEC-based emulsion.....	194
6.4. Conclusions.....	200

---

---

<b>Chapter 7 - Key findings and future research prospects.....</b>	<b>201</b>
7.1. Overall findings.....	201
7.2. Exploring possible mechanisms .....	202
7.2.1. Structural changes in the double-layer emulsion system under gastrointestinal digestion.....	202
7.2.2. Improvement of the emulsifying ability through the OSA modification .....	205
7.2.3. Resistance to intestinal digestion through manipulation of surface coverage .....	208
7.2.4. Resistance of M-CNC-based Pickering emulsion to the gastrointestinal digestion.....	211
7.3. Advantages and disadvantages of this study .....	212
7.3.1. <i>In vitro</i> digestion .....	212
7.3.2. <i>In vivo</i> digestion .....	214
7.4. Future research prospects .....	214
<b>Appendixes.....</b>	<b>239</b>

## List of figures

### For chapter 01

Figure 1.1. Two different digestive pathways of delivering SCFAs into the colon .... 26

### For chapter 02

Figure 2.1. SCFA production pathways in the colon ..... 33

Figure 2.2. Main chemical structure of inulin ( $GF_m$ ). G and F and  $m$  correspond to glucosyl, fructosyl units and the degree of polymerization of  $\beta(2\rightarrow1)$  linkage respectively. .... 50

Figure 2.3. Chemical structure of chitosan. DA corresponds to degree of acylation. 52

Figure 2.4. Starch co-polymer chain with amylose and amylopectin components ... 54

Figure 2.5. Schematic illustration of protein-containing pectin structure ..... 56

Figure 2.6. Emulsification mechanism of pectin in the presence of protein residue . 57

Figure 2.7. General structure of an O/W Pickering emulsion; shape of the solid stabilisers varies depending on the sources..... 60

Figure 2.8. TEM of a commercial CNC product..... 62

### For chapter 03

Figure 3.1. Chemical structure of TP..... 67

Figure 3.2. Molecular structures of native (A), modified (B) Inulin and octenyl succinate (C). .... 77

Figure 3.3.  $^1\text{H}$  NMR spectra of N-IN (A) and M-IN (B)..... 78

Figure 3.4. Particle size distribution of various emulsions encapsulated by N-IN (2.0 wt%) and M-IN (1.0–5.0 wt%) ..... 80

---

Figure 3.5. Particle size distributions of various fresh O/W emulsions. ....	82
Figure 3.6. Particle size distribution of double-layer O/W emulsions.....	84
Figure 3.7. Confocal images of WPI (A) and CS/WPI (1:5 weight ratio) (B) emulsions.. .....	86

#### **For chapter 04**

Figure 4.1. Preparation of the reconstituted emulsions .....	101
Figure 4.2. Droplet size distribution of various O/W emulsions stabilised by four types of PEC.....	107
Figure 4.3. Changes in microscopic structure of various PEC-based emulsions. ..	108
Figure 4.4. Confocal images and particle size distributions of O/W emulsions stabilised by pectin at various concentrations. ....	114
Figure 4.5. Hydrolysis of TP (%) and release of PA (%) from O/W emulsions stabilised by pectin at various concentrations .....	117
Figure 4.6. Hydrolysis profile of TP from reconstituted emulsions after the removal of free pectin in the gastric and intestinal phases.....	120
Figure 4.7. Kinetics of fatty acid release from O/W emulsions stabilised by pectin at various concentrations .....	123

#### **For chapter 05**

Figure 5.1. Structural profiles of unmodified cellulose nanocrystals (CNCs) (black line) and modified CNCs (MCNCs) (red dashed line) .....	137
Figure 5.2. (A) Mean droplet size distributions of emulsions stabilised by modified cellulose nanocrystals (MCNCs). ....	140

---

Figure 5.3. Confocal images of various modified cellulose nanocrystal (MCNC) emulsions .....	141
Figure 5.4. Visual images of creaming stability of emulsions stabilised by MCNCs. ....	147
Figure 5.5. (A) Mean droplet size distributions of emulsion E1.00 at various pHs, (B) apparent viscosities of emulsion E1.00 at pHs 7.0 and 3.0. ....	149
Figure 5.6. (A) Mean droplet size distributions of emulsion E1.00 at various ionic strengths, (B) apparent viscosities of emulsion E1.00.....	154
Figure 5.7. Confocal images of (A) freshly prepared emulsion at pH 7.0, (B) mixture of freshly prepared emulsion and SGF buffer at pH 3.0 without the addition of pepsin and (C) mixture of freshly prepared emulsion and SGF buffer at pH 3.0 with the addition of pepsin.....	160
Figure 5.8. Mean $\zeta$ -potential values of freshly prepared emulsion (pH 3.0 and pH 7.0) and mixtures of freshly prepared emulsion and SGF buffer at pH 3.0 without and with the addition of pepsin .....	161
Figure 5.9. Confocal images of the intestinal-digested samples at pH 7.0.....	164
Figure 5.10. Confocal images of the sequential gastrointestinal-digested samples at pH 7.0.....	168
Figure 5.11. Intestinal lipolysis profiles of the emulsions (experimental and theoretically fitted model) with or without passing through the gastric phase during <i>in vitro</i> digestion .....	170
 <b>For chapter 06</b>	
Figure 6.1. Diagrams of an ileal cannulated pig .....	184
Figure 6.2. Confocal images of PEC-based O/W emulsion.....	188

---

---

Figure 6.3. Confocal images of the <i>in vitro</i> gastric and intestinal digesta .....	190
Figure 6.4. Droplet size distribution of the fresh emulsion, gastric and intestinal digesta.....	193
Figure 6.5. Confocal images of the <i>in vivo</i> intestinal digesta.....	194

**For chapter 07**

Figure 7.1. Structural changes of CS-WPI O/W emulsion under the <i>in vitro</i> gastric conditions .....	204
Figure 7.2. Effects of OSA modification on emulsifying ability of IN and CNCs.....	207
Figure 7.3. Influence of PEC during the <i>in vitro</i> intestinal digestion .....	210

---

## List of tables

### For chapter 02

Table 2. 1. Beneficial effects of SCFA on the hosts .....	39
---	----

### For chapter 03

Table 3.1. Composition of 500-mL SGF buffer .....	70
Table 3.2. Composition of 500 mL SIF buffer .....	71
Table 3.3. Changes in average sizes ( $\mu\text{m}$ ) and $\zeta$ -potential (mV) of various emulsions .....	83
Table 3.4. Average sizes and of $\zeta$ -potential various double-layer emulsions .....	85
Table 3.5. Proportions of TP hydrolysis and PA release after 2 h incubation at <i>in vitro</i> intestinal condition.....	88
Table 3.6. Size ( $d_{32}$ ) changes of various O/W emulsions after gastric and intestinal digestion.....	89
Table 3.7. Proportions of hydrolysed TP and released PA.....	92
Table 3.8. Confocal pictures of single-layer emulsions, and double-layer emulsion before gastric, after gastric and intestinal digestion .....	93

### For chapter 04

Table 4.1. Particles sizes $d_{43}$ ( $\mu\text{m}$ ) of various PEC-based emulsions at various pH and ionic strength conditions.....	109
Table 4.2. $\zeta$ -potential (mV) of various pectin-based emulsions at various pH and ionic strength conditions .....	110

---

Table 4.3. Mean particle sizes ( $d_{32}$ and $d_{43}$ ), surface charge ( $\zeta$ -potential) and pectin coverage of freshly prepared O/W emulsions .....	113
Table 4.4. Lipolysis kinetic data of the <i>in vitro</i> intestinal digestion of various emulsions .....	122
Table 4.5. Effects of bile salts on surface charge ( $\zeta$ -potential) and pectin coverage .....	125

### For chapter 05

Table 5.1. Mean droplet sizes and $\zeta$ -potentials of modified cellulose nanocrystal (MCNC)-stabilised Pickering emulsions during 28 days of storage at 4 °C. ....	144
Table 5.2. Mean droplet sizes and $\zeta$ -potentials of emulsion E1.00 as a function of pH. ....	150
Table 5.3. Mean droplet sizes and $\zeta$ -potentials of emulsion E1.00 as a function of ionic strength. ....	153
Table 5.4. Kinetic parameters of the intestinal digestion during <i>in vitro</i> gastrointestinal digestion. ....	172

### For chapter 06

Table 6.1. Basal diet compositions for 192 Kg powder .....	183
Table 6.2. Mean droplet sizes and $\zeta$ -potentials of the emulsion, gastric and intestinal digesta. ....	189
Table 6.3. SCFAs and triglyceride profiles after <i>in vitro</i> gastric digestion (2 h), intestinal digestion (3 h) and fermentation (38 h) .....	191
Table 6.4. TP, TB, PA and BA profiles in the <i>in vivo</i> intestinal digesta and faecal samples. ....	198

---

## Acknowledgement

First of all, I would like to acknowledge my supervisors, i.e. Dist. Prof. Harjinder Singh, Dr Simon Loveday, Dr Emilia Nowak and Dr Zhigao Niu for their academic support during my PhD study. I specially thank Dr Loveday for his great assistance with academic writing and general English speaking when I started my PhD in 2017. Also, I express thanks to Dr Niu for his support with the experimental set-up in the first year. In addition, I am very grateful to Dr. Nowak for her encouragement to take part in “Strengths and Weaknesses” workshops at Massey University. I also would like to thank Prof. Singh for giving me a golden opportunity to visit University of Leeds, UK to conduct one chapter of my PhD project. The academic visit created great chance for me to learn new skills and knowledge, and extended my connections, all of which are extremely useful for my future career.

Also, I would like to deeply acknowledge Dr. Anwesha Sarkar at School of Food Science and Nutrition, University of Leeds, UK for her supervision during my academic visit at Leeds from Jan-2019 to May 2019. Although Anwesha was not my official supervisor, she contributed significantly to my PhD research with her involvement as corresponding author in two publications at high impact-factor journals. Anwesha was not only my supervisor but also my “sister” who taught and guided me in my academic expertise.

Furthermore, I specifically thank the nutrition team at Riddet Institute, Massey University, New Zealand for their help in my *in vivo* study with ileal-cannulated pigs (Ethics approval was obtained from the Massey University Animal Ethics Committee, Protocol No. 19/103). Many thanks to Dr. Suzanne Hodgkinson who supported me in

---

animal ethics application. Likewise, I am grateful to Dr. Natascha Stroebinger and Ms Paloma Craig for their technical contribution, i.e. TiO<sub>2</sub> analysis and the pig's diet preparation. Regarding the pig's daily feeding, I express thank to Ms Minke Buwalda and Mr Ravi Yadav.

Additionally, I would like to acknowledge Peter Zhu, Jack Cui, Maggie Zou and Chris Hall at Riddet Institute, Massey University and Dr. Matthew Savoian at MMIC (Manawatu Microscopy and Imaging Centre), Massey University for their technical support in training using various lab equipment, i.e. gas chromatography (Peter), pH-stat (Jack), lab induction and chemical purchases (Maggie), Mastersizer and Zetasizer (Chris) and Confocal microscopy (Matthew).

Next, I want to thank the NZAID-support team, i.e. Jamie Hooper and Saba Azeem. They are very dedicated and amazing people to work with. Thanks to them for hosting teamwork and outdoor activities, dinners and gatherings that helped me forget difficulty and complexity of my PhD research.

In addition, I thank friends, relatives, and colleagues for their support physically and mentally during my PhD candidacy. Many thanks to Ms. Hanh Nguyen and her family who looked after my son on weekends for 4 months (Jan-2019 to May-2019) when I was in the UK as part of the Riddet overseas placement. I also want to express gratitude to Murray Pirie for his great English tutoring that has significantly improved my English speaking.

Finally, I warmly thank my wife who dedicated her career and future to come to New Zealand with me. In the first 6 months in New Zealand, she spent most of her time looking after our son who was only 2 years old at that time. Also, she did not speak English very well, which made it impossible for her to get a job that suited her 8-year experience. She ended up working as a kitchenhand for a Chinese restaurant, then a Korean restaurant. During my academic visit in Leeds, UK, she stayed in New Zealand with my son. Without me, she had lots of sufferings physically and mentally but in the end, we both overcame all the difficulties. Words might not be enough to describe her sacrifice and dedication; I just want to say to her “I love you so much”.

## Publications and awards

### Publications

1. Le, H. D., M.Loveday, S., Nowak, E., Niu, Z., & Singh, H. (2020). Pectin emulsions for colon-targeted release of propionic acid. *Food Hydrocolloids*, 103, 105623.
2. Le, H. D., M.Loveday, S., Singh, H., & Sarkar, A. (2020). Pickering emulsions stabilised by hydrophobically modified cellulose nanocrystals: Responsiveness to pH and ionic strength. *Food Hydrocolloids*, 99, 105344.
3. Le, H. D., M.Loveday, S., Singh, H., & Sarkar, A. (2020). Gastrointestinal digestion of Pickering emulsions stabilised by hydrophobically modified cellulose nanocrystals: release of short-chain fatty acids. *Food Chemistry*, 320, 126650.

### Awards

1. Oct 2018 Winner of the Student Colloquium 2018 - Oral competition - Riddet Institute
2. Jan 2019 Recipient of the Overseas placement awards - Riddet Institute
3. Aug 2019 Winner of the People choice award of the 3-minute thesis (3MT) competition 2019 - Massey University
4. Oct 2019 Winner of Poster competition at the Food Structures, Digestion & Health 2019 International conference
5. Feb 2020 Recipient of FoodHQ IFAMA 2020 Scholarship. The recipient will be a member of a New Zealand team for a case study competition at the International Food and Agribusiness Management (IFAMA) 2020 conference in Rotterdam.

## List of abbreviations and terminology

<b>Abbreviations</b>	<b>Full terms</b>
ANOVA	Analysis of variance
AP	Apple
BA	Butyric acid
CA	Caproic acid
CE-SCFAs	Carbohydrate-encapsulated short chain fatty acids
CLSM	Confocal laser scanning microscopy
CNCs	Cellulose nanocrystals
CS	Chitosan
CT	Citrus
$d_{32}$	Sauter-average diameters
$d_{43}$	Volume-average diameters
DA	Degree of acylation
DMSO	Dimethyl sulfoxide
DP	Degree of polymerisation
DS	Degree of substitution
E0.05	Pickering emulsion stabilised by cellulose nanocrystals 0.05 wt%
E0.10	Pickering emulsion stabilised by cellulose nanocrystals 0.10 wt%
E0.20	Pickering emulsion stabilised by cellulose nanocrystals 0.20 wt%
E0.50	Pickering emulsion stabilised by cellulose nanocrystals 0.50 wt%

---

E1.00	Pickering emulsion stabilised by cellulose nanocrystals 1.00 wt%
EP1.0	Emulsions stabilised by citrus pectin 1.0 wt%
EP2.5	Emulsions stabilised by citrus pectin 2.5 wt%
EP5.0	Emulsions stabilised by citrus pectin 5.0 wt%
FDA	The Food and Drug Administration
FFAs	Free fatty acids
FTIR	Fourier-transform infrared spectroscopy
GalA	D-galacturonic acid
GC	Gas chromatography
GI	Gastrointestinal
GIT	Gastrointestinal tract
GPCR	G-protein-coupled receptors
GRAS	Generally Recognized As Safe
HDAC	Histone deacetylases
HG	Homogalacturonan
HM	High methoxyl
IN	Inulin
LM	Low methoxyl
LVR	Linear viscoelastic region
MCNCs	Modified cellulose nanocrystals
M-IN	Modified inulin
NF- $\kappa$ B	Nuclear factor kappa-light-chain-enhancer of activated B cells
NMR	Nuclear magnetic resonance
O/W	Oil-in-water
OSA	Octenyl succinate anhydride

---

PA	Propionic acid
PEC	Pectin
RGI	Rhamnogalacturonan
SCFAs	Short chain fatty acids
SFO	Sunflower oil
SGF	Simulated gastric fluid
SIF	Simulated intestinal fluid
SO	Soybean oil
TB	Tributylin (Glycerol tributyrinate)
TEM	Transmission electron microscopy
TP	Tripropionin (Glycerol tripropionate)
TV	Trivalerin (Glycerol trivalerate)
WPI	Whey protein isolate
XRD	X-ray diffractometry

## Terminology

$d_0$	the initial average diameter of the emulsion ( $d_{32}$ )
$G'$	the elastic modulus
$G''$	the viscous modulus
$k$	the lipid conversion rate per unit area of the droplet surface
$k_1$	the first-order rate constant of Free fatty acid release
$M_{\text{NaOH}}$	the molarity (M) of the NaOH solution
$M_{\text{w lipid}}$	the average molecular mass ( $\text{g mol}^{-1}$ ) of the triglycerides
$\rho_0$	the density of the lipid.
rev	the revolution of an engine per minute
$V_{\text{NaOH}}$	the volume (L) of NaOH solution
$W_{\text{lipid}}$	the total mass (g) of lipid present
$\Delta E$	the desorption energy
$\theta_w$	the static water contact angle
$\Phi_{\text{max}}$	the maximum total Free fatty acids level (%)

## Abstract

---

Short-chain fatty acids (SCFAs) are important functional metabolites. There is clinical evidence to show that they are useful in the prevention of the metabolic syndrome, bowel disorders and certain types of cancer. Therefore, supplementation of SCFAs to the daily diet brings benefits to human health. However, SCFAs are small and water-soluble molecules that are quickly absorbed in the upper gastrointestinal tract. This project aimed to develop carbohydrate-based systems to deliver tripropionin (TP, glycerol tripropionate) and tributyrin (TB, glycerol tributyrate) as sources of propionic and butyric acids into the colon. Two types of emulsion systems were employed, i.e. surfactant-stabilised oil-in-water (O/W) emulsions (single and double-layer systems) and particle-stabilised O/W emulsions (Pickering emulsions). The systems were characterised in terms of structural stability, surface charge, rheological properties, lipolysis degree and release of SCFAs under a static *in vitro* gastrointestinal digestion and an *in vivo* study with ileal-cannulated pigs.

In the screening experiments, several potential carbohydrate materials were explored, i.e. three modified starches (GUM, N46 and N-LOK), four pectins (PEC) and hydrophobically modified inulin (M-IN), to produce single-layer O/W emulsions. A double-layer O/W emulsion was also produced by combining whey protein isolate (WPI) and chitosan (CS) as the first and second layers, respectively. The capacity of emulsion systems for colon-targeted delivery of SCFAs was then tested using a static *in vitro* gastrointestinal digestion. The results show that PEC displayed the poorest emulsifying capacity amongst all investigated carbohydrates, leading to an emulsion droplets size ( $d_{32}$ ) of around 7.3  $\mu\text{m}$ . However, PEC-based formulation was the best

system for protection against gastric and intestinal conditions. On the other hand, other single-layer systems and the double-layer system proved to be unstable in the intestinal phase with a significant SCFA release. Deeper investigation on the emulsifying capacity showed that PEC stabilised the O/W emulsion mainly through steric effects. In addition, PEC had the ability to form thick layer around the O/W interface, which was evidenced by confocal laser scanning microscopy and the quantification of adsorbed PEC on the interface.

In addition to the above systems, a Pickering O/W emulsion stabilised by hydrophobically modified cellulose nanocrystals (CNCs) was also investigated. The hydrophobic modification of CNCs was carried out, resulting in an increase in static water contact angle from 56° (untreated CNCs) to 80.2° (MCNCs). As a result, the emulsifying capacity of MCNCs was significantly improved. The emulsions prepared from MCNCs  $\geq 0.20$  wt% were stable against droplet coalescence for up to 4-week storage. In addition, the Pickering emulsions were prone to droplet flocculation at ionic strength  $\geq 20$  mM NaCl (pH 7.0) or pH  $< 4.0$  (without addition of NaCl), which was due to the charge screening associated with the cellulose molecules at the surface. Similar droplet flocculation was also observed under *in vitro* gastric conditions, where the emulsions were exposed to low pH and high ionic strength. This gastric-induced structural changes improved physical strength of the emulsions and that enhanced resistance to bile-salt displacement and consequently delayed lipid digestion in the intestinal conditions. In addition, high desorption energy of the MCNC particles at O/W interface of the Pickering emulsion contributed to low lipolysis degree (30–35%).

High proportions of SCFAs remaining after the intestinal digestion observed in both PEC and MCNC-based emulsions show a strong promise their use in the colon-targeted delivery of SCFAs. However, CNCs are currently not considered as food-grade materials; therefore, PEC was chosen for the *in vivo* study using female ileal-cannulated pigs. The *in vivo* study demonstrated significant higher intestinal lipolysis (~ 51–53%) and lower SCFA release (~ 15%) as compared to the *in vitro* digestion (~ 40 and 35% respectively). The main reason for the difference between the two models was the absorption of the SCFAs in the pig's small intestine. However, high proportions of unhydrolysed triglycerides (~ 47–49%) and presence of oil droplets in the ileal-digesta demonstrated successful delivery of SCFAs.

Based on the findings in this research, we propose the use of PEC-based emulsion for human trials by incorporating the system into a daily diet or dessert liquid/gel products, such as drinking milk or yogurt. We also believe that the application of MCNC-based Pickering emulsions for colon-target delivery of could be of interest if the regulatory status could be confirmed. The study identifies promising directions for researchers who are interested in improving gut health through delivery of SCFAs to the colon.

# Chapter 1 - Introduction

---

## 1.1. General introduction

There is increasing evidence that short chain fatty acids (SCFAs), such as propionic and butyric acids, play an important role in mediating gut integrity, regulating the immune system and preventing bowel diseases, including cancer ([Besten, et al., 2013](#); [Mortensen & Clausen, 1996](#); [Tan, et al., 2014](#); [Venegas, et al., 2019](#)).

SCFAs, are saturated aliphatic acids containing six or fewer carbon molecules and include acetic, propionic, butyric, valeric and caproic acids. They are produced in the colon when microbiota ferment non-digestible carbohydrates (dietary fibre). However, in the modern way of life, people often do not consume enough fibre to bring the benefits in the colon. Also, the type of SCFAs produced through fermentation differ by fibre type, while some SCFAs are known to be more beneficial than the others. This leads to the need for supplementation of SCFAs in the daily diet. However, these SCFAs are known to absorb in the upper gastrointestinal tract. Therefore, there is a need for appropriate delivery systems that will prevent premature absorption (and/or degradation) to achieve a colon-targeted delivery in order to harness the benefits of SCFAs.

The development of target-delivery systems for SCFAs has attracted considerable attention from scientists worldwide. The research aimed to develop carbohydrate-based systems to deliver SCFAs into the colon. [Fig. 1.1](#) demonstrates two different pathways of delivering SCFAs into the colon, 1) *fermentation of fibre* that has been

---

widely described in the literature and 2) *carbohydrate-encapsulated SCFAs (CE-SCFAs)* that will be investigated thoroughly in this study.

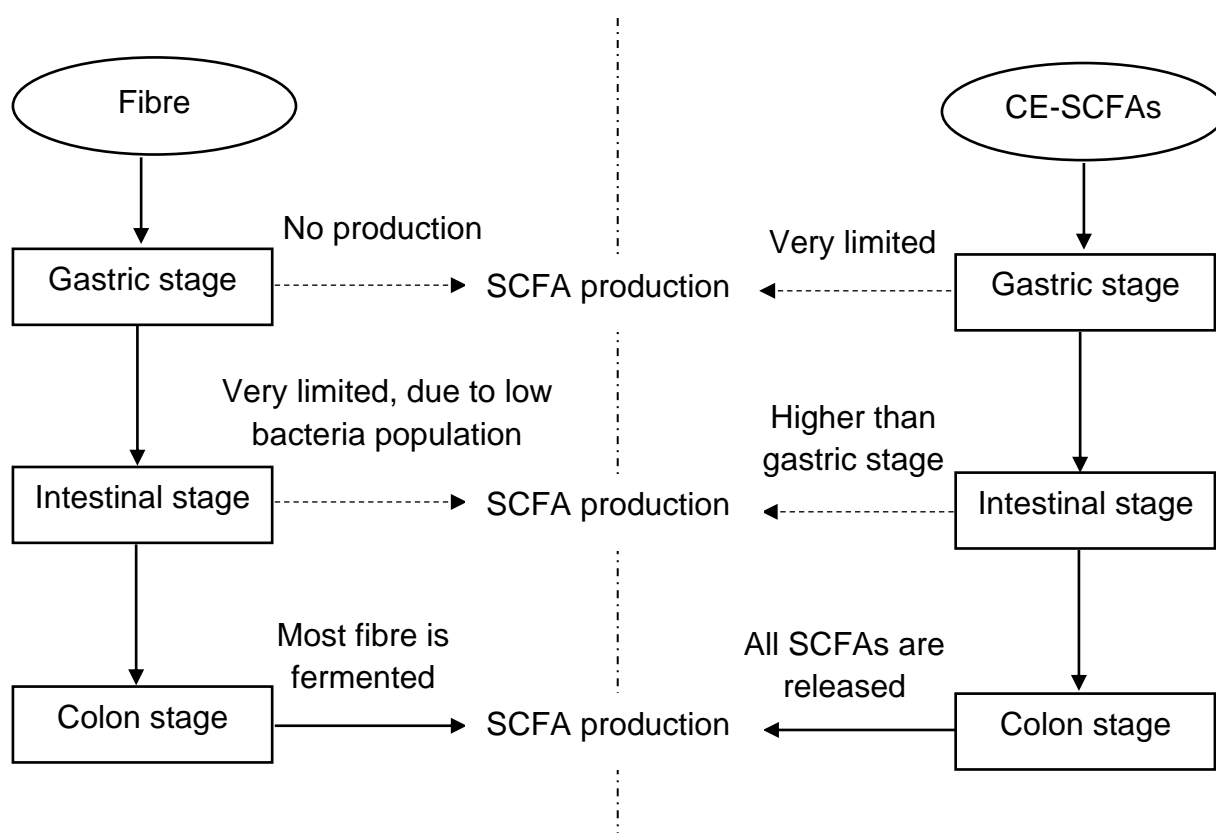


**Figure 1.1.** Two different pathways of delivering SCFAs into the colon

In the first pathway, SCFAs are mainly produced in the colon through the fermentation of fibre. However, the type of SCFAs produced varies depending on the fibre type and individuals. This drawback could be addressed by the use of CE-SCFAs. In this thesis, it is hypothesized that SCFA production from CE-SCFA systems at the gastric stage is limited due to resistance of carbohydrates to gastric digestion. In the small intestine, higher proportion of SCFAs is released, which depends on the resistance of the delivery systems to bile-salt displacement and in the colon, all SCFAs are released. SCFAs could also be produced from carbohydrates through the ileal and colon fermentation but the amount is insignificant due to low concentrations.

In this thesis, effective CE-SCFA systems were developed, and characterised in terms of particle size, surface charge, structural stability, degree of lipolysis and release of SCFAs during *in vitro* and *in vivo* gastrointestinal digestion. This thesis sought to answer the following questions:

1. a) How do O/W emulsions stabilised by different polysaccharides behave under *in vitro* gastrointestinal conditions?  
b) What is the impact of emulsifier surface coverage during this process?
2. How does a Pickering emulsion stabilised by cellulose nanocrystals (CNCs) behave under the *in vitro* gastrointestinal conditions?
3. Under *in vivo* conditions, to what extent are SCFAs released in the small intestine and in the colon?

## 1.2. Thesis structure

To achieve the project objectives, the study was conducted in four stages, organised into subsequent four research chapters.

### Chapter 2

*Literature review* provides a review the role of SCFAs in the maintenance of gut health and the importance of delivering them to the colon. This chapter also summarises the advantages and disadvantages of previously reported colon-targeted delivery systems. The comprehensive review of the colon-targeted delivery systems leads to the selection of the carbohydrates as emulsifiers for traditional and Pickering O/W emulsions.

### Chapter 3

---

A *screening study* (*research question 1a*) presents the use of various carbohydrate materials, i.e. modified inulin, modified starches, chitosan and various types of pectin to produce single and double-layer O/W emulsions. As a control, an emulsion stabilised by whey protein isolate, was used that is known to be susceptible to gastric destabilization. Changes in the emulsion structure, surface charge, lipolysis and release of SCFAs were investigated by an INFOGEST static *in vitro* gastrointestinal digestion (Minekus, et al., 2014). A selected carbohydrate will be used in [Chapter 4](#).

#### **Chapter 4**

*This chapter* (*research question 1b*) investigates the effects carbohydrate concentrations as well as coverage at the O/W interface on *in vitro* lipolysis and release of SCFAs. In addition, the displacement of the adsorbed carbohydrate at the O/W interface by bile salts was investigated quantitatively. The study provided an understanding of the carbohydrate-bile salt interactions, providing an evidence for the role of a thick layer at the O/W interface to improve resistance to bile salt displacement.

**Chapter 5** (*research question 2*) describes the formation of Pickering emulsions using hydrophobically-modified CNCs with octenyl succinate anhydride (OSA). Emulsion properties, including microscopic structure, surface charge, rheological properties and behaviours under various pH and ionic strengths were investigated. The INFOGEST static *in vitro* gastrointestinal digestion was performed to validate the suitability of the Pickering emulsions for delivery of SCFAs to the colon. This study revealed that adsorbed solid stabilisers could resist bile-salt displacement and delay digestion due to high desorption energy of the particles from the O/W interface.

**Chapter 6** (*research question 3*) details an *in vivo* study of the selected emulsions using cannulated pig model. The microstructure of the digested emulsion obtained at the terminal ileum was investigated with confocal laser microscopy. Lipolysis and release of SCFAs in the small intestine and the colon were determined. An *in vitro* digestion of the same emulsion system was also conducted to compare with the pig study. The study confirms the biological relevance of *in vitro* models by comparing with the *in vivo* results. This provides a better understanding of the fate of chosen carbohydrate-based emulsion in the GIT, and ultimately provides useful knowledge for designing delivery systems for future human studies.

**Chapter 7** summarises the main findings of this study as well as highlights the future research prospects for colon-targeted delivery of SCFAs.

The thesis structure, including main sections of each chapter is shown below.

Chapter 1 - Introduction

Chapter 2 - Literature review

Chapter 3 - *In vitro* digestion of SCFA-supplemented emulsions using various carbohydrate surfactants: a screening study

- Hydrophobic modification of inulin
- *In vitro* digestion of various single-layer carbohydrate-based emulsions
- *In vitro* digestion of a multi-layer emulsion using WPI and Chitosan

Chapter 4 - Optimising a carbohydrate-based system for colon-target delivery of SCFAs - an *in vitro* study

- Gastric digestion
- Intestinal digestion
- Interaction of adsorbed carbohydrate and bile salts

Chapter 5 - Design and *in vitro* evaluation of SCFA-supplemented Pickering emulsions using modified CNCs

- Hydrophobic modification of CNCs
- Responsiveness of modified CNCs-based emulsions to various pH and ionic strengths
- *In vitro* digestion of modified CNCs-based emulsions

Chapter 6 - *In vivo* digestion of SCFA-supplemented emulsions using cannulated pig model

- *In vitro* digestion
- *In vivo* study

Chapter 7 - Key findings and future research prospects

---

## Chapter 2 - Literature review

---

### 2.1. SCFAs and their main roles in gut health and the immune system

#### 2.1.1. Production of SCFAs

Although SCFAs can be naturally produced from the liver, the major production of them is in the colon through carbohydrate fermentation in the presence of SCFA-producing microbiota (Tan et al., 2014). They consist of six or less carbon molecules of which acetic, propionic (PA), and butyric acids (BA) are the majority (95% of the total SCFAs) (Besten, et al., 2013). The three SCFAs were mostly produced in the proximal colon in high concentration (70–140 mM). Their concentrations were much lower in the distal colon (20–70 mM) and in the distal ileum (20–40 mM) (Wong, deSouza, Kendall, Emam, & Jenkins, 2006). BA is mostly absorbed by the colonocyte to produce energy while PA and acetic acid reach the liver through the portal vein (Tan et al., 2014).

The major substrates of SCFA production in the colon are indigestible carbohydrates, such as pectin, inulin, chitosan, etc. The production of SCFAs in the colon involves various complex enzymatic pathways, all of which the most known pathway of SCFA production is via the glycolytic pathway (Tan et al., 2014). Fig. 2.1 demonstrates the production pathways of acetic acid, PA and BA. The type of SCFAs depends on the bacterial species. The recently reported list of butyrate-producing bacteria that included members of *Actinobacteria*, *Bacteroidetes*, *Fusobacteria*, *Proteobacteria*,

*Spirochaetes*, and *Thermotoga*. In addition, *Akkermansia muciniphila* (Phylum *Verrucomicrobia*) was reported to produce both propionate and acetate. Also, the production of acetic acid and PA is mediated by bacteria such as *Bifidobacterium* species (belonging to the Phylum *Actinobacteria*) ([Venegas, et al., 2019](#)).

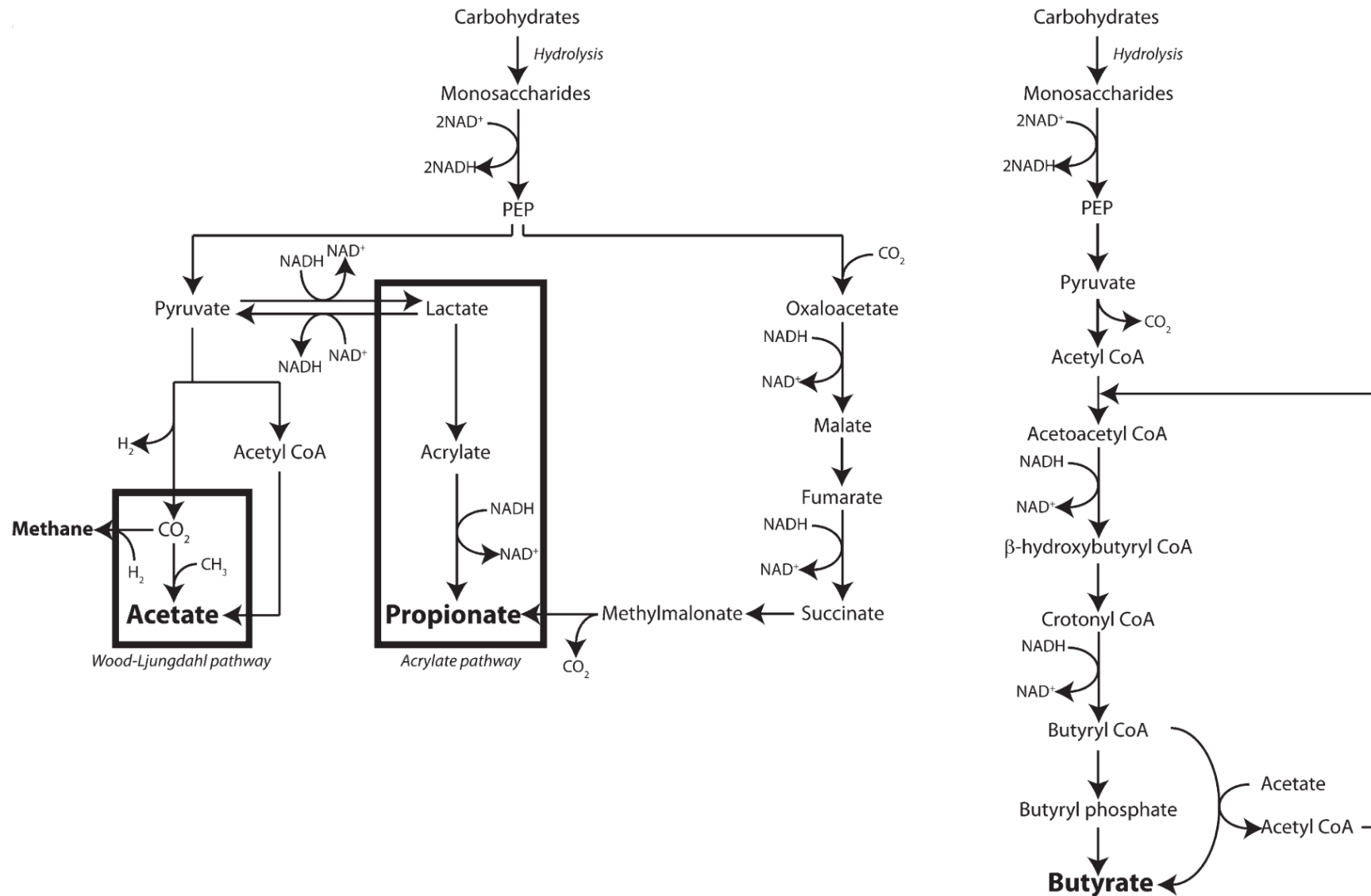


Figure 2.1. SCFA production pathways in the colon (adopted from Besten et al, 2013)

### 2.1.2. SCFA roles in gut health and the immune system

Recent studies have demonstrated their important roles for the maintenance of human health and the prevention of colon diseases (Besten, et al., 2013; Mortensen & Clausen, 1996; Tan, et al., 2014; Venegas, et al., 2019). Table 2.1 lists the biological functionality, including bioactivities of different SCFAs to the host and the corresponding working mechanisms.

#### ***Source of energy***

It was reported that 10% of human caloric requirements was provided by SCFAs (Bergman, 1990). In another study, Roediger and co-workers found that up to 70% energy for the epithelial cells of the rat colon was supplied by oxidation of SCFAs (Roediger, 1982). Although PA and BA are metabolised by gut epithelium and liver, a high proportion of BA is mainly removed by gut epithelium, whereas most of the PA is taken up by liver. Amongst all the SCFAs, BA is considered to be the most important source of energy for colonic cells due to its high affinity to the cells (Besten, et al., 2013; Roediger, 1982). In the colon, BA was mainly oxidised to produce energy for the epithelial cells. A small proportion of BA was converted to butyryl-CoA by the enzyme butyryl-CoA synthetase in the liver. After this reaction, it was quickly transferred to acetyl-CoA, longer chain fatty acids or to Ketone in the body. Similarly, most PA was converted to propionyl-CoA by the propionyl-CoA synthetase in the liver. However, the propionyl-CoA then goes through several enzymatic reactions to be converted to oxaloacetate before entering the tricarboxylic acid pathway to produce glucose. Amongst all SCFAs, PA is the only SCFA that could be a major source of glucose. Although PA is a potent glucogenic compound, it was challenging to assess accurate its contribution to glucose production of the whole animal body (Bergman, 1990).

---

### ***Inhibition of histone deacetylases (HDAC)***

Acetylation of the lysine within the histone induces gene activation while HDAC is responsible for removing the acetyl groups of the lysine (Tan, et al., 2014). Therefore, inhibition of HDAC expression might boost the gene transcription by increasing the histone acetylation. SCFAs were reported to inhibit HDAC (Boffa, Vidali, Mann, & Allfrey, 1978; Waldecker, Kautenburger, Daumann, Busch, & Schrenk, 2008) and this might increase the acetylation of the histone. SCFAs, therefore, alter gene transcription and subsequently gene expression of cells. However, the inhibition of HDAC depends on either the type of SCFAs or cell type that SCFAs interact with. Acetic, propionic and BAs increased histone acetylation when they were used in the treatment of hepatoma tissue (Sealy & Chalkley, 1978). BA was a more powerful inhibitor than propionic acid while acetic acid exhibited no effect when they acted on colonic cells (Tan, et al., 2014). In another study with colonic cancer cells, propionic, butyric and valeric acids demonstrated excellent inhibitory property against HDAC while acetic and caproic acid did not cause any effect on histone acetylation (Hinnebusch, Meng, Wu, Archer, & Hodin, 2002). In these studies, BA, amongst all the SCFAs, was considered as the most powerful inhibitor of HDAC.

### ***Activation of G-protein-coupled receptors (GPCR)***

GPCR, also called seven-transmembrane receptors or heptahelical receptors, are proteins located in the cell membrane that bind extracellular substances and transmit signals from these substances to an intracellular molecule called a G protein (guanine nucleotide-binding protein). One thousand types of GPCRs are encoded by the human genome alone, two of which (GPR43 and GPR41) have been reported to interact with

SCFAs in some previous studies ([Dewulfa, et al., 2011](#); [Poul, et al., 2003](#); [Tan, et al., 2014](#)). Activation of GPCR by SCFAs depends not only on the type of SCFAs but also on the type of GPCR. GPR43, also known as free fatty acid receptor 2, recognises most SCFAs, including acetic, propionic, BAs, valeric and caproic acids. However, GPR41, also known as free fatty acid receptor 3, was only activated by acetic and propionic acids. In both cases, propionic acid was considered as the most potent activator ([Tan, et al., 2014](#)).

### ***Anti-inflammatory role***

SCFAs have anti-inflammatory effects through various mechanisms. The most common way is by regulating NF- $\kappa$ B (nuclear factor kappa-light-chain-enhancer of activated B cells) activity ([Ni, et al., 2010](#)). NF- $\kappa$ B is a protein complex found in almost all cell types of animals and plays a very important role in controlling the transcription of DNA. Incorrect regulation of NF- $\kappa$ B possibly leads to inflammation or even cancer. However, SCFAs, especially propionic and BAs are known to ameliorate it, i.e., BA can affect the transcription of NF- $\kappa$ B by regulating the nuclear transcription factor group box-1, and hence inhibit the inflammation ([Huuskonen, Suuronen, Nuutinen, Kyrlylenko, & Salminen, 2004](#); [Tan, et al., 2014](#)).

The maintenance of mucous homeostasis is an essential factor in the prevention of colonic diseases, such as inflammatory bowel disease and irritable bowel syndrome. Mucus forms a physical barrier to limit the access of external bacteria to epithelial cells ([Moughan, Rutherford, & Bala, 2013](#)), that maintain the integrity of the colon. Any deficiencies in the mucous layer could, therefore, possibly exacerbate various diseases. But this could be modulated with efficient supplementation of SCFA ([Tan,](#)

---

et al., 2014). In a study, the oral supplementation of BA in a mice model was reported to alter colon permeability and therefore, enhanced colon integrity (Ferreira, et al., 2012). There was another theory that SCFA could enhance gut integrity through the maintenance of symbiosis (Tan, et al., 2014).

### ***Anti-cancer effect***

On the one hand, in an *in vivo* study with mice, SCFAs was reported to regulate epithelial gene expression involved in energy metabolism, such as lipid metabolism and promote the development of mouse intestinal organoids, subsequently strengthening their part in supporting epithelial cell proliferation (Venegas, et al., 2019). On the other hand, a study showed that BA had different on the intestinal stem cells, inhibiting their proliferation and delaying wound repair through the transcription factor Foxo3 (Kaiko et al., 2016).

In addition, telomerase, or terminal transferase, was one of the most important factors to maintain cancer cell proliferation. SCFAs, in particular BA, can inhibit telomerase activity, thereby playing a key role in the prevention of cell proliferation. Although all SCFAs were reported to have anticancer effect, BA is likely the most potent candidate (Gupta, Martin, Prasad, & Ganapathy, 2006; Gurav, et al., 2015; Kilner, et al., 2012).

### ***Anti-microbial activity***

SCFAs have been used in food and agriculture for several decades due to their antimicrobial properties. Acetic and propionic acids, for instance, are usually used in food as anti-microbial additives while BA is used to control *Salmonella* infections (Liick

& Jager, 1997a, 1997b). All SCFAs can change the pH balance, and subsequently affect the nutrient uptake of bacteria. Some researchers found that propionic and caproic acids could promote the expression of host anti-microbial peptide (Alva-Murillo, Ochoa-Zarzosa, & López-Meza, 2012). In a human study, the activity of an antimicrobial agent (cathelicidin) released polymorphonuclear leukocytes was induced by butyrate via its HDAC inhibitory activities (Tan et al., 2014). Therefore, SCFAs supplemented or produced by microbiota will play a vital role in shaping the microbial ecology of the colon.

### ***Promoting metabolic health***

Firstly, SCFAs were reported to regulate the glucose metabolism in the host body. The plasma glucose level is determined by the composition of the food, gluconeogenesis and the involvement of multi organs. As reviewed by Besten et al. (2013), oral addition of acetic acid and PA reduced glycemia in diabetic hyperglycemic KK-A(y) mice and normal rats. SCFAs might also reduce the plasma glucose level through increasing the gut hormone PYY that is known as a satiety hormone.

Acetic and propionic acids were reported to decrease the plasma concentration of cholesterol in rats (Fushimi, et al., 2006) and human (Kondo, Kishi, Fushimi, Jin, & Kaga, 2009). Supplementation with acetic acid affected cholesterol 7 $\alpha$ -hydroxylase which was involved in the conversion of cholesterol to bile acid while propionic acid could reduce the activity of 3-hydroxy-3-methylglutaryl-CoA reductase, a rate-limiting enzyme in the synthesis of cholesterol. Acetic and propionic acids, therefore, could play an important role in regulating cholesterol metabolism (Besten, et al., 2013).

**Table 2.1.** Beneficial effects of SCFA on the hosts

Beneficial effects	SCFAs involved	Short description of main mechanism	References
Source of energy	C2, C3, C4	SCFA are oxidised inside the colonocytes to produce up to 70% of the required energy for the cells.	( <a href="#">Bergman, 1990</a> ; <a href="#">Besten, et al., 2013</a> ; <a href="#">Hinnebusch, et al., 2002</a> ; <a href="#">Mortensen, et al., 1996</a> ; <a href="#">Roediger, 1982</a> )
Inhibition of HDAC	“C4>C3>C2”, C5	SCFA may enter the cells via transporters and subsequently inactivate the enzymes by occupying one part of the active site of HDAC.	( <a href="#">Boffa, et al., 1978</a> ; <a href="#">Tan, et al., 2014</a> ; <a href="#">Waldecker, et al., 2008</a> )
Activation of GPCR	C2, C3, C4, C5	The absorption of SCFA into the colonic cells of animal models, such as rats and rabbits results in the release of intestinal peptide YY that exerts anorexigenic effects.	( <a href="#">Dewulfa, et al., 2011</a> ; <a href="#">Poul, et al., 2003</a> ; <a href="#">Tan, et al., 2014</a> )
Anti-inflammatory role	“C4>C3>C2”, C5, C6	SCFA can regulate the immune cell chemotaxis as well as the release of cytokine. In addition, SCFA can remediate deficiency in the mucous layer of the intestine.	( <a href="#">Huuskonen, et al., 2004</a> ; <a href="#">Kilner, et al., 2012</a> ; <a href="#">Mortensen, et al., 1996</a> ; <a href="#">Scheppach, 1995</a> ; <a href="#">Tan, et al., 2014</a> ; <a href="#">Voltolini, et al., 2012</a> )

---

Anticancer role	C2, C3, C4, C5, C6	Inhibition of HDAC by SCFA results in a reduction in telomerase activity that may possibly reverse the malignant phenotype.	(Gupta, et al., 2006; Gurav, et al., 2015; Kilner, et al., 2012; Narayanan, Baskaran, Amalaradjo, & Venkitanarayanan, 2015)
Antimicrobial activity	C1, C2, C3, C4, C5, C6	SCFA can alter the pH, effect osmotic balance, nutrient uptake and energy generation of the cells.	(Liick, et al., 1997a, 1997b; Mortensen, et al., 1996; Tan, et al., 2014)
Regulation of cholesterol metabolism	C2, C3	Cholesterol metabolism is a complex pathway involving 3-hydroxy 3-methylglutaryl-CoA reductase, which is inhibited by SCFA, especially propionic acid.	(Besten, et al., 2013; Cummings, Rombeau, & Sakata, 2004; Fushimi, et al., 2006; Kondo, et al., 2009)

---

C1, C2, C3, C4, C5 and C6: formic, acetic, propionic, butyric, valeric and caproic acids, respectively.

SCFA\*: either one or more SCFA result in the benefits because current understanding is unclear.

## **2.2. Targeted delivery of SCFAs to the digestive tract**

Although SCFAs can be supplied by non-digestible carbohydrates (fibre), many people do not consume sufficient dietary fibre. Therefore, extra supplementation of SCFAs might be a good nutritional strategy to provide health benefits to the colon as discussed in [section 1.1](#).

### **2.2.1. Supplementation of SCFAs to animals**

There has been an increasing amount of published work regarding the application of encapsulated SCFAs, especially BA, to enhance body weight of broilers, pig, and egg production of laying hens ([Levy, et al., 2015](#); [Mallo, Balfagón, Gracia, Honrubia, & Puyalto, 2012](#); [Sobczak & Kozłowski, 2016](#)). Encapsulated BA formulations used in these studies were commercial products (ButiPEARL™) that are designed for animals, specially hens and pigs. In the studies, BA was encapsulated by fat matrix, which was then embedded in the silica MicroPEARLS matrix during the manufacturing process. The MicroPEARLS were used to supplement into basal diets of hen, pigs and broilers to improve weight and egg productivity. For example, in the study of [Sobczak & Kozłowski \(2016\)](#), two groups of hens (48 weeks of age) were investigated. The control group was fed on a basal diet (wheat, triticale, soybean meal and maize, with no feed additives), while the experimental group was fed on a similar basal diet supplemented with encapsualted BA at a weigh ratio of 500 g of encapsulated BA to 1 ton of feed. The experiment was conducted for 24 weeks. The results showed that supplementation of the basal diet with encapsulated BA significantly increase the eggshell thickness and eggshell weight as a percentage of total egg weight. In addition, supplementing encapsulated BA to animal diets was also reported to

increase BA concentrations in the colon of pigs and hens (Mallo, et al., 2012; Sobczak, et al., 2016).

### **2.2.2. Supplementation of SCFAs to human**

SCFAs have been used to treat patients with irritable bowel syndrome (Banasiewicz, et al., 2012; Scarpellini, et al., 2007). The direct supplementation of BA via a tablet led to clear therapeutic effect, such as abdominal pain reduction at a dose of 1g BA/day for 30 days (Scarpellini, et al., 2007) or 0.3g/day after 28 days (Banasiewicz, et al., 2012). For example, in the study of Scarpellini, et al. (2007), the patients were divided into two subgroups: constipation-predominant irritable bowel syndrome (IBS) and diarrhoea-predominant IBS. The IBS variant and symptom scores of patients were recorded before and after treatment by questionnaires. At the end of the trial, the symptom scores demonstrated a significant improvement in patients with the diarrhoea variant compared with those with the constipation variant ( $p < 0.05$ ), showing that oral supplementatin of BA is a promising method to regulate the status and to improve the gastrointestinal symptoms in patients with the diarrhoea-predominant irritable bowel syndrome. Further information about the formulation used in these studies was not mentioned due to commercial sensitivity. However, unpleasant smell from SCFAs was also reported, making direct supplementation of such SCFAs to daily diet rather restricted. To overcome this drawback, different approaches have been suggested, but the most popular method is the use of SCFA precursors, including non-digestible carbohydrates and triglycerides of SCFAs.

### ***Non-digestible carbohydrates***

Polysaccharides such as inulin, cellulose and oligosaccharides are the main substrates for a complex bacterial fermentation to produce SCFAs in the colon. Up to 95% of SCFAs formed in the colon are rapidly adsorbed by colonocytes while the remaining part is excreted to the faeces (Boets, et al., 2015). Non-digestible carbohydrates are resistant to digestion by gastrointestinal enzymes and, hence can directly reach the colon.

To date, it has been widely reported that SCFAs can be produced by non-digestible carbohydrates *in vivo*. The amount and type of SCFAs have also been analysed (Besten, et al., 2013; Brestensky, et al., 2016; Knudsen, Jørgensena, & Theil, 2016; Wang, et al., 2017). The concentration of SCFAs generated in the colon varies, depending on various factors such as diet and difference between individuals. SCFAs accumulate in two parts of the colon respectively, ranging from 70 to 140 mM in the proximal colon, and 20 to 70 mM in the distal colon (Besten, et al., 2013; Tan, et al., 2014). In an *in vivo* study, the total amount of SCFAs produced from inulin in the whole colon was around 168 mM (Boets, et al., 2015). Amongst all the SCFAs, acetic, propionic, and BAs are dominant, contributing around 95% of total SCFAs (Besten, et al., 2013). Different molar ratios between acetic, propionic, and BAs have been reported, depending on the type of substrates, microbiota and individuals. For example, the molar proportions of acetic : propionic : BAs reported by different groups were 82:6:12 (Boets, et al., 2015), approximately 80:10:10 (Wang, et al., 2017) and 60:20:20 (Besten, et al., 2013; Tan, et al., 2014). In all cases, acetic acid was the dominant product, while propionic and BAs, which bring more proven health benefits to the gut, contribute to less than 40% of the total SCFAs. On the other hand, the type and amount of SCFAs supplied by carbohydrates to the colon is uncontrollable. These

drawbacks might be addressed by targeted delivery of desired-SCFAs precursors to the gut.

### ***Triglycerides of SCFAs***

Short-chain triglycerides, such as tripropionin (TP) and tributyrin (TB) are sources of propionic and BAs respectively. The triglycerides are hydrolysed by either pancreatic or microbial lipases to produce SCFAs. Some research groups have developed oil-in-water (O/W) emulsion systems to deliver TB ([Augustina, et al., 2011](#); [Y. Li, Maux, Xiao, & Mcclements, 2009](#)). Other researchers have encapsulated TB in O/W emulsions and spray dried as powder form. The release profile of BA from emulsion powders has been tested in simulated gastrointestinal fluids ([Donovan, Bauer, Jr, & Lee, 2017](#); [Donovan, Cadwallader, & Lee, 2016](#); [Donovan, Lee, & Lee, 2016](#); [Sanguansri, et al., 2013](#)). In these studies, authors used whey protein isolate, anhydrous milk fat, short-chain inulin and gamma-cyclodextrin as wall materials. It was reported that all the spray-dried samples containing TB released approximately 2–3% and up to 93.88% BA at gastric and intestinal phases respectively. This was attributed to the enzymatic hydrolysis of TB in the small intestinal phase ([Donovan, et al., 2017](#)). Most protein-stabilized emulsions tend to be destabilized and coalesced in the gastric phase owing to pepsin-induced interfacial proteolysis ([Sarkar, Goh, Singh, & Singh, 2009](#); [Sarkar, Zhang, Murray, Russell, & Boxal, 2017](#); [Torres, Murray, & Sarkar, 2019](#)). Bearing this in mind, understanding the interaction of gastrointestinal fluids with triglycerides and interfacial materials is crucial to select suitable materials for designing delivery systems. In our work, to prevent premature absorption of SCFAs, various indigestible carbohydrates were selected as emulsifiers.

### 2.3. Release of SCFAs from emulsions: dynamics of lipid digestion

There are three main stages in the human digestive system that affect the release of SCFAs from O/W emulsion, i.e. lingual, gastric and intestinal stages.

In the first stage, emulsion will be mixed with saliva and interact with enzymes. Ptyalin, or  $\alpha$ -amylase, a common enzyme found in saliva, hydrolyses carbohydrates, especially starches to maltose (Pedersen, Bardow, Jensen, & Nauntofte, 2002; Wilde & Chu, 2011). In addition, no specific human lipase, such as lingual lipase in the case of rodents, was identified at the oral phase although lipase activity was identified at this stage (Brignot & Feron, 2019). Moreover, the retention time in the oral stage is short, the lipid digestion is therefore limited. It was reported that less than 2% of BA was released from an emulsion containing TB encapsulated by whey protein using *in vitro* oral phase (Donovan, et al., 2017).

In the gastric stage, emulsions encounter low pH, various enzymes, high ionic strength and stomach contraction. This process can last up to 4 hours and pepsin can digest most proteins present in emulsions (McClements, 2013). Therefore, triglycerides encapsulated by protein emulsifiers will be significantly influenced in this stage. Gastric lipase also has surface activity and commences the hydrolysis by interfacial interaction with lipid similar to lingual lipase (Chahinian, Snabe, Attias, Fojan, Petersen & Carriere, 2006). In the presence of an emulsifier on the O/W interface, gastric lipase must overcome the protection of this layer to initiate the digestion. *In vivo* studies have shown that up to 30% of dietary lipids are hydrolysed within lingual and gastric phases (Carrière, Barrowman, Verger & Laugier, 1993; Armand, et al., 1999). The main reason for low lipolysis in the oral and gastric phase is product inhibition. Product of

the lipolysis in the gastric phase are fatty acids and diglycerides that are polar lipids, so tend to be more surface active than the neutral triglycerides. Therefore, the lipolysis products tend to accumulate at the O/W interface, sometimes forming solid or crystalline phases which prevent lipase from gaining access to the interface (Wilde, et al., 2011).

Subsequently, intestinal digestion is responsible for most of the lipolysis. Intestinal fluid contains a mixture of bile salts, pancreatic enzymes including lipase, co-lipase, and various salts that digest any macronutrients to be absorbed by the epithelial cells. In contrast to lingual and gastric lipases, pancreatic lipase has no surface activity, so it relies on bile salts to initiate the hydrolysis. Bile salts displace any emulsifiers that have weaker surface activity. In addition, the influence of hydrolysis products in the intestinal stage is rather restricted. Fatty acids, monoglycerides and/or diglycerides that accumulate at the O/W interface will be solubilised and displaced by bile salt to allow the hydrolysis to continue. However, because the bile salts are more surface active than any materials that they displace from the O/W interface, this makes it difficult for lipase to adsorb on the interface. In other words, bile salts will inhibit pancreatic lipase activity. To solve this problem, the pancreatic lipase has a cofactor, a small protein that is able to adsorb on the bile salt dominated interface. In addition, the cofactor can form a complex with lipase, therefore facilitating the adsorption of lipase to the interface in the presence of bile salt (McClements, 2008 & 2013).

For the purpose of colon-targeted delivery, lipid hydrolysis in all phases, especially gastric and intestinal stages must be restricted. Strategies for a) gastric and b) intestinal digestion prevention are:

a) Gastric digestion can be limited by using emulsifiers that are resistant to pepsin. While protein emulsifiers are mostly digested in the gastric phase, carbohydrates are potential candidates due to their resistant properties to gastric enzymes.

b) The restriction of intestinal digestion may be accomplished by interfering with bile salt adsorption, preventing lipase adsorption and therefore slowing down lipid hydrolysis. There are two approaches to reduce bile salt adsorption:

- The first solution is the employment of emulsifiers that have stronger surface activity than bile salts. Galactolipids are emulsifiers from plants and they have the ability to restrict bile salts adsorption ([Diaz, Cordova, Baratti, Carriere, & Abousalham, 2007](#)). However, the emulsifiers are very costly (e.g. 1-mg commercial product costs 600 NZD) and therefore the application of such emulsifiers is limited.
- The second method is designing systems that are mechanically strong enough to resist displacement. Some studies attempted to strengthen a protein-oil complex by heat-treatment ([Sandra, Decker, & McClements, 2008](#)), or forming cross-linking with small molecular substances ([Hu, et al., 2015](#)). Heating allows the rearrangement of intermolecular bonds between the protein molecules, thus promoting the formation of intermolecular disulphide bonds. Disulphide bonds induced by heat-treatment resulted in improvement in resistance to displacement of bile salts. However, these crossed-linked proteins failed to prevent lipid hydrolysis in an *in vitro* study ([Sandra, et al., 2008](#)). This was probably due to the destruction of WPI caused by pancreatic protease. In a different study, cross-linking between protein and genipin significantly delayed lipid hydrolysis ([Hu, et al., 2015](#)). In addition to cross-linking, layer-by-layer encapsulation systems made

of lecithin and chitosan was also reported to delay lipid hydrolysis (Mun, Decker, Park, Weiss, & McClements, 2006).

Overall, to delay the intestinal lipolysis, an emulsifier must possess two vital properties; resistant against human enzymes and mechanically strong enough to resist competitive displacement by bile salts (Hu, et al., 2015; Mun, et al., 2006; Sandra, et al., 2008). Most protein emulsifiers tend to be hydrolysed by pepsin at the gastric stage, leading to destabilized and coalesced emulsions (Sarkar, et al., 2009; Sarkar, et al., 2017; Torres, et al., 2019). Carbohydrates, such as inulin, chitosan, pectin and cellulose are resistant to pepsin and pancreatic enzymes. Although non-digestible carbohydrates have been extensively used as emulsifiers to produce O/W emulsions (Funamia, et al., 2007; Miao, Tayebi, & Hamad, 2017; Verkempinck, et al., 2018), limited studies focused on their application to deliver SCFAs to targeted-digestive tracts (Donovan, et al., 2017).

## **2.4. Conventional O/W emulsions and carbohydrate-based emulsifiers**

This section summarises overall O/W emulsion formation process and structural properties of various carbohydrates, i.e. inulin, chitosan, modified starches, pectin and cellulose nanocrystals (CNCs), and their applications for producing O/W emulsions as delivery vehicles of bioactive compounds. That will set the scene for better understanding the potential application of these carbohydrates to produce delivery systems for SCFAs.

### **2.4.1. O/W emulsion formation process**

To produce an O/W emulsion, the oil phase and aqueous phase are mixed and homogenised to breakdown large droplets into smaller ones, which significantly increases the surface area of oil droplets. In food processing, the homogenisation could be achieved using a high-speed mixer, or a high-pressure valve homogenizer. From a thermodynamics perspective, if the surface area is increased by an amount  $\Delta A$  through the homogenisation, the energy require of this process is  $\Delta G = \gamma\Delta A$ , where  $\gamma$  is the interfacial tension. Without the presence of emulsifiers, oil droplets will coalesce with their neighbours to reform larger droplets. To prevent coalescence, the emulsifiers present in the aqueous phase will adsorb at the surface of the freshly formed droplets. The rate of adsorption depends on the emulsifying ability of the emulsifiers. Therefore, an effective emulsifier should possess three crucial properties: (i) rapidly reduce the interfacial tension at the freshly formed O/W interface, (ii) bind strongly to the interface once adsorbed, and finally (iii) protect the newly formed droplets against flocculation or coalescence. The emulsifier layer surrounding the oil droplet surface creates a barrier that prevents droplet coalescence through electrostatic and steric stabilization mechanisms depending on the structure of the emulsifiers (Dickinson, 2009). The next section will briefly summarise structural properties of some potential carbohydrate materials and throughout the thesis, mechanisms of the emulsification by these carbohydrates and their behaviours under *in vitro* gastrointestinal digestion will be thoroughly discussed.

### **2.4.2. Carbohydrate-based emulsifiers**

#### ***Inulin***

Inulin is a generic term to cover all  $\beta(2\rightarrow1)$  linear fructans. The degree of polymerisation (DP) of inulin varies depending on the resources and manufacturing procedure. For instance, chicory inulin has a DP from 2 to 60 while its partial enzymatic hydrolysis product has DP of 2 to 8 (Roberfroid, 2005). The main chemical structure of inulin is illustrated in Fig. 2.2. It consists of a chain-terminating glucosyl moiety and a repetitive fructosyl moiety (Morrosa, Leveckeb, & Infantea, 2011). Inulin is listed in the prebiotic group which are non-digestible carbohydrates. Inulin is resistant to human digestive enzymes, but fermentable by the intestinal microbes, therefore, it promote the growth of bacteria such as *Bifidobacterium sp.* and *Lactobacillus sp.* (Singh, Jadaun, Narnoliya, & Pandey, 2017). In addition, inulin is fermented by colon microbiota to produce a wide range of metabolites in the gut, e.g., short-chain fatty acids (Boets, et al., 2015; Singh, et al., 2017).

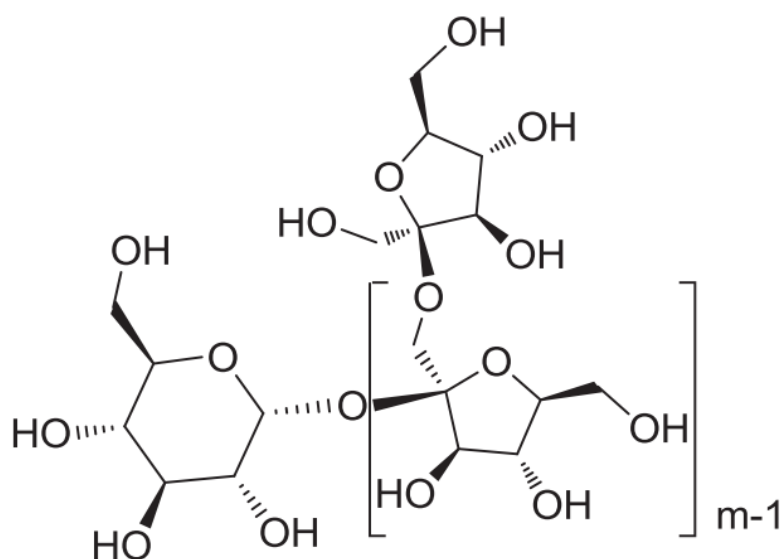


**Figure 2.2.** Main chemical structure of inulin ( $GF_m$ ). G and F and  $m$  correspond to glucosyl, fructosyl units and the degree of polymerization of  $\beta(2\rightarrow1)$  linkage respectively (Morrosa, et al., 2011).

Inulin is soluble in water and the solubility level depends on its polymer chain length (Kokubun, Ratcliffe, & Williams, 2013). At high concentration, typically >15%, longer chain length inulin forms gels on cooling (Kim, Faqih, & Wang, 2001; Kokubun, et al., 2013). The application of inulin in the food sector has been increasing not only because of its gelling properties but also because of its nutritional values. For delivery of bioactive compounds to targeted digestive tracts, the application of inulin in emulsion systems is very limited due to its poor surface activity. Chemical modification of inulin with hydrophobic groups has been proposed to overcome this drawback (Kokubun, et al., 2013; Kokubun, Ratcliffe, & Williams, 2015; Morrosa, et al., 2011). Various chemicals have been used to modify inulin but the most common one is 2-octen-1-yl-succinic anhydride (OSA). The attachment of OSA groups onto an inulin backbone significantly improves its hydrophobicity, and the amphiphilicity provides better emulsifying capacity than unmodified inulin (Kokubun, et al., 2015). It is reported that O/W emulsions stabilised by OSA-modified inulin remain stable up to 21 days at 25 and 50°C storage condition (Kokubun, Ratcliffe, & Williams, 2018). The excellent emulsification property of modified inulin makes it a promising candidate to prepare gastrointestinal resistant emulsions for targeted delivery of bioactive compounds in the digestive tract. However, no relevant work has been reported until now.

### **Chitosan**

Chitosan, or  $\beta$ -(1-4) linked 2-amino-2-deoxy-D-glucose, is a linear polymer conventionally produced by partial alkaline deacetylation of chitin (Kean & Thanou, 2010). For chitosan production, the deacetylation of chitin usually reaches about 50% depending on the origin of the polymer (Rinaudo, 2006). Chemical structure of chitosan is illustrated in Fig. 2.3 where DA stands for degree of acylation (Rinaudo,

2006). Chitosan can be degraded by enzymes which hydrolyse glucosamine–glucosamine, glucosamine–N-acetyl-glucosamine and N-acetyl-glucosamine–N-acetyl-glucosamine linkages. In vertebrates, chitosan could be degraded by lysozyme and by bacterial enzymes in the colon. As reviewed by Kean, et al., (2010), eight human chitinases (in the glycoside hydrolase 18 family) have been identified, three of which have shown enzymatic activity. In other words, the hydrolysis of chitosan in human digestive system is very limited until it reaches the colon.

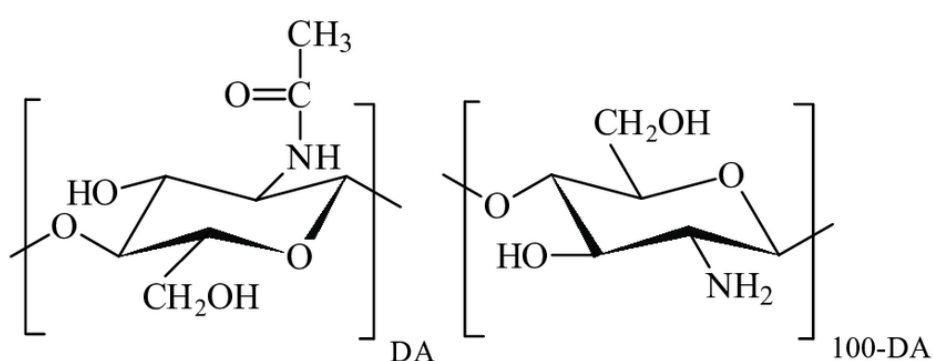


**Figure 2.3.** Chemical structure of chitosan. DA corresponds to degree of acylation.

Chitosan is soluble at pH below 6.0 and usually dissolved in 1% or 0.1M acetic acid to form a solution. However, the solubility depends on various factors, such as DA, the ionic concentration, the pH and the distribution of acetyl groups along the chain. The solubilization happens by protonation of the  $-NH_2$  groups on the C-2 position of the D-glucosamine unit, whereby the polysaccharide is converted to a polyelectrolyte in the acidic media (Rinaudo, 2006).

As a naturally occurring polysaccharide, chitosan is considered Generally Recognized As Safe (GRAS) by FDA. It has many applications in food and pharmaceutical sectors, including drug/bioactive delivery and tissue engineering (Kean, et al., 2010). Chitosan

is natural positively charged carbohydrate having pKa of around 6.6–7.0 (Schulz, Rodríguez, Blanco, Pistonesi, & Agulló, 1988). In food and pharmaceutical formulations, chitosan is often used to coat an emulsion to form a multilayer system, interacting with the oppositely charged emulsifiers. The multilayer systems have been used to deliver various bioactive compounds, such as curcumin,  $\beta$ -carotene and Intranasal vaccine (Fang, Zhao, Liu, Liang, & Yang, 2019; Li, Hwang, Chen, & Park, 2016). Such applications were based on the fact that chitosan has good resistance to human digestive enzymes. In fact, chitosan is frequently used for delivering drugs, but not food bioactives, to the lower gastrointestinal tract.

### ***Modified starches***

Starch is one of the most abundant storage polymers, found in a variety of plants and widely used in food, pharmaceutical and other industries. This co-polymer comprises of two macromolecular moieties, i.e. amylose and amylopectin, the proportion of which varies depending on the sources. Amylose is a linear polysaccharide of glucose units that is linked through  $\alpha$ -1-4 glycosidic bonds, on average it accounts for 20–30% of the starch composition. Amylopectin is a more branched macromolecular polysaccharide that has additional  $\alpha$ -1-6 links and it accounts for 70–80% of the starch composition. The chemical structures of amylose and amylopectin are illustrated in Fig. 2.4 (Masina, et al., 2017).

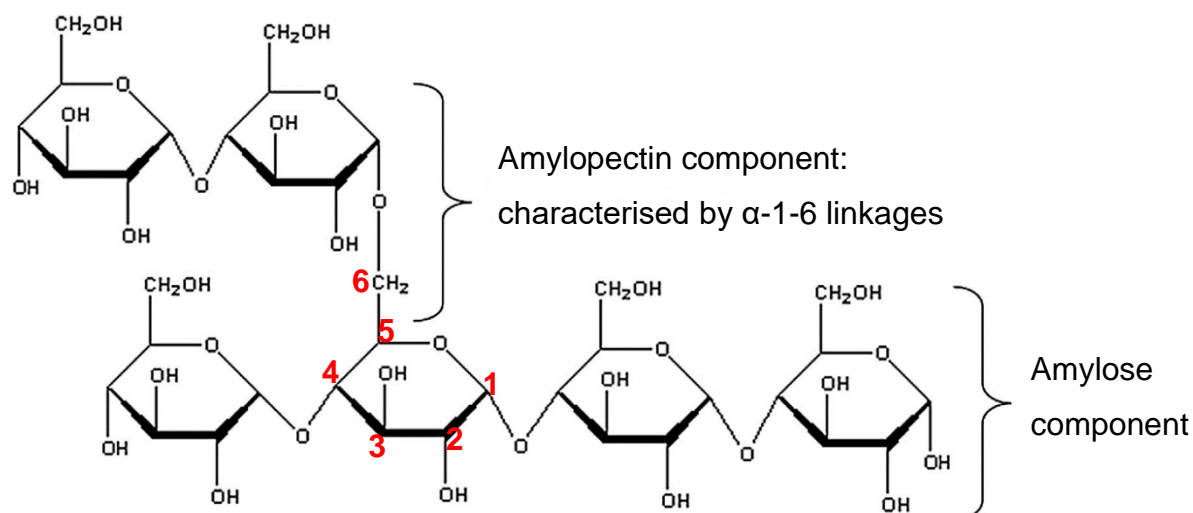


**Figure 2.4.** Starch co-polymer chain with amylose and amylopectin components

To maximise the potential of starch in food applications for delivering bioactive compounds, the physicochemical and physicommechanical properties can be modified to fit the required properties of the designed delivery systems. The three available hydroxyl groups (at position: C2, C3 and C6) can be chemically modified through esterification, etherification and oxidation (Masina, et al., 2017). In food applications, esterification of starch with OSA is one of the most common chemical modifications to improve starch emulsifying capacity (Jaina, Winuprasith, & Suphantharika, 2019; Lin, Liang, Zhong, Ye, & Singh, 2018a, 2018b). After the OSA-modification, the starch has OSA tails added to its backbone which provides whole starch molecules with an amphiphilic property. A previous study reported that OSA-modified starches had similar surface activity to gum Arabic (Chanamai & McClements, 2002). OSA-modified starches primarily stabilise O/W emulsions through a steric hindrance mechanism due to its branched amylopectin chains. In addition, the presence of OSA groups in the polymer backbone also gives the starch anionic property that stabilises emulsion droplets by electrostatic repulsive forces (Lin, et al., 2018a).

In the food sector, OSA starches have been used to stabilise aroma retention, coffee oil, rice bran oil,  $\beta$ -carotene and to deliver other bioactive compounds such as  $\beta$ -carotene (Chanamai, et al., 2002; Charoen, et al., 2011; Jaina, et al., 2019; Lee, Liu, Wong, & Liu, 2017; Lin, et al., 2018b). However, modified starches have not yet been used to encapsulate and deliver SCFAs, which will be thoroughly investigated in this PhD research.

### ***Pectin***

Pectin represents a family of heterogeneous polysaccharides, mainly located in the primary cell wall of plant cells (Ngouémazong, Christiaens, Shpigelman, Loey, & Hendrickx, 2015). Most commercial pectin products have a small proportion of protein residue. Pectin itself is one of the most structurally complex plant macromolecules. The molecular structure of pectin is very diverse depending on the sources and extraction process. Although the fine structure of pectin is not fully unravelled (Ngouémazong et al., 2015), the extracted pectin mainly includes to some extent heterogeneous homogalacturonan (HG), rhamnogalacturonan-I (RGI) structural elements, as well as limited proportion of the conserved rhamnogalacturonan-II (RGII) domain. HG is a homopolymer of up to 200 units of  $\alpha(1\rightarrow4)$ -linked D-galacturonic acid (GalA), and it is the most abundant component accounting for about 65% of the total pectin. RGI is a branched and heterogeneous polysaccharide, characterised by a long sequence of  $[\rightarrow2)\text{-}\alpha\text{-L-rhamnose-(1}\rightarrow4)\text{-}\alpha\text{-D-GalA(1}\rightarrow]$  alternating residues, which could be possibly be O-acetylated at O-2 and/or O-3 positions of GalA residues. It makes up approximately 20 to 35% of pectin. Another complex structural element of pectin, RGII, includes a backbone composed of approximately 9  $\alpha(1\text{-}4)$ -linked D-GalA residues, to which 4 heteropolymeric side chains of consistent structure and known

composition are attached (Nkouémazong, et al., 2015). It makes up approximate 10% of pectin. Fig. 2.5. represents pectin chemical structure with protein residue attaching to the chain.

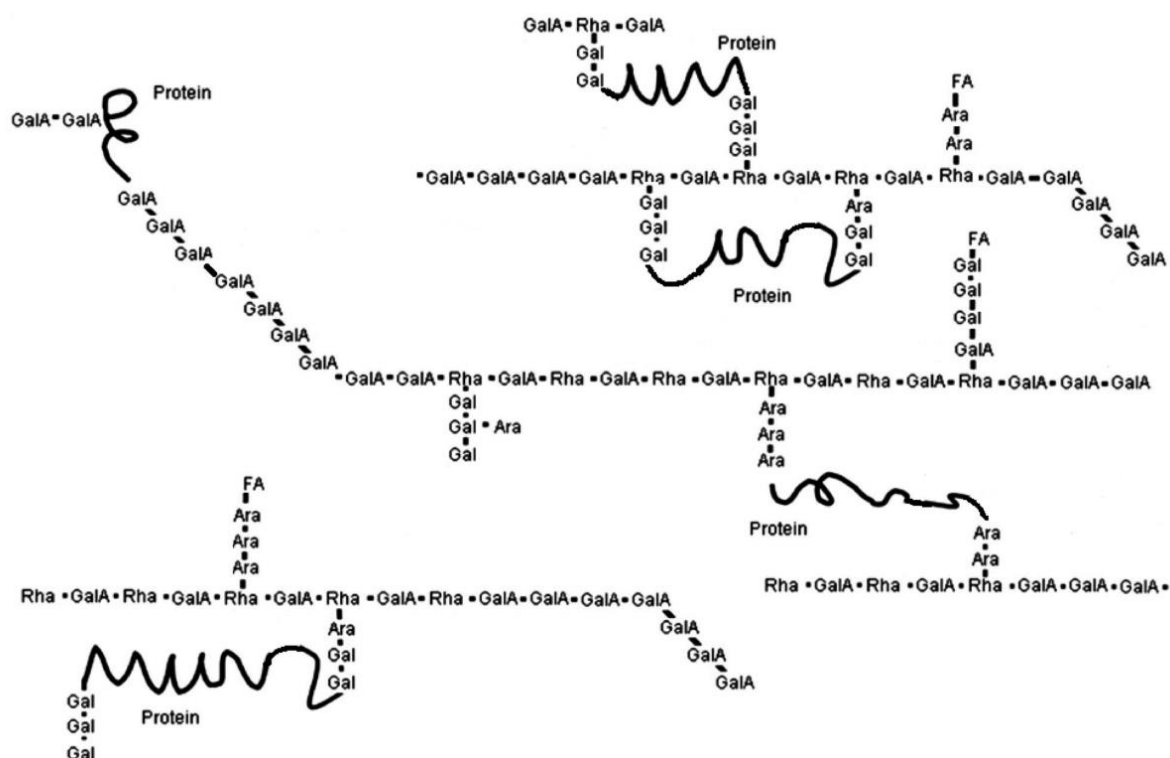


**Figure 2.5.** Schematic illustration of protein-containing pectin structure (adopted from Nkouémazong, et al., 2015)

During the past few decades, pectin has been perceived as a stabilising agent, mainly improving the shelf-life of the emulsions or solutions by increasing the viscosity of the continuous phase. However, recent studies have proven to some extent surface activity of pectin at the oil–water interface, mainly due to the presence of protein in most extracted pectin products (Siew, Williams, Cui, & Wang, 2008). Pectin emulsion stabilisation is achieved through steric and/or electrostatic stabilisation. As the molecular structure of pectin contains highly branched polysaccharide units covalently linked to a common protein core, the emulsification is hypothesised to initiate through

the adsorption of protein anchor onto the oil–water interface. In addition, the charged polysaccharide units extend into the aqueous solution, thereby providing a steric barrier against droplet coalescence, flocculation and further instability during storage, including creaming (Ngouémazong, et al., 2015). The emulsification mechanism “Loop and tail pectin adsorption model” in the presence of protein is illustrated in Fig. 2.6. In addition to steric and electrostatic interactions, viscosity might also play an important role in the emulsification process. Through increasing the viscosity of the aqueous phase of the emulsions, pectin restricts the mobility of the dispersed oil droplets, thus slowing down the tendency to coalesce and to cream.

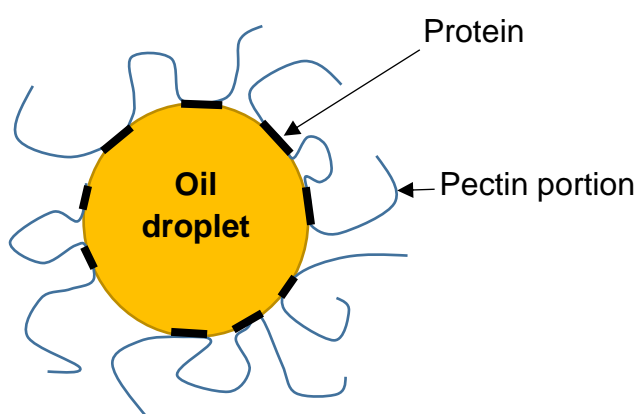


**Figure 2.6.** Emulsification mechanism of pectin in the presence of protein residue (the model was reproduced from Ngouémazong, et al., 2015).

Pectin appears to be a potential candidate as a digestion-resistant emulsifier because of three important properties. Firstly, pectin was successfully used as the sole emulsifier to produce stable oil-in-water (O/W) emulsions (Ngouémazong, et al., 2015). However, few studies on the specific influences of pectin as an emulsifier on lipid digestion have been reported (Verkempinck, et al., 2018; Verrijssen, et al., 2016; Verrijssen, Verkempinck, Christiaens, Loey, & Hendrickx, 2015). Secondly, it was

reported that pectin (2.0 wt% in the final emulsion) had the ability to form a thick layer (20 mg m<sup>-2</sup>) around the oil droplets at pH 4.0 because of the formation of multilayers (Siew, et al., 2008). This property is essential for slowing down the displacement by bile salts and eventually delaying lipid digestion. Finally, pectin is non-digestible by human digestive enzymes and is easily obtainable from plant cell wall material (Funami, et al., 2011; Funamia, et al., 2007; Ngouémazong, et al., 2015; Verkempinck, et al., 2018). Therefore, pectin can potentially produce a stable barrier that can prevent enzymatic destruction better than other types of emulsifiers, such as proteins.

## 2.5. Pickering emulsions – Cellulose nanocrystals (CNCs)

### 2.5.1. Pickering emulsions

Pickering emulsions, i.e. emulsions stabilised by solid particles, have gained significant research attention from food colloid scientists because of their combined advantages of high resistance to coalescence and the ability to delay lipid digestion (Dickinson, 2012; Sarkar, Zhang, Holmes, & Ettelaie, 2019). The preparation of a Pickering emulsion involves the addition of solid particles into the continuous phase, and then the homogenisation of the dispersed and continuous phases. Based on the particle's partial wettability in each of the two immiscible phases, they adsorb at the oil/water interface to form an effective steric and electrostatic protective shield for the emulsified droplets (Tang, Quinlan, & Tam, 2015). Pickering emulsions can be either oil-in-water (O/W) or water-in-oil (W/O) depending on the preferential wettability of the stabilising particles (Chevalier & Bolzinger, 2013). Hydrophilic particles that can adsorb at the oil-water interface favour the formation of O/W emulsions, whereas hydrophobic particles are generally suitable for W/O emulsions (Zembyla, Murray, &

[Sarkar, 2018](#)). In food applications, O/W emulsions are the most common systems. The general structure of an O/W Pickering emulsion, which is emulsified by spherical stabilisers is demonstrated in [Fig. 2.7](#). However, the shape of the stabilisers varies depending on the sources. Pickering O/W emulsions using inorganic particles have been studied extensively, but the use of biocompatible particles, such as protein microgels ([Destribats, Rouvet, Gehin-Delval, Schmitt, & Binks, 2014](#); [Hu, et al., 2016](#); [Sarkar, et al., 2016](#)), modified starch and non-starch polysaccharide particles ([Xia Li, et al., 2018](#); [Marefati, Matos, Wiege, Haase, & Rayner, 2018](#); [Tzoumaki, Moschakis, Kiosseoglou, & Biliaderis, 2011](#); [Yusoff & Murray, 2011](#)), protein–protein particle composites ([Liu, Huang, Chen, Deng, & Yang, 2019](#)), protein–polysaccharide particle composites ([Doost, et al., 2019](#); [Sarkar, Ademuyiwa, et al., 2018](#)) and polysaccharide–polysaccharide particle composites ([Xiaomin Li, et al., 2019](#)), for generating particle-stabilised interfaces is relatively recent. Such particles have been studied mainly to stabilise Pickering emulsions with the ultimate aim to alter the kinetics of lipid digestion. Protein microgels from WPI, for instance, were created by adjusting the pH, temperature and/or ionic strength to a specific value where the protein solution formed a gel. The gel was then broken down into micro/nano size by using a homogenizer. The WPI microgel Pickering emulsions were reported to resist pepsin hydrolysis due to thick interfacial loading ( $\sim 14 \text{ mgm}^{-2}$ ) that was nearly 12-fold higher than a WPI monolayer at the interface. However, protein microgel Pickering emulsions failed to protect intestinal lipolysis ([Sarkar et al, 2019](#)). Various forms of starch used for making Pickering emulsions with length scales from native to OSA-modified starch granules of mean diameter of 1–50  $\mu\text{m}$  have been reported ([Xia Li, et al., 2018](#); [Marefati, Matos, Wiege, Haase, & Rayner, 2018](#); [Tzoumaki, Moschakis, Kiosseoglou, & Biliaderis, 2011](#); [Yusoff & Murray, 2011](#)). The starch-based Pickering emulsions were stable in

the gastric phase but coalesced in the intestinal phase, which was explained by the easy accessibility of bile salts and lipolytic enzymes to the interface in the particle-free area. The protein–polysaccharide and polysaccharide–polysaccharide particle composites usually have some advantages over starches or proteins due to better resistance of the polysaccharides to intestinal digestion.

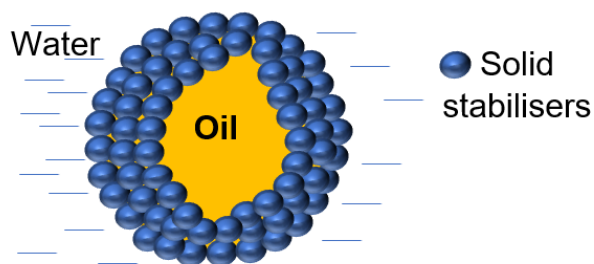


**Figure 2.7.** General structure of an O/W Pickering emulsion; shape of the solid stabilisers varies depending on the sources

In food systems, droplet size between 0.2 and 50  $\mu\text{m}$  was reported to have a significant impact on overall sensory perception of the consumers. For example, creaminess and thickness significantly decreased with increasing droplet size (Lett et al., 2016). For the design of small-sized ( $\leq 10 \mu\text{m}$ ) oil droplets, solid stabilisers must be in the nanometric size range. In this case, modified starch granules might not be suitable Pickering stabilisers because they are generally several microns in size unless they have been modified by physical approaches (Yusoff, et al., 2011). Although protein and inulin particles have been reported to have nanometric sizes, emulsions stabilised by protein/inulin composites or protein particles as the sole stabiliser had droplet sizes ( $d_{43}$ ) of up to 24.7  $\mu\text{m}$  (Sarkar, Li, Cray, & Boxall, 2018) and larger than 100  $\mu\text{m}$  in the case of zein particles (Folter, Ruijven, & Velikov, 2012). In addition, as protein-based particle-stabilised emulsions are generally sensitive to coalescence under physiological conditions because of their susceptibility to proteolytic enzymes (Sarkar,

[Ademuyiwa, et al., 2018](#)). There has recently been a demand for particles that are resistant to human gastrointestinal enzymes as potential Pickering stabilisers.

### **2.5.2. Cellulose nanocrystals (CNCs)**

Needle shaped cellulose nanocrystals (CNCs) are human-enzyme-resistant particles that have attracted recent research attention for the production of stable Pickering emulsions. ([Chen, et al., 2018](#); [Lee, et al., 2011](#); [Yan, et al., 2017](#)). CNCs have a characteristic length of around 100–200 nm and a diameter of 8–86 nm, depending on their sources. TEM of needle shaped CNCs is demonstrated in [Fig. 2.8](#).

Commercial CNCs are usually produced by hydrolysis of plant cellulose with concentrated  $H_2SO_4$ . CNCs are highly charged due to the presence of sulphate group in the backbone, their partial wettability by oil is poor, with very large contact angles (much greater than  $90^\circ$ ), which may limit their direct use as Pickering stabilisers. Hence, various methods have been used to tackle this drawback. The first method to improve the wettability of these CNCs was to combine them with surfactants. For example, CNCs were blended with surfactants and these particle–surfactant mixtures were used to create the particle-laden interface ([Hu, Ballinger, Pelton, & Cranston, 2015](#)). Another approach was to use protein as a primary layer and then to add CNCs to the system as a second layer to form a composite protein-CNC interface ([Sarkar, Li, et al., 2018](#); [Sarkar, et al., 2017](#)); however, whether such a system was a true Pickering emulsion can be argued. In both approaches, as the emulsions were probably stabilised by surfactants and not by the solid CNCs, the high desorption energies associated with true Pickering stabilisers might not be achieved in these systems.

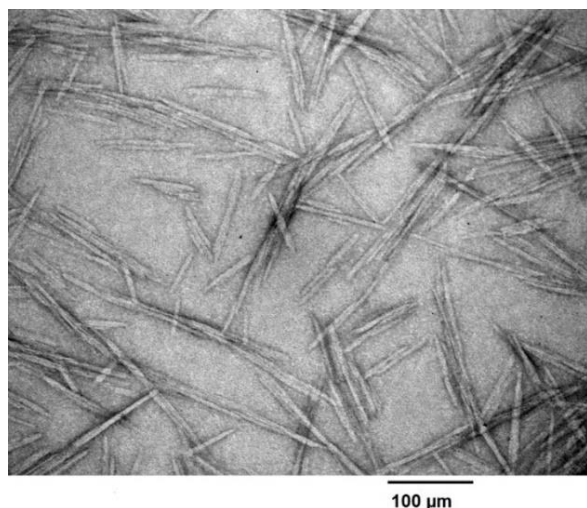


**Figure 2.8.** TEM of a commercial CNC product which was purchased from [CelluForce, Montreal, Quebec, Canada](#) (the image was taken in our lab).

An alternative approach is hydrophobic modification of the CNCs with various substances, such as succinic anhydride ([Liu, Sun, Zhang, Ren, & Geng, 2006](#)), octenyl succinic anhydride (OSA) ([Chen, et al., 2018](#)), phenyltrimethylammonium chloride ([Gong, Wang, & Chen, 2017](#)) and organic acids (hexanoic acid and dodecanoic acid) ([Lee, et al., 2011](#)). Such modified CNCs (MCNCs) can be used as the sole stabiliser without the need for any surfactant or protein. Of all the chemicals mentioned above, OSA, which has been used for decades in the food industry for the modification of starch ([Nilsson & Bergenståhl, 2007](#); [Silva, et al., 2013](#)), seems to be the most straightforward. Only one study has reported on the modification of CNCs using OSA to produce high internal phase emulsion gels ([Chen, et al., 2018](#)). To our knowledge, there is no published literature on the creation of Pickering O/W emulsions using OSA-modified CNCs. In addition, it is not known how such emulsions behave on exposure to different environmental stresses, such as pH and ionic strength as well as *in vitro* digestion.

## 2.6. Summary

For colon-targeted delivery of SCFAs, short-chain triglycerides are potential sources. SCFAs delivered to the colon can be controlled by using different types of triglycerides, bringing more health benefits through precision nutrition.

Carbohydrates that are surface active and able to produce a thick adsorbed layer at the O/W interface of emulsion systems are potential emulsifiers to resist bile salts displacement and the subsequent digestion. In addition, multilayer emulsion systems that combine advantages of various emulsifiers could also be promising to delay the lipolysis. Furthermore, Pickering emulsions with high desorption energy are promising systems to delivery SCFAs to the colon. Up until now, such carbohydrate surfactants and Pickering emulsions have not been used for the colon-targeted delivery of SCFAs.

To evaluate the possibility of using carbohydrates to prepare conventional emulsions and Pickering emulsions for SCFAs delivery, in this PhD project:

- ✓ *In vitro* digestion of O/W emulsions (single and multilayer systems) stabilised by various carbohydrates will be examined and compared ([chapter 3](#)).
- ✓ The effect of carbohydrate concentration and coverage at the O/W interface on lipolysis and release of SCFAs will be explored ([chapter 4](#)).
- ✓ A novel Pickering O/W emulsion system stabilised by hydrophobically modified CNCs will be used to investigate the delivery of SCFAs to the colon ([chapter 5](#)).
- ✓ *In vivo* study in pigs will be used to evaluate the capability of selected carbohydrate-based O/W emulsion to deliver SCFAs to the colon ([chapter 6](#)).

## Chapter 3 – Preparation and *in vitro* digestion of SCFA-supplemented emulsions made using various carbohydrate materials: a screening study

---

### Abstract

The main objective of this chapter was to evaluate the potential applications of various carbohydrates to produce surfactant-stabilised O/W emulsion systems to deliver tripropionin (glycerol tripropionate, TP) as source of propionic acid (PA) to the colon. While the emulsifying capacity of various carbohydrates was compared, the behaviours of the corresponding emulsion systems, i.e. microscopic structure, surface charge, lipolysis and release of PA under a static INFOGEST *in vitro* gastrointestinal (GI) conditions were investigated.

In this study, several potential carbohydrate materials were investigated to produce O/W emulsions. They were three commercial modified starches (GUM, N46 and N-LOK), a citrus high-methoxyl pectin (PEC) and a hydrophobically modified inulin (M-IN), which was synthesised via chemical modification of native inulin (N-IN) with octenyl succinic anhydride (OSA). In addition, an emulsion stabilised by whey protein isolate (WPI) was used as a control system. A double-layer emulsion system was also explored by coating the WPI-stabilised emulsion droplets with chitosan (CS) at pH 5.5. The results showed that while WPI, GUM and M-IN displayed excellent ability to form emulsions with an average size  $d_{32}$  of around 0.11–0.13  $\mu\text{m}$ , PEC had compromised emulsification ability, leading to the formation of emulsion droplets with an average

size  $d_{32}$  of around 7.3  $\mu\text{m}$ . Coating WPI-stabilised emulsion droplets with CS significantly increased droplet size by around 100 times. Under gastrointestinal conditions, nevertheless, PEC emulsion was the most stable system while the other emulsions (including the double-layer system) were destabilised with high degree of coalescence. In addition, the PEC-based formulation showed the lowest release of PA ( $\approx 30\%$ ) in the intestinal conditions while WPI, GUM, M-IN and the double-layer systems proved to be unstable with a significant PA release (95.6, 91.9, 74.0 and 91.4% respectively) in the stomach and the small intestine. Results suggested that amongst various investigated emulsion systems, the PEC-based emulsion was the most promising one in terms of colon-targeted delivery of PA. The system would be investigated in [Chapter 4](#) in a greater depth.

### 3.1. Introduction

PA which possesses some beneficial effects on the gut ([Tan, et al., 2014](#)) was selected as a SCFA model. In this chapter, TP was chosen as source of PA. Mixture of short-chain triglycerides would be used in [Chapter 5](#) and [Chapter 6](#). The study consisted of 5 parts: *a*) chemical modification of inulin; *b*) emulsifying capacity of various carbohydrate emulsifiers: a comparison study; *c*) design of a double-layer O/W emulsion; *d*) *in vitro* intestinal digestion of various O/W emulsions that bypassed the gastric stage; and *e*) *in vitro* sequential gastrointestinal digestion of various O/W emulsions.

### 3.2. Materials and methods

#### 3.2.1. Materials

Food-grade glyceryl tripropionate (TP,  $\geq 97.1\%$ ), octenyl succinic anhydride (OSA), medium molecular weight chitosan (CS, deacetylation degree of 75-85%), porcine pepsin (P7000), porcine bile extract (B8631), porcine pancreatin (P7545, 8 × USP), analytical-grade TP and tributyrin (TB), PA and caproic acid (CA) were purchased from [Sigma-Aldrich Co. LLC, USA](#). Modified starches (with commercial names GUM, N46 and N-LOK) were bought from [Ingredion, New Zealand](#). Whey protein isolate (WPI, 93.0% protein) was obtained from [Fonterra Co-operative Group, New Zealand](#). Inulin (IN) was bought from [THEHUT Group, Cheshire, UK](#). High-methoxyl pectin (PEC) from citrus peel was supplied by [Herbstreith & Fox KG, Germany](#). Soybean oil (SO) was obtained from a local market in [Palmerston North, New Zealand](#). SO was used directly for producing O/W emulsions without treatment. Other chemicals (NaOH, KCl,  $\text{KH}_2\text{PO}_4$ ,  $\text{NaHCO}_3$ , NaCl,  $\text{MgCl}_2(\text{H}_2\text{O})_6$  and  $\text{CaCl}_2(\text{H}_2\text{O})_2$ ) were supplied by [Sigma-](#)

Aldrich Co. LLC, USA. Milli-Q water (electrical resistance of 18.2 MΩ.cm at 25 °C) was purified by a Milli-Q apparatus, Millipore Corp., USA. Acetate buffer pH 5.5 was made from glacial acetic acid (Merck KGaA, 64271 Darmstadt Germany) and milli-Q water.

***TP properties as provided by the supplier:***

- Linear formula:  $(C_2H_5CO_2CH_2)_2CH(O_2CC_2H_5)$
- Molecular weight: 260.28 g/mol
- Water solubility at 37 °C: 3.07 mg/mL
- Density: 1.08 g/mL
- Boiling temperature: 175–175 °C at 20 mmHg
- White in colour

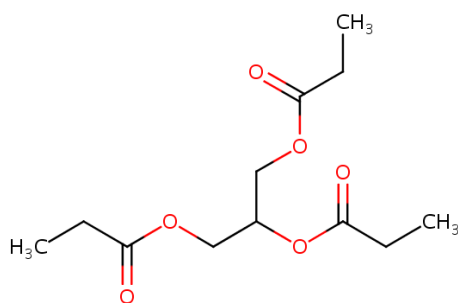


**Figure 3.1.** Chemical structure of TP

### 3.2.2. Preparation of carbohydrate solutions

The polymer solutions with various concentrations were used. WPI and modified starch solutions were made by dispersing the powder into acetate buffer pH 5.5 and subsequently stirred for 1 h at 25 °C. CS solutions were prepared by dissolving the powder into 90 mL of 0.5% v/v acetic acid solution, stirring for 12 h at 25 °C, then adjusting the pH to 5.5 by NaOH 1.0 N. Pectin solutions were produced by adding the powder into acetate buffer pH 5.5, stirring for 12 h at 50 °C.

### 3.2.3. Preparation of M-IN

Our preliminary work showed that IN had poor emulsifying ability, but it could be improved by hydrophobic modification with OSA. The OSA molecules were expected to react with -OH group on the IN backbones to enhance its hydrophobicity. The modification of N-IN was adopted from [Kokubun, Ratcliffe, & Williams \(2013\)](#) with some changes. One hundred mL of N-IN solution (30 wt%) in water was prepared by a magnetic stirrer at 50 °C for 1 h. The pH was adjusted to  $8.30 \pm 0.1$  using 1.0 N NaOH solution. OSA (3.56 g) was added to 10 mL of ethanol (> 99.5%) and the mixture was stirred for 1 h. OSA and N-IN solutions were blended, and the reaction was conducted at 25 °C under 100 rpm with continuous addition of NaOH to maintain pH 8.3 was done using a pH-stat ([TIM856, Radiometer Analytical, Hach Company, Loveland, CO, USA](#)) for around 7 h. The obtained products were neutralised by 1.0 N HCl solution to pH 7.0 and subsequently freeze-dried. The freeze-dried powder was placed into Soxhlet bag and then purified with ethanol (> 99.5%) at 78°C for 12 h remove any leftover OSA from the powder. Finally, it was air dried in an oven at 40 °C overnight to remove the ethanol. This powder is referred to as M-IN and was used to create O/W emulsions. The degree of substitution was analysed as presented in [section 3.2.10](#) while the changes in emulsifying capacity were thoroughly discussed in [section 3.3.1](#).

### 3.2.4. Preparation of single-layer O/W emulsions

An O/W emulsion was prepared by mixing TP with WPI solution (1.0 wt%). The obtained emulsion was unstable due to high water solubility of TP. A similar observation has also been reported in a previous study when TB was encapsulated

by Tween 20 (Li, Maux, Xiao, & McClements, 2009). To improve the emulsion stability, a mixture of TP and SO at various ratios was tested. At a ratio of 1:1 (w/w), the obtained emulsion was stable for a 4-day preservation at 4 °C (see [appendix Fig. 3A.1](#), [Table 3A.1](#) and [Table 3A.2](#)). This ratio was then applied for designing other O/W emulsions.

Emulsions were made by blending oil phase (TP-SO mixture with a weight ratio of 1:1) with aqueous phase (WPI, modified starches, M-IN and PEC solutions) to obtain a final oil concentration of 10 wt%. Various concentrations (0.5–7.0 wt%) of the emulsifiers were tested in trial experiments to find the most appropriate conditions (see [appendix Fig. A3.1–Fig. A3.5](#)). Selected concentrations of WPI (1.0 wt%), modified starches (5.0 wt%), PEC (2.5 wt%) and M-IN (5.0 wt%), at which droplet sizes and  $\zeta$ -potential remained unchanged as concentration increased, were applied for the *in vitro* digestion studies. In the next step, the mixture was pre-homogenised by a high-speed blender (D500 series, Biolab Ltd, Germany) at 10,000 rpm for 3 min and subsequently fed to a high pressure homogeniser (Homolab 2 series, FBF Italia Srl, Italia) at first/second stage pressures of 300/50 bar for five passes. The obtained emulsions were used for storage and *in vitro* digestion studies. All the experiments were done in triplicate.

### 3.2.5. Preparation of a double-layer O/W emulsion

Firstly, a single-layer O/W emulsion was prepared from WPI solution (1.0 wt%) and TP-SO mixture as described in [Section 3.2.4](#). The double-layer emulsion was produced by drop-by-drop adding the WPI-stabilised emulsion to CS solution pH 5.5 at a volumetric ratio of 1:1 under magnetic stirring at 100 rpm. Various concentrations

of CS solutions were used to obtain different CS:WPI ratios (w/w) of 1:10, 1:5; 1:4; 1:3; 1:2 and 1:1. The formulations were equilibrated for 15 min before analysing particle size,  $\zeta$ -potential and *in vitro* digestion studies.

### 3.2.6. Static *in vitro* GI digestion

The gastrointestinal digestion was carried out using the static INFOGEST digestion protocol as described by [Minekus et al. \(2014\)](#) without the oral phase.

**For gastric digestion**, freshly prepared emulsions were mixed with simulated gastric fluid (SGF) buffer at a volumetric ratio of 1:1 under magnetic stirring at 350 rpm. The composition of the SGF buffer was demonstrated in [Table 3.1](#), while pepsin activity in the final mixture was 2000 U mL<sup>-1</sup>. The temperature was maintained at 37 °C during the digestion and the initial pH was adjusted to pH 3.0. Aliquots were collected during 2 h incubation for analysis of particle size,  $\zeta$ -potential, microstructural changes, and quantification of PA and TP.

**Table 3.1.** Composition of 500-mL SGF buffer

	Stock concentration	Volume of stock	Concentration in SGF
	g L <sup>-1</sup>	mL	mmol L <sup>-1</sup>
KCl	37.3	6.9	6.9
KH <sub>2</sub> PO <sub>4</sub>	68.0	0.9	0.9
NaHCO <sub>3</sub>	84.0	12.5	25.0
NaCl	117.0	11.8	47.2
MgCl <sub>2</sub> (H <sub>2</sub> O) <sub>6</sub>	30.5	0.4	0.1
(NH <sub>4</sub> ) <sub>2</sub> CO <sub>3</sub>	48.0	0.5	0.5
CaCl <sub>2</sub> (H <sub>2</sub> O) <sub>2</sub> is added separately when emulsion and SGF are mixed			
CaCl <sub>2</sub> (H <sub>2</sub> O) <sub>2</sub>	44.1 g L <sup>-1</sup> or 0.3 M	CaCl <sub>2</sub> in the final mixture is 0.075 mM	

**For intestinal digestion**, the gastric digesta were mixed with simulated intestinal fluid (SIF) buffer with added bile salts and pancreatin at a ratio of 1:1 v/v at 37 °C under magnetic stirring at 350 rpm for 3 h. For the intestinal digestion that bypassed gastric stage, freshly prepared emulsions were diluted twice with Mili-Q water before mixing with SIF buffer, bile salts and pancreatin. The composition of the SIF buffer is shown in [Table 3.2](#), with 10 mM bile salts and pancreatin (lipase activity of 2000 mL<sup>-1</sup> in the final mixture). The temperature was maintained at 37 °C during the digestion and the initial pH was adjusted to pH 7.0. Aliquots were collected over 3 h intestinal digestion for analysis of particle size,  $\zeta$ -potential, microstructural changes, and analysis of PA, and TP. To stop the hydrolysis reaction, samples were immediately blended with a mixture of extraction solvents (hexane–isopropanol) or were rapidly cooled using ice.

**Table 3.2.** Composition of 500 mL SIF buffer

Constituent	Stock concentration	Volume of stock	Concentration in SIF
	g L <sup>-1</sup>	mL	mmol L <sup>-1</sup>
KCl	37.3	6.8	6.8
KH <sub>2</sub> PO <sub>4</sub>	68.0	0.8	0.8
NaHCO <sub>3</sub>	84.0	42.5	85.0
NaCl	117.0	9.6	38.4
MgCl <sub>2</sub> (H <sub>2</sub> O) <sub>6</sub>	30.5	1.1	0.33
CaCl <sub>2</sub> (H <sub>2</sub> O) <sub>2</sub> is added separately when emulsion and SIF are mixed			
CaCl <sub>2</sub> (H <sub>2</sub> O) <sub>2</sub>	44.1 g L <sup>-1</sup> or 0.3 M	CaCl <sub>2</sub> in the final mixture is 0.30 mM	

### 3.2.7. Characterisation of O/W emulsions and digesta

The emulsion and digesta samples were characterised using droplet size and  $\zeta$ -potential while the microstructure was assessed using confocal laser scanning microscopy (CLSM). The samples were diluted to a droplet concentration of around 0.01% w/v using phosphate buffer pH 7.0 before analysing the  $\zeta$ -potential. For size measurement, the undiluted emulsions or the digesta samples were added to a dispersion unit Hydro EV to reach an obscuration of around 10%. The stirring speed of the dispersion unit was set at 2000 rpm. The droplet size distribution was determined at room temperature (25 °C) by a static light scattering technique using a Mastersizer (2000S series, Malvern Instruments Ltd, Malvern, UK). The relative refractive index, i.e. the ratio of oil (1.456) to the dispersion medium (1.33), was 1.095. Mean droplet sizes were reported as Sauter-average diameters ( $d_{32}$ ) and volume-average diameters ( $d_{43}$ ) from the size distribution results. Each individual  $d_{32}$  and  $d_{43}$  value was reported as the mean and standard deviation of at least three reported readings made on triplicate samples.

The  $\zeta$ -potential of the emulsion droplets was measured using a Zetasizer (ZS Nano, Malvern Instruments Ltd, Malvern, UK). The diluted samples (freshly prepared emulsions and digesta) were transferred into DTS1070 folded capillary cells, followed by 2 min of equilibration within the equipment to reach a temperature of 37 °C. The machine was controlled by Zetasizer 3000 software that applied an electrical field across the sample, inducing the movement of charged particles. The ratio between the particle velocity and the external applied field, known as electrophoretic mobility, was then measured and converted to the zeta potential using the classical

[Smoluchowski](#) equation. Each  $\zeta$ -potential value was reported as the mean and standard deviation of at least three reported readings made on triplicate samples.

CLSM images of the emulsions and the digesta were taken at 25 °C using a [Leica SP5 DM6000B](#) Scanning Confocal Microscope equipped with 3 tunable PMT detectors. Each 500  $\mu$ L of emulsion was added to a 1.5 mL Eppendorf tube followed by 10  $\mu$ L of Nile Red (1 mg/mL in methanol) and 30  $\mu$ L of Fast Green FCF (1 mg/mL in water). The mixture was vortexed for 10 seconds and equilibrated for 10 min before deposited 30  $\mu$ L onto a slide. The sample was fixed by adding 50  $\mu$ L of agarose 1.0% w/w and placing a coverslip.

### 3.2.8. Quantification of TP

TP was measured using a gas chromatographic method ([Donovan, Cadwallader, & Lee, 2016](#)) with some modifications.

#### ***Sample preparation***

TP was extracted by mixing 100  $\mu$ L sample emulsion with 900  $\mu$ L mixture of hexane and isopropanol (3:2 w/w ratio) in a 1.5 mL Eppendorf tube. The mixture was vortexed for 20 seconds and subsequently centrifuged at 17,000  $g$ , 2° C for 20 min. The supernatant (200  $\mu$ L) was then blended with 1600  $\mu$ L hexane-isopropanol mixture and 200  $\mu$ L of internal standard (TB, 1 mg mL<sup>-1</sup>). The mixture was then centrifuged at 17000  $g$ , 2° C for 20 min. The supernatant was collected for GC analysis. Standard curves ([appendix Fig. A3.6](#)) were prepared from TP standard at various concentrations and TB as internal standard with the same procedure.

### **Chromatographic analysis**

TP was quantified using an [Agilent 7890A](#) GC system equipped with a flame ionization detector, a liquid injector, a [7683B](#) Auto-sampler and an [Agilent 19091Z-413 HP-1](#) capillary column (30 m x 0.32 mm x 0.25  $\mu\text{m}$ ). The carrier gas was helium at 7.5 PSI pressure, flow rate of 0.65 mL min<sup>-1</sup>,  $\mu = 22.3 \text{ cm s}^{-1}$ . The injection port was set at 300 °C. The oven temperature programme was installed as follow; 125 °C for 5 min and then increased at 10 °C min<sup>-1</sup> to 325 °C, where the temperature was kept constantly for 20 min. TP concentration was calculated based on standard curve. An example of GC spectrum was presented in the [appendix section](#) ([Fig. 3A.7](#)).

### **Measurement of hydrolysed TP**

The amount of hydrolysed TP was calculated as the difference between TP in the initial emulsion (emulsion without digestion) and TP in the corresponding digesta. TP in the initial emulsion was calculated based on emulsion formulation and confirmed by GC analysis.

Percentage of hydrolysed TP (%) was quantified as the ratio of hydrolysed TP to TP in the initial emulsion.

### **3.2.9. Quantification of PA**

PA was measured using GC protocol ([Bindelle, Pieper, Montoya, & Kessel, 2011](#)) protocol with some modifications.

### **Sample preparation**

A 1.0 mL aliquot of sample (emulsion or digesta) was added to a 1.5 mL Eppendorf tube and centrifuged at 17,000 *g*, 2 °C for 20 min. The supernatant (200 µL) was then transferred to a 2.0 mL Eppendorf tube followed by 800 µL of acetonitrile, 60 µL of phosphoric acid (25% w/w) and 400 µL of internal standard (caproic acid; 30 mL of Milli-Q water was measured and 15 µL of caproic acid was added to prepare the internal standard). The mixture was centrifuged at 17,000 *g*, 2 °C for 20 min. The supernatant was transferred into a vial for GC analysis. A standard curve ([appendix Fig. 3A.8](#)) was prepared with the PA standard at various concentrations using the same sample preparation procedure.

### ***Chromatographic analysis***

PA was quantified using a [Shimadzu-2010](#) GC system equipped with a flame ionisation detector, a liquid injector and a [Shimadzu-AOC-5000](#) autosampler. Samples were run on a fused-silica capillary column (30 m x 0.32 mm x 0.25 µm, [ZB-FFAP](#), [Zebron](#)). The flow rate of helium (as the carrier gas) was 1.24 mL min<sup>-1</sup>. The split mode was run with a split ratio of 20:1 at a pressure of 54.4 kPa and a total flow of 29 mL min<sup>-1</sup>. The temperature programme was set as follows: initial temperature, 100 °C for 4 min, then 170 °C for 5 min and a final temperature of 220 °C for 2 min. The PA concentration was calculated based on the peak area associated with PA and the standard curve. An example of GC spectrum was presented in the [appendix section \(Fig. 3A.9\)](#).

### ***Measurement of released PA***

The amount of released PA was calculated as the difference between PA in the digesta and PA in the freshly prepared emulsion.

Percentage of released PA (%) was quantified as the ratio of released PA to maximum theoretical PA after the *in vitro* digestion. According to [McClements, Decker, Park, & Weiss \(2008\)](#), pancreatic lipase hydrolyses triacylglycerols into two fatty acid and one monoacylglycerol molecules. Theoretically, 260 g of TP will release maximum 148 g of PA.

### **3.2.10. Nuclear magnetic resonance (NMR) determination of Inulin**

Approximate 100 milligrams of either native or modified inulin and 0.5 mL of  $d_6$ -Dimethyl sulfoxide (DMSO) were blended and gentle shaken for 5 min at 50 °C to dissolve inulin completely. Inulin solutions were then added into an NMR tube and the  $^1\text{H}$  NMR spectra were measured at 500.13 MHz magnet, 25 °C using a [Bruker Avance 500 MHz NMR spectrometer \(Bruker BioSpin GmbH - Rheinstetten, Germany\)](#) equipped with a QXI probe.

### **3.2.11. Statistical analysis**

Analysis of variance (ANOVA) was conducted using [Minitab® version 17.3.1](#) to detect overall significant differences ( $p < 0.05$ ).

### 3.3. Results and discussion

#### 3.3.1. Hydrophobic modification of inulin and its emulsifying capacity

The purpose of this experiment was to examine structural changes of N-IN after the chemical modification and investigate the changes in its emulsifying ability.

##### *Characterization of M-IN*

The changes of native N-IN structure were determined by NMR. Molecular structures of N-IN, M-IN and octenyl succinate are shown in Fig. 3.2. During the modification of N-IN, the chemical reactions took place at hydroxyl groups of C3, C4 and C6 of fructose units, as the hydrogens in the hydroxyl groups were replaced by octenyl succinate. Degree of substitution (DS) is defined as the average number of octenyl succinate derivatives per fructose unit. In this study, DS was determined using  $^1\text{H}$  NMR spectra of N-IN and M-IN (Fig. 3.3).

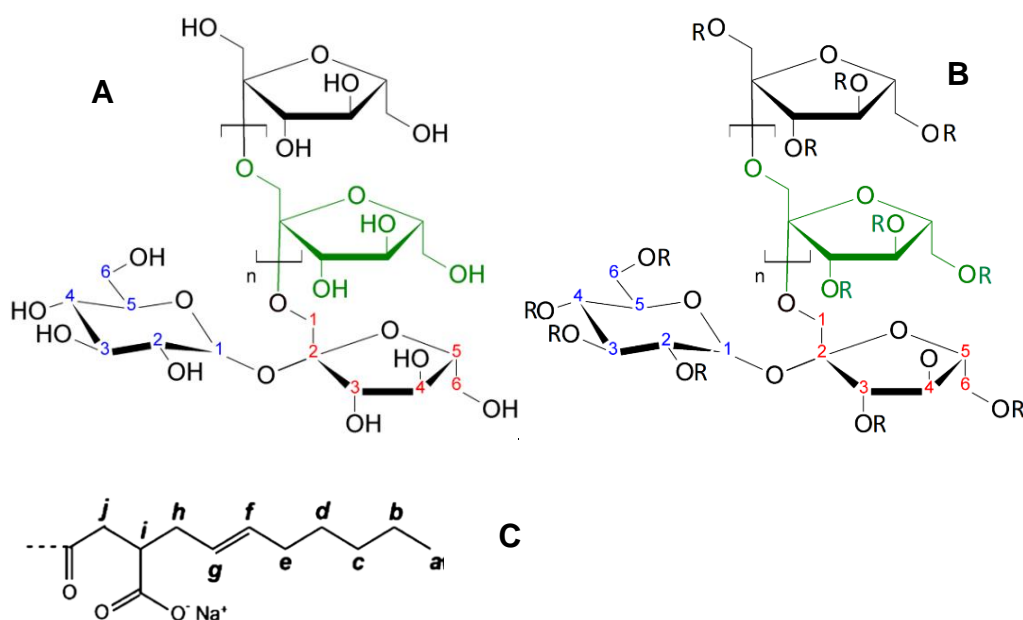


**Figure 3.2.** Molecular structures of native Inulin (A) and modified Inulin (B) and octenyl succinate (C). R in modified the M-IN structure is either H or octenyl succinate.

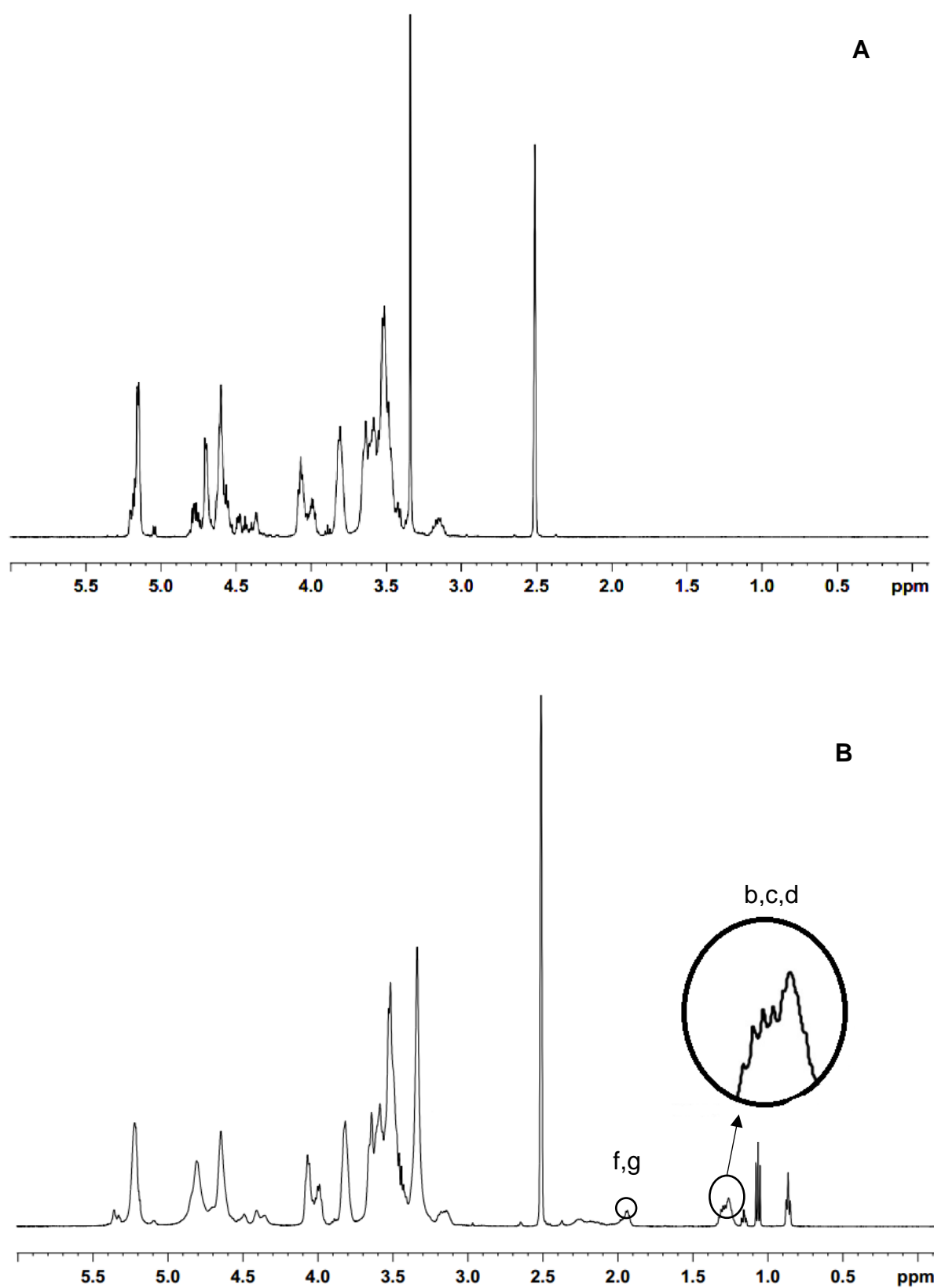


**Figure 3.3.**  $^1\text{H}$  NMR spectra of N-IN (A) and M-IN (B)

As can be seen in Fig. 3.3, the noticeable peaks at 2.54 ppm and 3.34 ppm were from the solvents (DMSO and H<sub>2</sub>O which were used to dissolve M-IN respectively) while the peaks at 3.14 ppm to 5.16 ppm were from the inulin structure. New <sup>1</sup>H NMR signals that appeared in spectrum of M-IN at 0.85 ppm and 1.26 ppm were related to the methyl groups at positions “a” and “b,c,d” while <sup>1</sup>H NMR signals at 1.94 ppm correspond to the methylene groups at carbon “f” and “g” in octenyl succinate backbone. Carbon positions in octenyl succinate were marked as in Fig. 3.2. DS was calculated as the ratio of the area of the peak at 0.85 ppm to the total area of the peaks from 3.14 to 5.16 ppm from inulin structure (Kokubun, et al., 2013). In this study, the degree of substitution was 1.7%.

#### *Emulsification capacity of M-IN: a comparison with N-IN*

In this experiment, N-IN (2.0 wt%) and M-IN (1.0, 2.0 and 5.0 wt%) solutions were used to produce O/W emulsions by the procedure described in Section 3.2.3. The results in Fig. 3.4 clearly showed a significant improvement in the emulsifying capacity of N-IN after the hydrophobic modification. As can be seen in Fig. 3.4, N-IN had a poor emulsifying ability. Particle size of N-IN emulsion showed a trimodal distribution with the biggest peak ranging from around 2 to 30 μm. On the other hand, M-IN demonstrated better emulsifying ability even at the lowest concentration (1.0 wt%). For instance, emulsion made of 1.0 wt% M-IN solution had a narrow distribution with  $d_{32}$  and  $d_{43}$  of 0.4 and 0.6 μm, respectively. Apart from this, increase in M-IN concentration from 1.0 to 5.0 wt% resulted in a significant decrease in sizes, in which  $d_{32}$  and  $d_{43}$  of 5.0% M-IN emulsion were around 0.12 and 0.16 μm, a 4-fold decrease. Emulsification properties of inulin modified by OSA were also examined in a previous study in which M-IN at various concentrations (0.5–2.5 wt%) was used to create

emulsions with medium chain triglyceride by a high-speed mixer (Kokubun, Ratcliffe, & Williams, 2015). It was reported that 2% M-IN (DS of around 5–7%) was the lowest concentration required to stabilize the 15% w/v O/W emulsions while  $d_{43}$  of all emulsions was higher than 4  $\mu\text{m}$  (Saki Kokubun, et al., 2015). Difference between our results and findings of Kokubun, et al. (2015) was possibly due to different oil concentrations, DS and homogenisation methods.

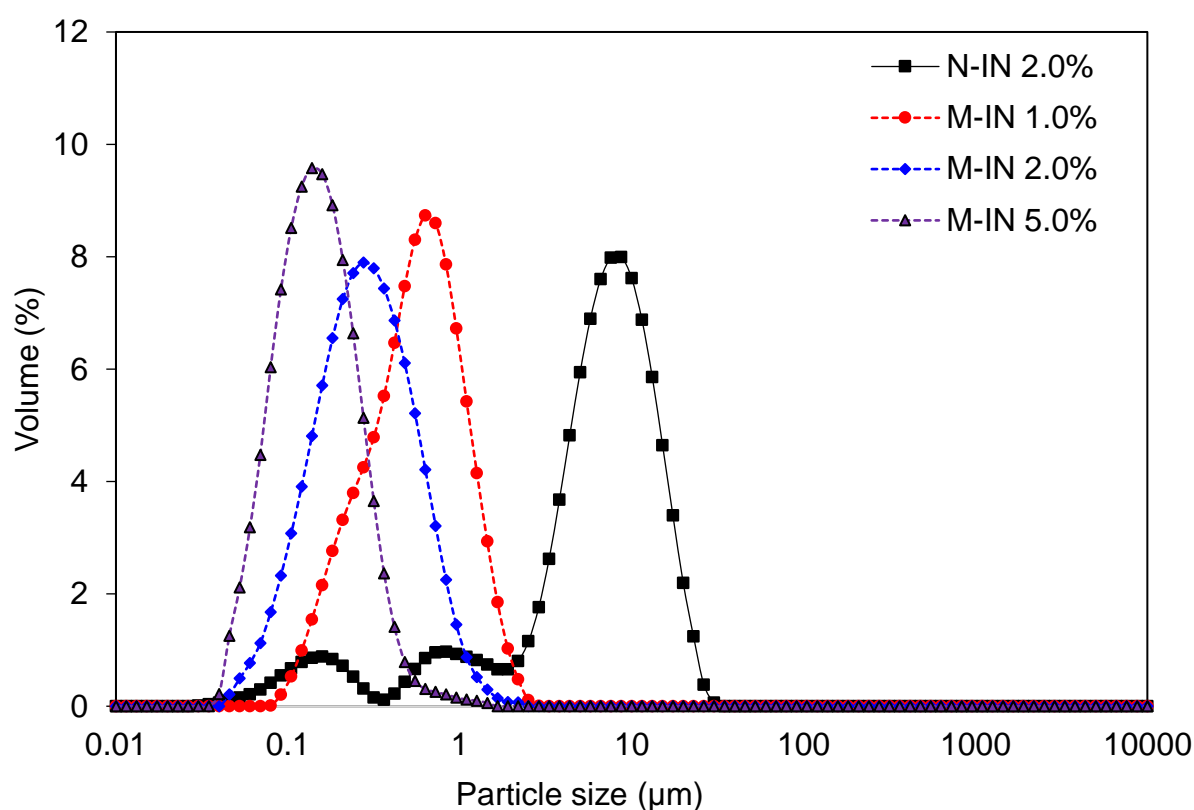


**Figure 3.4.** Particle size distribution of various emulsions encapsulated by N-IN (2.0 wt%) and M-IN (1.0–5.0 wt%)

### 3.3.2. Single-layer O/W emulsions - emulsification ability of various carbohydrates

The aim of this experiment was to compare emulsifying ability of WPI, PEC, modified starches (GUM, N46 and N-LOK) and M-IN in term of particle sizes and stability. The modified starches originated from waxy maize have been chemically modified with OSA to improve the emulsifying capacity. The degree of modification was not provided by the suppliers. Preliminary tests were conducted to find a suitable concentration of each materials from a range of concentrations (0.5–7.0 wt%; see [appendix Fig. A3.1](#) to [Fig. A3.5](#) for details). Selected concentrations (1.0 wt% for WPI, 2.5 wt% for PEC and 5.0 wt% for other emulsifiers) were used to produce 10 wt% O/W emulsions as described in [Section 3.2.4](#). The obtained emulsions were sampled for analysis of particle size,  $\zeta$ -potential and for storage at 4 °C for 4 days.

As can be seen from [Fig. 3.5](#), WPI, GUM and M-IN emulsions exhibited narrow particle size distribution and had comparatively similar  $d_{32}$  and  $d_{43}$  of around 0.11 and 0.13  $\mu\text{m}$  respectively. On the other hand, other modified starches, such as N46 and N-LOK, demonstrated poorer emulsifying ability with bigger sizes and wider distribution ranging from 0.1 to 10  $\mu\text{m}$ , probably due to different degrees of OSA substitution in the starch backbones. PEC had the lowest emulsifying ability amongst the investigated materials. The PEC emulsion showed bimodal size distribution with a size range of around 0.5–13  $\mu\text{m}$ . Average sizes ( $d_{32}$  and  $d_{43}$ ) of PEC emulsion, for example, were around 70 times higher than those of WPI emulsion. However, PEC emulsion had a  $\zeta$ -potential of -17.6 mV at pH 5.5, around 2 and 3 times higher than that of WPI and GUM emulsions respectively. High negative charge of PEC emulsion was due to the presence of carboxylic groups in the backbone of PEC that are adsorbed onto the O/W

interface (Ngouémazong, Christiaens, Shpigelman, Loey, & Hendrickx, 2015). As demonstrated in Table 3.3, modified starches N46 and N-LOK possessed the lowest absolute  $\zeta$ -potential (around -6.0 mV) while M-IN had the highest absolute value of  $\zeta$ -potential (-35.3 mV), which was due to the presence of OSA group in their backbone. A previous study on  $\zeta$ -potential of M-IN emulsions also reported a similar value (Kokubun, et al., 2015).

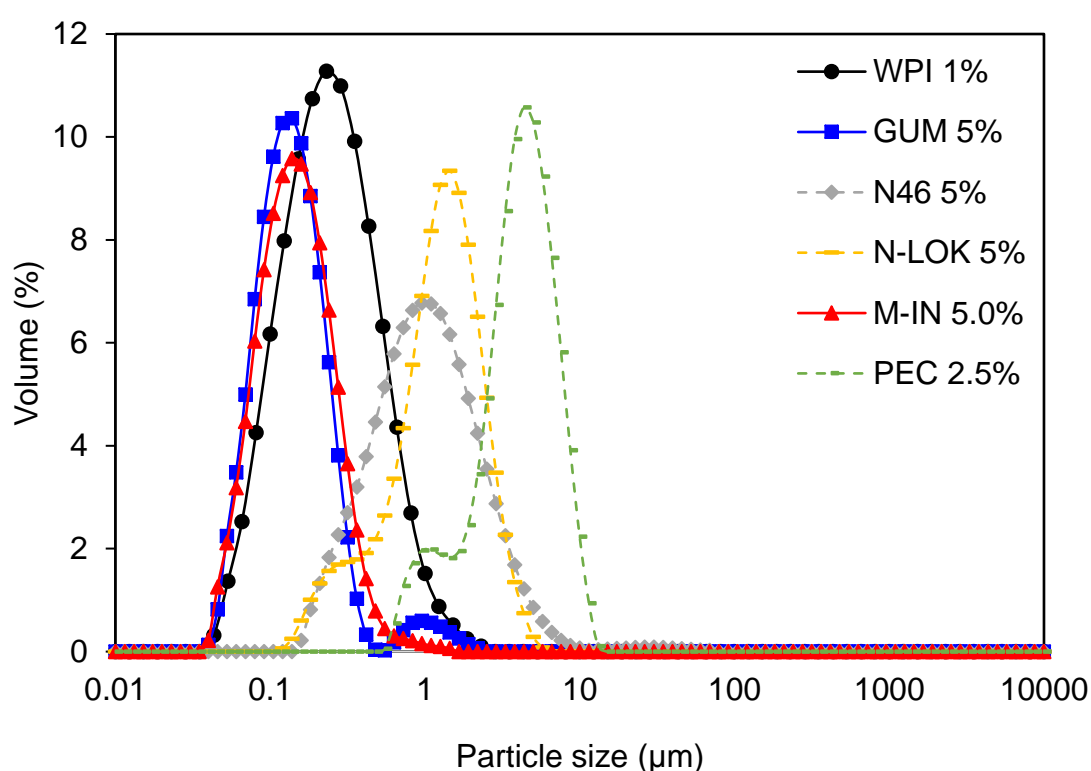


**Figure 3.5.** Particle size distributions of various fresh O/W emulsions produced from WPI, modified starches (GUM, N46 and N-LOK), PEC and M-IN.

To evaluate the emulsion stability, particle sizes and  $\zeta$ -potential of the emulsions were determined for 4-day storage at 4 °C. The results in Table 3.3 showed insignificant change in  $d_{32}$ ,  $d_{43}$  and  $\zeta$ -potential of all emulsions ( $p \leq 0.05$ ).

**Table 3.3.** Changes in average sizes ( $\mu\text{m}$ ) and  $\zeta$ -potential (mV) of emulsions stabilised by WPI, modified starches (GUM, N46 and N-LOK), PEC and M-IN after 4-day storage at 4 °C.

Emulsifiers			$d_{32}$ ( $\mu\text{M}$ )	$d_{43}$ ( $\mu\text{M}$ )	$\zeta$ -Potential (mv)
WPI	Fresh		$0.127 \pm 0.014^c$	$0.194 \pm 0.029^d$	$-10.4 \pm 0.2^c$
	4 days		$0.130 \pm 0.018^c$	$0.195 \pm 0.035^d$	$-10.2 \pm 0.2^c$
Modified Starches	GUM	Fresh	$0.111 \pm 0.001^d$	$0.169 \pm 0.005^{cd}$	$-7.4 \pm 0.3^d$
		4 days	$0.114 \pm 0.001^d$	$0.170 \pm 0.005^{cd}$	$-7.5 \pm 0.3^d$
	N46	Fresh	$0.698 \pm 0.021^b$	$1.464 \pm 0.357^b$	$-5.8 \pm 0.5^e$
		4 days	$0.702 \pm 0.019^b$	$1.472 \pm 0.417^b$	$-6.0 \pm 0.5^e$
	N-LOK	Fresh	$0.790 \pm 0.046^b$	$1.312 \pm 0.028^b$	$-5.6 \pm 1.2^e$
		4 days	$0.805 \pm 0.021^b$	$1.391 \pm 0.052^b$	$-5.6 \pm 1.0^e$
PEC	Fresh		$7.266 \pm 0.108^a$	$9.215 \pm 0.020^a$	$-17.6 \pm 0.9^b$
	4 days		$7.862 \pm 0.150^a$	$9.521 \pm 0.09^a$	$-18.1 \pm 1.2^b$
M-IN	Fresh		$0.115 \pm 0.00^d$	$0.160 \pm 0.001^c$	$-35.3 \pm 1.4^a$
	4 days		$0.114 \pm 0.00^d$	$0.160 \pm 0.001^c$	$-35.6 \pm 1.1^a$

<sup>a</sup> Samples within the same column with the same superscript letters are not different from one another ( $p < 0.05$ )

### 3.3.3. A double-layer O/W emulsion

The aim of this experiment was to characterise the structure of a double-layer O/W emulsion produced from WPI as the first layer and CS as the second layer, as well as

to optimise the formulation (CS/WPI weight ratio). The preparation of the emulsion was described in [Section 3.2.5](#).

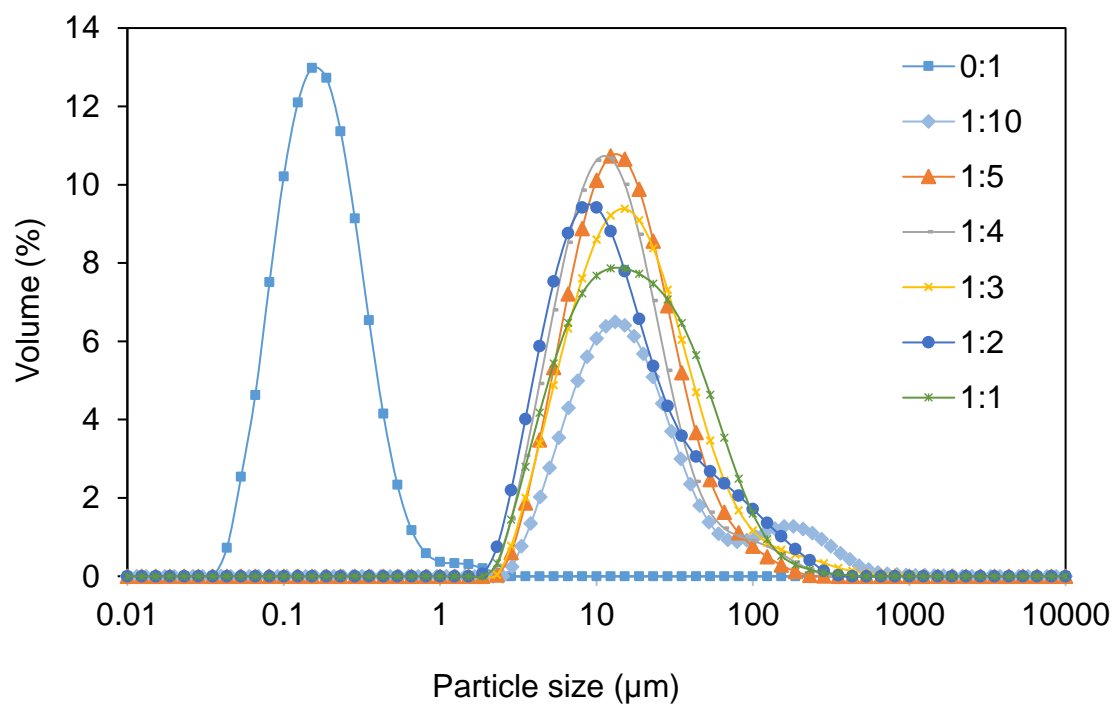


**Figure 3.6.** Particle size distribution of double-layer O/W emulsions at various CS/WPI weight ratios (0:1, 1:10, 1:5, 1:4, 1:3, 1:2, 1:1)

As can be seen from [Fig. 3.6](#), monomodal distribution within a narrow size range of 0.43–2.31  $\mu\text{m}$  was observed in the emulsion without chitosan. The average sizes  $d_{32}$  and  $d_{43}$ , and  $\zeta$ -potential of the emulsion were 0.130  $\mu\text{m}$ , 0.195  $\mu\text{m}$  and -10.4 mV respectively ([Table 3.4](#)). Coating the WPI-stabilised emulsion droplets with CS at a CS/WPI weight ratio of 1:10 significantly increased the sizes (by around 100 times) and reversed the surface charge from a negative to a positive value ([Table 3.4](#)). However, when CS/WPI ratio decreased from 1:10 to 1:5,  $d_{43}$  significantly dropped from 41.6 to 18.2  $\mu\text{m}$  while  $\zeta$ -potential went up from +22.1 to +27.5 mV. Further changes in CS/WPI ratio did not result in significant change in either size or  $\zeta$ -potential.

**Table 3.4.** Average particle sizes and  $\zeta$ -potential of various double-layer emulsions

CS/WPI ratios	$d_{32}$ ( $\mu\text{m}$ )	$d_{43}$ ( $\mu\text{m}$ )	$\zeta$ -potential (mV)
0:1	$0.127 \pm 0.014^b$	$0.194 \pm 0.029^d$	$-10.4 \pm 0.9^d$
1:10	$12.0 \pm 0.6^a$	$41.6 \pm 5.6^a$	$22.1 \pm 1.1^c$
1:5	$10.3 \pm 1.2^a$	$18.2 \pm 1.0^c$	$27.5 \pm 2.0^b$
1:4	$9.0 \pm 1.5^a$	$17.5 \pm 2.0^c$	$28.1 \pm 1.0^b$
1:3	$11.0 \pm 0.6^a$	$27.0 \pm 4.2^b$	$29.2 \pm 1.5^b$
1:2	$8.5 \pm 1.6^a$	$21.6 \pm 4.1^{bc}$	$30.5 \pm 0.5^b$
1:1	$10.7 \pm 2.5^a$	$23.7 \pm 2.6^{bc}$	$33.2 \pm 0.9^a$

<sup>a</sup> Samples within the same column with the same superscript letters are not different from one another ( $p < 0.05$ )

For better understanding of the influence of CS on particle sizes, confocal microscopy analysis of the emulsions with and without CS were carried out (Fig. 3.7). An emulsion with CS/WPI ratio of 1:5 was chosen as a representative. Figure 3.7A shows that WPI-stabilised emulsion had uniform size and homogenous structure. Droplets were well separated and mostly covered by WPI. On the other hand, a considerable proportion of large droplets was clearly seen in the CS-WPI emulsion (Fig. 3.7B). In addition, the large droplets were surrounded by a thick layer of protein that was also covering many smaller droplets. Aggregation of most small droplets was also detected in the whole emulsion.

At pH 5.5, CS is positively charged while WPI has a negative charge. The adsorption of CS onto droplet surface, due to electrostatic attraction, resulted in the reversion of surface charge from negative to positive value. However, CS might play a role as a cross-linker to connect protein backbones that were covering different droplets, resulting in aggregation. When more CS was added to the emulsion, more CS molecules adsorbed onto the O/W interface, thereby increased the  $\zeta$ -potential as can be seen in [Table 3.4](#). As a result, electrostatic interactions between emulsion droplets increased and that led to the separation of oil droplets within the aggregates when CS/WPI ratio augmented from 1:10 to 1:5. At the CS/WPI ratio of 1:5, the amount of adsorbed CS on the O/W interface might reach a saturated level; therefore, no alternation in size and surface charge were observed.

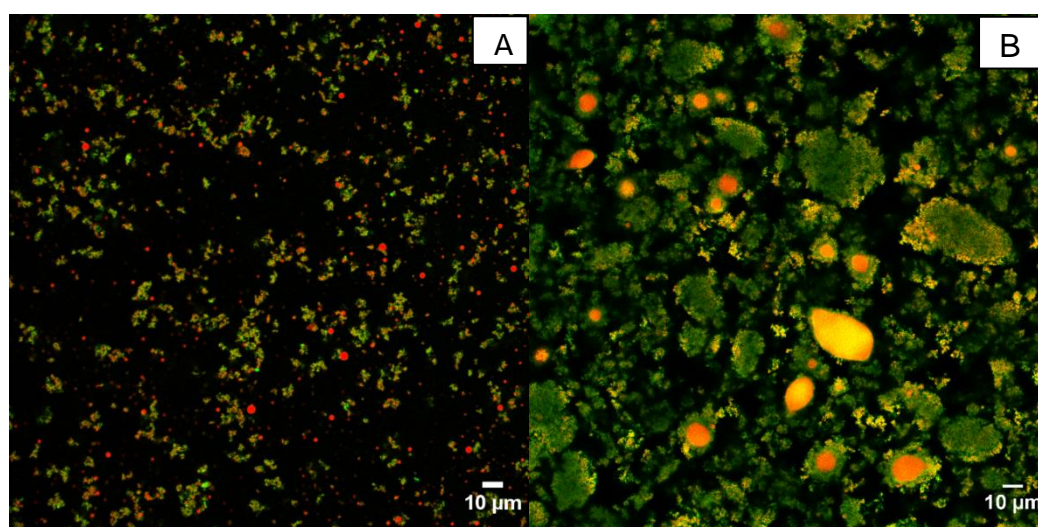


**Figure 3.7.** Confocal scanning laser microscope images of WPI (A) and CS/WPI (1:5 weight ratio) (B) emulsions. The oil droplets stained by Nile Red have red or orange colour, and WPI stained by Fast Green has green colour.

### 3.3.4. Performance of various O/W emulsions in *in vitro* intestinal phase

The objective of this study was to understand the behaviour of various O/W emulsions under the *in vitro* intestinal conditions bypassing the gastric phase. Single-layer emulsions stabilised by WPI (1.0 wt%), GUM (5.0 wt%), M-IN (5.0 wt%) and PEC (2.5 wt%), and a double-layer emulsion produced from WPI in combination with CS (CS/WPI ratio of 1:5) were chosen for the experiment. Modified starches N46 and N-LOK was not selected for this study due to their low emulsifying ability as compared to GUM as reported in [Section 3.3.2](#).

The percentages of released PA and hydrolysed TP are presented in [Table 3.5](#). As can be seen, nearly all TP in WPI and CS-WPI emulsions was hydrolysed, leading to the release of around 88% of PA. In other words, CS failed to protect WPI from pancreatic hydrolysis. At pH 7.0 of the intestinal phase, both CS (isoelectric point of 6.3) ([Popat, Liu, Lu, & Qiao, 2012](#)) and WPI (isoelectric point of 4.6) ([Chanamai & McClements, 2002](#)) had negative charge and repelled each other. The desorption of CS favoured the access of pancreatic enzymes onto the O/W interface to break down WPI and that facilitated the hydrolysis of TP. On the other hand, GUM and M-IN had better protection from intestinal digestion than WPI. One possible explanation for better protection from GUM and M-IN is the higher concentration used, 5 wt% of GUM and M-IN as compared to 1 wt% of WPI. High concentration created thick layers around oil particles and delayed the adsorption of lipase. However, the hydrolysis mechanisms for GUM and M-IN were probably different. GUM is an OSA-modified starch and hence digested by amylase present in the pancreatin. Simultaneously, GUM may be displaced by bile salt. After the bile-salt displacement, lipase adsorbed onto the O/W interface to commence the lipolysis. Inulin, on the other hand is a non-

digestible carbohydrate with resistant properties to human digestive enzymes (Tadrosa, Vandamme, Booten, Leveck, & Stevens, 2004). M-IN was not hydrolysed by pancreatic enzymes but probably displaced by bile salts to facilitate the hydrolysis of emulsion droplets.

**Table 3.5.** Proportions of TP hydrolysis and PA release after 2 h incubation at *in vitro* intestinal condition (TP: tripropionin; PA: propionic acid)

Delivery systems	[TP] (mg/mL)	Hydrolysis (%)	[PA] (mg/mL)	Release (%)
WPI	0.23 ± 0.17 <sup>d</sup>	98.2 ± 1.3 <sup>a</sup>	6.3 ± 0.2 <sup>a</sup>	88.4 ± 2.7 <sup>a</sup>
GUM	1.85 ± 0.16 <sup>c</sup>	85.2 ± 1.3 <sup>b</sup>	5.7 ± 0.1 <sup>b</sup>	80.0 ± 1.5 <sup>b</sup>
M-IN	2.90 ± 0.10 <sup>b</sup>	76.9 ± 0.8 <sup>c</sup>	4.5 ± 0.3 <sup>c</sup>	63.4 ± 3.5 <sup>c</sup>
PEC	7.52 ± 0.23 <sup>a</sup>	47.3 ± 4.1 <sup>d</sup>	2.4 ± 0.1 <sup>e</sup>	29.6 ± 4.4 <sup>d</sup>
WPI-CS	0.05 ± 0.27 <sup>d</sup>	99.2 ± 0.4 <sup>a</sup>	3.1 ± 0.1 <sup>d</sup>	87.3 ± 2.1 <sup>a</sup>

[TP] and [PA] were TP and PA concentrations in the digested emulsions.

<sup>a</sup> Samples within the same column with the same superscript letters are not different from one another ( $p < 0.05$ )

Amongst all the investigated systems, PEC emulsion had the lowest hydrolysis of TP (47.3%) and release of PA (29.6%). It is also worth noting that although the emulsions stabilised by WPI, GUM and M-IN had smaller particle size as compared to PEC emulsions, they demonstrated higher level of lipolysis. In other words, WPI, GUM and M-IN had excellent emulsifying ability even at a low concentration but did not produce a stable adsorbed layer against intestinal digestion. Amongst these three systems, the

emulsions with smaller particle size demonstrated higher degree of hydrolysis, which might contribute the larger surface area as the particle size decreased. Better protection achieved from PEC system was probably due to three possible reasons. Firstly, PEC is a non-digestible carbohydrate and therefore resist hydrolysis by pancreatic enzymes. Another possibility is the binding of calcium present in the intestinal fluid, which might restrict lipase action. Finally, PEC could form a thick adsorbed layer around lipid droplets (Ngouémazong, Christiaens, Shpigelman, Loey, & Hendrickx, 2015). As reported by Wilde & Chu (2011), densely packed adsorbed layer and strong interfacial network could resist bile-salt displacement and delay lipid digestion.

### 3.3.5. Performance of various O/W emulsions in *in vitro* gastrointestinal phase

The objective of this study was to understand behaviours of various emulsions under sequential gastrointestinal digestion. Similar emulsion systems from Section 3.3.4 were chosen for this study. Changes of particle size, hydrolysis of TP and the release of PA are illustrated in Tables 3.6 and 3.7.

Under the gastric conditions, the structures of WPI and WPI-CS emulsions were changed significantly, and a phase separation was observed after 2 h incubation. Confocal images of the WPI emulsions in Fig. 3.8A show substantial structural changes with high degree of droplet coalescence. These changes were due to the sensitivity of WPI-stabilised emulsion to pepsinolysis that hydrolysed adsorbed WPI at the O/W interface to facilitate the coalescence (Sarkar, Li, Cray, & Boxall, 2018). Regarding to the double-layer emulsion, at pH 2.0, both WPI and CS had positive charge and repelled each other. Therefore, CS would separate from the adsorbed WPI

layer at the O/W interface to enable the pepsinolysis. As can be seen in Fig. 3.8E, droplet coalescence was clearly observed in the gastric digesta of the WPI-CS emulsion, showing the instability of the system under gastric condition. However, TP hydrolysis and PA release in both WPI and WPI-CS emulsions were low, at around 2.0–5.0%. Similar results (from 0.66 to 2.66%) were also reported when WPI-encapsulated tributyrin was *in vitro* digested in SGF without gastric lipase (Donovan, Bauer, Jr, & Lee, 2017). Although gastric lipase was not present, the low degree of lipolysis observed in these systems was probably due to acid hydrolysis.

**Table 3.6.** Size ( $d_{32}$ ,  $\mu\text{m}$ ) changes of various O/W emulsions after gastric and intestinal digestion

Delivery systems	Fresh emulsion	Gastric digesta	Intestinal digesta
WPI	$0.127 \pm 0.014^c$	Phase separation	Phase separation
GUM	$0.111 \pm 0.001^{cA}$	$0.139 \pm 0.002^{cB}$	Phase separation
M-IN	$0.115 \pm 0.001^{cA}$	$5.538 \pm 0.124^{aB}$	$10.296 \pm 0.225^{aC}$
PEC	$7.266 \pm 0.108^{bA}$	$7.387 \pm 0.044^{bAB}$	$7.828 \pm 0.267^{bB}$
WPI-CS	$18.243 \pm 0.987^a$	Phase separation	Phase separation

<sup>a</sup> (lower case letter) Samples within the same column with the same superscript letters (lower case) are not significantly different from one another ( $p < 0.05$ )

<sup>A</sup> (upper case letter) Samples within the same column with the same superscript letters (upper case) are not significantly different from one another ( $p < 0.05$ )

Values on the tables are the average of at least three measurements on triplicate samples ( $n = 3 \times 3$ ).

Gastric digestion also had a considerable influence on the particle size of M-IN emulsions, in which  $d_{32}$  of the emulsions increased from 0.115 to 5.538  $\mu\text{m}$ . Also, the size change was evidenced in the confocal images of M-IN emulsions before and after gastric digestion (Fig. 3.8C). That as a significant drop in  $\zeta$ -potential from -35.3 mV of the fresh emulsion (measured at pH 7.0) to -10.3 mV of the corresponding digesta (measured at pH 2.0, appendix Table A3.3). The emulsion stability was possibly associated with electrostatic interaction rather than steric effects because M-IN has a short molecular chain length. Such dramatic drop in  $\zeta$ -potential induced droplets getting closer, which led to the formation of aggregates and/or droplet coalescence. However, the TP hydrolysis and PA release from M-IN emulsion were 6.0 and 4.7% respectively. By contrast, GUM emulsion was less affected by gastric digestion. The  $d_{32}$  of GUM emulsions, for example, increased from 0.111 to 0.139  $\mu\text{m}$ . Confocal images of GUM emulsions also demonstrated a slight change in particle size after gastric digestion (Fig. 3.8B). PEC emulsion was the only emulsion system that was not influenced by gastric digestion. The particle size remained unchanged after 2 h incubation under gastric condition. Regardless of the size, production of PA and lipolysis observed in both GUM and PEC emulsions were similar to those in WPI, M-IN and WPI-CS stabilised emulsions.

Under the intestinal conditions, WPI, GUM and WPI-CS emulsions were unstable. High degree of coalescence was observed in all three systems after the intestinal digestion. In addition, most of the TP was hydrolysed up to 95.6, 91.4 and 91.9% PA release in the WPI, GUM and WPI-CS emulsions, respectively. Previously, Donovan, et al., (2017) reported that 93.88% of butyric acid was produced when WPI-stabilised emulsion enriched with tributyrin was *in vitro* digested in the intestinal phase. High

release of PA was due to the sensitivity of the systems to enzymatic destruction and consequently lipolysis.

**Table 3.7.** Proportions of hydrolysed TP and released PA under gastrointestinal digestion

Delivery system	Hydrolysis of TP (%)		Release of PA (%)	
	Gastric stage	Intestinal stage	Gastric stage	Intestinal stage
WPI	4.9 ± 2.8 <sup>a</sup>	97.6 ± 0.8 <sup>a</sup>	3.4 ± 0.5 <sup>b</sup>	95.6 ± 3.0 <sup>a</sup>
GUM	9.2 ± 2.5 <sup>a</sup>	89.2 ± 2.5 <sup>b</sup>	5.3 ± 3.8 <sup>ab</sup>	91.4 ± 1.8 <sup>a</sup>
M-IN	6.0 ± 2.2 <sup>a</sup>	82.6 ± 0.6 <sup>c</sup>	4.7 ± 0.2 <sup>a</sup>	74.0 ± 1.9 <sup>b</sup>
PEC	6.0 ± 2.2 <sup>a</sup>	39.8 ± 1.9 <sup>d</sup>	5.8 ± 0.6 <sup>b</sup>	34.1 ± 1.8 <sup>c</sup>
WPI-CS	5.6 ± 2.4 <sup>a</sup>	97.8 ± 0.8 <sup>a</sup>	2.0 ± 1.3 <sup>b</sup>	91.9 ± 2.3 <sup>a</sup>

<sup>a</sup> Samples within the same column with the same superscript letters are not different from one another ( $p < 0.05$ )

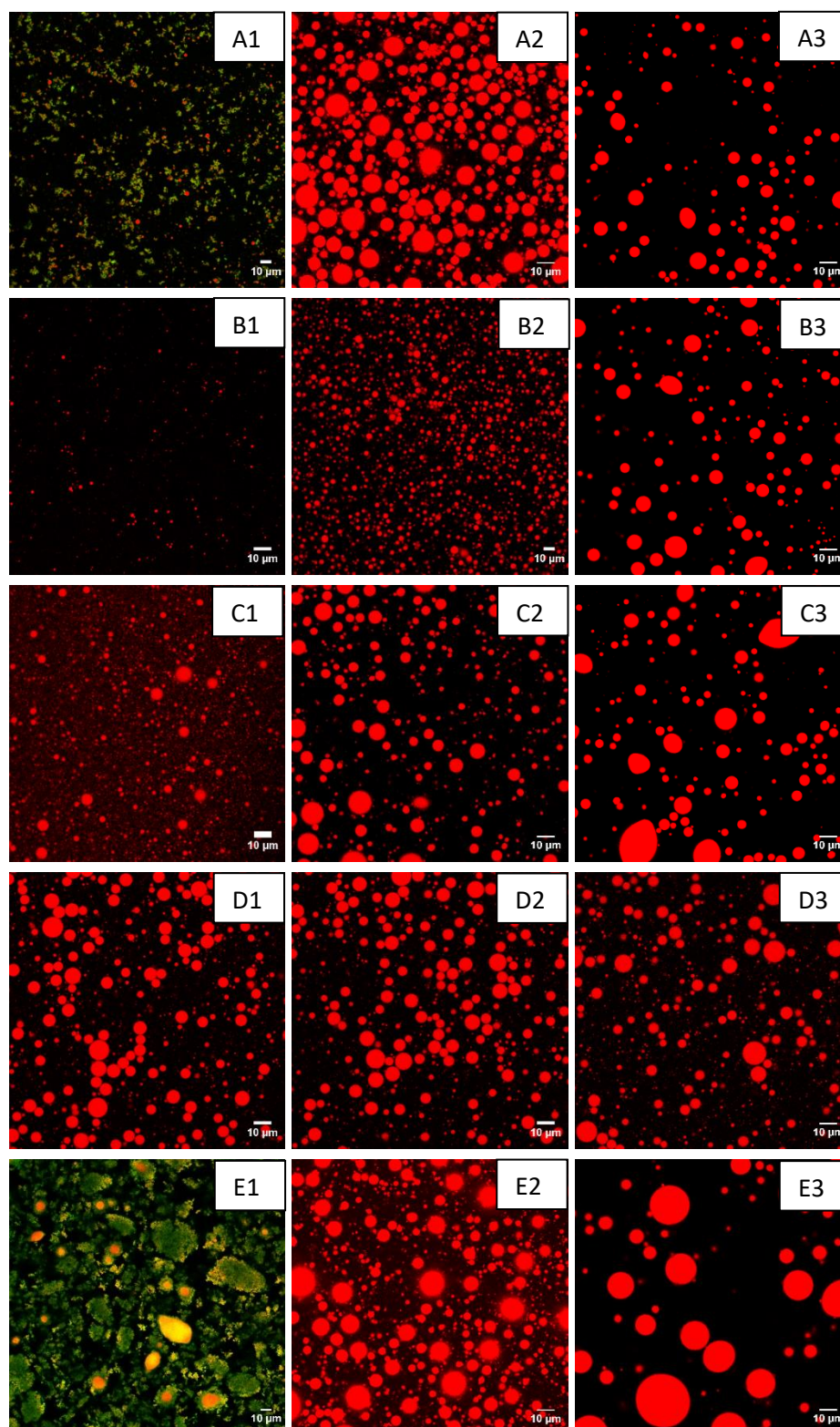


**Figure 3.8.** Confocal pictures of single-layer WPI (A1, A2, A3), GUM (B1, B2 and B3), M-IN (C1, C2 and C3) and PEC (D1, D2 and D3) emulsions, and double-layer WPI-CS (E1, E2 and E3) emulsion before gastric, after gastric and after intestinal digestion respectively. The oil droplets stained by Nile Red have red or orange colour, and WPI stained by Fast Green has green colour.

On the other hand, M-IN and PEC emulsions demonstrated lower degree of lipolysis. In case of M-IN emulsion, 82.6% of TP was hydrolysed and that resulted in a release of 74.0% PA. Compared to WPI emulsion, the release of PA from M-IN emulsion was around 20% lower. One possible explanation for that is the resistance of inulin to enzymatic action (Singh, Jadaun, Narnoliya, & Pandey, 2017). Although M-IN could be replaced by bile salts, M-IN remaining on droplet surface might play a role in delaying the hydrolysis of TP. Amongst all the investigated emulsions, PEC system had the lowest production of PA (34.1%) and hydrolysis of TP (39.8%). Although a slight size change was observed (Table 3.7), the overall appearance of PEC emulsions remained unchanged after gastric and intestinal digestion (Fig. 3.8D). Resistance to bile salt displacement, lipase action and binding of calcium to PEC to inhibit lipase activity were possibly responsible for the emulsion stability and low lipolysis degree observed in the PEC-based emulsion system.

As can be seen from Table 3.5 and Table 3.7, the hydrolysis of the intestinal digestion that bypassed gastric stage and the sequential gastrointestinal digestion were not significantly different. In other words, structural changes induced by gastric digestion did not influence the hydrolysis at the intestinal stage.

### 3.4. Conclusion

The OSA modification of inulin significantly enhanced its emulsification ability and improved the stability of the M-IN stabilised emulsion under storage at 4°C for 4 days. In terms of the emulsifying capacity, the TP-SO emulsified by WPI, GUM and M-IN showed particle sizes between 0.11 and 0.13 µm while those stabilised by PEC displayed a particle size of around 70-times higher.

In respect to the protection against hydrolysis, WPI (alone or in combination with CS) and GUM failed to protect TP from gastrointestinal digestion whereas M-IN and PEC showed higher potential in this regard. Amongst all the emulsions, PEC system had the lowest release of PA (34.1%) under gastrointestinal digestion, which was due to three possible mechanisms, the resistance against enzymatic degradation and bile salt displacement offered by PEC and the binding of calcium that inhibited lipase activity. It could be concluded that particle size did not have significant impact on triglyceride protection while enzymatic and bile-salt resistant properties of emulsifiers are the main factors to for controlling lipolysis. In the next chapter, the formulation of the PEC-based O/W emulsion for PA delivery was optimised and the mechanism behind low degree of lipolysis under the *in vitro* gastrointestinal digestion was explained.

---

## Chapter 4 – Optimisation of PEC-based emulsion system for delivery of SCFAs - an *in vitro* study

---

### Abstract

In this chapter, we aimed to design O/W emulsion systems, using PEC as an emulsifier that could resist gastric and intestinal digestion, and deliver tripropionin (TP) as propionic acid (PA) precursor to the colon. The stability of four O/W emulsions stabilised by four types of PEC, i.e. apple-high methoxyl (AP-HM), apple-low methoxyl (AP-LM), citrus-high methoxyl (CT-HM) and citrus-low methoxyl (CT-LM) were determined. The results showed that citrus PEC demonstrated better emulsifying ability than apple PEC, and that all the emulsions showed good stability under various pH and ionic strength conditions. Amongst all the investigated PEC, the CT-HM PEC was the most promising candidate and, therefore was chosen for the *in vitro* gastrointestinal digestion.

The stability and the lipolysis of the emulsions stabilised by CT-HM PEC (1.0–5.0 wt%) under *in vitro* gastrointestinal digestion were assessed using droplet sizing, microscopy,  $\zeta$ -potential and quantification of TP, PA and the PEC coverage. The emulsions were stable in the gastric stage, but the stability under intestinal conditions was dependent on the concentration of pectin. The microscopic analysis demonstrated a certain degree of droplet coalescence of all emulsions after intestinal digestion, with the most affected emulsion being that at the lowest PEC concentration. PEC concentrations of  $\geq 2.5$  wt% improved the resistance of the emulsion to coalescence

and reduced the rate and extent of lipolysis. This apparently improved the resistance of the interfacial PEC layer to displacement by bile salts and to the subsequent adsorption of colipase and lipase that occur in the initial phase of lipid digestion. The use of PEC to form gastrointestinal-resistant emulsions is a promising approach to delaying the digestion of TP, or other lipid-based materials, and to deliver TP to the colon. Further investigation of this emulsion system using an *in vivo* study are explored in [Chapter 6](#).

## 4.1. Introduction

In the previous chapter, CT-HM PEC-based O/W emulsions that were stable under *in vitro* gastrointestinal digestion were produced. The stability and low degree of lipolysis of the emulsion systems were due to three main possible mechanisms as described in section 3.4, the resistance of PEC to enzymatic destruction and bile-salt displacement, and the binding of calcium. In this chapter, various types of PEC were studied to find the most suitable system based on the emulsification capacity of these PEC and the emulsion stability under various pH and ionic strengths. Also, the chosen system with various PEC concentrations was used for an *in vitro* gastrointestinal digestion to deliver TP into the colon. The particle size, surface charge and microscopic structure of the emulsions were determined before and after the *in vitro* digestion. To confirm the findings in [Chapter 3](#), the displacement of pectin by bile salts was assessed based on  $\zeta$ -potential measurement and the amount of PEC adsorbed at the O/W interface. The hydrolysis of TP and the kinetics of free fatty acid release during the intestinal digestion were analysed to assess the resistance of the emulsion systems to lipolysis.

---

## 4.2. Materials and methods

### 4.2.1. Materials

Four different types of PEC (AP-HM, AP-LM, CT-HM and CT-LM) were kindly gifted by [Hawkins Watts Limited \(Auckland, New Zealand\)](#). Kjeldahl analysis showed the presence of around 1.0% (w/w) in all PEC products. Food-grade TP (glyceryl tripropionate  $\geq 97.1\%$ ), TB (glyceryl tributyrates, analytical grade), porcine pancreatin (P7545, 8 x USP), porcine pepsin (P7000,  $\geq 250$  units  $\text{mg}^{-1}$ ), porcine bile extract (B8631), propionic acid (PA, analytical grade) and caproic acid (analytical grade) were purchased from [Sigma-Aldrich Co. LLC \(St. Louis, MO, USA\)](#). Soybean oil (SO) was obtained from a local supermarket ([Palmerston North, New Zealand](#)) and was used without purification. Other chemicals were of analytical grade and were obtained from [Sigma-Aldrich Co. LLC](#). Milli-Q water (ionic purity of 18.2 M $\cdot$ cm at 25 °C), purified by a [Milli-Q apparatus \(Millipore Corp., USA\)](#), was used for all experiments.

### 4.2.2. Preparation of emulsions

For the stability experiment, PEC solutions (1.0 wt%) were prepared from four types of PEC by gradually adding the powder into magnetically stirred water at 50 °C for 12 h. Further steps for producing the emulsions were conducted similar to the procedure reported in [Section 3.2.4](#).

For the *in vitro* digestion, various concentrations (1.0, 2.5 and 5.0 wt%) of PEC solutions chosen from the selection experiment were used to produce O/W emulsions. Emulsions stabilised by PEC (1.0, 2.5 and 5.0 wt%), hereafter referred to as EP1.0, EP2.5 and EP5.0 respectively, were made by blending the oil phase with pectin

solutions at a ratio of 1:9 (w/w). Further steps for producing the emulsions were conducted similar to the procedure reported in [Section 3.2.4](#). All the experiments were performed in triplicate.

### **4.2.3. Stability and *In vitro* gastrointestinal digestion studies**

#### *4.2.3.1. Stability study*

Freshly prepared emulsions stabilised by four types of PEC (1.0 wt%) were used for this experiment. The emulsions were subjected into four different pH and ionic strength conditions, i.e. pH 2.0 in 10 mM NaCl solution, pH 2.0 in SGF buffer, pH 7.0 in 10 mM NaCl solution and pH 7.0 in SIF buffer. For each condition, 10 mL of each emulsion in a 50 mL beaker was added to 10 mL of 20 mM NaCl solution, or 10 mL of SGF buffer, or 10 mL of SIF buffer. The mixture was then adjusted to the desired pH by drop-by-drop addition of NaOH or HCl under constant stirring at 500 rev min<sup>-1</sup>. Subsequently, the samples were analysed for any changes in droplet size,  $\zeta$ -potential and microstructure (CLSM). All measurements were done in triplicate and were reported as the mean and standard deviation.

#### *4.2.3.2. In vitro digestion study*

*In vitro* digestion of EP1.0, EP2.5 and EP5.0 was conducted using the static INFOGEST digestion protocol ([Minekus, et al., 2014](#)) which as in [Section 3.2.6](#).

#### 4.2.4. *In vitro* gastrointestinal digestion of emulsions after the removal of free pectin

In this study, free pectin was defined as pectin that did not adsorb on to the droplet surface but was present in the aqueous phase of the emulsion. The free pectin was separated by centrifugation of the freshly prepared emulsions at 10,000 *g* for 1 h. The cream phase was collected and rinsed with water to remove any free-pectin residue. The rinsing process was done by adding water to the cream phase at a weight ratio of 1:1 (water:cream). The mixture was then shaken gently and recentrifuged at 10,000 *g* for 30 min to allow phase separation. The cream phase was collected and rinsed with water again. The washed cream phase was gently mixed with Milli-Q water at a 1:9 (w/w) ratio. A schematic diagram on preparation of the reconstituted emulsions is shown in Fig. 4.1. The emulsions obtained were used for *in vitro* gastrointestinal digestion according to the protocol described in Section 3.2.6.

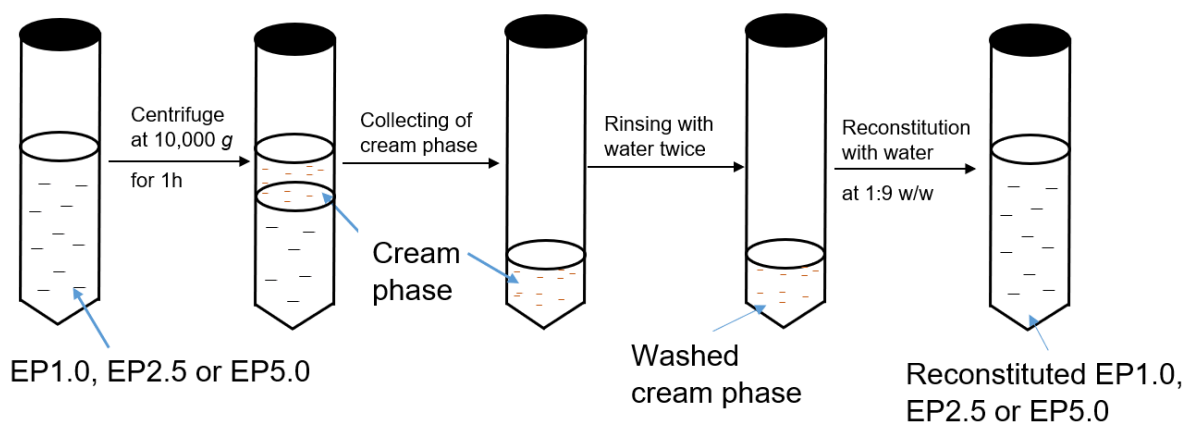


**Figure 4.1.** Preparation of the reconstituted emulsions

#### 4.2.5. Kinetics of free fatty acid release

The release of free fatty acids (FFAs) during simulated intestinal digestion was quantified over 2 h while maintaining the pH at 7.0 by the addition of 0.05 M NaOH using a pH-stat (TIM 854, Radiometer). The percentage of FFAs released was calculated based on the volume of NaOH consumed, assuming that lipase will hydrolyse two FFAs per triglyceride molecule (Li & McClements, 2010):

$$\%FFA = 100 \times \left( \frac{V_{NaOH} \times M_{NaOH} \times M_w \text{ lipid}}{2 \times W_{lipid}} \right) \quad (1)$$

where  $V_{NaOH}$  is the volume (L) of 0.05 M NaOH solution consumed to neutralise the FFAs produced,  $M_{NaOH}$  is the molarity (M) of the NaOH solution used,  $M_w \text{ lipid}$  is the average molecular mass ( $\text{g mol}^{-1}$ ) of the triglycerides and  $W_{lipid}$  is the total mass (g) of lipid present in the sample used for titration.

The kinetic parameters for the initial FFA release were calculated using Equation (2) (Li & McClements, 2010):

$$\Phi_t = \Phi_{\max} [1 - (1 + k_1 t)^{-2}] \quad (2)$$

where  $t$  is the intestinal digestion time (min),  $\Phi_{\max}$  is the maximum total FFA level (%) and  $k_1$  is the first-order rate constant of FFA release ( $\%FFA \text{ min}^{-1}$ ), which was calculated using the following equation:

$$k_1 = \frac{3kM_w}{2d_o \cdot \rho_o} \quad (3)$$

where  $k$  ( $\text{mol s}^{-1} \text{m}^{-2}$ ) is the lipid conversion rate per unit area of the droplet surface, occurring at maximum lipase surface coverage,  $M_w$  is the molecular weight of the lipid,  $d_o$  is the initial average diameter of the emulsion ( $d_{32}$ ) and  $\rho_o$  is the density of the lipid.

In this study, Equation (2) was used as the mathematical model that gave the best fit to the experimental data. Non-linear regression analyses were done with R version 3.6.0 (R Core Team, 2019) using RStudio 1.1.447 (RStudio, Boston, MA, USA) and the nls function in the stats package (version 3.6.0). The lipolysis half time ( $t_{1/2}$ , min), i.e. the time required to achieve half lipid digestion, was obtained from the experimental FFA curve.

#### 4.2.6. Interactions of adsorbed pectin on the interface with bile salts

Possible interaction between adsorbed pectin and bile salts was determined by measuring the changes in surface charge and pectin coverage in the presence of bile salts. After the removal of free pectin, the emulsions were mixed with bile salts (10 mM in the final mixture, i.e. the same concentration as used for the *in vitro* digestion). The mixtures were then incubated at 37 °C, pH 7.0 under magnetic stirring at 350 rev min<sup>-1</sup> for 2 h. They were then diluted 50 times before analysis of the surface charge.

For analysis of the pectin coverage on the droplet surface, the emulsions were centrifuged at 10,000 *g* for 1 h to separate the free pectin in the aqueous phase, which was then quantified using a spectrometric method as described in Section 4.2.9. The pectin adsorbed on the droplet surface was quantified as the difference between the pectin content in the original emulsion and the free pectin after centrifugation. All experiments were performed in triplicate.

#### **4.2.7. Characterisation: droplet size distribution, droplet $\zeta$ -potential and microstructure**

The emulsions and digesta samples were characterised using droplet size and  $\zeta$ -potential measurements, and the microstructure was determined using confocal laser scanning microscopy. These procedures were described in [Section 3.2.7](#).

#### **4.2.8. Quantification of TP and PA**

TP and PA were measured using the gas chromatographic (GC) methods as described in [Section 3.2.8](#) and [Section 3.2.9](#).

#### **4.2.9. Determination of pectin coverage**

Samples were taken from freshly prepared emulsions and emulsions that had been incubated with bile salts ([Section 4.2.6](#)). The free pectin was separated by centrifuging the emulsions at 10,000 *g* for 1 h. The aqueous phase was sampled for analysis of the pectin content using a spectrometric method ([Kintner & buren, 1982](#)). The cream phase was then washed twice with water. The washed liquid was collected for determination of the pectin content.

Free pectin was defined as the total amount of pectin in the aqueous phase after centrifugation and the pectin in the wash liquid. Pectin adsorbed on the droplet surface was calculated as the difference between the pectin in the initial emulsion and the free pectin quantified by the spectrometric method. In brief, 1 mL PEC solution was added to 16 x 150 mm test tubes and placed in an ice-water bath to cool. Subsequently, 6 ml of chilled, concentrated sulfuric acid/ tetraborate solution (0.0125M solution of sodium tetraborate was prepared in concentrated sulfuric acid) was added to the tube and the

mixture was vortexed gently. The tubes were then heated in a boiling water bath for 5 min, then cooled in tap water. A 60  $\mu\text{L}$  aliquot of m-hydroxydiphenyl reagent was added to develop colour. The final solution was mixed promptly, and the absorbance was read at 520 nm. Standard curve was prepared from pure galacturonic acid using the same procedure.

#### 4.2.10. Calculation of pectin coverage on the interface

The surface area was calculated based on the droplet size ( $d_{32}$ ) (Cameron, Weber, Idziak, Neufeld, & Cooper, 1991) as follows:

$$\text{Surface area (m}^2 \text{ mL}^{-1}\text{)} = \frac{\text{Volume of particles}}{d_{32}} \times 6 \quad (4)$$

The coverage of pectin on the interface was calculated as the ratio of the amount of pectin adsorbed on the interface to the surface area.

$$\text{Pectin coverage (mg m}^{-2}\text{)} = \frac{\text{Pectin adsorbed on the interface (mg mL}^{-1}\text{)}}{\text{Surface area (m}^2 \text{ mL}^{-1}\text{)}} \quad (5)$$

#### 4.2.11. Statistical analysis

Analysis of variance was conducted using Minitab® version 17.3.1 to detect overall significant differences ( $p < 0.05$ ).

### 4.3. Results and discussion

#### 4.3.1. Formation and stability of PEC emulsions

The droplet size distributions in [Fig. 4.2](#), [Fig. 4.3](#) and [Table 4.1](#) clearly show significant differences in the emulsifying properties of PEC from different sources. The emulsions were prepared from 1.0 wt% PEC solution at pH 5.5, and the oil phase in the final emulsion was 10 wt%. PEC from citrus and apple formed emulsions with a bimodal distribution with the droplet size of the second peak from citrus PEC-based emulsions ranging from 2.4 to 22  $\mu\text{m}$ . Similar size range of O/W emulsions prepared from citrus PEC was also reported in previous studies ([Verkempinck, et al., 2018](#); [Verrijssen, et al., 2016](#)). According to [Ngouémazong et al. \(2015\)](#), PEC emulsification capacity was achieved through the adsorption of the protein fraction of PEC on the interface, and steric and/or electrostatic interaction played a role in the emulsion stability. While  $\zeta$ -potential values of all the emulsions were not significantly different ([Table 4.2](#)), steric effect might be the main mechanism to maintain the stability of these emulsions.

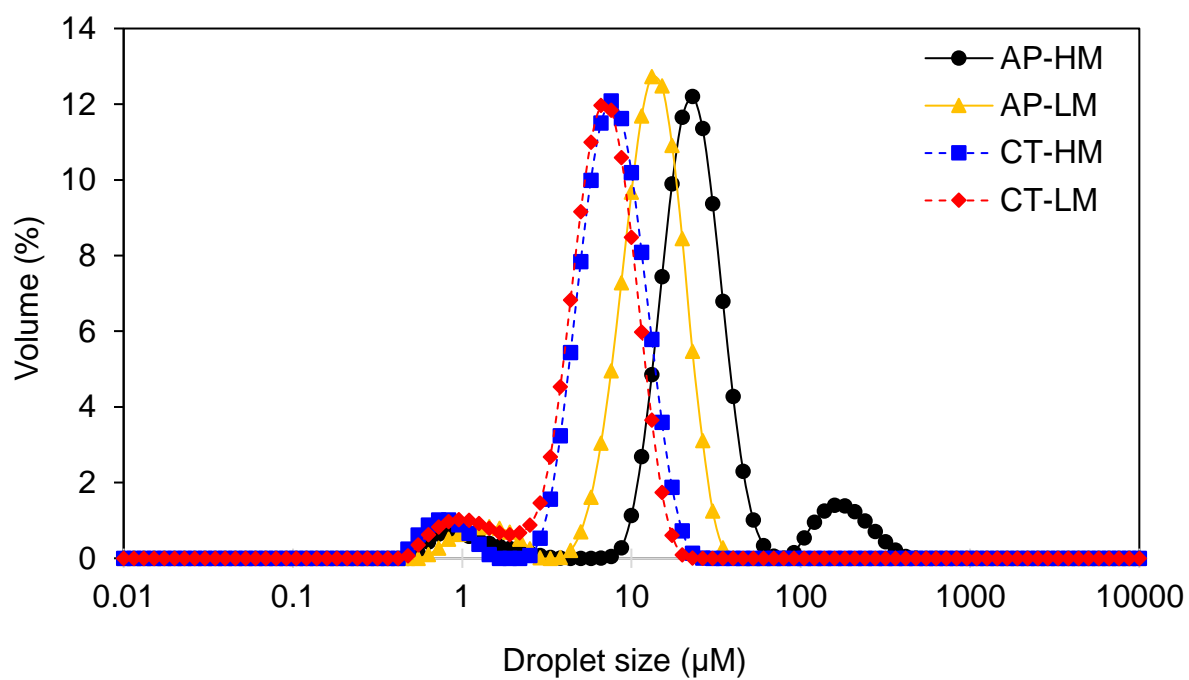


**Figure 4.2.** Droplet size distribution of various O/W emulsions stabilised by four types of PEC

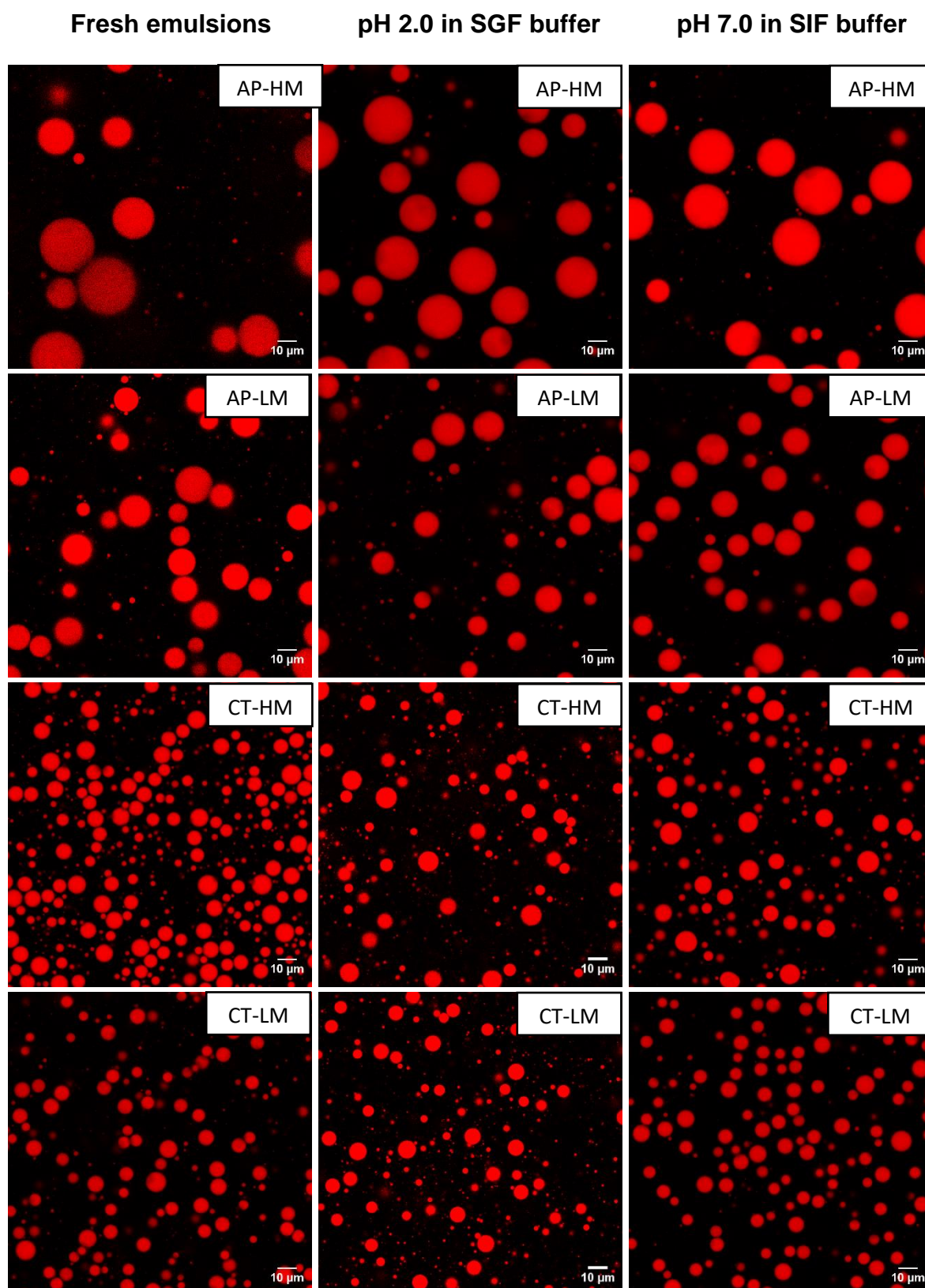


**Figure 4.3.** Changes in microscopic structure of various PEC-based emulsions under pH 2.0 in SGF buffer and pH 7.0 in SIF buffer.

PEC from citrus and apple may vary in molecular structures and that lead to different emulsifying capacities. In addition, the methods of production of these commercial products might also play a role in this regard. In terms of DM influence, there was no significant difference in droplet size and structure of the CT-HM and CT-LM PEC emulsions. Previously, it was reported that PEC (from citrus) with various DM (Verkempinck, et al., 2018; Verrijssen, et al., 2016) had significant differences in droplet size, which was explained through the organization of the hydrophilic and hydrophobic groups within the PEC backbones, such as galacturonic acid, acetyl, methyl, ferulic acid and the presence of protein in most PEC commercial products. In this study, the protein content of the four PEC products was around 1.0 %. In addition, electrostatic interaction was also reported as the main mechanism to stabilise the emulsions (Verkempinck, et al., 2018). In this study, the characteristics of the emulsions stabilised by CT-HM and CT-LM were similar.

**Table 4.1.** Particles sizes  $d_{43}$  ( $\mu\text{m}$ ) of various PEC-based emulsions at various pH and ionic strength conditions

	AP-HM	AP-LM	CT-HM	CT-LM
Fresh emulsions	$36.5 \pm 0.8^a$	$12.6 \pm 1.1^a$	$7.4 \pm 0.6^a$	$6.4 \pm 1.5^a$
pH 2.0 at 10 mM	$37.9 \pm 4.3^{ab}$	$12.8 \pm 1.5^a$	$6.7 \pm 0.7^a$	$5.7 \pm 1.6^a$
pH 2.0 in SGF buffer	$40.2 \pm 6.5^{ab}$	$13.2 \pm 1.9^{ab}$	$7.7 \pm 2.2^a$	$7.1 \pm 0.5^a$
pH 7.0 at 10 mM	$42.4 \pm 1.4^b$	$13.8 \pm 1.2^{ab}$	$7.1 \pm 1.3^a$	$5.8 \pm 1.5^a$
pH 7.0 in SIF buffer	$41.7 \pm 2.4^b$	$14.7 \pm 0.1^b$	$7.5 \pm 1.9^a$	$6.0 \pm 1.9^a$

<sup>a</sup> Samples within the same column with the same superscript letters are not different from one another ( $p < 0.05$ )

On the other hand, PEC from apple demonstrated low emulsification ability, while AP-LM PEC showed a better emulsifying ability than AP-HM PEC. Emulsion produced from AP-HM PEC showed a bimodal distribution with the second peak ranging from around 80 to 350  $\mu\text{m}$ . Also, the AP-HM PEC emulsion had an average size of around 3 times bigger than that from AP-LM PEC (Table 4.1), which was also evidenced in Fig. 4.3.

**Table 4.2.**  $\zeta$ -potential (mV) of various pectin-based emulsions at various pH and ionic strength conditions

		AP-HM	AP-LM	CT-HM	CT-LM
Fresh emulsions	pH 2.0	$-0.9 \pm 0.1^a$	$-0.9 \pm 0.3^a$	$0.3 \pm 1.3^a$	$0.8 \pm 0.6^b$
	pH 7.0	$-17.4 \pm 1.1^c$	$-16.4 \pm 0.4^b$	$-18.9 \pm 2.7^b$	$-17.0 \pm 1.1^c$
pH 2.0 at 10 mM		$0.3 \pm 1.1^a$	$0.0 \pm 1.3^{ab}$	$-0.9 \pm 0.3^a$	$1.3 \pm 0.7^a$
pH 2.0 in SGF buffer		$-1.1 \pm 0.3^a$	$-0.7 \pm 0.1^a$	$-0.8 \pm 0.1^a$	$-0.1 \pm 1.1^a$
pH 7.0 at 10 mM		$-17.6 \pm 1.1^{bc}$	$-21.4 \pm 0.7^d$	$-16.4 \pm 2.1^b$	$-17.8 \pm 2.4^b$
pH 7.0 in SIF buffer		$-14.9 \pm 0.5^b$	$-21.2 \pm 2.0^d$	$-15.2 \pm 1.1^b$	$-24.1 \pm 4.5^b$

<sup>a</sup> Samples within the same column with the same superscript letters are not different from one another ( $p < 0.05$ )

Although significant differences in droplet sizes amongst the four emulsions was observed,  $\zeta$ -potentials of the emulsions were not significantly different. All the emulsions had negative  $\zeta$ -potential value of around -18.9 to -17.0 mV at pH 7.0 and around 0 mV at pH 2.0. Negative surface charge of PEC emulsions at pH 7.0 was due to the presence of galacturonic groups in PEC molecular backbone, while pH 2.0 was

---

close to pKa of PEC, leading to neutral net value of  $\zeta$ -potential (Ngouémazong, Christiaens, Shpigelman, Loey, & Hendrickx, 2015).

Under various pH and ionic strength conditions, all the emulsions demonstrated excellent stability as can be seen in Fig. 4.3. Although the  $\zeta$ -potential dropped in negative value from around -17 mV to almost 0 mV in all the emulsions as pH decrease from 7.0 to 2.0 at 10 mM electrolytes, droplet size remained unchanged. Similar to the pH effects, the changes in ionic strength did not result in any changes in microscopic structure of the emulsions. A previous study reported opposite results when citrus PEC (DE of 55, 70 and 84%) was used to make O/W emulsions and the stability of the emulsions were tested under various ionic strengths (Schaaf, Schütz, & Karbstein, 2017). In this study, the authors reported the changes in ionic strength altered the electrostatic interactions of adsorbed PEC at the O/W interface and consequently the emulsion size and stability were affected.

To summarise, PEC from citrus showed better emulsification capacity than PEC from apple, while all PEC appeared to stabilise O/W emulsions through the adsorption of protein fraction on the interface and the steric effects were responsible for the emulsion stability. In addition, there was no DM effect on emulsifying ability of citrus PEC. Also, it was previously reported that increasing in methoxylation led to an increase in the number of non-polar (hydrophobic) groups on the molecules, and a decrease in the number of negatively charged groups. Consequently, HM PEC had better resistance to intestinal lipolysis than LM PEC (Verrijssen et al., 2016). In the current study, therefore, CT-HM PEC was chosen for the *in vitro* digestion.

### 4.3.2. *In vitro* digestion of pectin-based emulsions

The emulsions stabilised by CT-HM-PEC at different concentrations (1.0, 2.5 and 5.0 wt%) were subjected to gastric and then intestinal *in vitro* simulated digestion as described in [Section 4.2.3](#). After each stage of the digestion, samples were taken for analysis of droplet size, surface charge, hydrolysis of TP and release of PA.

Firstly, the effects of PEC concentration on the emulsion properties, including sizes ( $d_{32}$  and  $d_{43}$ ), surface charge ( $\zeta$ -potential) and pectin coverage were briefly described. Clearly, all the original emulsions showed bimodal size distributions, with the second dominant peak spanning a size range of 5–30  $\mu\text{m}$  ([Fig. 4.4](#)). The average droplet size increased with increasing pectin concentration, which was possibly caused by the loss of the first peak. The pectin coverage increased as the pectin concentration was increased from 1.0 to 2.5 wt%, but a further increase in pectin concentration to 5.0 wt% did not significantly affect the coverage ( $p > 0.05$ ). [Siew et al. \(2008\)](#) reported a coverage of around 20  $\text{mg m}^{-2}$  when sugar beet pectin (2.0 wt%) was used to stabilise limonene O/W emulsions. The difference in the level of pectin coverage was probably due to the different sources of pectin. Other studies stated that the rhamnogalacturonan-I in the pectin backbone initiated the intermolecular associations between pectin chains, therefore leading to the formation of thick adsorbed pectin layers ([Funamia, et al., 2007](#); [Ngouémazong, Christiaens, Shpigelman, Loey, & Hendrickx, 2015](#)). However, PEC concentration did not affect  $\zeta$ -potential, possibly due to the saturation of adsorbed PEC on the interface.

**Table 4.3.** Mean particle sizes ( $d_{32}$  and  $d_{43}$ ), surface charge ( $\zeta$ -potential) and pectin coverage ( $\text{mg}/\text{m}^2$ ) of freshly prepared O/W emulsions stabilised by pectin at various concentrations, i.e. 1.0 wt% (EP1.0), 2.5 wt% (EP2.5) and 5.0 wt% (EP5.0), and corresponding gastric and intestinal digesta

	Freshly prepared emulsion				Gastric digesta			Intestinal digesta		
	$d_{32}$ ( $\mu\text{m}$ )	$d_{43}$ ( $\mu\text{m}$ )	$\zeta$ -potential (mV) pH 7.0	Pectin coverage ( $\text{mg m}^{-2}$ )	$d_{32}$ ( $\mu\text{m}$ )	$d_{43}$ ( $\mu\text{m}$ )	$\zeta$ -potential (mV) pH 2.0	$d_{32}$ ( $\mu\text{m}$ )	$d_{43}$ ( $\mu\text{m}$ )	$\zeta$ -potential (mV) pH 7.0
EP1.0	$4.1 \pm 0.3^b$	$6.3 \pm 0.1^b$	$-18.6 \pm 1.2^a$	$4.6 \pm 0.9^b$	$4.1 \pm 0.2^b$	$6.7 \pm 0.2^b$	$-1.5 \pm 0.5^a$	$7.7 \pm 0.3^a$	$33.1 \pm 8.4^a$	$-25.2 \pm 0.7^b$
EP2.5	$7.3 \pm 0.1^a$	$9.2 \pm 0.1^a$	$-17.6 \pm 0.9^a$	$7.7 \pm 0.6^a$	$7.4 \pm 0.0^a$	$9.2 \pm 0.1^a$	$-1.6 \pm 0.2^a$	$7.8 \pm 0.3^a$	$15.8 \pm 5.0^b$	$-22.8 \pm 0.6^a$
EP5.0	$7.2 \pm 0.2^a$	$9.2 \pm 0.1^a$	$-18.9 \pm 1.1^a$	$8.4 \pm 0.8^a$	$7.4 \pm 0.0^a$	$9.2 \pm 0.0^a$	$-1.4 \pm 0.1^a$	$7.8 \pm 0.3^a$	$17.0 \pm 5.0^b$	$-21.4 \pm 0.8^a$

Samples in the same column with the same superscript letters are not significantly different ( $p < 0.05$ ). The values are the mean and standard deviations are of at least three measurements from triplicate samples.

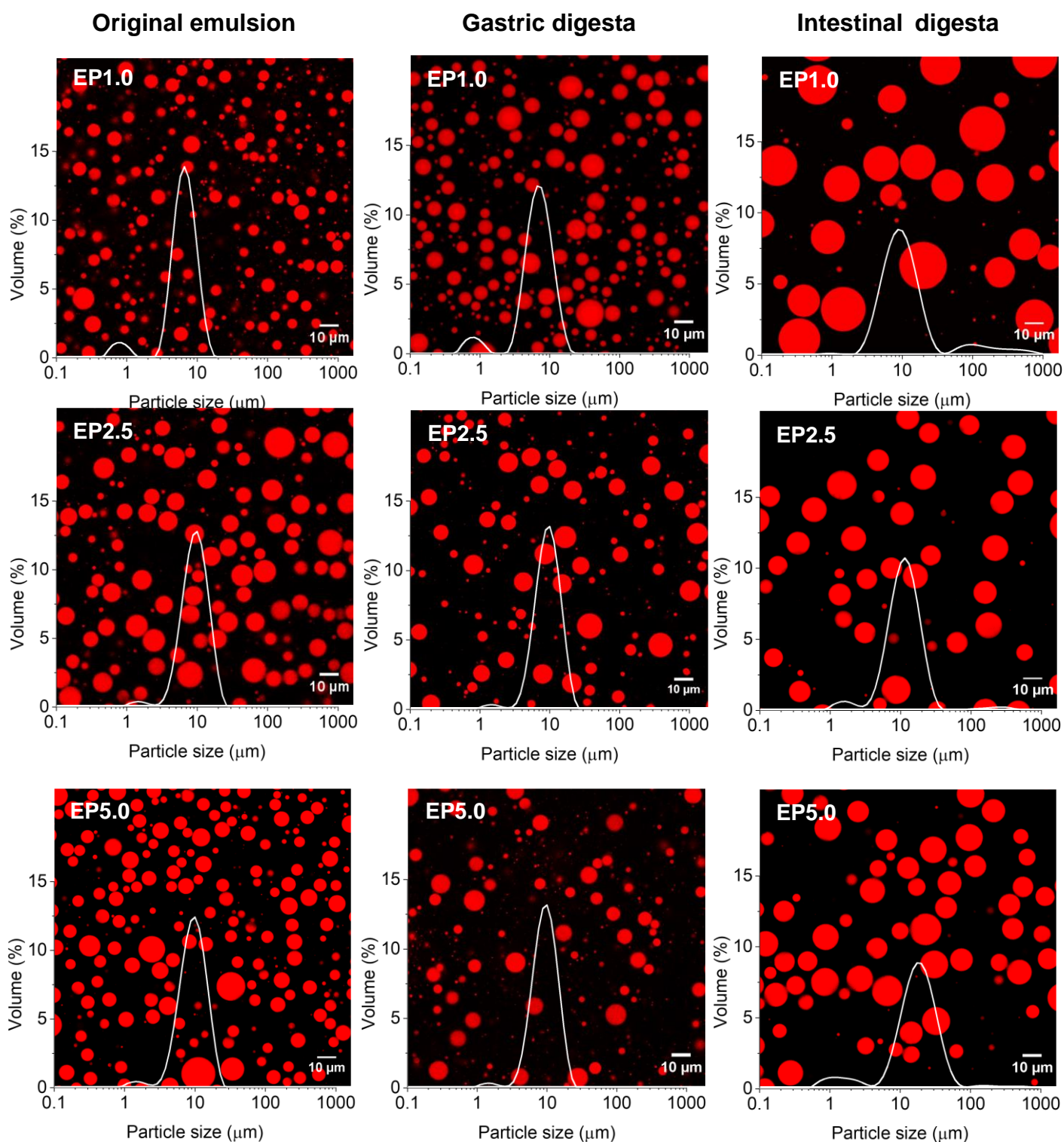


**Figure 4.4.** Confocal images and particle size distributions of O/W emulsions stabilised by pectin at various concentrations, i.e. 1.0 wt% (EP1.0), 2.5 wt% (EP2.5) and 5.0 wt% (EP5.0), and corresponding gastric and intestinal digesta. The red colour represents the oil phase (stained by Nile Red).

#### 4.3.2.1. Gastric digestion

The results in [Fig. 4.4](#) and [Table 4.3](#) show high stability of the emulsions during gastric digestion, regardless of the pectin concentration (1.0–5.0 wt%). The confocal images in [Fig. 4.4](#) clearly showed that most oil droplets were distributed individually in the emulsions without sign of flocculation and coalescence. The structures of the three emulsions before and after gastric digestion were identical, and differences in the surface charges were insignificant ( $p > 0.05$ ).

As pectin is an indigestible carbohydrate ([Mudgil & Barak, 2013](#)), the emulsions were stable under gastric conditions. Such resistance was previously reported when citrus pectin was used to stabilise  $\beta$ -carotene-enriched O/W emulsions ([Verrijssen, et al., 2016](#)). Emulsions stabilised by pectin with a high degree of methylesterification (DM) were stable under gastric conditions, whereas low DM pectin emulsions were unstable. The pectin used in this study had a DM of around 70%. In contrast, [Verkempinck, et al., \(2018\)](#) reported that, in the presence of SGF, the emulsions stabilised by citrus pectin at various DMs from 10 to 82% showed bimodal droplet size distributions, with the new peak appearing in a larger size range. According to the authors, the presence of the new peak was due to the interaction of pectin with gastric electrolytes such as  $\text{Ca}^{2+}$ ,  $\text{K}^{+}$  and  $\text{H}^{+}$ , which shielded surface charges, leading to droplet flocculation. The differences observed across different studies of the gastric stability are probably due to the different structures of the PEC used.

The lipid hydrolysis results showed that approximately 6.0–7.1% of the TP was hydrolysed after gastric digestion, producing 3.0–5.8% PA ([Fig. 4.5A](#)). This observation was in agreement with a previous study ([Donovan, Bauer, Jr, & Lee, 2017](#))

on the gastric digestion of reconstituted emulsions from spray-dried powder containing TB. According to [Donovan, et al., \(2017\)](#), the emulsions released approximately 5% of the total butyric acid content in the gastric phase, which was attributed to acid degradation.

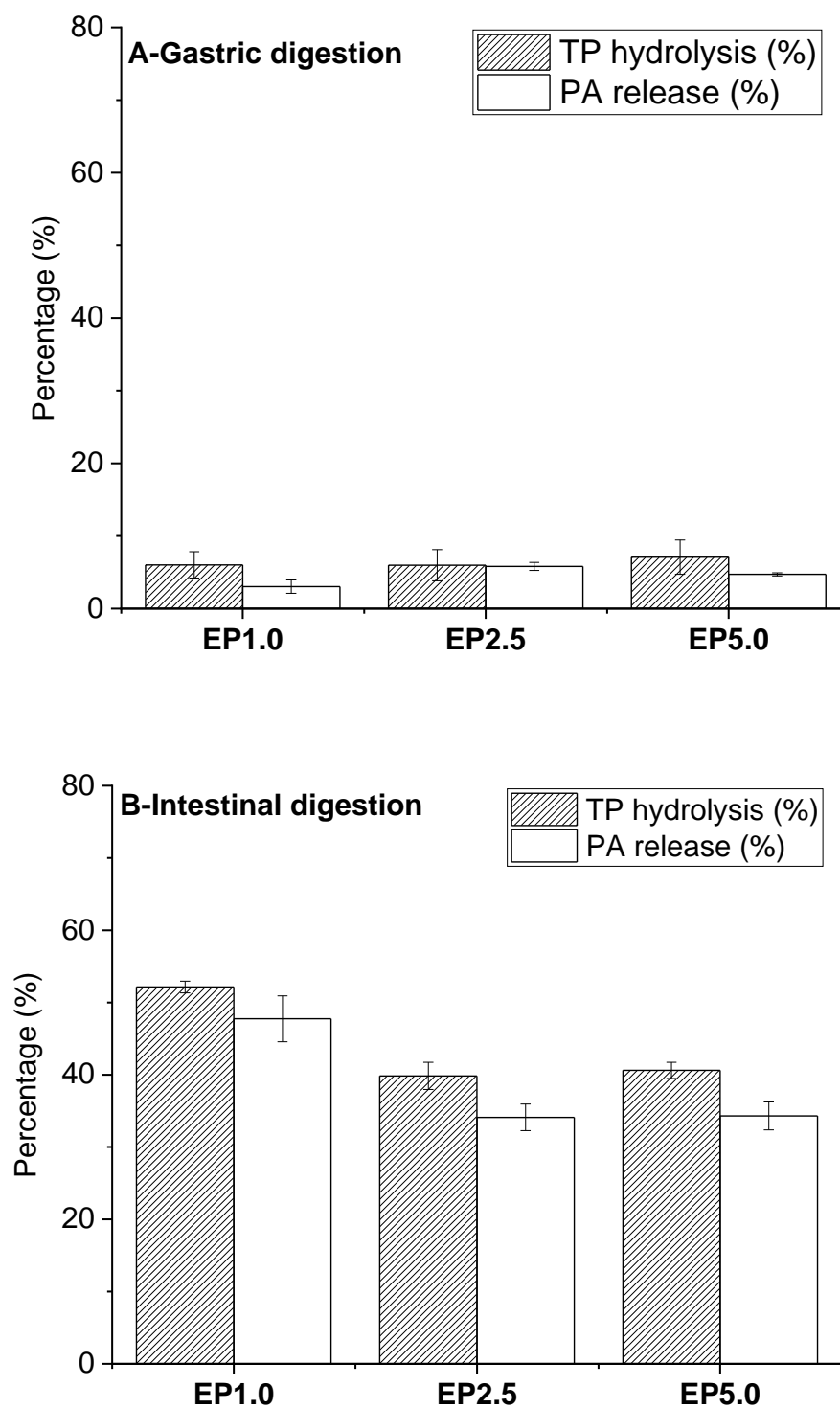


**Figure 4.5.** Hydrolysis of TP (%) and release of PA (%) from O/W emulsions stabilised by pectin at various concentrations, i.e. 1.0 wt% (EP1.0), 2.5 wt% (EP2.5) and 5.0 wt% (EP5.0), in the gastric (A) and intestinal (B) phases. Error bars denote standard deviations of three measurements.

#### 4.3.2.2. *Intestinal digestion*

In contrast to the gastric digestion, the sizes and surface charges of all the emulsions were significantly affected by the intestinal digestion. All the emulsions demonstrated a certain degree of coalescence according to the droplet size distribution results and the confocal images (Fig. 4.4). The most affected emulsion contained the lowest pectin concentration. For example, the size ( $d_{43}$ ) of EP2.5 increased 1.7 times compared with a 4.4-fold increase for EP1.0. Such dramatic changes in droplet size after the intestinal digestion of pectin-based emulsions are in agreement with the results of Verkempinck et al. (2018). In that work, the droplet size ( $d_{43}$ ) of emulsions stabilised by 1.0 wt% pectin (82% DM) increased 4.6 times after 2 h of intestinal digestion. Such an increase in size was probably due to the displacement of pectin at low concentration by bile salts.

The surface charges of all the emulsions also increased significantly after intestinal digestion ( $p < 0.05$ ). This can be attributed to the production of fatty acids and di- and/or monoglycerides and bile salt accumulating on the droplet surface (Sarkar, Li, Cray, & Boxall, 2018; Wilde & Chu, 2011).

Lipid hydrolysis showed that more than half of the TP in EP1.0 was hydrolysed (Fig. 4.5B), whereas only 40% lipolysis occurred for EP2.5 and EP5.0. Surprisingly, for all emulsions, the proportions of TP hydrolysis were approximately 5–6% higher than those of PA release (Fig. 4.5B). This was due to the difference between the theoretical and real enzymatic reactions. The proportion of PA release was calculated with the hypothesis that one triglyceride molecule produced two fatty acid molecules, but it appears that a single hydrolysis event occurred for a small proportion of TP molecules.

However, the release of PA in EP2.5 and EP5.0 was still significantly lower than that in EP1.0.

Two main explanations for the significant drop in lipid digestion at higher pectin concentrations can be proposed. The first explanation is related to the accumulation of more pectin on the droplet surface as the pectin concentration is increased. Lipid digestion is widely reported to be an interfacial process that is initiated when bile salts displace emulsifier to facilitate the adsorption of lipase and colipase (Parker, Rigby, Ridout, Gunning, & Wilde, 2018; Wilde, et al., 2011). Therefore, emulsifiers with the ability to form a physically strong layer around lipid droplets can slow down lipid digestion (Wilde, et al., 2011). In our study, the increase in pectin concentration from 1.0 to 2.5 wt% enhanced the surface coverage by 67.4% (Table 4.3). However, a further increase in pectin concentration to 5.0 wt% did not significantly change the surface coverage ( $p > 0.05$ ). The increase in surface pectin coverage may have conferred resistance to the displacement of pectin by bile salts, inhibiting the subsequent adsorption of lipolytic enzymes.

The second possible explanation is that the interaction of free pectin in the aqueous phase with components of the intestinal fluid can inhibit lipid hydrolysis. It was previously reported that free pectin in the aqueous phase could reduce the extent of lipid digestion because of its binding interactions with bile salts and lipases (Espinal-Ruiz, Parada-Alfonso, Restrepo-Sánchez, Narváez-Cuenca, & McClements, 2014). In this study, Espinal-Ruiz et al. (2014) mixed pectin solution (4.0 wt%) with stabilised emulsion and examined the interactions of free pectin with gastrointestinal components, such as lipase and  $\text{CaCl}_2$ . They reported that free pectin increased

droplet flocculation or microgel formation through cross-linking and that these factors would therefore reduce the droplet surface area available for lipid digestion. In another study, pectin was reported to possess pancreatic-lipase-inhibiting properties, because of its ability to form a complex with the enzyme, thus preventing digestion (Kumar & Chauhan, 2010).

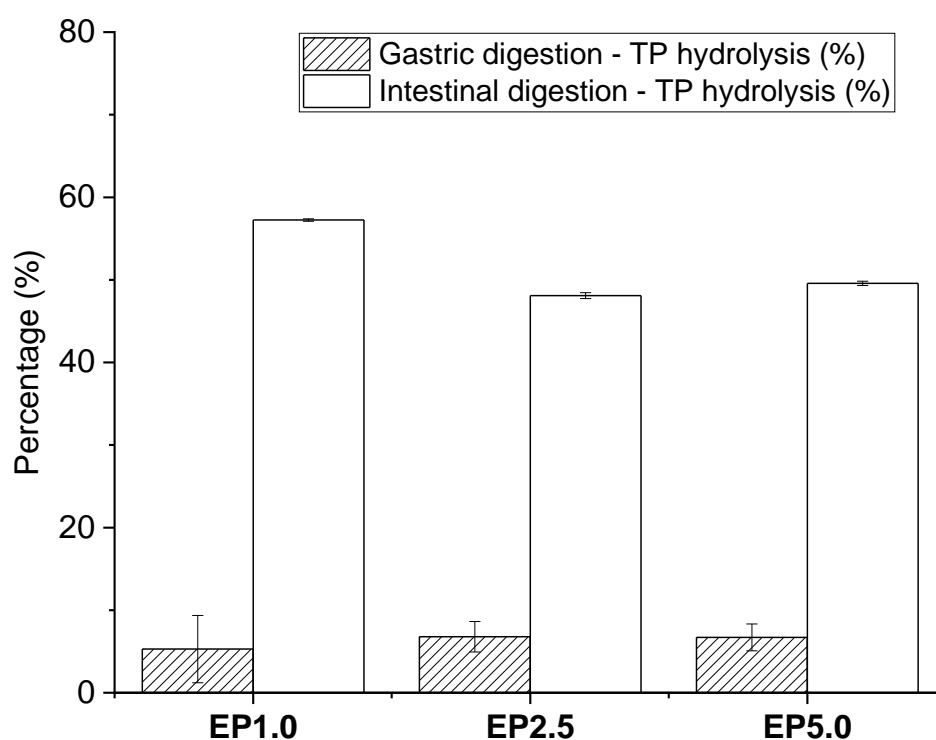


**Figure 4.6.** Hydrolysis profile of TP from reconstituted emulsions after the removal of free pectin in the gastric and intestinal phases. The initial concentration of TP in the reconstituted emulsions was around 26.7–26.9 mg mL<sup>-1</sup>. Error bars denote standard deviations of three measurements.

It was not clear how these mechanisms contributed to the inhibition of lipolysis seen in the current study. For a better understanding of the effects of these two factors on

lipid digestion, free pectin was separated from the emulsion by centrifugation and the cream phase was collected as described in [Section 4.2.4](#). After removal of the free pectin, these reconstituted emulsions were used for gastrointestinal digestion; the hydrolysis of TP is reported in [Fig. 4.6](#). The removal of free pectin made little difference to the gastric hydrolysis of TP. The intestinal hydrolysis of TP was 5–10 percent points higher as a result of the removal of the free pectin. However, the TP hydrolyses of the reconstituted EP2.5 and EP5.0 were still 8–9 percent points lower than that of the reconstituted EP1.0. Therefore, it appears that both factors, i.e. pectin coverage and free pectin, contributed to mitigating lipolysis.

#### 4.3.3. Kinetics of fatty acid release

The lipid hydrolysis profiles at the small intestinal phase of all the pectin-based emulsions were assessed by quantifying the release of FFAs using a pH-stat titration method. The results in [Fig. 4.7](#) clearly show the effects of pectin concentration on the extent of FFA release. At the lowest pectin concentration, approximately 25% of the FFA was produced within 6 min. The reaction rate then reduced and the maximum release was around 33% after 60 min of digestion. Interestingly, the release of PA, which was quantified by GC analysis (47.7%), was higher than the release of FFAs, as measured by titration. The oil phase used in this study was a mixture of SO and TP (50:50 w/w); SO consists of a mixture of long chain triglycerides. It was previously reported that lipase had greater activity against short chain triglycerides than long chain triglycerides when using pancreatic lipase from pig ([Liang, et al., 2016](#); [Nini, et al., 2001](#)), rat and human ([Cohen, Morgan, & Hofmann, 1971](#)). As short chain triglycerides are relatively more water soluble than long chain triglycerides, lipase has

greater accessibility to make contact with and hydrolyse them. In addition, the products of the hydrolysis of short chain triglycerides are SCFAs and short chain mono- and diglycerides, which can diffuse more easily into the surrounding aqueous phase than those from the hydrolysis of long chain triglycerides. The diffusion of these products into the aqueous phase will release more available surface for further lipid hydrolysis. Therefore, over the same period of time, more SCFAs than long chain fatty acids were released; however, in this study, FFA was calculated as the average amount of total fatty acids released. Hence, the release of SCFAs as quantified by GC analysis was significantly higher than the average release of total free fatty acids as determined by titration.

**Table 4.4.** Lipolysis kinetic data of the *in vitro* intestinal digestion of various emulsions

Emulsion	$k_1$ (%FFA min <sup>-1</sup> )	$\Phi_{\max}$ (%)	$t_{1/2}$ (min)	Residual standard error
EP1.0	0.101 ± 0.001	32.9 ± 0.8 <sup>a</sup>	4.33 ± 0.14 <sup>c</sup>	0.5841
EP2.5	0.036 ± 0.000	18.8 ± 0.1 <sup>b</sup>	9.67 ± 0.08 <sup>b</sup>	0.2861
EP5.0	0.033 ± 0.000	17.6 ± 0.2 <sup>c</sup>	10.64 ± 0.21 <sup>a</sup>	0.2349

Samples in the same column with the same superscript letters are not significantly different ( $p < 0.05$ ). The values are the mean and standard deviations are of at least three measurements from triplicate samples.

As the pectin concentration was increased to 2.5 and 5.0 wt%, the hydrolysis rate was significantly reduced, compared with 1.0 wt% pectin (Table 4.4). The fatty acid release rate of EP1.0 was around three times higher than those of EP2.5 and EP5.0.

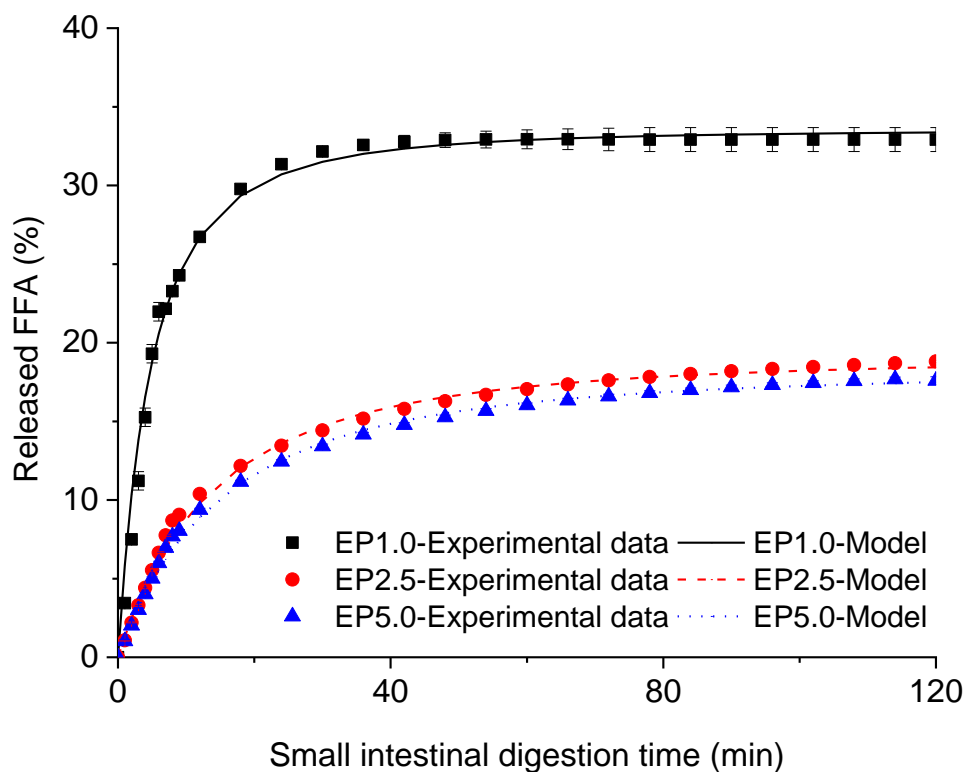


**Figure 4.7.** Kinetics of fatty acid release from O/W emulsions stabilised by pectin at various concentrations, i.e. 1.0 wt% (EP1.0), 2.5 wt% (EP2.5) and 5.0 wt% (EP5.0). The curves are the best fits to the experimental data predicted using Equation (2) for EP1.0 (black solid line), EP2.5 (red dashed line) and EP5.0 (blue dotted line). Error bars denote standard deviations of three measurements.

In addition, the lipolysis half time of EP1.0 was approximately 5.3–6.3 min shorter than those of EP2.5 and EP5.0. After 60 min of digestion, the release of fatty acids in EP1.0 was maximum and was around two times greater than that in EP2.5 and EP5.0. As explained in [Section 4.3.2](#), both the interactions of free pectin with the components of the intestinal fluid and the thick layer around the interface formed at high pectin concentrations were responsible for the low rate of hydrolysis at high pectin concentrations. For a better understanding of the pectin-bile salts interaction, a

displacement study was conducted, in which the amounts of pectin adsorbed on the interface before and after the addition of bile salts were measured.

#### 4.3.4. Displacement of adsorbed pectin by bile salts

Possible interactions of pectin and bile salts were observed through  $\zeta$ -potential measurement and pectin coverage (Table 4.5). EP1.0 was the most sensitive emulsion to the effects of bile salts; the  $\zeta$ -potential increased significantly to a higher negative charge after the addition of bile salts. In contrast, EP2.5 and EP5.0 showed better resistance to the displacement by bile salts. The net surface charges of the two emulsions also increased ( $p < 0.05$ ) but the changes were smaller than that of EP1.0. That is, in the presence of bile salts, the proportion of displaced pectin was more significant at a lower pectin concentration (EP1.0) than at higher concentrations (EP2.5 and EP5.0).

To confirm this hypothesis, the pectin adsorbed on the interface was determined. Because free pectin had been removed from the prepared emulsions, it was hypothesised that all the pectin present in the emulsion was adsorbed pectin and that the emulsions therefore had similar pectin coverages to the freshly prepared emulsion. Table 4.5 shows that more than half of the pectin adsorbed at the interface in EP1.0 was displaced by bile salts. However, the displacements for EP2.5 and EP5.0 were much lower. Therefore, this might suggest that the thick pectin coverage obtained at higher concentration produced a stronger barrier to displacement by bile salts and, as a result, better protection against lipid digestion.

**Table 4.5.** Effects of bile salts on surface charge ( $\zeta$ -potential) and pectin coverage (mg/m<sup>2</sup>)

		EP1.0	EP2.5	EP5.0
Reconstituted emulsions	$\zeta$ -Potential (mV) at pH 7.0	$-18.3 \pm 0.5^a$	$-18.0 \pm 0.4^a$	$-19.1 \pm 0.8^a$
	Adsorbed pectin ( $\mu\text{g mL}^{-1}$ )	$422 \pm 73^b$	$631 \pm 50^a$	$709 \pm 70^a$
	Pectin coverage ( $\text{mg m}^{-2}$ )	$4.6 \pm 0.9^b$	$7.7 \pm 0.6^a$	$8.4 \pm 0.8^a$
Reconstituted emulsions and bile salts	$\zeta$ -Potential (mV) at pH 7.0	$-23.5 \pm 0.1^b$	$-20.5 \pm 0.2^a$	$-20.8 \pm 0.5^a$
	Adsorbed pectin ( $\mu\text{g mL}^{-1}$ )	$196 \pm 4^c$	$398 \pm 18^b$	$503 \pm 16^a$
	Pectin coverage ( $\text{mg m}^{-2}$ )	$3.4 \pm 0.1^c$	$4.3 \pm 0.2^b$	$5.8 \pm 0.1^a$
Displacement (%)		$53.7 \pm 0.0^a$	$37.0 \pm 0.0^b$	$29.1 \pm 0.0^c$

Samples in the same row with the same superscript letters are not significantly different ( $p < 0.05$ ). The values are the mean and standard deviations are of at least three measurements from triplicate samples.

## 4.4. Conclusions

In this chapter, we demonstrated that citrus PEC had better emulsification capacity than apple PEC; all the investigated PEC stabilised O/W emulsions were stabilised through steric effect. All PEC-based emulsions were resistant to gastric digestion whereas changes in the emulsion structure and the release of SCFAs were observed in the intestinal phase, in which the release profile could be modulated by the concentration of pectin. At a sufficient concentration (2.5 wt% or higher), pectin produced a thick coverage around the oil droplets, which provided strong resistance to displacement by bile salts and, as a consequence, delayed lipid digestion. Free pectin in the aqueous phase also played an important role in delaying the hydrolysis through interacting with components of the intestinal fluid such as bile salts and lipase. These results provide new ideas for the future design of emulsion systems that can protect bioactive compounds and deliver them to the targeted large intestinal lumen. The suitability of these pectin-based emulsions for the delivery of SCFAs, including mixture of propionic and butyric acids would be investigated by an *in vivo* study using a cannulated pig model described in [Chapter 6](#).

## Chapter 5 - Design and *In vitro* digestion of SCFA-supplemented Pickering emulsions using hydrophobically modified CNCs

---

### Abstract

The three main objectives of this research were to **1)** hydrophobically modify cellulose nanocrystals (CNCs), **2)** investigate the ability of such modified CNCs (MCNCs) to stabilise Pickering oil-in-water (O/W) emulsions and understand their stability under storage for 4 weeks, different pHs (2.0–7.0) and ionic strengths (0–150 mM NaCl), and **3)** to understand their behaviour during the *in vitro* digestion.

**1)** Structural changes resulting from esterifying CNCs with octenyl succinic anhydride (OSA) were determined using Fourier transform infrared (FTIR) spectroscopy, X-ray diffractometry (XRD), transmission electron microscopy (TEM) and wettability analysis. FTIR spectroscopy confirmed a decrease in the intensity of the –OH-associated band because of reaction of the hydroxyl group with OSA. XRD indicated a lower (11.5%) crystallinity index in MCNCs. TEM revealed that there was no change in morphology of the needle-shaped CNCs upon OSA modification (length/diameter = 40–100 nm/2–4 nm). Hydrophobic modification of CNCs with OSA was evidenced by an increase in static water contact angle from 56° (untreated CNCs) to 80.2° (MCNCs) allowed the MCNCs to be partially wetted by both phases and stabilise O/W emulsions.

**2)** The stability of the Pickering O/W emulsions (20 wt% oil, 0.05–1.00 wt% MCNCs) was assessed using droplet sizing, microscopy,  $\zeta$ -potential, apparent viscosity and oscillatory rheological measurements. Emulsions prepared from MCNCs  $\geq 0.20$  wt% were resistant to droplet coalescence for over 4-week storage at 4°C. The Pickering emulsions showed droplet flocculation at pH < 4.0 (without addition of NaCl) or ionic strength  $\geq 20$  mM NaCl (pH 7.0), with a predominant elastic gel-like behaviour observed at  $\geq 20$  mM NaCl.

**3)** The emulsions (20 wt% oil, 1 wt% MCNCs) were subjected to two *in vitro* digestion pathways. In the first pathway, the emulsions were used for direct intestinal digestion by bypassing the gastric phase while in the second pathway, the emulsions were subjected to sequential gastrointestinal digestion. Flocculation of emulsion droplets occurred because of charge screening effects by the gastric electrolytes. Such gastric flocculation reduced the droplet surface area, overall lipolysis and consequently decreased the extent of SCFA release, latter was 40–45% in the gastric-bypassed emulsions and 30–35% in the sequentially-digested emulsions. High proportion of SCFAs remaining after the intestinal digestion (~ 65%) shows promise in the use of Pickering emulsions for the colon-targeted delivery of SCFAs.

## 5.1. Introduction

Pickering emulsions are stabilised by solid particles that have a strong resistance to bile salt displacement by virtue of their high desorption energy once adsorbed (Sarkar, et al., 2016; Tzoumaki, Moschakis, Kiosseoglou, & Biliaderis, 2011). Needle-shaped cellulose nanocrystals (CNCs) are human-enzyme-resistant particles that have recently attracted research attention in the production of such Pickering emulsions (Chen, Zheng, Xu, et al., 2018; Lee, et al., 2011; Yan, et al., 2017). To our knowledge, there is no published literature on the creation of Pickering O/W emulsions stabilised by CNCs to deliver SCFA.

In this study, we aim to hydrophobically modify CNC with OSA, test the stability of the MCNC-based Pickering emulsions and to apply the emulsion for delivery of PA and BA. The hypothesis of this study was that particle-stabilised emulsions would protect SCFAs during intestinal digestion and thus allow more colon-targeted release. In addition, exposure to gastric conditions may induce microstructural changes in the Pickering emulsions, which might influence the rate and extent of lipolysis and consequently SCFA release profiles. Therefore, we analysed the *in vitro* digestion of the emulsions using the two routes i.e. sequential gastric and intestinal digestion and intestinal digestion bypassing the gastric step (i.e. without the gastric digestion step).

## 5.2. Materials and methods

### 5.2.1. Materials

Sulphated cellulose nanocrystal (CNC, 94–96%) powder was purchased from [CelluForce™, Montreal, Quebec, Canada](#). The CNCs used in this study were intended for research purposes and not for consumption. Sunflower oil (SO) was purchased from a local supermarket ([Morrisons, Leeds, UK](#)). Food-grade TP (glyceryl tripropionate  $\geq 97.1\%$ ) and TB (glyceryl tributyrate  $\geq 97.1\%$ ), and analytical grade TP, TB, OSA, propionic acid (PA), butyric acid (BA), caproic acid (CA), porcine pepsin (P7000), porcine bile extract (B8631) and porcine pancreatin (P7545, 8 × USP) were purchased from [Sigma–Aldrich Company Ltd, Dorset, UK](#). The standards TP, TB, PA and BA were later used for gas chromatography (GC) analysis. All other chemicals were of analytical grade and were also purchased from [Sigma–Aldrich Company Ltd, Dorset, UK](#). Milli-Q water (electrical resistance of 18.2 M $\Omega$ .cm at 25 °C) purified by a [Milli-Q apparatus, Millipore Corp., USA](#), was used as a solvent for all experiments.

### 5.2.2. Hydrophobic modification of CNCs

Hydrophobic modification of CNCs was conducted according to a method that has previously been used for inulin ([Han, Ratcliffe, & Williams, 2015](#)) with some modifications. All reactions were performed in a 500 mL round-bottomed flask at 25 °C. The CNC dispersion (3.0 wt% in water) was mixed with OSA at a ratio of 1:0.15 (w/w). The pH was adjusted to pH  $8.30 \pm 0.1$  using 0.5 N NaOH. During the esterification reaction of hydroxyl groups on the CNC backbone with OSA, the pH was maintained by the continuous addition of 0.5 N NaOH using a pH-stat ([TIM856, Radiometer Analytical, Hach Company, Loveland, CO, USA](#)). The reaction was carried

out until no further NaOH was needed to neutralise the acidic products to ensure that all the OSA had been consumed; typically, the time required was around 7.0 h. Once the reaction was complete, the resultant product was neutralised to pH 7.0 with 1.0 N HCl and then lyophilised, yielding a white powder. The powder was purified by Soxhlet extraction for 12 h using ethanol to remove any leftover OSA from the powder. Finally, it was air dried in an oven at 40 °C overnight to remove the ethanol. This powder is referred to as modified cellulose nanocrystals (MCNCs) and was used to create Pickering O/W emulsions.

### **5.2.3. Structural analysis of MCNCs**

#### *5.2.3.1. Fourier transform infrared (FTIR) spectroscopy*

Before measurement, the MCNCs were ground sufficiently with a mortar and pestle; all samples were then pressed into pellets. The measurements were carried out using a Bruker ATR-FTIR spectrometer ([Bruker Optics GmbH, Ettlingen, Germany](#)) in the mid-IR region (400–4000  $\text{cm}^{-1}$ ), with a resolution of 4  $\text{cm}^{-1}$  for at least 64 scans. The FTIR spectra of unmodified CNCs and MCNCs were collected as average values of 64 scans using [Mobility Series™](#) software before being exported to Origin 2016 Sr2 ([OriginLab Corp., Northampton, MA, USA](#)) for peak fitting.

#### *5.2.3.2. X-ray diffractometry (XRD)*

XRD profiles of unmodified CNCs and MCNCs were obtained using a [Bruker AXS D8 Advance diffractometer](#) with LINXEYE detector using  $\text{Cu K}\alpha$  ( $\lambda = 0.154 \text{ nm}$ ). The XRD analysis was performed at room temperature at 40 kV and 40 mA, with  $2\theta$  ranging from 0 to  $60^\circ$ , at a scan rate of  $0.02^\circ \text{ min}^{-1}$ . The crystallinity indexes (CIs) of the CNCs

and MCNCs were calculated using the Segal method, as described previously (Lee, et al., 2011):

$$CI = \left( \frac{I_{002} - I_{AM}}{I_{002}} \times 100\% \right) \quad (6)$$

where  $I_{002}$  is the peak intensity of plane 002 and  $I_{AM}$  is the minimum intensity between planes 002 and  $10\bar{1}$  in the XRD profiles.

### 5.2.3.3. Wettability

Static water contact angles of unmodified CNCs and MCNCs were determined at 25 °C with the sessile drop method using an OCA25 drop-shape tensiometer ([DataPhysics Instruments, Filderstadt, Germany](#)) fitted with a microsyringe and a high speed IDS camera. Before measurement, both CNCs and MCNCs were pressed, under a weight of 6 tonnes for 30 s, between the plates of a hydraulic bench press (Clarke, Kempston, UK) into discs with diameters of 15 mm and thicknesses of approximately 2 mm, according to a previous method ([Zembyla, Murray, & Sarkar, 2018](#)). A straight needle (0.52 mm outer diameter and 0.26 mm internal diameter) was used to produce 5.0 µL water droplets that formed sessile drops on the discs made from unmodified CNCs or MCNCs. The water droplet contour was recorded using a video camera and was immediately fitted using the [SCA202 V5.0.15](#) software. Static water contact angles ( $\theta_w$ ) between the CNC or MCNC disc and the water were then measured. All measurements were done in triplicate and were reported as the mean and standard deviation.

### 5.2.3.4. Transmission electron microscopy (TEM)

TEM was used to observe the structural changes in the CNCs (if any) after modification with OSA. Both CNC and MCNC samples (10  $\mu\text{L}$ ) were stabilised with 2.5% (v/v) glutaraldehyde, fixed in 0.1% (w/v) osmium tetroxide and then embedded in araldite. Ultra-thin sections (80–100 nm) were then placed on 3.05 mm grids and stained with 8% (v/v) uranyl acetate and lead citrate. The imaging was carried out using a [CM10 TEM microscope \(Philips, Guildford, UK\)](#).

#### **5.2.4. Preparation of Pickering O/W emulsions**

The MCNCs were used as Pickering stabilisers at various concentrations to create O/W emulsions. The oil phase (TP–TB–SFO mixture with a weight ratio of 1:1:2) was pre-homogenised at an oil:aqueous phase ratio of 1:4 (w/w) using a high speed blender ([D500 series, Biolab Ltd, Germany](#)) at 10,000  $\text{rev min}^{-1}$  for 3 min. The emulsions were prepared using various concentrations of MCNCs, i.e. 0.05, 0.10, 0.20, 0.50 and 1.0 wt% in the final emulsions, hereafter referred to as emulsions E0.05, E0.10, E0.20, E0.50 and E1.00 respectively. In the next step, the coarse emulsions were homogenised using a two-stage valve homogeniser ([Panda Plus, GEA Niro Soavi, Parma, Italy](#)) at pressures of 200/50 bar for three passes. The resulting emulsions were used for analysis of droplet size,  $\zeta$ -potential, microstructure and stability. Control emulsions were also prepared from unmodified CNCs using 1.0 wt% CNCs.

#### **5.2.5. Stability of MCNC-based emulsions under different stresses**

##### *5.2.5.1. Storage at 4 °C*

The emulsions E0.05 – E1.00 were stored at 4 °C in capped vials and were monitored using visual observation and droplet sizing and  $\zeta$ -potential measurements for 4 weeks.

#### 5.2.5.2. pH and ionic strength conditions

Freshly prepared emulsions (E1.00) had a pH of approximately pH 6.8. For the pH study, the emulsions were adjusted to pH 7.0 using 1 N NaOH and then to pH 6.0, 5.0, 4.0, 3.0 and 2.0 using 1 N HCl. For each pH study, 20 mL of emulsion E1.00 in a 50 mL beaker was adjusted to the desired pH by drop-by-drop addition of NaOH or HCl under constant stirring at 500 rev min<sup>-1</sup>. In separate experiments, emulsions (E1.00) were adjusted to various ionic strengths from 10 to 150 mM NaCl by mixing 10 mL of emulsion with a suitable quantity of solid NaCl under constant stirring at 500 rev min<sup>-1</sup>. Subsequently, samples were analysed for any change in droplet size,  $\zeta$ -potential and microstructure (CLSM). All measurements were done in triplicate and were reported as the mean and standard deviation.

#### 5.2.6. *In vitro* digestion study

The *in vitro* digestion was conducted using the static INFOGEST digestion protocol (Minekus, et al., 2014) which was described in Section 3.2.6. For the intestinal digestion, freshly prepared emulsions as well as gastric digesta (with added pepsin) were used, the latter representing sequential digestion.

#### 5.2.7. Kinetics of free fatty acid release

The release of free fatty acids (FFAs) during simulated intestinal digestion was quantified over 2 h while maintaining the pH at 7.0 by the addition of 0.05 M NaOH using a pH-stat (TIM 854, Radiometer) similar to the procedure in Section 4.2.5.

### 5.2.8. Characterisation of the Pickering O/W emulsion and digesta

The emulsions and digesta samples were characterised using droplet size and  $\zeta$ -potential measurements, and the microstructure was determined using confocal laser scanning microscopy. The analysis procedures were described in [Section 3.2.7](#).

A Kinexus ultra rheometer ([Malvern Instruments Ltd, Malvern, UK](#)) was used to measure the apparent viscosity, elastic modulus ( $G'$ ) and viscous modulus ( $G''$ ) of the emulsions and the digesta. The samples were added to a double gap geometry DG 24/27, followed by 5 min of equilibration to reach a temperature of 37 °C. Subsequently, steady shear experiments were performed; apparent viscosities, as a function of shear rate in the range from 0.1 to 1000 s<sup>-1</sup>, were recorded. A strain amplitude sweep from 0.1 to 20% was performed for each sample in an attempt to achieve linear viscoelastic region (LVR). Dynamic frequency sweep tests were then carried out at a strain amplitude selected from the strain amplitude sweep (1.0%) and with an angular frequency range of 0.01–20 s<sup>-1</sup>. The frequency-dependent curves of  $G'$  and  $G''$  were recorded. All measurements were done in triplicate and were reported as the mean and standard deviation.

### 5.2.8. Quantification of TP, TB and SCFAs

Determination of short-chain triglycerides and SCFAs were done using GC methods as described in [Section 3.2.8](#) and [Section 3.2.9](#).

### 5.2.9. Statistical analysis

Analysis of variance was conducted using [Minitab® version 17.3.1](#) to detect overall significant differences ( $p < 0.05$ ).

---

## 5.3. Results and discussion

### 5.3.1. Hydrophobic modification of CNCs

#### 5.3.1.1. Characteristics of MCNCs

The modification of the CNCs using OSA and any effects of this hydrophobic modification on the particle behaviour and morphology were measured for the CNCs and MCNCs with a range of complementary techniques, such as FTIR spectroscopy, XRD profiles, static water contact angles and TEM (Fig. 5.1). This sets the scene for understanding the behaviour of the MCNCs when they are present at an interface. As expected, the modification reduced the number of hydroxyl ( $-OH$ ) groups in the cellulose backbone because of their replacement by OSA in MCNCs; this was clearly observed in the FTIR absorbance spectra (Fig. 5.1A). The intensity of the band at  $3400\text{ cm}^{-1}$ , which corresponds to the  $-OH$  groups, decreased by approximately 14% in the MCNC sample, which was in agreement with a previous study (Chen, Zheng, Yan-TengXu, et al., 2018), in which the intensity of the same band also decreased because of the substitution by OSA. There was a significant increase in the band at  $1600\text{ cm}^{-1}$ ; this corresponded to an increase in the water content of the MCNCs and was associated with the addition of some water molecules during the modification process, which was also observed in the previous study (Chen, Zheng, Yan-TengXu, et al., 2018).

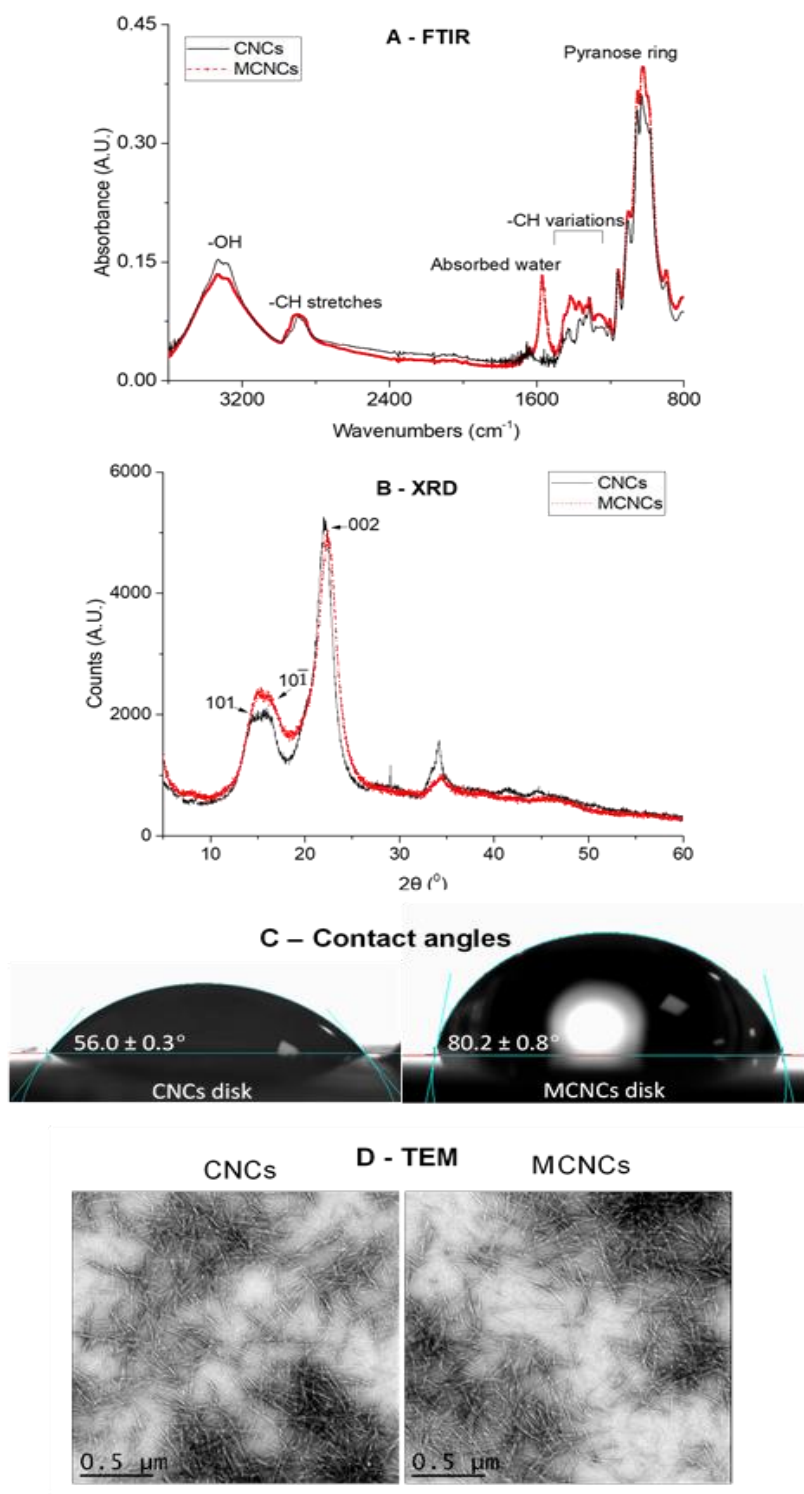


**Figure 5.1.** (A) Fourier transform infrared (FTIR) spectra and (B) X-ray diffractometry (XRD) profiles of unmodified cellulose nanocrystals (CNCs) (black line) and modified CNCs (MCNCs) (red dashed line) and corresponding (C) static water contact angles and (D) transmission electron microscopy (TEM) images.

Modification with OSA also led to changes in the crystalline form (allomorph) of cellulose I, the diffraction pattern of which was between planes 101 and 002, as indicated in Fig. 5.1B (Ciolacu, Ciolacu, & Popa, 2011). There was an increase in the intensity of the peak between diffraction planes 101 and  $10\bar{1}$ , which indicated increased amorphousness or decreased crystallinity. This observation was in contrast to previous studies on the OSA modification of cotton CNCs (Chen, Zheng, Yan-Teng Xu, et al., 2018) and the organic acid modification of bacterial cellulose nanofibres (Lee, et al., 2011), in which the intensity of the peak between planes 101 and  $10\bar{1}$  decreased. In our study, the CIs of the CNCs and MCNCs were 77.7 and 68.8% respectively. That is, modification led to an around 11.5% decrease in the CI of the cellulose structure. This change was nearly three times higher than that reported by Chen et al., 2018; Lee et al., (2011), which was around 4.5% and 5.0%, respectively. This discrepancy in the crystallinities of the MCNCs in the present study versus previous studies (Chen et al., 2018; Lee et al., 2011) might be attributed to the differences in source of CNCs used and the modification methods. For instance, Lee et al. (2011) used bacterial cellulose nanofibres while we used a commercial CNCs synthesised by sulphuric acid treatment of cellulose derived from bleached kraft pulp (Reid et al., 2017), both materials have different original crystallinity indices (CIs) before the modification, i.e. 90.2 and 77.7 % for cellulose nanofibres and CNCs in the current study, respectively. The differences might affect their behaviour and reaction during the subsequent modification process. In the present study, we controlled the pH at a constant value for at least 7 h, which was an important factor in improving the degree of substitution of OH by OSA. In contrast, Chen et al., (2018) did not control the pH and mixing with OSA was carried out for only 1 min.

As a result of this OSA substitution, the hydrophobicity of the MCNCs was significantly enhanced; this was clearly demonstrated by the dramatic increase in the water contact angle from  $56.0 \pm 0.3^\circ$  (CNCs) to  $80.2 \pm 0.8^\circ$  (MCNCs) (Fig. 5.1C). The differences in the organisation of the crystal as shown in XRD data in Fig. 5.1B upon modification with OSA might also explain the shifting of static water contact angle in Fig. 5.1C towards more hydrophobicity. That is, MCNCs will be wetted preferentially by water and only partially wetted by the oil phase; thus, they will stabilise O/W emulsions, as opposed to unmodified CNCs, which are too hydrophilic and will probably remain in the aqueous phase (Cherhal, Cousin, & Capron, 2016; Kalashnikova, Bizot, Cathala, & Capron, 2012). Changes in the surface charge of the CNCs were also determined, by comparing the  $\zeta$ -potentials of CNCs and MCNCs in 1 wt% solution at pH 7.0. The CNCs had a high negative charge of  $-39.3 \pm 1.0$  mV because of the presence of sulphated groups in the cellulose backbones. In addition, the  $\zeta$ -potential ( $-39.1 \pm 2.1$  mV) of the MCNCs was similar to that of the unmodified CNCs. Although some changes in crystallinity were evident in the XRD profiles, the TEM images (Fig. 5.1D) of the CNCs and the MCNCs were indistinguishable, showing a needle-like shape and a similar aspect ratio (length:diameter) of 20:1, with a diameter of 2–4 nm and a length of 40–100 nm.

### **5.3.1.2. Characteristics of MCNC-based Pickering O/W emulsions**

MCNCs at various concentrations (0.05–1.00 wt%) were used to produce 20 wt% Pickering O/W emulsions. As a control, emulsions were also prepared using 1.00 wt% unmodified CNCs. Fig. A5.1 (appendix) confirms that the unmodified CNCs did not have emulsifying capacity; phase separation with a clear oil layer occurred almost immediately after preparation of the emulsions, and exceptionally large oil droplets

were observed in the confocal micrographs. This is in agreement with the low water contact angle observed in Fig. 5.1C and again confirms the need for hydrophobic modification to enable the formation of stable oil droplets. The MCNC-stabilised emulsions were characterised by droplet size distribution (Fig. 5.2A), confocal microscopy (Fig. 5.3) and  $\zeta$ -potential (Table 5.1).

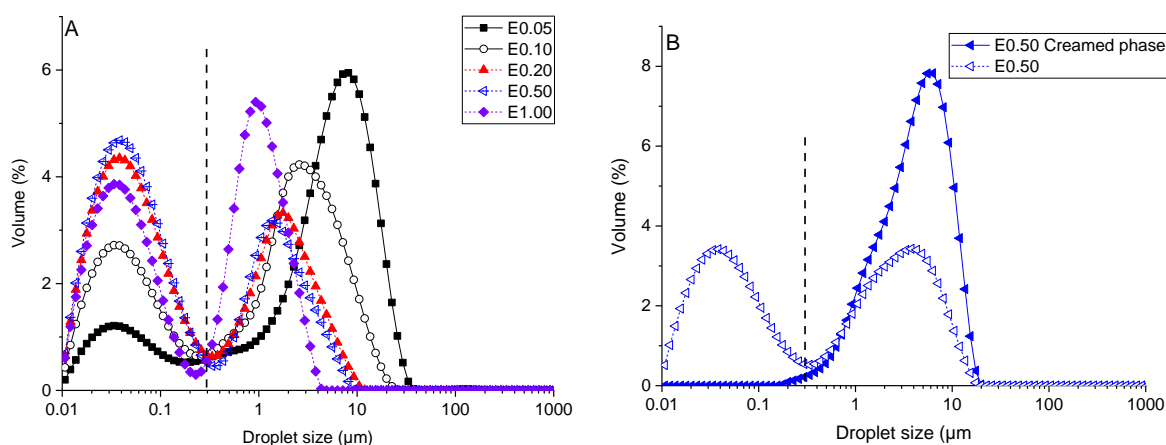


**Figure 5.2.** (A) Droplet size distributions of emulsions stabilised by modified cellulose nanocrystals (MCNCs) at various concentrations: E0.05, 0.05 wt% MCNCs; E0.10, 0.10 wt% MCNCs; E0.20, 0.20 wt% MCNCs; E0.50, 0.50 wt% MCNCs; E1.00, 1.00 wt% MCNCs. (B) Droplet size distributions of emulsion E0.50 and its creamed phase after centrifugation at 14,500 g for 40 min followed by dilution to a similar droplet concentration to that of emulsion E0.50. The plotted values are the average of at least three measurements on triplicate samples ( $n = 3 \times 3$ ).

Fig. 5.2A clearly shows that all emulsions had bimodal distributions, with similar first peaks in the range 0.01–0.3 μm. As the MCNC concentration increased, the first peak became more prominent and the second peak narrowed and shifted to a lower size range. In all emulsions, the first peaks were too small to represent emulsion droplets;

they probably represented the MCNCs, which had a needle-like shape with a length of 40–100 nm (Fig. 5.1D). Hence, a possible explanation for the first peak was the presence of unadsorbed MCNCs in the aqueous phase. In a previous study on emulsions stabilised by CNC–protein composites, a similar small-sized peak was observed; it was hypothesised to be unadsorbed CNCs (Sarkar, Li, Cray, & Boxall, 2018).

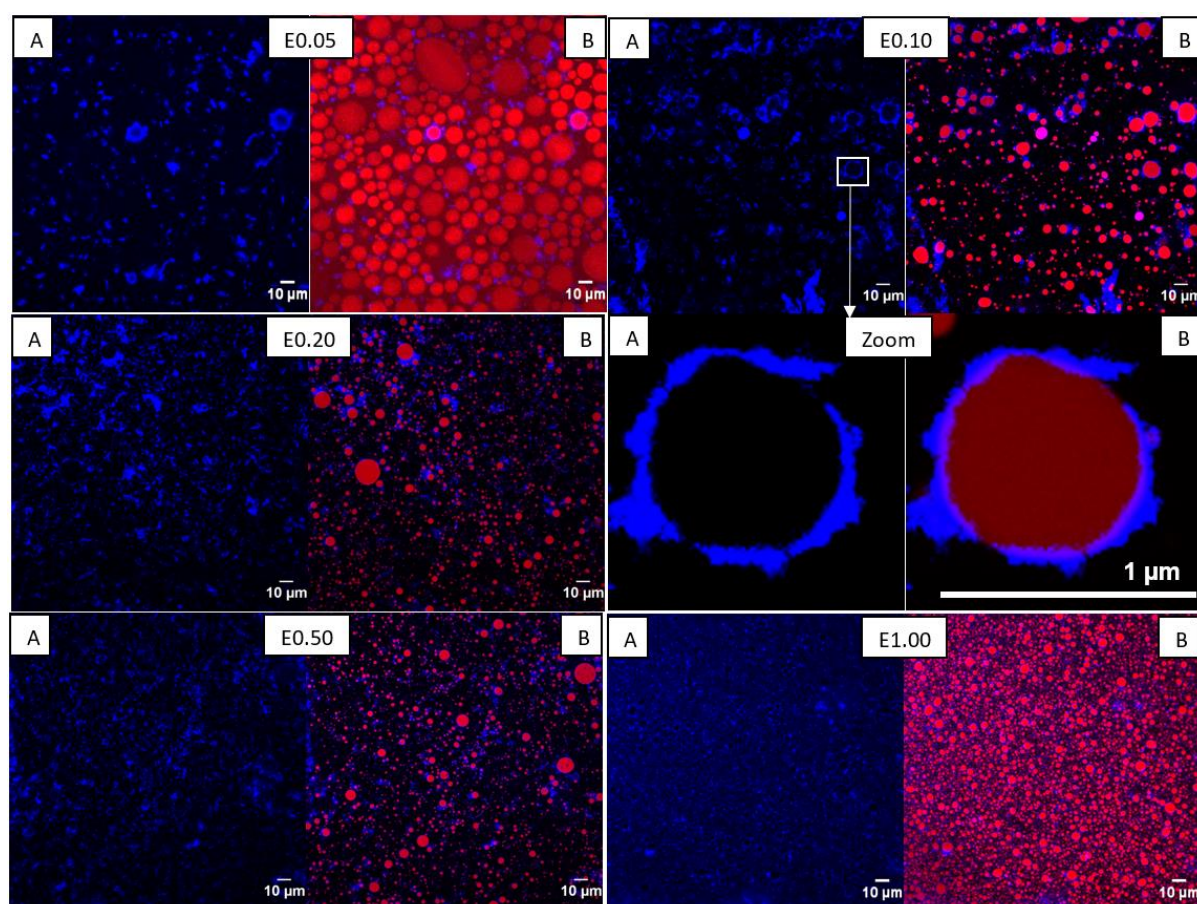


**Figure 5.3.** Confocal images of various modified cellulose nanocrystal (MCNC) emulsions: A, MCNC channel; B, merge channel of MCNCs and oil droplets. The red colour represents the oil phase (stained by Nile Red); the blue colour represents the MCNCs (stained by Calcofluor-white). Zoomed image was created from the E0.10.

To prove this hypothesis, we centrifuged an emulsion at 14,500 *g* for 40 min at 4 °C, collected the cream layer, diluted it in Milli-Q water to a droplet concentration similar to that of the original emulsion and analysed it for droplet size distribution. The droplet size distributions of emulsion E0.50 and the cream phase of emulsion E0.50 confirm that the first peak was unadsorbed MCNCs, as it did not appear in the diluted cream phase in [Fig. 5.2B](#). In addition, we also measured the particle size distribution of the MCNC solution using dynamic light scattering (DLS) ([appendix Fig. A5.2](#)). The MCNC solution had a multimodal distribution, in which the main peak was in the size range 100–300 nm, closely resembling that of the first peak of the droplet size distribution in [Fig. 5.2A](#). Although the DLS size is in agreement with the characteristic length of the MCNCs ([Fig. 5.1D](#)), caution should be used in interpreting the DLS data, recognising the limitation that DLS assumes particles to be spherical; MCNCs are rod shaped ([Boluk & Danumah, 2014](#)). Therefore, in this study, the calculation of average particle sizes  $d_{32}$  and  $d_{43}$  were done after removal of the first peak in the range 0.01–0.3  $\mu\text{m}$  (the peaks were separated by a dashed line, see [Fig. 5.2A](#)) similarly to a previous study ([Zembyla, Murray, & Sarkar, 2018](#)). In addition,  $d_{32}$  and  $d_{43}$  of the first peaks of all the freshly prepared emulsions were quantified and presented in [appendix Table A5.1](#). As can be clearly seen in [appendix Table A5.1](#), the  $d_{32}$  and  $d_{43}$  of all the first peaks were around 33–38 and 58–86 nm, respectively, which were within the range of lengths observed for the needle-shaped MCNCs (40–100 nm) TEM (see [Fig. 5.1D](#)). This analysis again confirmed that the first peak was due to the presence of free MCNCs in the continuous phase.

The results also confirmed the nature of the Pickering emulsions, in which the diameter of the Pickering droplets was around 10–100 times larger than that of the solid

---

particles, which has been reported in many previous studies (Hu, Ballinger, Pelton, & Cranston, 2015; Marefati, Matos, Wiege, Haase, & Rayner, 2018; Sarkar, et al., 2016). Furthermore, in our study, the average droplet size ( $d_{43} = 2.29 \mu\text{m}$ ) obtained at low MCNC concentration (0.20 wt%) was smaller than that of most Pickering droplets that have been reported (Li, et al., 2018; Marefati, et al., 2018; Tzoumaki, Moschakis, Kiosseoglou, & Biliaderis, 2011; Yusoff & Murray, 2011). This indicates the excellent partial wetting of these MCNCs by either of the two phases.

Confocal micrographs of the Pickering emulsions are shown in Fig. 5.3, in which A represents the Calcofluor-white channel (MCNCs) and B illustrates the merge channel of Calcofluor-white and Nile Red (oil droplets). It can be seen clearly that the amount of MCNCs in emulsion E0.05, with an oil volume fraction of 20 wt%, was not high enough to prevent coalescence. This is in agreement with a previous study on emulsion gels stabilised by OSA-modified CNCs, which reported substantial coalescence when low concentrations (less than 0.3 wt%) were used (Chen, Zheng, Yan-TengXu, et al., 2018). However, the 'clear blue ring' in Fig. 5.3 (zoomed image) highlights the signature of the MCNCs acting as Pickering stabilisers. An increase in the MCNC concentration from 0.05 to 0.10 wt% resulted in a 1.97-fold decrease in average droplet size ( $d_{43}$ ) to  $4.02 \mu\text{m}$  (Table 5.1). In addition, the MCNC coverage on the interface was evident in the confocal images (Fig. 5.3), with smaller droplets being formed at higher MCNC concentration (0.05–0.10 wt%) and with a greater amount of unadsorbed MCNCs being present in the continuous phase, in agreement with the size distribution results (Fig. 5.2A).

**Table 5.1.** Mean droplet sizes (population in the second peak representing the emulsion-relevant sizes) and  $\zeta$ -potentials of modified cellulose nanocrystal (MCNC)-stabilised Pickering emulsions during 28 days of storage at 4 °C. The values are the mean and standard deviation of at least three measurements on triplicate samples (n = 3 × 3).

MCNC concentration (wt%)		E0.05	E0.10	E0.20	E0.50	E1.00
Freshly prepared emulsions	$d_{32}$ ( $\mu\text{m}$ )	3.27 ± 0.14 <sup>a</sup>	1.95 ± 0.05 <sup>b</sup>	1.39 ± 0.02 <sup>c</sup>	1.31 ± 0.01 <sup>d</sup>	0.92 ± 0.01 <sup>e</sup>
	$d_{43}$ ( $\mu\text{m}$ )	7.82 ± 0.62 <sup>a</sup>	4.02 ± 0.15 <sup>b</sup>	2.29 ± 0.06 <sup>c</sup>	2.01 ± 0.02 <sup>d</sup>	1.22 ± 0.01 <sup>e</sup>
	$\zeta$ -Potential (mV)	-60.3 ± 4.0 <sup>bc</sup>	-57.8 ± 2.2 <sup>c</sup>	-62.6 ± 3.0 <sup>bc</sup>	-64.3 ± 3.0 <sup>ab</sup>	-68.7 ± 2.7 <sup>a</sup>
Day 07	$d_{32}$ ( $\mu\text{m}$ )			1.60 ± 0.03 <sup>b</sup>	2.08 ± 0.32 <sup>a</sup>	0.98 ± 0.02 <sup>c</sup>
	$d_{43}$ ( $\mu\text{m}$ )			3.88 ± 0.19 <sup>a</sup>	4.04 ± 0.85 <sup>a</sup>	1.39 ± 0.06 <sup>b</sup>
	$\zeta$ -Potential (mV)			-60.9 ± 2.6 <sup>b</sup>	-63.7 ± 4.4 <sup>ab</sup>	-66.6 ± 2.4 <sup>a</sup>
Day 14	$d_{32}$ ( $\mu\text{m}$ )	Because of phase separation, measurement was not carried out.		1.86 ± 0.15 <sup>a</sup>	1.61 ± 0.02 <sup>b</sup>	0.97 ± 0.00 <sup>c</sup>
	$d_{43}$ ( $\mu\text{m}$ )			13.76 ± 2.67 <sup>a</sup>	2.92 ± 0.07 <sup>b</sup>	1.37 ± 0.01 <sup>c</sup>
	$\zeta$ -Potential (mV)			-50.7 ± 7.1 <sup>b</sup>	-66.6 ± 7.7 <sup>a</sup>	-65.4 ± 4.9 <sup>a</sup>
Day 28	$d_{32}$ ( $\mu\text{m}$ )			2.21 ± 0.32 <sup>a</sup>	1.71 ± 0.02 <sup>b</sup>	0.96 ± 0.00 <sup>c</sup>
	$d_{43}$ ( $\mu\text{m}$ )			36.22 ± 14.56 <sup>a</sup>	3.05 ± 0.10 <sup>b</sup>	1.36 ± 0.01 <sup>c</sup>
	$\zeta$ -Potential (mV)			-54.1 ± 2.5 <sup>b</sup>	-60.9 ± 2.2 <sup>a</sup>	-66.9 ± 3.8 <sup>a</sup>

Different superscripts (a–e) in the same row represent significant differences between different samples at the  $p < 0.05$  level

Another study on 20 wt% O/W emulsions stabilised by carboxylated CNCs (0.1 wt%) reported similar droplet sizes ([Mikulcov, Bordes, Minarik, & Kasparkov, 2018](#)) to those obtained in our study. However, in their study, the microscopic structure of the emulsions was not examined. In our study, there was significant improvement when the concentration of MCNCs was further increased to  $\geq 0.20$  wt%. Most droplets in these emulsions appeared to be fully covered by MCNCs and, even in a populated area, the droplets were well separated with distinctive layers of MCNCs on the interface without any sign of uncoated droplets. Also, there was no sign of droplet aggregation. This may have been associated with the higher negative surface charge ( $-68.7$  mV) obtained at higher MCNC concentration ([Table 5.1](#)), which prevented the droplets from coming in close vicinity of each other. In comparison with the surface charge of the aqueous dispersion of MCNCs ( $-39.1 \pm 2.1$  mV), as reported in [Section 5.3.1.2](#), the surface charges of all emulsions were significantly higher. This might be due to the difference in the arrangement of the MCNCs between bulk solution and the oil droplet surface after exposing to homogenisation, which needs to be investigated in future using XRD. The MCNCs were more densely packed at the surface of the droplets than in the solution.

A similar difference in particle charge between in the bulk phase and at the interface has been reported previously ([Sarkar et al., 2016](#)). Electrostatic repulsion is generally common in Pickering emulsions when the particles carry a surface charge ([Araki, 2013](#); [P.Binks, 2002](#); [Ridel, Bolzinger, Gilon-Delepine, Dugas, & Chevalier, 2016](#)). Therefore, the MCNCs allowed the formation of Pickering O/W emulsion droplets that carried large desorption energies, because of their particle-stabilised interface, and at

the same time were electrostatically stabilised, because of the high charge densities of the MCNCs at the interface.

### **5.3.2. Responsiveness of modified CNCs-based emulsions to various pH and ionic strengths**

The emulsions were also examined for their microstructural stability and their physicochemical properties when subjected to storage at 4 °C and to different pHs (pH 2.0–7.0) and ionic strengths (0–150 mM NaCl).

#### *5.3.2.1. Storage for 4 weeks at 4 °C*

[Fig. 5.4](#) shows the appearance of freshly prepared emulsions and emulsions after 1, 2 and 4 weeks of storage under refrigerated conditions. Apart from emulsion E0.05, in which a thin oil layer had separated from the remaining emulsion, all emulsions were stable, without any signs of creaming or separation. After 1 week of storage, there was clear phase separation in emulsions E0.05 and E0.10. Instability of the emulsions was due to an insufficient amount of emulsifier available to stabilise all the interfacial area at the chosen oil content (20 wt% oil).

This phenomenon was also in line with the CLSM images ([Fig. 5.3](#)), which showed large droplets in emulsions E0.05 and E0.10. In contrast, the droplet sizes of emulsions E0.20, E0.50 and E 1.00 changed slightly ([Table 5.1](#)) but the appearance of the emulsions was rather homogeneous. The  $\zeta$ -potentials of emulsions E0.20, E0.50 and E1.0 remained constant after 1-week storage, suggesting that the high net negative surface charges were providing electrostatic repulsive forces to prevent flocculation. After 2 weeks of storage, emulsion E0.20 showed almost an order of

magnitude change in droplet size. The zeta-potential of E0.20 significantly decreased, i.e.  $-60.9 \pm 2.6$  and  $-50.7 \pm 7.1$  mV after 1 and 2 weeks respectively ( $p < 0.05$ ). This was in agreement with increase in droplet size (3.55 times) and associated emulsion instability. Although creaming was clearly seen in both emulsion E0.50 and emulsion E1.00, both emulsions returned to a visually homogeneous appearance after a gentle shake, and there were no signs of coalescence. The creaming observed in this study was probably due to density difference between the two phases. However, the oil droplets were still stabilised by M-CNC. Therefore, there was no significant change in droplet size and  $\zeta$ -potential in emulsions E0.50 and E1.00 after 4 weeks of storage.

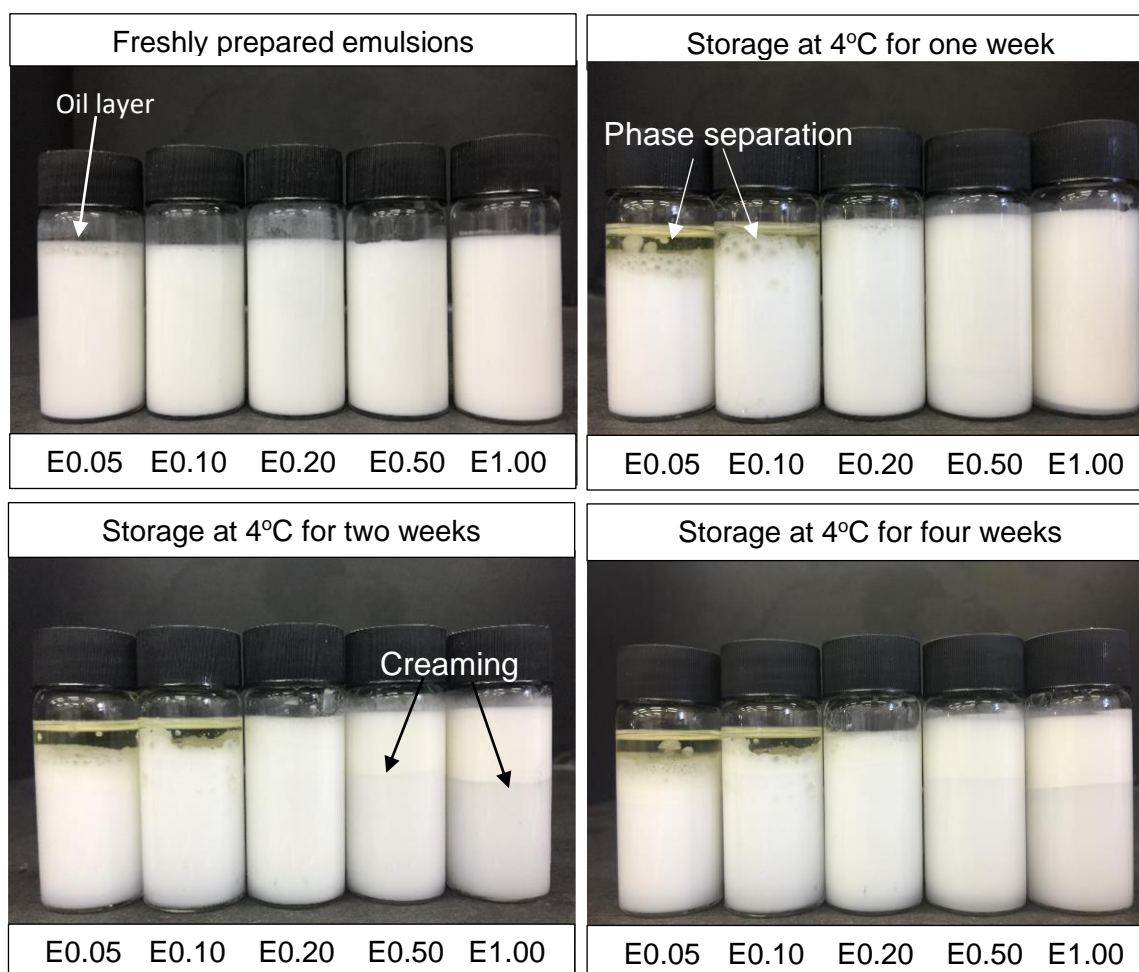


**Figure 5.4.** Visual images of creaming stability of emulsions stabilised by 0.05–1.00 wt% modified cellulose nanocrystals during 28 days of storage at 4 °C.

In a previous study (Mikulcov et al., 2018), emulsions stabilised by less than 0.3 wt% carboxylated CNCs showed clear separation of bulk oil from the remaining emulsion, indicating coalescence. In our study, for MCNC concentrations higher than 0.20 wt%, creaming was detected only after 14 days. Overall, this suggests that 0.50–1.00 wt% of MCNC was sufficient to create fine droplets with sufficient particle coverage, as shown in the confocal micrographs (Fig. 5.3), a high negative charge (Table 5.1) and resistance to coalescence over the storage period.

#### 5.3.2.2. pH conditions

The emulsions subjected to different pH conditions (pH 2.0–7.0) were characterised using droplet sizing (Fig. 5.5A), flow curves (Fig. 5.5B) and confocal micrographs (Fig. 5.5C), with mean sizes and  $\zeta$ -potentials shown in Table 5.2. Fig. 5.5A and Table 5.2 show that decreasing the pH from pH 7.0 to pH 5.0 slightly affected the sizes (1.3 times) and net negative surface charge of the emulsions. However, when the pH was decreased to  $\leq$  pH 4.0, the droplet size increased significantly, by approximately 2.7 times, and the magnitude of the  $\zeta$ -potential decreased from  $-30.4$  mV at pH 4.0 to  $-20.5$  mV at pH 2.0. In addition, when the pH was  $\leq$  4.0, the first peak of the size distribution decreased in height and the second peak shifted to a larger droplet size range.

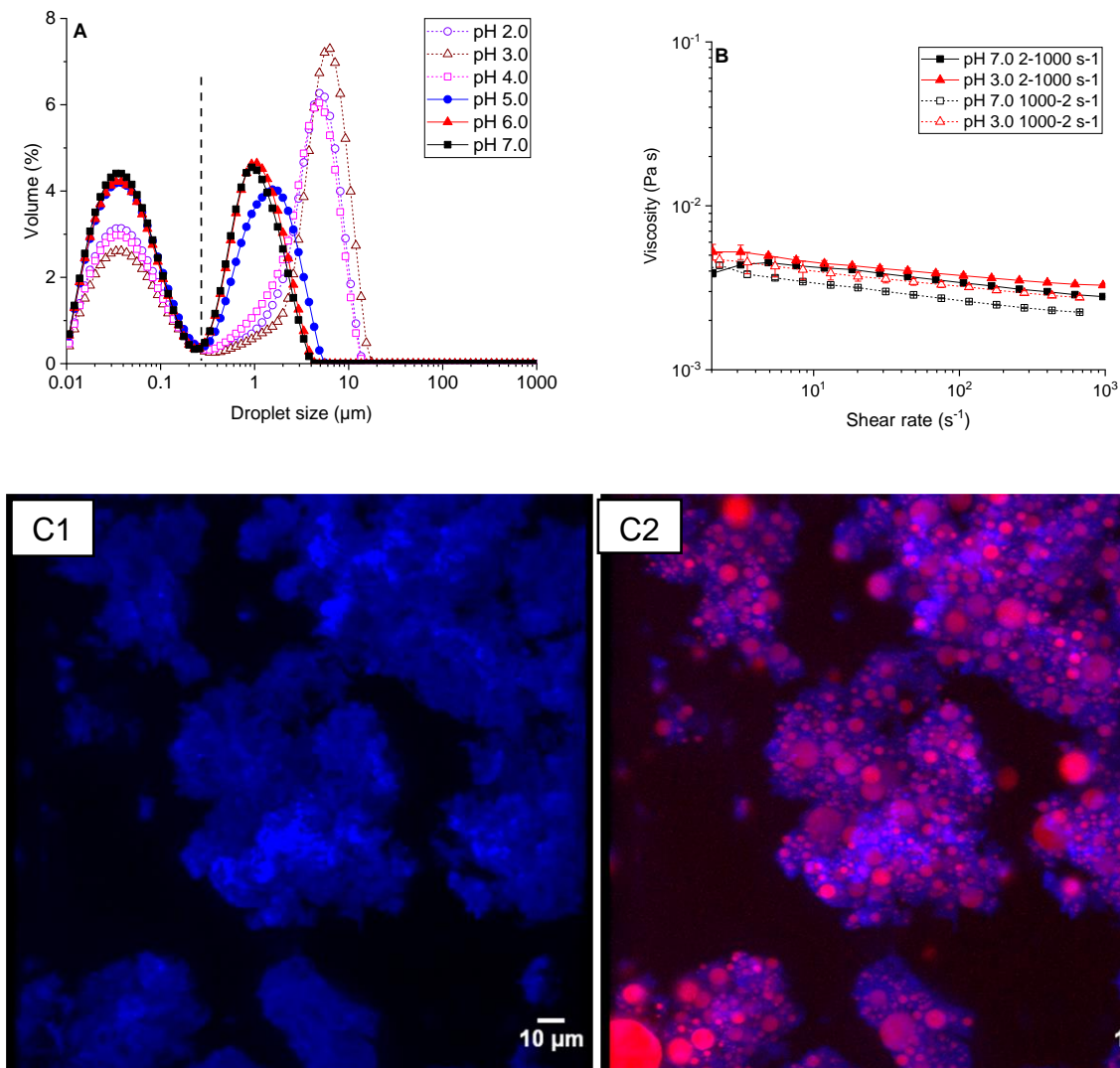


**Figure 5.5.** (A) Droplet size distributions of emulsion E1.00 at various pHs, (B) apparent viscosities of emulsion E1.00 at pHs 7.0 and 3.0 at shear rates from 2 to 1000  $\text{s}^{-1}$  and then from 1000 to 2  $\text{s}^{-1}$  and (C) corresponding confocal micrographs at pH 3.0 (C1, Calcofluor-white channel; C2, merge channel of Calcofluor-white and Nile Red). The red colour represents the oil phase (stained by Nile Red, excitation 514 nm, emission 539–648 nm); the blue colour represents the modified cellulose nanocrystals (stained by Calcofluor-white, excitation 405 nm, emission 410–523 nm). The plotted values of the mean droplet size distribution are the average of at least three measurements on triplicate samples ( $n = 3 \times 3$ ).

**Table 5.2.** Mean droplet sizes (population in the second peak representing the emulsion-relevant sizes) and  $\zeta$ -potentials of emulsion E1.00 as a function of pH. The values are the mean and standard deviation of at least three measurements on triplicate samples ( $n = 3 \times 3$ ).

pH	$d_{32}$ ( $\mu\text{m}$ )	$d_{43}$ ( $\mu\text{m}$ )	$\zeta$ -Potential (mV)
2.0	$2.92 \pm 0.05^b$	$4.72 \pm 0.10^b$	$-20.5 \pm 0.6^e$
3.0	$3.61 \pm 0.24^a$	$5.86 \pm 0.32^a$	$-29.1 \pm 1.8^d$
4.0	$2.58 \pm 0.29^b$	$4.35 \pm 0.47^b$	$-30.4 \pm 2.1^{cd}$
5.0	$1.15 \pm 0.01^c$	$1.62 \pm 0.01^c$	$-33.6 \pm 2.2^c$
6.0	$0.95 \pm 0.00^d$	$1.26 \pm 0.01^d$	$-50.0 \pm 2.9^b$
7.0	$0.92 \pm 0.00^e$	$1.21 \pm 0.01^e$	$-64.3 \pm 3.0^a$

Different superscripts (a–e) in the same column represent significant differences between different samples at the  $p < 0.05$  level.

For understanding of the role of MCNCs when present at the particle-stabilised interface, we first evaluated the effects of pH on the behaviour of aqueous dispersions of MCNCs (1.0 wt%) ([appendix Fig. A5.3](#)), which demonstrated a significant decline in the magnitude of the  $\zeta$ -potential as the pH was decreased from pH 5.0 to pH 4.0. Behaviour of MCNCs in the aqueous dispersions and in the emulsions was not in complete agreement but the changes in  $\zeta$ -potential were similar within the pH range 4-5. This phenomenon might be due to the difference in alignment and concentrated coverage of the MCNCs at the emulsion droplet surface as compared to that in the bulk aqueous dispersions. In addition, as discussed in [Section 5.3.1.2](#), the high surface charge of the emulsions contributed by the MCNCs would guarantee strong

electrostatic repulsion to prevent droplet aggregation. At lower pH, the net negative charge was reduced, resulting in insufficient electrostatic repulsion to prevent closer approach of the oil droplets. As a consequence, there was droplet aggregation. The confocal images of the emulsion at pH 3.0 in [Figs. 5.5C1](#) and [5.5C2](#) clearly illustrate emulsion flocculation. Aggregation of the emulsion droplets was associated not only with the MCNCs on the droplet surface but also with the unadsorbed MCNCs in the aqueous phase. This might explain the decrease in the first peak of the size distribution, which represented the unadsorbed MCNCs, as explained in [Section 5.3.1.2](#). Interestingly, there was no sign of coalescence in the emulsions on pH adjustment. That is, weak electrostatic interaction of the droplets at low pH induced aggregation but did not cause desorption of the MCNCs.

Studies on Pickering emulsions stabilised by CNCs from various sources have also reported the same trend, in which the changes in the magnitude of the  $\zeta$ -potential were a function of pH ([Liu et al., 2018](#); [Mikulcov et al., 2018](#); [Wen, Yuan, Liang, & Vriesekoop, 2014](#)). However, in these studies, the authors did not characterise the microscopic structure of the Pickering emulsions under various pH conditions.

For a better understanding of the effects of pH, the bulk rheological properties of the emulsions at pH 7.0 and pH 3.0, hereafter referred to as emulsion E7.0 and emulsion E3.0 respectively, were determined by applying shear rates from 2 to 1000 s<sup>-1</sup> and then from 1000 to 2 s<sup>-1</sup> to the emulsions to observe hysteresis (if any) ([Fig. 5.5B](#)). In general, the viscosity of E3.0 was higher than that of E7.0 due to droplet flocculation at lower pH. In addition, the viscosities of the emulsions at both pHs decreased as the shear rate increased within the investigated shear rate ranges, exhibiting a slight

shear-thinning behaviour. Interestingly, both emulsions demonstrated negligible hysteresis within the range of shear rate investigated, indicating their stability during the shearing. In a previous study on Pickering emulsions stabilised by fumed silica, it was reported that the emulsions were stable against coalescence at a shear stress up to 1000 Pa and the emulsions reversed to its original state after the removal of the stress (Lee et al., 2014). However, this observation was in contrast to some other findings on Pickering emulsions stabilised by silica particles (French, Taylor, Fowler, & Clegg, 2015; Whitby & Krebsz, 2014; Whitby, Fischer, Fornasiero, & Ralston, 2011), where shearing from 0.1 to 1000 s<sup>-1</sup> resulted in droplet coalescence (Whitby, Fischer, Fornasiero, & Ralston, 2011). In our study, no such shear-induced droplet coalescence was observed. In our study, emulsions E7.0 and E3.0 had  $\zeta$ -potentials of -64.3 and -29.1 mV respectively. Sufficient negative charge of the emulsion droplets possibly prevented the droplets from coming in close vicinity and the higher mechanical strength of the MCNC-laden interface limited shear-induced coalescence.

#### 5.3.2.3. Ionic strength conditions

On exposure to different ionic strengths (0–150 mM NaCl), the emulsions were assessed using droplet sizing (Fig. 5.6A) and apparent viscosity (Fig. 5.6B) measurements to understand the flocculation behaviour. In addition, the frequency dependence of the curves of storage modulus ( $G'$ ) and loss modulus ( $G''$ ) (Fig. 5.6C) together with their corresponding confocal images (Fig. 5.6D and 5.6E) gave an understanding of the ion-induced evolution in the material properties of these Pickering emulsions. The MCNC-stabilised Pickering emulsions were highly sensitive to changes in ionic strength at a critical electrolyte concentration (threshold) of  $\geq 20$  mM NaCl (Fig. 5.6A and Table 5.3). The volumetric proportion of the second peak

increased significantly at the expense of the first peak. The average size  $d_{43}$  increased significantly from 1.21  $\mu\text{m}$  in the absence of added NaCl to 2.04 and 76.86  $\mu\text{m}$  at 20 and 100 mM NaCl respectively. Further increases in ionic strength did not lead to significant changes in the droplet size. In addition, the net surface charge of the emulsions decreased significantly from  $-64.3$  mV in the absence of added NaCl to  $-34.6$  and  $-18.6$  mV at 20 and 100 mM NaCl respectively (Table 5.3). It can be clearly seen that within the NaCl concentration range of 20-100 mM, addition of more electrolytes resulted in higher degree of reduction of net surface charge. This observation was due to salt induced electrostatic screening of droplet charge and eventually formation of aggregates, as clearly observed in Fig. 5.6D and 5.6E.

**Table 5.3.** Mean droplet sizes (population in the second peak and third peaks representing the emulsion-relevant sizes) and  $\zeta$ -potentials of emulsion E1.00 as a function of ionic strength. The values are the mean and standard deviation of at least three measurements on triplicate samples ( $n = 3 \times 3$ ).

NaCl concentration (mM)	$d_{32}$ ( $\mu\text{m}$ )	$d_{43}$ ( $\mu\text{m}$ )	$\zeta$ -Potential (mV)
0	$0.92 \pm 0.00^e$	$1.21 \pm 0.01^d$	$-64.3 \pm 3.0^a$
10	$0.93 \pm 0.01^e$	$1.23 \pm 0.01^d$	$-68.7 \pm 2.7^a$
20	$1.23 \pm 0.11^d$	$2.04 \pm 0.28^c$	$-34.6 \pm 2.6^b$
50	$1.85 \pm 0.25^c$	$4.01 \pm 0.78^b$	$-21.7 \pm 1.2^c$
100	$15.99 \pm 1.5^b$	$76.86 \pm 9.65^a$	$-18.6 \pm 2.3^d$
150	$26.76 \pm 2.22^a$	$86.78 \pm 8.17^a$	$-18.1 \pm 1.1^d$

Different superscripts (a–e) in the same column represent significant differences between different samples at the  $p < 0.05$  level.

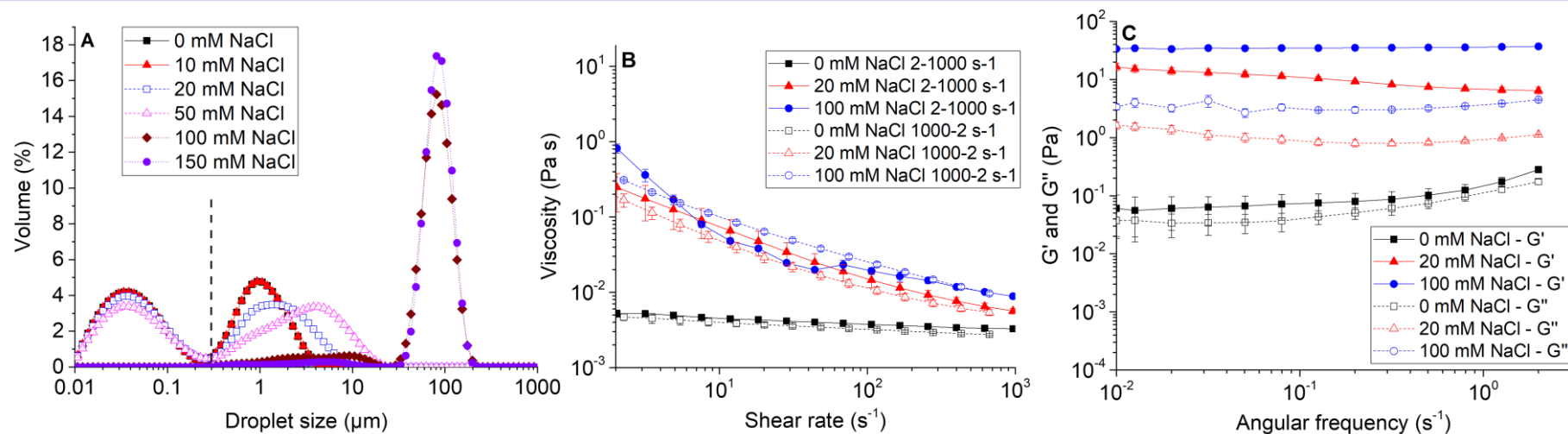


**Figure 5.6.** (A) Droplet size distributions of emulsion E1.00 at various ionic strengths, (B) apparent viscosities of emulsion E1.00 at 0, 20 and 100 mM NaCl at shear rates from 2 to 1000  $\text{s}^{-1}$  and then from 1000 to 2  $\text{s}^{-1}$ , (C) frequency sweep curves of storage ( $G'$ ) and loss ( $G''$ ) moduli of emulsion E1.00 at 0, 20 and 100 mM NaCl in the angular frequency range 0.01–2.0  $\text{s}^{-1}$  and at a strain of 1.0% and corresponding confocal micrographs at (D) 20 mM NaCl and (E) 100 mM NaCl (D1 and E1, Calcofluor-white channel; D2 and E2, merge channel of Calcofluor-white and Nile Red).

For comparative purposes, the  $\zeta$ -potentials of aqueous dispersions of 1.0 wt% MCNCs at various NaCl concentrations (0–150 mM) were also determined ([appendix Fig. A5.4](#)). The net surface charge of the aqueous dispersion of MCNCs decreased as a function of NaCl concentration from 0 to 100 mM but a further increase in concentration did not lead to any significant changes in the  $\zeta$ -potential. This trend agreed with the effects of ionic strength on the surface charge of the emulsion E1.00 droplets. This indicates that the behaviour of the MCNCs in the bulk phase at various ionic strengths may also influence the behaviour of the MCNCs at the droplet surface. The addition of electrolytes above the threshold of 20 mM NaCl will screen the charges associated with the cellulose molecules at the surface. This might result in a reduction in electrostatic repulsion, and van der Waals' interactions might dominate, leading to aggregation ([Boluk, Lahiji, Zhao, & McDermott, 2011](#); [Chau et al., 2015](#); [Prathapan, Thapa, Garnier, & Tabor, 2016](#); [Zhong, Fu, Peng, Zhan, & Sun, 2012](#)). Indeed, such aggregation of the MCNCs was evident in the confocal images of emulsion E1.00 at 20 mM NaCl ([Fig. 5.6D](#)). The decrease in the volumetric proportion of the first peak ([Fig. 5.6A](#)) was probably due to the utilisation of unadsorbed MCNCs to form bridges with the MCNCs adsorbed at the droplet surface, resulting in such aggregation. A further increase in the NaCl concentration to 100 mM led to the formation of a gel-like structure ([Fig. 5.6E](#)).

The apparent viscosities of the emulsions at 20 and 100 mM NaCl, hereafter referred to as emulsion E20 and emulsion E100 respectively, were also determined at shear rates from 2 to 1000 s<sup>-1</sup> (ramp up) and then from 1000 to 2 s<sup>-1</sup> (ramp down) ([Fig. 5.6B](#)). At both NaCl concentrations, the emulsions showed strong shear-thinning behaviour, with two orders of magnitude reduction in the apparent viscosity as a function of shear

---

rate. This may have been due to reversible shear-induced breakdown of the flocs, supporting the gel-like behaviour observed in the confocal micrographs (Figs. 5.6D and 5.6E). The changes in the viscosity of emulsion E20 when the shear rate was ramped up and then down within the range 2–1000 s<sup>-1</sup> were identical, showing no hysteresis (Fig. 5.6B). In contrast, the viscosity curve of emulsion E100 (ramp up) should be taken with some cautions as the emulsion E100 showed wall slip, most likely due to the higher stress required to shear this sample (data not shown). Particularly, during the ramp down, the apparent viscosity was higher in the region 10–100 s<sup>-1</sup> but lower at 2–5 s<sup>-1</sup>. At a shear rate of 2 s<sup>-1</sup>, the apparent viscosity of emulsion E100 was about 50% lower at the end of the ramp down than at the start of the ramp up, largely associated with the slip, latter leads to apparent decrease in the measured viscosity during ramp up (Franco, Gallegos, & Barn, 1998). Such pronounced slip might be associated the emulsion E100 gel-forming gel-like network at low shear rate. A similar phenomenon has been reported in previous studies (Kim, Song, Lee, & Park, 2003; Nandi, Khakhar, & Mehra, 2001; Schokker & Dalgleish, 1998; Whitby et al., 2011). Strong shearing may destroy the gel network (Kim et al., 2003). Although at higher shear rates, 100 to 1000 s<sup>-1</sup> and the corresponding downward shear rate sweep test overlap, the contribution of slip cannot be neglected. Such flow behaviour of E100 needs further attention in future studies using serrated geometry with rough surfaces (Sánchez, Valencia, Franco, & Gallegos, 2001). In our study, emulsion E20 was partially aggregated, i.e. some droplets were still well separated. In addition, emulsion E20 had a relatively high negative charge (–34.6 mV) (Table 5.3). In contrast, emulsion E100, as shown in Fig. 5.6E, was completely aggregated, meaning that the mobility of the droplets in the system was very restricted. Furthermore, emulsion E100 had quite a weak negative charge (–18.6 mV), approximately half that of emulsion E1.00 in the

absence of NaCl. Therefore, during the shearing, the ion-induced droplet network of emulsion E100 was prone to breakdown, caused by the shear-induced disruption of flocs, but the effect was largely reversible.

To understand the gel-like behaviour of these flocculated Pickering emulsions in the presence of ions, dynamic oscillatory measurements were performed (Fig. 5.6C). The response of the Pickering emulsions to the applied frequency was determined at a constant strain (1.0%) within the linear viscoelastic region. The dominance of  $G'$  over  $G''$  in Fig. 5.6C convincingly confirmed the elastic gel-like structure of the emulsion at NaCl concentrations of  $\geq 20$  mM, which is in agreement with the network-like structure in Fig. 5.6E. Such observations can be attributed to the flocculation of droplets through the sharing of MCNC particles at the interface, as discussed above. The formation of an elastic network can also be explained by the tight packing of droplets that is associated with the charge screening by ions. As expected, the first peak in the size distribution almost disappeared when the NaCl concentration was  $\geq 100$  mM (Fig. 5.6A), which suggested that the unadsorbed MCNCs in the bulk phase associated strongly with the MCNCs at the interface, where the droplets behaved as 'active fillers' (Torres, Murray, & Sarkar, 2016). Interestingly, although sensitive to aggregation, the emulsions as a whole were resistant to coalescence. This might be associated with the fact that the rod-shaped MCNCs in the bulk phase had a strong tendency to collectively form a 'space-filling isotropic gel' (Oguzlua, Danumah, & Boluk, 2017) in the presence of ions that were somehow entrapping the droplets in a gel-like network, preventing further inter-droplet interactions.

### 5.3.3. *In vitro* digestion of modified CNCs-based emulsions

#### 5.3.3.1. *Microstructural fate of the emulsions – gastric digestion*

Pickering emulsions stabilised by 1.0 wt% MCNCs had  $d_{32}$  and  $d_{43}$  values of 0.92 and 1.21  $\mu\text{m}$  respectively (Table 5.2). The freshly prepared emulsions had a bimodal particle size distribution, with the first peak ranging from around 0.01 to 0.30  $\mu\text{m}$  and with the second peak being distributed in the narrow droplet size range of 0.30–6.31  $\mu\text{m}$ . The first peak was associated with unadsorbed MCNCs in the aqueous phase. The emulsions had a homogeneous distribution of droplets, as shown in the CLSM images, with most droplets being well separated and covered by a thin layer of MCNCs (Fig. 5.7A). In addition, the emulsions were negatively charged at both pH 7.0 and the gastric pH of 3.0 (–68.7 mV and –30.1 mV respectively) (Fig. 5.8), in line with a previous report (Sarkar et al., 2017). The high negative charges ensured sufficient electrostatic repulsion between the emulsion droplets to prevent aggregation, as shown in the CLSM image in Fig. 5.7A. On exposure to SGF buffer, the droplet size increased by approximately eight times ( $p < 0.05$ ), with the second peak showing broadening and with the simultaneous appearance of a third peak at around 100  $\mu\text{m}$ ; the first peak remained in the same size range but with a lower volumetric proportion (Fig. 5.7B).

The confocal images of the emulsion–SGF buffer mixture in Fig. 5.7B clearly demonstrate flocculation of the oil droplets. Such an increase in droplet size suggests flocculation. The reduction in the volumetric proportion of the first peak demonstrates the involvement of the unadsorbed MCNCs in the droplet aggregation as shown in section 5.3.1 or involvement of MCNCs to create smaller droplets (Qiu-Hong Chen, Tong-Xun Liu, & Chuan-He Tang, 2019). Our observation was in line with the results

---

of previous studies that have reported the aggregation of oil droplets stabilised by modified or unmodified CNCs at low pH (Le et al., 2020; Liu et al., 2018; Mikulcov, Bordes, Minarik, & Kasparkov, 2018) and the formation of a gel-like structure at high ionic strengths (Chau et al., 2015; Le et al., 2020; Prathapan, Thapa, Garnier, & Tabor, 2016). In the current study, the simultaneous effects of pH 3.0 and the ionic strength of the gastric conditions led to a significant screening of charges and a reduction in the  $\zeta$ -potential to  $-14$  mV, compared with  $-30.1$  and  $-68.7$  mV for the freshly prepared emulsion at pH 3.0 and pH 7.0, respectively (Fig. 5.8). Consequently, the repulsive forces between the droplets were not sufficient to prevent droplet aggregation. However, droplet coalescence was not observed in the emulsion–SGF buffer mixture.

Cellulose is known to be not responsive to human proteolytic enzymes such as pepsin (Sarkar et al., 2019), which was the main reason for using this interfacial material for the delivery of SCFAs in this study. As expected, the addition of pepsin did not alter the droplet size of the emulsions significantly ( $p < 0.05$ ) and the overall microstructure showed no droplet coalescence (Fig. 5.7C), similar to that of the emulsion–SGF buffer (Fig. 5.7B). Preliminary works (data not shown) showed that 20 wt% O/W emulsions stabilised by pepsin (1.0 wt%) had  $\zeta$ -potential value of  $-3.3$  mV at pH 3.0. Thus, pepsin would be electrostatically repelled from the anionic MCNC-stabilised emulsions. The  $\zeta$ -potential data also showed no obvious change on the addition of pepsin ( $p > 0.05$ ) compared with the emulsion–SGF buffer (Fig. 5.8). In addition, the confocal images in Fig. 5.7C showed similar droplet aggregation to that in Fig. 5.7B, confirming the limited contribution of pepsin to the gastric flocculation of MCNC-stabilised emulsions, which is in contrast to most protein-stabilised emulsions, which are highly susceptible to interfacial proteolysis (Sarkar et al., 2009, 2017; Torres et al., 2019).

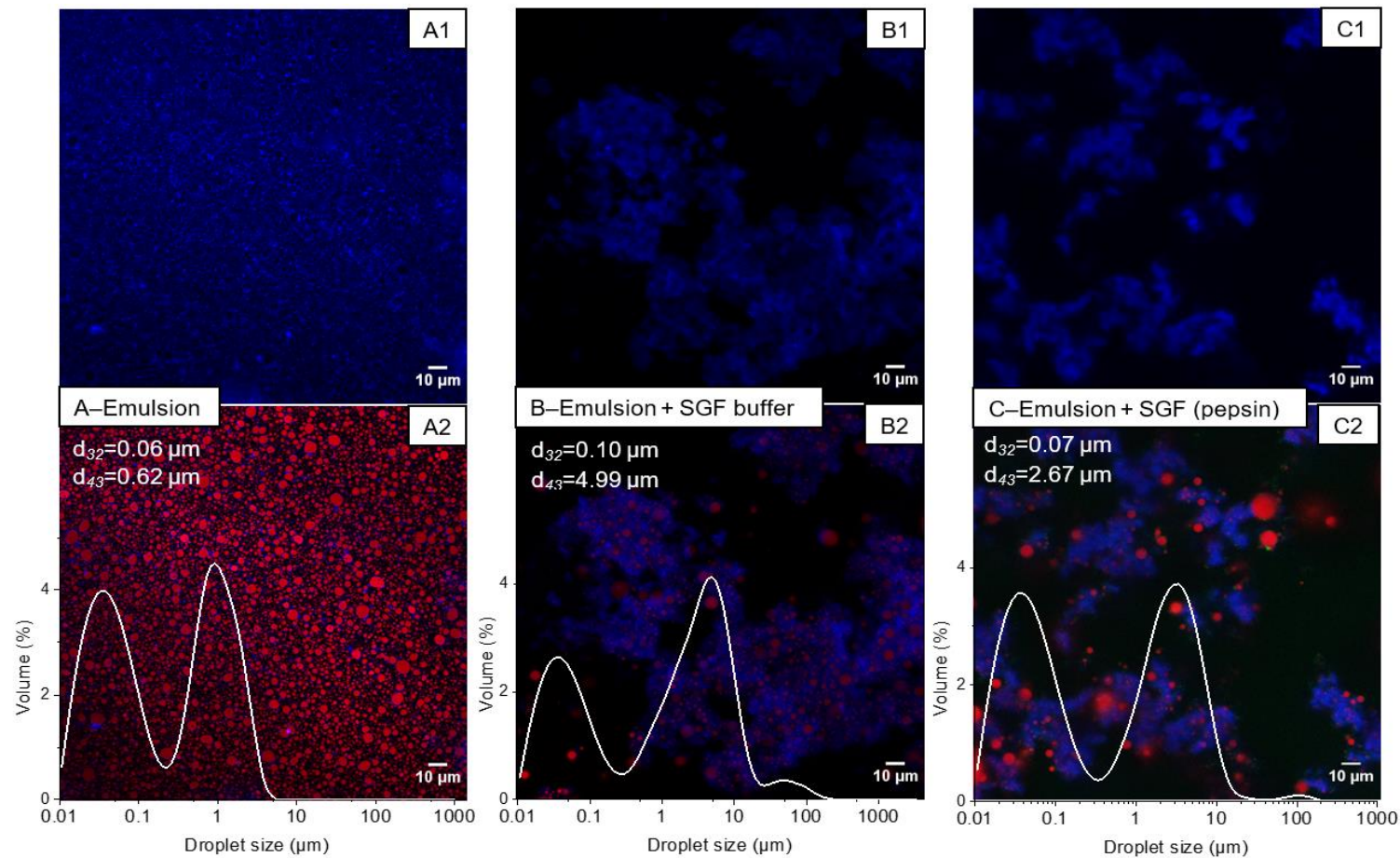


**Figure 5.7.** Confocal images of (A) freshly prepared emulsion at pH 7.0, (B) mixture of freshly prepared emulsion and SGF buffer at pH 3.0 without the addition of pepsin and (C) mixture of freshly prepared emulsion and SGF buffer at pH 3.0 with the addition of pepsin after 2 h of incubation at 37 °C (A1, B1 and C1: MCNC channels; A2, B2 and C2: merged channels of MCNCs, pepsin and oil droplets); blue colour represents the MCNCs, green colour represents the pepsin and red colour represents the oil phase; the insets provide the corresponding droplet size distribution,  $d_{32}$  and  $d_{43}$ , values of the emulsion or digesta.

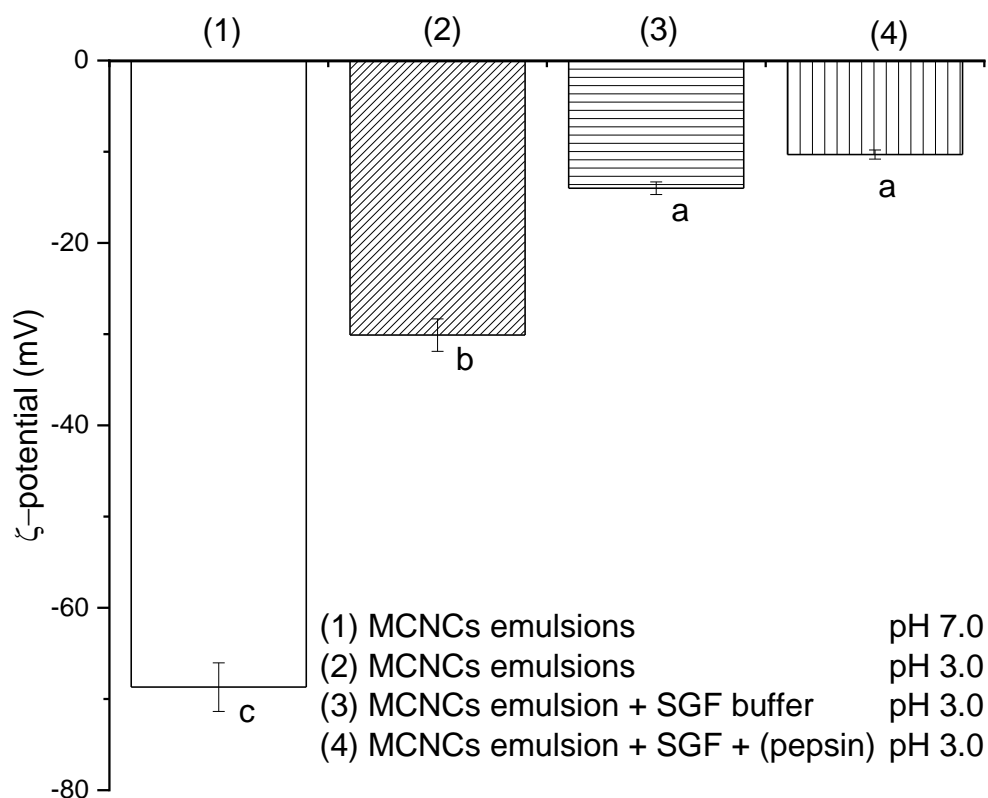


**Figure 5.8.** Mean  $\zeta$ -potential values of freshly prepared emulsion (pH 3.0 and pH 7.0) and mixtures of freshly prepared emulsion and SGF buffer at pH 3.0 without and with the addition of pepsin after 2 h of incubation at 37 °C (pH 3.0). Error bars represent the standard deviations. Different superscripts (a–c) represent significant differences at the  $p < 0.05$  level.

The effects of SGF buffer, without and with the addition of pepsin, on the rheological properties (apparent viscosity, elastic modulus and viscous modulus) of the emulsions were determined ([appendix Fig. A5.5](#)). Freshly prepared emulsions with 10 wt% oil had a low viscosity and Newtonian behaviour. The presence of SGF buffer with or without pepsin led to significant changes in the rheological properties of the emulsion. For example, at a shear rate of  $10 \text{ s}^{-1}$ , the viscosity increased by approximately 27

times (Fig. A5.5A), which was due to floc formation under the SGF conditions, in line with a previous study (Le et al., 2020). In addition, the elastic and viscous moduli presented in Fig. A5.5B clearly demonstrate the formation of a gel-like structure; the elastic modulus was approximately 10 times higher than the viscous modulus and there was little frequency dependence of the two moduli (Ikeda & Nishinari, 2001). In summary, it appears that the electrostatic charge screening of the emulsion droplets was the main mechanism behind the flocculation under gastric conditions.

### 5.3.3.2. Microstructural fate of the emulsions – intestinal digestion

#### *a) Bypassing gastric digestion*

The purpose of this intestinal digestion was to understand the ability of Pickering emulsions on their own to protect SCFAs in the intestine. Therefore, freshly prepared emulsions were diluted twice (10 wt% oil) and subsequently used for intestinal digestion without going through the gastric stage. Three different systems were used for this intestinal digestion: emulsion–SIF buffer; emulsion–SIF buffer containing bile salts; emulsion–SIF buffer containing bile salts and pancreatin. Fig. 5.9A shows that the addition of SIF buffer slightly increased the average size ( $d_{43}$ ) of the emulsion droplets (Fig. 5.7A). The confocal image demonstrated some degree of droplet flocculation but the majority of the droplets were still well separated. In addition, the  $\zeta$ -potential of the emulsions decreased significantly from  $-68.7$  mV (freshly prepared emulsion) to  $-47.8$  mV in the emulsion–SIF mixture.

The aggregation of the emulsion droplets was due to the reduction in the electrostatic repulsion in the presence of electrolytes. Similar observations have been reported in

---

previous studies ([Chau et al., 2015](#); [Le et al., 2020](#); [Prathapan et al., 2016](#)). In addition, SIF contains divalent cations ( $\text{Ca}^{2+}$  ions), which might induce ion bridging between MCNCs adsorbed on to different droplets. Such ion binding could have resulted in a more viscous shear-thinning structure compared with the freshly prepared emulsions ([appendix Figs. A5.5 and A5.6](#)).

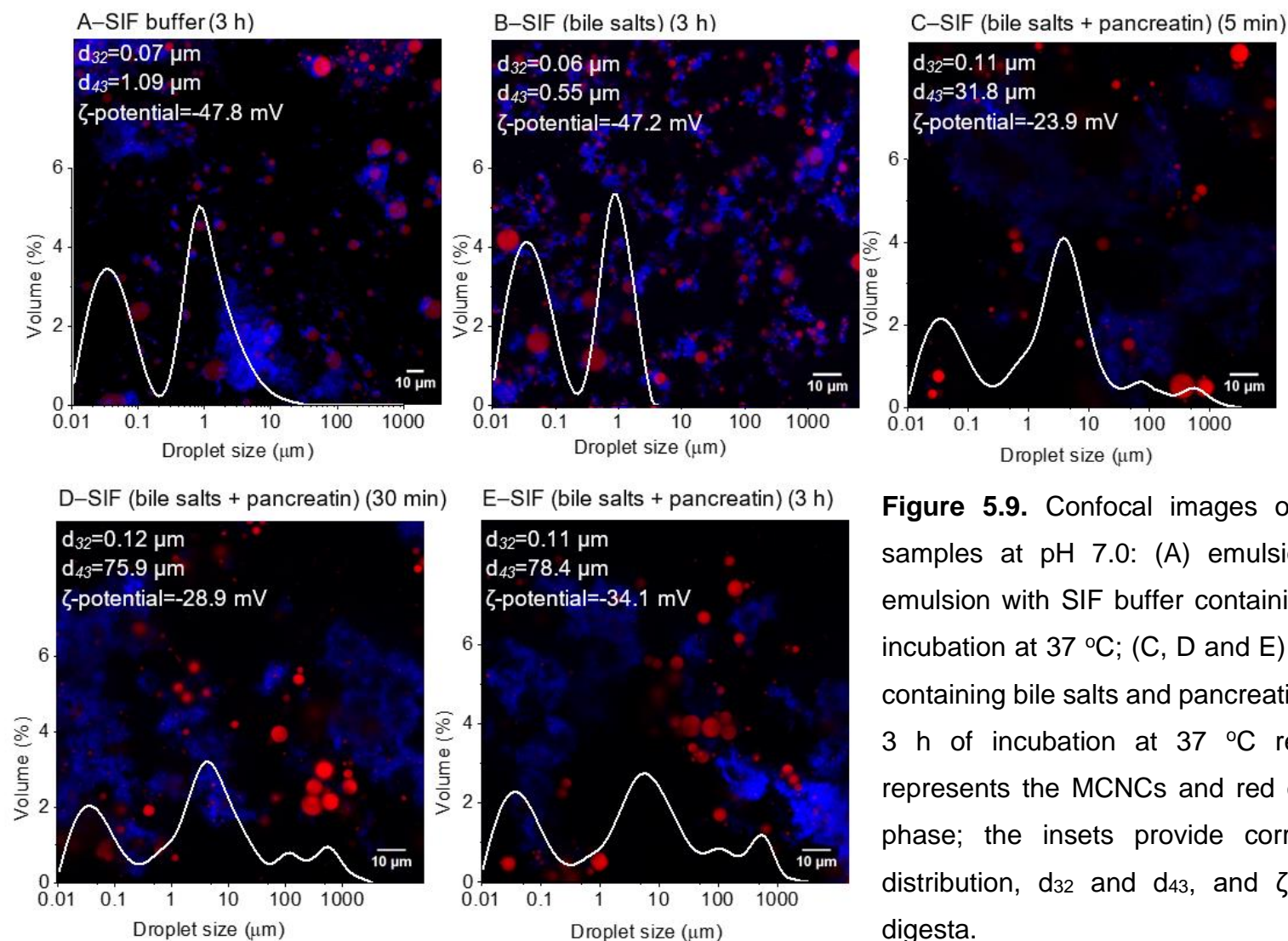


**Figure 5.9.** Confocal images of the intestinal-digested samples at pH 7.0: (A) emulsion with SIF buffer; (B) emulsion with SIF buffer containing bile salts after 3 h of incubation at 37 °C; (C, D and E) emulsion with SIF buffer containing bile salts and pancreatin after 5 min, 30 min and 3 h of incubation at 37 °C respectively; blue colour represents the MCNCs and red colour represents the oil phase; the insets provide corresponding droplet size distribution,  $d_{32}$  and  $d_{43}$ , and  $\zeta$ -potential values of the digesta.

The addition of bile salts had limited effect on the  $\zeta$ -potential and the overall microscopic structure remained unchanged. In addition, the apparent viscosity did not change in the presence of bile salts (Fig. A5.6). The confocal image in Fig. 5.9B clearly shows that, in the presence of bile salts, most oil droplets were still remained within the MCNC-stabilised shell and that small aggregates of several oil droplets that had formed through treatment with the buffer remained. This suggests that the displacement by bile salts of MCNCs adsorbed on to the droplet surface was rather restricted.

Two main factors may have contributed to the resistance of the MCNCs to bile salt displacement. The first and the most important factor was the high desorption energy of the MCNC-laden interface (Sarkar et al., 2016a; Wu & Ma, 2016; Zoppe, Venditti, & Rojas, 2012). It is noteworthy that MCNCs with  $r \approx 20$  nm (the width is taken as the radius given that the MCNCs lie flat at the interface) at a contact angle of  $86^\circ$  at the oil–water interface (typical value of  $\gamma_{ow} \approx 50$  mN m<sup>-1</sup>) will have a desorption energy ( $\Delta E = \gamma_{ow}\pi r^2(1 - |\cos\theta|)^2$ ) of nearly  $10^5 k_B T$ , where  $k_B$  is the Boltzmann constant and  $T$  is the temperature in Kelvin. Thus, it is unlikely that bile salts can overcome such high energies and thus they cannot displace MCNCs from the interface. Surface charge could be the second factor for the emulsion stability in the presence of bile salts. Under SIF conditions (pH 7.0), both the MCNCs and the bile salts had negative charges. It has been reported that a 20 wt% O/W emulsion stabilised by bile salts (1.0 wt%) had a  $\zeta$ -potential of around  $-46$  mV at pH 7.0 (Sarkar et al., 2016b). However, MCNCs contain hydroxyl, sulphate and OSA groups in their backbones, which make them negatively charged at pH 7.0. Thus, it is highly likely that MCNCs will repel anionic bile salts from the vicinity of negatively charged emulsion droplets. A similar observation was reported in a previous study (Sarkar, Li, Cray, & Boxall, 2018), in which the

authors investigated the duodenal digestion of O/W emulsions stabilised by protein coated with unmodified CNCs as primary and secondary layers respectively.

The addition of pancreatin significantly increased the droplet size ( $d_{43}$ ) of the emulsions, changing the droplet distribution from bimodal to trimodal (Fig. 5.9C). After 5 min of incubation in SIF containing bile salts and pancreatin, the  $d_{43}$  of the emulsions increased 50-fold from 0.62  $\mu\text{m}$  (freshly prepared emulsion) or 0.55  $\mu\text{m}$  (emulsion + SIF containing bile salts) to 31.8  $\mu\text{m}$  ( $p < 0.05$ ), whereas the apparent viscosity of the digesta remained unchanged (appendix Fig. A5.7). The confocal image in Fig. 5.9C shows the presence of some larger coalesced droplets, corroborating the third peak in the size distribution, but the majority of the droplets were still encapsulated by MCNCs or trapped within the droplet aggregates. Therefore, the significant increase in size was probably due to both droplet flocculation and some degree of coalescence. Pancreatin addition also resulted in a significant increase in the  $\zeta$ -potential to  $-23.9$  mV, compared with  $-47.2$  mV in the systems without pancreatin (Fig. 5.9B). After 30 min of incubation in SIF containing pancreatin and bile salts, the  $d_{43}$  value increased to 75.9  $\mu\text{m}$  (Fig. 5.9D), i.e. twice the size at 5 min, and the confocal image demonstrated a higher degree of coalescence, suggesting that the lipolysis was not complete within the first 5 min. After 3 h of digestion (Fig. 5.9E), although there was a high degree of coalescence, a significant proportion of the droplets were still intact inside the aggregates. The increase in the negative  $\zeta$ -potential ( $-34.1$  mV), compared with that after 5 min (Fig. 5.9C) ( $p < 0.05$ ), might be attributed to the release of lipid digestion products, such as fatty acids and mono- and/or diglycerides, that accumulated on the droplet surface. Similar observations on the changes in surface charge have been reported in previous studies (Sarkar et al., 2018; Wilde & Chu,

2011). Although the Pickering emulsions were capable of resisting bile salt displacement, they did not prevent lipolysis of the oil droplets. This might be expected as the size of the interfacial pores at the MCNC-coated droplets might be an order of magnitude greater than the 2.5-nm-sized lipase molecules (Sarkar et al., 2016a), allowing easy access of lipase to the lipidic substrate.

*b) With gastric digestion – sequential gastrointestinal digestion*

The emulsions were first subjected to gastric digestion and then the gastric digesta were used for an intestinal digestion in SIF buffer without and with bile salts, and with both bile salts and pancreatin. Fig. 5.10A shows that the droplet size became smaller after 3 h of incubation in SIF buffer, compared with the gastric digesta (Fig. 5.7C). The confocal image also revealed the presence of aggregates, which were smaller than those in the gastric digesta (Fig. 5.7C). A possible explanation for this observation was the change in pH, which allowed the  $\zeta$ -potential to increase from  $-10.4$  mV in the gastric digesta (pH 3.0) to  $-19.8$  mV in the presence of SIF buffer (pH 7.0). As a result, the repulsive forces between the emulsion droplets increased, allowing better separation of the droplets. However, the  $\zeta$ -potential of the gastric digesta in SIF was significantly lower ( $p < 0.05$ ) than that in the sample without gastric digestion ( $-47.8$  mV) (Fig. 5.9A). In other words, gastric digestion affected the surface properties of the emulsions and, even after changing the pH, some of the flocculated droplets did not revert to their original individual droplets. In addition, it should be noted that these gastric digesta in SIF contained electrolytes of both the SGF and the SIF; non-gastric-digested samples contained only SIF ions, explaining the lower  $\zeta$ -potential in the gastric-digested system.

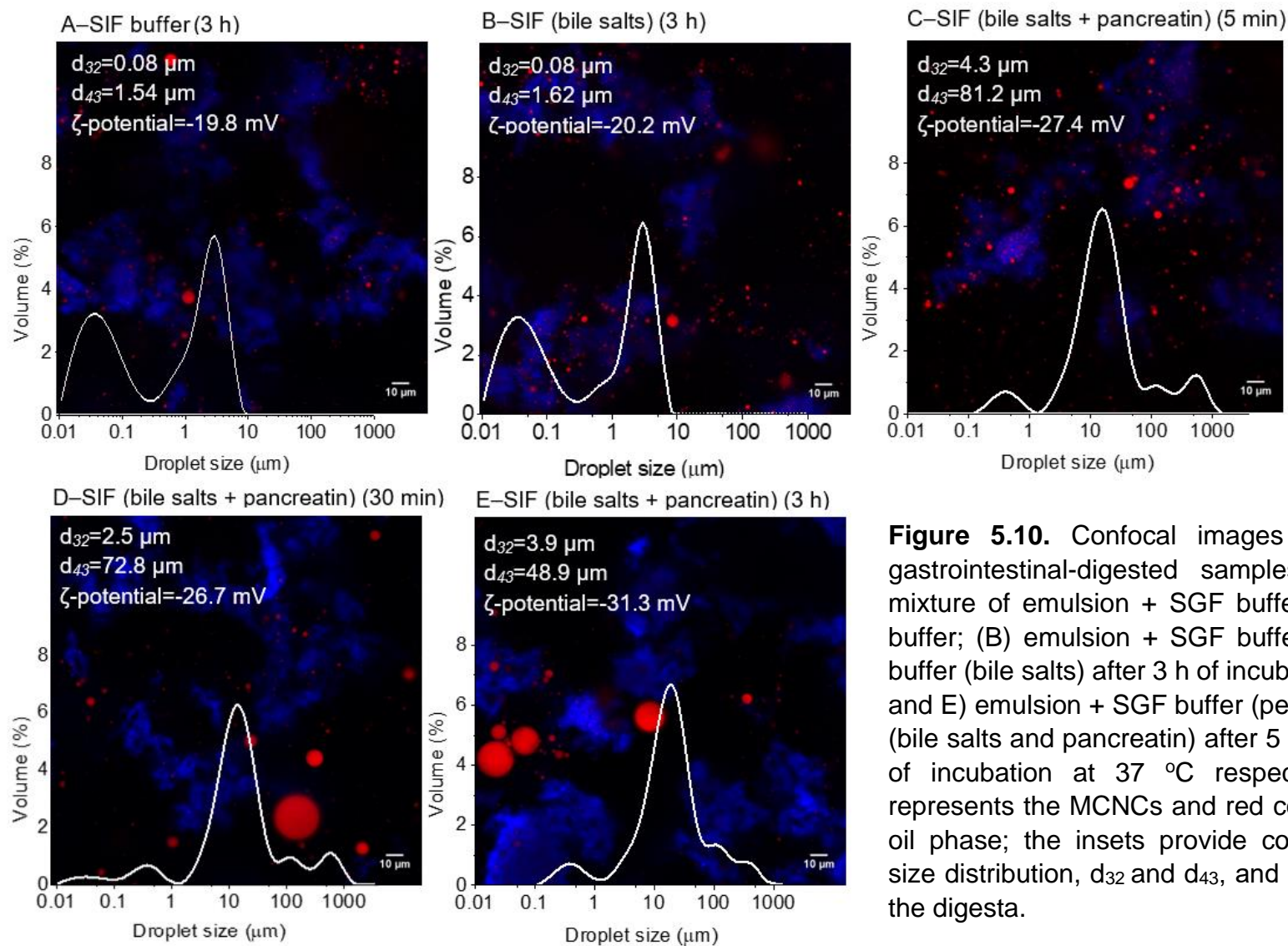


**Figure 5.10.** Confocal images of the sequential gastrointestinal-digested samples at pH 7.0: (A) mixture of emulsion + SGF buffer (pepsin) with SIF buffer; (B) emulsion + SGF buffer (pepsin) with SIF buffer (bile salts) after 3 h of incubation at 37 °C; (C, D and E) emulsion + SGF buffer (pepsin) with SIF buffer (bile salts and pancreatin) after 5 min, 30 min and 3 h of incubation at 37 °C respectively; blue colour represents the MCNCs and red colour represents the oil phase; the insets provide corresponding droplet size distribution,  $d_{32}$  and  $d_{43}$ , and  $\zeta$ -potential values of the digesta.

---

The addition of bile salts did not influence the size,  $\zeta$ -potential, microscopic structure (Fig. 5.10B) and apparent viscosity of the gastric digesta (appendix Fig. A5.7). This observation was in line with the results reported in section 5.3.3.2.a, again confirming the resistance of MCNCs to bile salt displacement. The presence of pancreatin altered the droplet size, surface charge and microscopic structure (Figs. 5.10C–5.10E) dramatically but did not significantly alter the apparent viscosity (Fig. A5.7). The effects of pancreatin that were observed in these gastric-digested samples were similar to those observed in the gastric-bypassed samples but with a smaller change in absolute values. Qualitatively, after 30 min of incubation in SIF, the  $\zeta$ -potential of the gastric digesta remained unchanged ( $p > 0.05$ ) compared with that at 5 min. Although the droplet size increased dramatically after 5 min of digestion, increasing the incubation time further did not alter the droplet size significantly ( $p > 0.05$ ). In addition, the confocal images did not show any difference in the degree of coalescence (Figs. 5.10C–5.10E).

### **5.3.3.3. Kinetics of fatty acid release and short-chain triglyceride hydrolysis**

To quantitatively observe the kinetics of total FFA (including long- and short-chain fatty acids) release in the intestinal phase, titration was employed, followed by fitting with a theoretical model; the release of individual SCFAs, including PA and BA, was quantified by GC. In addition, the degree of lipolysis was determined through quantification of short-chain triglycerides, i.e. TP and TB. Typical GC profile of a sequential gastrointestinal-digested sample after 10 min of digestion is reported in Fig. A5.8 (appendix). Fig. 5.11 show Intestinal lipolysis profiles of the emulsions with or without passing through the gastric phase during *in vitro* digestion.

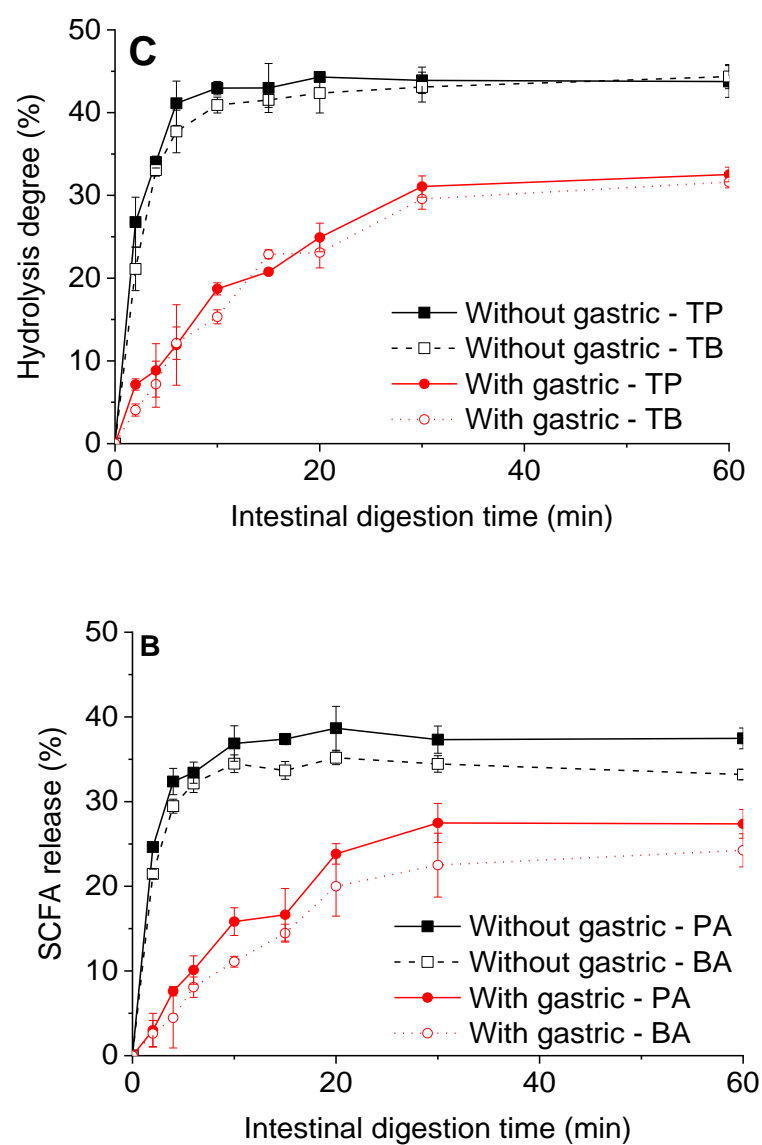


**Figure 5.11.** Intestinal lipolysis profiles of the emulsions (experimental and theoretically fitted model) with or without passing through the gastric phase during in vitro digestion: (A) kinetics of total FFAs were determined by titration; (B) release of individual SCFAs (PA and BA) was quantified by GC; (C) hydrolysis proportions of TP and TB were analysed by GC. Error bars represent the standard deviations.

[Fig. 5.11A](#) shows that the Pickering emulsions prepared using MCNCs without going through the gastric route had a relatively slow rate of initial lipid digestion as compared to other Pickering emulsion systems, such as those stabilized by protein-based particles. For instance, the  $k$  value ( $0.046 \mu\text{mol s}^{-1} \text{m}^{-2}$ ) was nearly 10-fold lower in this study using MCNCs as Pickering stabilizers compared to that observed in case of proteinaceous-microgel particle-stabilized Pickering emulsions ( $0.31 \mu\text{mol s}^{-1} \text{m}^{-2}$ ) ([Sarkar et al., 2016a](#)). It should also be noted that this initial rate of lipolysis of 1 wt% MCNC-stabilised emulsions is in line with the values reported in the literature when CNCs (3 wt%) were used as a secondary layer to coat protein-stabilised emulsions ([Sarkar et al., 2018](#)). This highlights that CNCs, when modified and presented directly at the interface, provide a better barrier to the diffusion of lipase to the droplet surface than the proteinaceous Pickering stabilisers or protein–CNC composite interfacial layers studied previously.

Of more importance is that gastric digestion had a significant effect on the degree and the rate of FFA release ([Fig. 5.11A](#)). In the first 10 min, up to 27.5% FFAs were produced in freshly prepared emulsions whereas the release was around 3-fold lower for the gastric-digested emulsions. From the initial hydrolysis period obtained from the fitted parameters as described in [section 4.2.5](#), freshly prepared emulsions that bypassed the gastric route were digested significantly faster than their gastric-digested counterparts ([Table 5.4](#)). Passing through gastric digestion increased the overall hydrolysis half time by around 9 min and decreased the maximum FFA release by 27% ([Table 5.4](#)). The delay of the lipolysis after exposing the emulsion to gastric digestion was due to the formation of aggregates and consequently a reduction in the droplet surface area. Our results are in line with a previous study ([Golding et al., 2011](#)),

in which the authors also highlighted that the rate of intestinal lipolysis was significantly influenced by changes in the droplet surface area that were induced at the gastric stage. In addition to the reduction in surface area, the MCNC-led flocculation also played an important role in trapping a high proportion of the oil droplets inside the aggregates (Figs. 5.10C–5.10E), with extra protection from lipase, helping to delay the digestion. The flocculation in the gastric phase thus reduced the available surface area for lipase to bind to and probably created a barrier to the droplets that were trapped inside the aggregates. Also, it is also possible that the packing of droplets within the aggregates might have reduced the available interfacial pores in which lipase could diffuse or from which lipolytic products (e.g. FFAs, mono- and/or diglycerides) could diffuse out to the aqueous media for analysis by the pH-stat technique.

**Table 5.4.** Kinetic parameters of the intestinal digestion during *in vitro* gastrointestinal digestion.

	$k$ ( $\mu\text{mol s}^{-1} \text{m}^{-2}$ )*	$\Phi_{max}$ (%)	$t_{1/2}$ (min)
With gastric digestion	0.001752 (0.00006090)	20.8 (0.09842)	10.98
Without gastric digestion	0.04608 (0.001039)	28.6 (0.07093)	1.93

\*Data in parentheses represent the standard errors of the estimates.

$k$ , lipid conversion rate per unit area of the droplet surface.

$\Phi_{max}$ , maximum total FFA level.

$t_{1/2}$ , lipolysis half time.

The results in [Fig. 5.11B](#) show a similar pattern to that in [Fig. 5.11A](#). It is worth noting that there was a significant difference between the release of FFAs ([Fig. 5.11A](#)) and the release of SCFAs ([Fig. 5.11B](#)). During the intestinal digestion, SCFA release was approximately 5–7% higher than FFA release. The difference was due to various lipolysis rates of the different triglycerides, depending on the fatty acid chain length, which has been explained in [section 4.3.3](#). The release patterns of PA and BA were almost identical, with slightly more release of PA (2–3% higher) than of BA.

Even though the patterns of TP and TB hydrolysis ([Fig. 5.11C](#)) were similar to those of the fatty acid release seen in both [Fig. 5.11A](#) and [Fig. 5.11B](#), the hydrolysis proportions of the two short-chain triglycerides were around 5–8% higher than the release proportions of the corresponding SCFAs. In this study, the proportions of short-chain triglyceride hydrolysis were quantified based on the difference between the amounts of short-chain triglycerides present in the emulsions before and after the intestinal digestion. For SCFAs, the release proportion was quantified with the hypothesis that one triglyceride molecule would produce two molecules of corresponding SCFAs. However, it seems that a small proportion of TP and TB produced only one molecule of SCFAs.

## 5.4. Conclusions

This study showed that OSA-modified CNCs have excellent emulsifying capacity because of a significant increase in hydrophobicity, which resulted in partial wettability by an oil phase without the need for an additional surfactant. Pickering O/W emulsions (20 wt% oil) stabilised by 1.0 wt% MCNCs had very small droplet sizes (1.22  $\mu\text{m}$ ) relative to those in other studies, and they resisted phase separation for up to 4 weeks of storage under refrigerated conditions. The emulsions were sensitive to aggregation at  $\text{pH} < 4.0$  and at ionic strength higher than 20 mM NaCl. The formation of aggregates under these conditions was associated with a reduction in electrostatic repulsive forces between the droplets. These aggregated emulsions at low pH and high ionic strength responded differently under shearing conditions; in particular, emulsions at higher ionic strength ( $\geq 20$  mM NaCl) had a prominent gel-like character. Nevertheless, the emulsions were strongly resistant to coalescence under all pH and ionic strength conditions investigated, which might be associated with the formation of a thick and dense layer of MCNCs around the oil droplets as well as with the MCNCs in the bulk phase forming strong bridges with the MCNCs at the interface, resulting in a gel-like network that reduced the mobility of the droplets.

The study also demonstrated that Pickering O/W emulsions stabilised by MCNCs were prone to flocculation in a gastric environment. The formation of aggregates was due to a reduction in the electrostatic repulsive force between the emulsion droplets, which was induced by low pH and high ionic strength. Under intestinal conditions, the lipolysis rates were associated with a reduction in the droplet surface area because of gastric structuring, with the gastric-digested emulsions being digested more slowly than freshly prepared emulsions. In addition, electrostatic repulsion of MCNCs to bile

salts and the high desorption energy of the MCNCs particles were responsible for the resistance to bile salt displacement, which occurred in the initial stage of the digestion process. The resistance of the MCNC-stabilised emulsion to lipolysis shows its suitability as a delivery system for SCFAs. The responsiveness of these emulsions to gastrointestinal conditions, as shown in this study, might allow the development of novel foods that can deliver other bioactive compounds to target regions of the digestive tract.

---

## Chapter 6 - *In vivo* digestion of SCFA-supplemented emulsions using cannulated pigs

---

### Abstract

This research aimed to deliver TP and TB as sources of PA and BA respectively into the colon using an O/W (20 wt% oil) emulsion stabilised by CT-HM PEC (2.5 wt%). To investigate the delivery capacity of the system, an *in vivo* study using ileal-cannulated pigs was undertaken. Twelve pigs were randomly divided into experimental and control groups (n = 6; average body weight, BW, of  $69.2 \pm 5.2$  and  $68.7 \pm 6.3$  Kg) and they were fed with either a diet enriched in TP and TB via CT-HM PEC emulsion, or a control diet with SCFA-free CT-HM PEC emulsion. A static *in vitro* digestion study with the same emulsion system was also conducted to compare with the *in vivo* study.

The *in vitro* results showed no significant impact of gastric digestion on the microscopic structure of the emulsion; SCFA release and lipolysis were both less than 5%. Under the *in vitro* intestinal digestion, the emulsion droplets showed some degree of coalescence that led to the SCFA release and lipolysis of approximately 40%. However, the *in vivo* study demonstrated lipolysis degree of around 51-53%, while the SCFA release was only 15% at the intestinal phase. The main reason for this observation was the absorption of the SCFAs within the small intestine. Therefore, SCFA release in the collected ileal digesta was significantly lower than the hydrolysis of TP and TB. Also, the production of SCFAs was also observed in the ileal digesta of the control group, which was due to the fermentation of pectin and other carbohydrates

presence in the control diet. In the faeces, TP and TB was not detected, while the concentrations of PA and BA in both experimental and control groups were not significantly different. A high proportion of short-chain triglycerides remained after the *in vivo* intestinal digestion (~ 47–49%), indicating successful delivery of around half of SCFAs into the colon. The emulsion shows promise not only in the use of the PEC-based emulsions for the colon-targeted delivery of SCFAs for future human study but also for delivery of other bioactive compounds.

## 6.1. Introduction

SCFAs are important functional metabolites. Recent clinical evidence has shown that they play an important role in the prevention of the metabolic syndrome, bowel disorders and certain types of cancer (Besten, et al., 2013; Gurav, et al., 2015; Tan, et al., 2014; Venegas, et al., 2019). SCFAs are fermentation products of non-digestible carbohydrates, such as pectin and inulin by gut microbiota. They consist of six or less carbon molecules of which acetic acid, PA and BA are the main products of the fermentation (95% of the total SCFAs) (Besten, et al., 2013). In addition, the total amount and their relative proportions vary depending on the sources of the carbohydrates in the diet while PA and BA are the most effective acids in terms of gut-related disease prevention (Boets, et al., 2015; Brestenský, et al., 2016; Knudsen, Jørgensena, & Theil, 2016; Tan, et al., 2014; Wang, et al., 2017). Therefore, delivering PA and BA in the colon might be a good nutritional strategy to achieve therapeutic benefits.

To date, oil-in-water (O/W) emulsions using surfactant emulsifiers (inulin, gamma-cyclodextrin, soy protein isolate and whey protein isolate) are the most common systems for the delivery of SCFAs to the colon (Donovan, Bauer, Jr, & Lee, 2017; Donovan, Cadwallader, & Lee, 2016; Donovan, Lee, & Lee, 2016). However, in these studies, only a limited proportion of the SCFAs was eventually delivered to the colon. For instance, the *in vitro* gastrointestinal digestion of spray-dried TB-loaded powder demonstrated a release of approximately 94% butyric acid before reaching the colonic regime (Donovan, et al., 2017). This was attributed to the enzymatic hydrolysis of the TB in the small intestinal phase.

In [Chapter 3](#), it was shown that the O/W (10 wt% oil) emulsion systems stabilised by CT-HM PEC ( $\geq 2.5$  wt%) could protect up to 60% PA (as a SCFA model) from the *in vitro* gastrointestinal digestion prior reaching the colon. The result shows potential application of the system for colon-targeted delivery of SCFAs. In this chapter, we further investigated the system using an *in vivo* study with an ileal-cannulated pig model that has been used in many previous studies due to similarity of the gastrointestinal digestion between pigs and humans ([Hooda, Metzler-Zebeli, Vasanthan, & Zijlstra, 2011](#); [Le, Buchet, Beltranena, Gerrits, & Zijlstra, 2017](#); [Montoya, Rutherford, & Moughan, 2016](#); [Montoya, Saigeman, Rutherford, & Moughan, 2016](#)).

Regarding the use of emulsifiers in this study, it is also worth to noting that although the Pickering emulsion stabilised by MCNCs reported in [Chapter 5](#) shows a strong promise for future applications, the use of MCNCs is not yet approved for use in animal and human consumption. Therefore, CT-PEC was chosen for these experiments. An O/W (20 wt% oil, mixture of TP, TB and SO) emulsion stabilised by CT-HM PEC (2.5 wt%) was used for the *in vivo* study. The oil concentration was doubled as compared to that used in [Chapter 3](#) to improve the bioactive loading of the emulsions. As the oil phase composition was changed from the [Chapter 3](#), a static *in vitro* digestion of the emulsion was conducted to compare with the *in vivo* study. To our knowledge, this is the first study that investigated the relevance of *in vitro* and *in vivo* studies of a vehicle system for delivery of SCFAs into the colon.

---

## 6.2. Materials and methods

### 6.2.1. Materials

Food-grade TP (glyceryl tripropionate  $\geq 97.1\%$ ), TB (glyceryl tributyrate  $\geq 97.1\%$ ), porcine pepsin (P7000,  $\geq 250$  units/mg solid), porcine bile extract (B8631), porcine pancreatin (P7545, 8  $\times$  USP), analytical-grade TP, TB, TV, PA, BA and CA were purchased from [Sigma-Aldrich Co. LLC, USA](#). High-methoxyl PEC from citrus peel was supplied by [Herbstreith & Fox KG, Germany](#). SO was obtained from a local market in [Palmerston North, New Zealand](#). SO was used directly for producing O/W emulsions without treatment. Other chemicals (NaCl, NaOH, NaHCO<sub>3</sub>, KCl, KHCO<sub>3</sub>, KH<sub>2</sub>PO<sub>4</sub>, MgO, MgCl<sub>2</sub>(H<sub>2</sub>O)<sub>6</sub>, CaCO<sub>3</sub>, CaCl<sub>2</sub>(H<sub>2</sub>O)<sub>2</sub>) and TiO<sub>2</sub> were supplied by [Sigma-Aldrich Co. LLC, USA](#). Milli-Q water (electrical resistance of 18.2 M $\Omega$ .cm at 25 °C) was purified by a [Milli-Q apparatus, Millipore Corp., USA](#). Acetate buffer (pH 5.5) was made from glacial acetic acid ([Merck KGaA, 64271 Darmstadt Germany](#)) and milli-Q water.

For preparation of the pig diet, food-grade ingredients were provided by different suppliers in New Zealand, i.e. starch and sugar ([Davis Trading, Palmerston North](#)), grain bread ([Countdown, Palmerston North](#)), vitamin mineral mix ([Nutritech International, Auckland](#)), casein and whey powder ([Fonterra, Palmerston North](#)).

### 6.2.2. Preparation of the emulsion

The experimental emulsion was made by blending oil phase (TP-TB-SO mixture with a weight ratio of 1:1:2) with PEC solution (2.5 wt%) at a 2:8 weight ratio to obtain a final oil concentration of 20 wt%. For the control emulsion, the oil phase (SO only) was blended with PEC solution (2.5 wt%) at a 1:8 weight ratio. Homogenisation steps were carried out similar to the procedure reported in [Section 3.2.4](#).

### 6.2.3. Static *in vitro* GI digestion and fermentation

*In vitro* gastrointestinal digestion of the experimental emulsion was conducted using the static INFOGEST digestion protocol (Minekus, et al., 2014) as described in Section 3.2.6.

The *in vitro* fermentation was carried out using a pig faecal inoculum as previously described (Montoya, Rutherford, et al., 2016). In short, fresh faeces samples were collected from five healthy pigs into isolated containers flushed with CO<sub>2</sub> at 37°C. The pig faecal inoculum was prepared by blending the faeces with 0.1 M-phosphate buffer at pH 7 (1:5, w/v). The homogenate was then filtered to remove undissolved residue. Inoculum (5 ml) was added to a McCartney bottle containing 1 g of intestinal digesta collected from the *in vitro* digestion. All the bottles were flushed with CO<sub>2</sub>, capped and incubated with the pig inoculum for 38 h at 37°C. After incubation, samples were taken and transferred into an aliquot (2 ml) to an Eppendorf tube, which placed in ice. The samples were used for analysis of TP and TB that was described in section 6.2.6. SCFAs were not quantified due to significant evaporation during the incubation period of 38 h.

### 6.2.4. *In vivo* assay using ileal-cannulated pigs

An *in vivo* study was undertaken using 12 female ileal-cannulated pigs. Ethics approval was obtained from the Massey University Animal Ethics Committee, Protocol No. 19/103.

Twelve pigs cannulated (simple T-cannula) at the terminal ileum were randomly allocated to 2 different diets (n = 6 pigs/diet) and kept individually in 1.5 × 1.5-m cages.

---

The location of cannula is illustrated in [Fig. 6.1](#). The simple T-cannula has a lid that was used to collect digesta.

The experimental group (BW of  $69.2 \pm 5.2$  Kg) was fed with a mixture of grain bread, basal diet and the experimental emulsion at a weight ratio of 10.8:3.4:1.0. The composition of the basal diet is presented in [Table 6.1](#).  $\text{TiO}_2$  was introduced into the basal diet as an inert marker, which was then used to calculate the dilution factor.

The control group (BW of  $68.7 \pm 6.3$  Kg) was fed with a mixture grain bread, basal diet and the control emulsion at a weight ratio of 10.8:3.4:0.9. The daily ration was 8% of the metabolic BW ( $\text{BW}^{0.75}$ ) and fed to the pigs as 2 equal meals at 8:00 am and 17:00 pm for 7 days. Fresh water was freely available. Ileal digesta were continuously collected over a 7-h period starting 1 h after feeding on days 5 and 6. The ileal digesta were collected in plastic bags that were changed every 30 min. The collected bags were immediately stored in a  $-20^\circ\text{C}$  freezer to minimize further digestion. The ileal digesta was then used for analysis of SCFAs, short-chain triglycerides and  $\text{TiO}_2$ .

For analysis of microscopic structure, the digesta collected 5 h after feeding was used immediately for observation in a confocal microscope. The faecal samples were taken on days 6 and 7 by collecting fresh faeces at around 1-4 h after feeding. The faecal samples were also placed in plastic bags and immediately covered by dry ice. For long-term storage, all the faecal samples were transferred into a  $-80^\circ\text{C}$  freezer before analysis of SCFAs, triglycerides and  $\text{TiO}_2$ .

**Table 6.1.** Basal diet compositions (g/kg dry matter)

Ingredient	<i>g/kg dry matter</i>
Grain bread	760.6
Wheat flour	74.9
Soybean Oil	37.4
Casein	32.7
Wheat gluten meal	24.5
Whey powder	24.5
Dicalcium phosphate	18.7
Skim milk powder	8.1
KHCO <sub>3</sub>	7.5
CaCO <sub>3</sub>	2.2
NaHCO <sub>3</sub>	2.2
Lysine	1.5
Vit/Min Premix <sup>1</sup>	1.5
MgO	0.7
TiO <sub>2</sub>	3.0

<sup>1</sup> Contains in the final diet: Ca 461 mg.kg<sup>-1</sup>; Cu 10 ppm; I 1.3 ppm; Fe 125 ppm; Mn 60 ppm; Se 0.3 ppm; Zn 100 ppm; niacin 44 mg; vitamin B12 0.03 mcg; pantothenic acid 24 mg; riboflavin 6.6 mg; vitamin K 1.4 mg; biotin 0.44 mg; vitamin A 11 IU; vitamin D3 2.2 IU; vitamin E 66 IU; pyridoxin 0.24 mg; folate 1.6 mg and thiamin 0.24 mg.

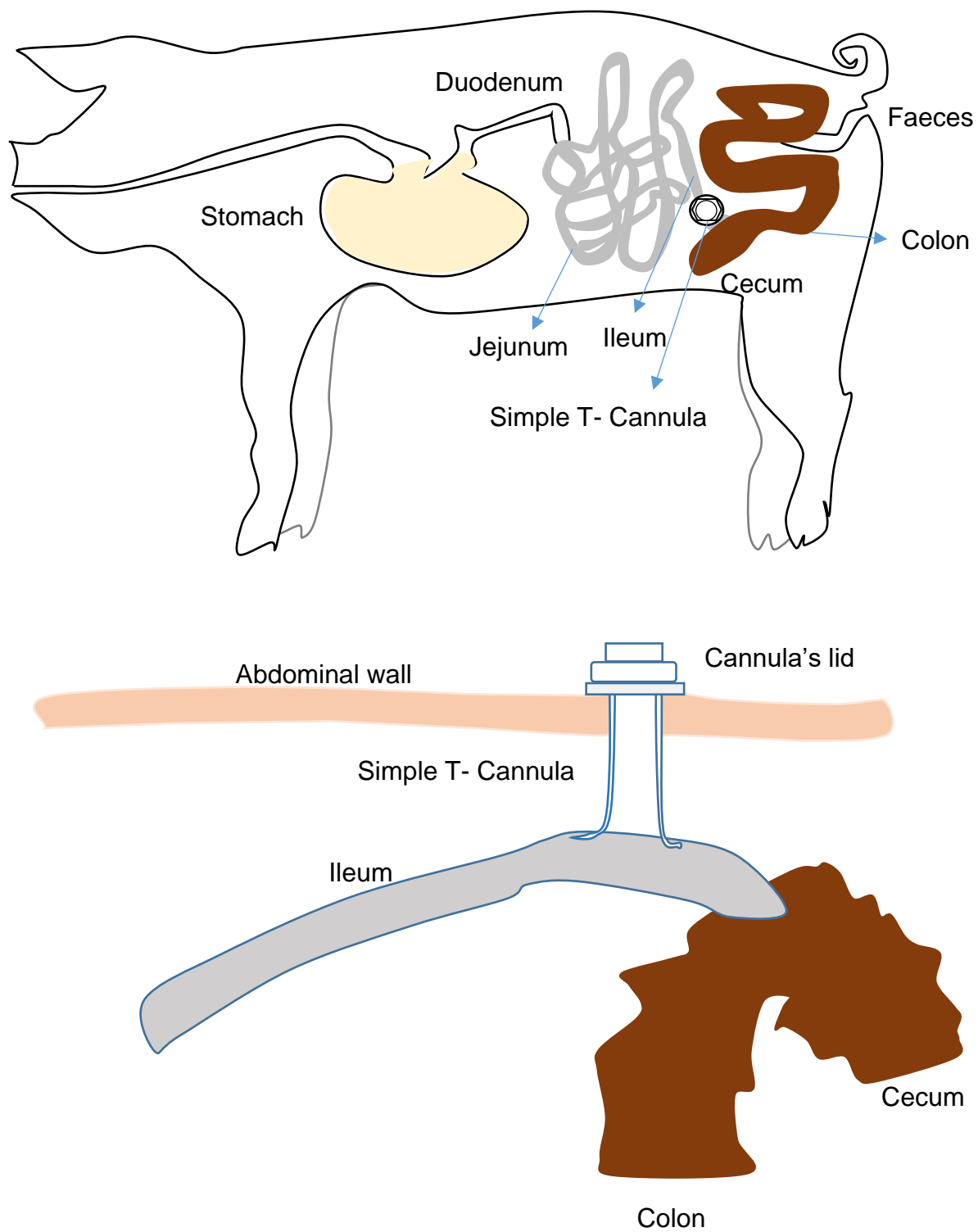


**Figure 6.1.** Diagrams of an ileal cannulated pig

### 6.2.5. Characterisation of the O/W emulsions and digesta

The emulsions and digesta samples were characterised using droplet size and  $\zeta$ -potential measurements, and the microstructure was determined using confocal laser scanning microscopy. The analysis of size and  $\zeta$ -potential were described in [Section 3.2.7](#).

CLSM images of the emulsions and the digesta (*in vitro* and *in vivo*) were taken at 25°C using a [Leica SP5 DM6000B](#) Scanning Confocal Microscope equipped with 3 tunable PMT detectors. Each 1000  $\mu\text{L}$  of the sample was added to a 1.5 mL Eppendorf tube followed by 20  $\mu\text{L}$  of Nile Red (1 mg/mL in methanol). The mixture was vortexed for 10 seconds and equilibrated for 10 min before depositing 20  $\mu\text{L}$  onto a slide. Approximately 20  $\mu\text{L}$  of calcofluor white (1 wt% in water) was added onto the sample and mixed gently with a pipet tip, then covered with a coverslip.

### 6.2.6. Quantification of TP, TB, BA and PA

#### *Homogenisation of the samples*

Frozen samples (digesta and faeces) were defrosted at 4°C for approximately 48h. Samples from different plastic bags of the same pig were mixed manually and subsequently taken for analysis.

#### *GC analysis*

TP, TB, PA and BA contents of the emulsions and defrosted digesta were measured using the GC methods as described in [Section 3.2.8](#) and [Section 3.2.9](#). The faecal samples were diluted with mili-Q water 3 times and then analysed similar to digesta

samples. TV and CA were used and external standards for analysis of short-chain triglycerides and SCFAs respectively.

### 6.2.7. Quantification of TiO<sub>2</sub>

#### *Sample preparation*

Frozen samples (diets, digesta and faeces) were freeze dried to yield powder. The obtained powder was then ground with an electric grinder to achieve a powder size that passed through the 1 mm-size mesh.

#### *Analytical method*

TiO<sub>2</sub> contents of the diets, digesta and the faeces were determined by a spectrophotometric method (Short, Gorton, Wiseman, & Boorman, 1996) with slight modifications. In short, triplicate aliquots (~100 mg) of each sample were ashed in porcelain crucibles for 13 h at 580°C. Subsequently, 2 mL of milli-Q water was added to each crucible upon cooling, followed by 10 mL of concentrated H<sub>2</sub>SO<sub>4</sub> (7.4 M). All the samples were then boiled at 200°C for approximately 90 min. After cooling, the solutions were transferred quantitatively into 10 mL volumetric flasks, then adjusted the whole volume to 10 mL by milli-Q water. Aliquots (1 mL) of the resulting solutions were measured on a spectrophotometer at 410 nm. A standard curve was prepared by a standard solution (0.5 mg.mL<sup>-1</sup> TiO<sub>2</sub>) using the same procedure.

### 6.2.8. Statistical analysis

Analysis of variance (ANOVA) was conducted using Minitab® version 17.3.1 to detect overall significant differences (p < 0.05).

## 6.3. Results and discussion

### 6.3.1. *In vitro* digestion of the PEC-based emulsions

Fig. 6.2 shows that the emulsion had a monomodal droplet size distribution with a size range of around 10–60  $\mu\text{m}$ . Average sizes ( $d_{32}$  and  $d_{43}$ ) of the emulsions were 21.8 and 23.4  $\mu\text{m}$  respectively, which were  $\sim 3$  times larger than sizes reported in Chapter 3. The main reason for this size change was due to higher oil content (20 wt%) of this emulsion as compared to that used in Chapter 3 (10 wt%). A previous study (Schaaf, Schütz, & Karbstein, 2017) demonstrated similar size range of the emulsion droplets when O/W (30 wt%) emulsions were prepared from CT-HM PEC (1.0 wt%). However, another study (Verkempinck, et al., 2018) reported smaller size range ( $<30 \mu\text{m}$ ) of an 5% (w/v) carrot-enriched olive O/W emulsion stabilised by CT-HM PEC 1.0 wt%. In addition to the influence of the oil content, PEC concentrations and sources might also be associated with the obtained droplet size.

Confocal images of the emulsion are shown in Fig. 6.2, in which A represents the Calcofluor-white channel (PEC) and B illustrates the merged channels of Calcofluor-white and Nile Red (oil droplets). Most droplets in the emulsion appeared to be fully covered by PEC with distinctive layers of PEC on the surface. In addition, thick layers of PEC adsorbed at the O/W interface were observed in most of the oil droplets. Previous studies (Funamia, et al., 2007; Ngouémazong, Christiaens, Shpigelman, Loey, & Hendrickx, 2015) suggested that the formation of thick layers of adsorbed PEC through the interaction of rhamnogalacturonan-I in the pectin backbones. However, these studies did not show any evidence at such a microscopic level as that seen in the current study. To our knowledge, this is the first study that clearly shows

microscopic evidence of thick PEC layer adsorbed at the O/W interface. In this study, the  $\zeta$ -potential of the emulsion was -18.2 mV, which was similar to that reported in Chapter 3.

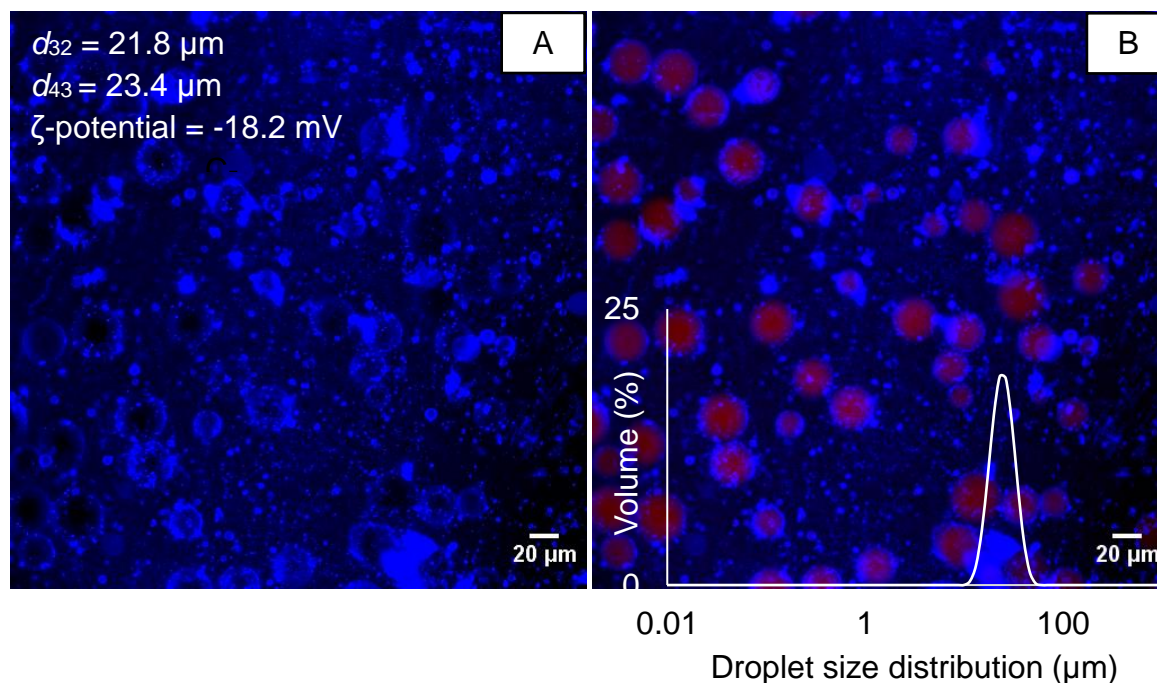


**Figure 6.2.** Confocal images of PEC-based O/W emulsion: A, PEC channel; B, merge channel of PEC and oil droplets. The red colour represents the oil phase (stained by Nile Red); the blue colour represents the PEC (stained by Calcofluor-white).

The results in Fig. 6.3A and Table 6.2 show high stability of the emulsions during *in vitro* gastric digestion. The confocal image in Fig. 6.3A clearly shows that most oil droplets were distributed evenly in the emulsions without sign of droplet flocculation or coalescence. Clear distinctive layers of PEC on the interface were observed in most droplets, and the difference in the  $\zeta$ -potential before and after the gastric digestion was not significant ( $p \geq 0.05$ ). In addition, the release of SCFAs and hydrolysis were less than 5% (Table 6.3). Similar observation was also reported in Chapter 3. High stability of the emulsion under gastric conditions was due to resistance of PEC to pepsinolysis (Mudgil & Barak, 2013; Sarkar, Li, Cray, & Boxall, 2018). When gastric lipase was

included in the SGF, the lipid hydrolysis under gastric *in vitro* conditions was around 5.6–22.6%, depending on the sources of gastric lipase and the type of lipid substrates (Bourlieu, et al., 2014; Capolino, et al., 2011; Pafumi, et al., 2002; Sassene, et al., 2016)

**Table 6.2.** Mean droplet sizes and  $\zeta$ -potentials of the emulsion, *in vitro* gastric and intestinal digesta. The values are the mean and standard deviation of at least three measurements on triplicate samples ( $n = 3 \times 3$ ).

	$d_{32}$ ( $\mu\text{m}$ )	$d_{43}$ ( $\mu\text{m}$ )	$\zeta$ -Potential (mV)
Fresh emulsion, pH 3.0	....	....	$-1.99 \pm 0.34^a$
Fresh emulsion, pH 7.0	$21.8 \pm 0.2^b$	$23.5 \pm 0.2^c$	$-18.2 \pm 1.00^b$
Gastric digesta	$21.7 \pm 0.3^b$	$23.4 \pm 0.1^c$	$-2.3 \pm 0.27^a$
Intestinal digesta (5 min)	$27.6 \pm 0.1^a$	$35.5 \pm 1.0^b$	$-20.7 \pm 1.60^{bc}$
Intestinal digesta (30 min)	$28.5 \pm 0.5^a$	$49.6 \pm 4.6^a$	$-19.6 \pm 1.00^b$
Intestinal digesta (3 h)	$29.1 \pm 0.3^a$	$52.9 \pm 2.3^a$	$-23.9 \pm 1.21^c$

Different superscripts (a–e) in the same column represent significant differences between different samples at the  $p < 0.05$  level. Droplet sizes of the fresh emulsion were only measured using water as dispersion medium (pH 7.0).

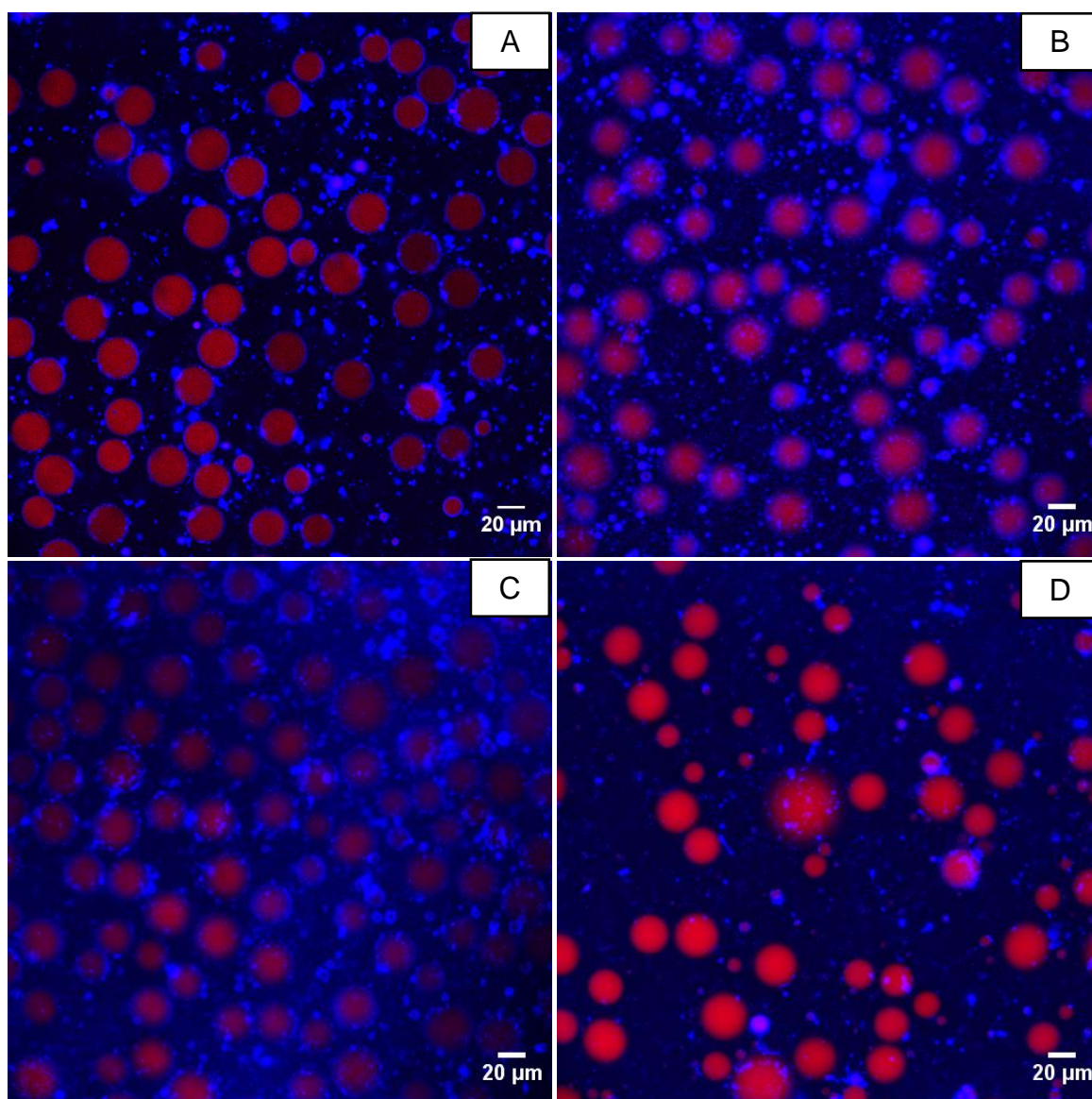


**Figure 6.3.** Confocal images of the *in vitro* gastric and intestinal digesta (A) gastric digesta after 2 h incubation at 37 °C and pH 3.0; (B, C and D) the intestinal digesta after 5 min, 30 min and 3 h of incubation at 37 °C and pH 7.0 respectively; blue colour represents the PEC (stained by Calcofluor white) and red colour represents the oil phase (stained by Nile red).

**Table 6.3.** SCFAs and triglyceride profiles after *in vitro* gastric digestion (2 h), intestinal digestion (3 h) and fermentation (38 h)

	Gastric digestion		Intestinal digestion		Fermentation	
	Concentration [mg/mL]	Hydrolysis/release (%)	Concentration [mg/mL]	Hydrolysis/release (%)	Concentration [mg/mL]	Hydrolysis/release (%)
PA	0.37 ± 0.02 <sup>b</sup>	2.63 ± 0.11 <sup>a</sup>	2.92 ± 0.16 <sup>b</sup>	42.35 ± 0.67 <sup>a</sup>	Analysis was not done due to evaporation of SCFAs in 38h fermentation	
BA	0.41 ± 0.07 <sup>b</sup>	2.93 ± 0.51 <sup>a</sup>	2.85 ± 0.08 <sup>b</sup>	40.50 ± 1.07 <sup>a</sup>		
TP	25.80 ± 0.49 <sup>a</sup>	0.73 ± 1.34 <sup>a</sup>	13.55 ± 0.64 <sup>a</sup>	41.05 ± 5.66 <sup>a</sup>	Undetected by GC	....
TB	24.87 ± 0.98 <sup>a</sup>	1.13 ± 1.73 <sup>a</sup>	13.17 ± 0.62 <sup>a</sup>	45.55 ± 2.56 <sup>a</sup>	Undetected by GC	....

Different superscripts (a–b) in the same column represent significant differences between different samples at the  $p < 0.05$  level.

In contrast to the gastric digestion, the droplet sizes and  $\zeta$ -potential of the emulsion were significantly impacted by the *in vitro* intestinal digestion. During the first 5 min, the emulsion structure remained stable. Although sizes ( $d_{32}$  and  $d_{43}$ ) increased  $\sim 1.3$  and 1.5 times respectively (Table 6.2), the overall structure of the emulsion remained unchanged with clear layers of PEC covering most oil droplets without any sign of coalescence (Fig. 6.3B). In addition,  $\zeta$ -potential of the emulsion did not change significantly, which was attributed to a high proportion of PEC remaining at the O/W interface.

After 30 min, the average droplet sizes ( $d_{32}$  and  $d_{43}$ ) were  $\sim 1.3$  and 2.1 times larger compared to those of the freshly prepared emulsion. Such increase in  $d_{43}$  was due to the presence of a new small peak in a size range of larger than 100  $\mu\text{m}$  (Fig. 6.4). However, the emulsion microstructure was not significantly different to that at 5 min. Also, the  $\zeta$ -potential remained unchanged. This observation indicates a strong resistance of PEC to bile-salt displacement in the first 30 min of the *in vitro* intestinal digestion. After 3 h digestion, the average droplet sizes ( $d_{32}$  and  $d_{43}$ ) increased 1.3- and 2.3-fold as compared to those of the freshly prepared emulsions. Such changes in the droplet size after the intestinal digestion of pectin-based emulsions were also reported in a previous study (Verkempinck, et al., 2018). In that work, the droplet size ( $d_{43}$ ) of emulsions stabilised by 1.0 wt% pectin (82% DM) increased 4.6 times after 2 h of intestinal digestion. Higher extent of size change observed by Verkempinck, et al. (2018) was probably due to the lower PEC concentration used by these researchers.

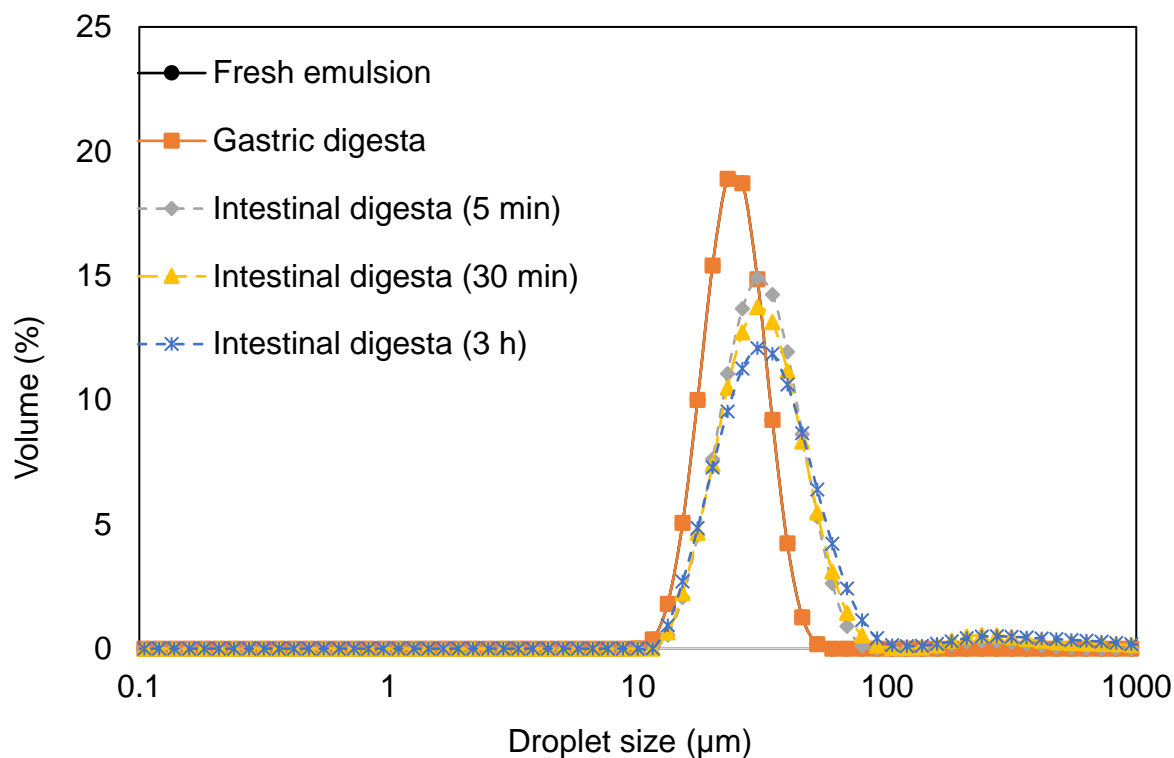


**Figure 6.4.** Droplet size distribution of the fresh emulsion, *in vitro* gastric and intestinal digesta (5 min, 30 min and 3 h).

The confocal image in Fig. 6.3C showed a certain degree of coalescence, as a consequence of displacement of high proportion of adsorbed PEC by bile salts. However, the image also showed a certain proportion of intact oil droplets with almost full coverage of PEC. The  $\zeta$ -potential of the emulsion became more negative after 3-h digestion ( $p < 0.05$ ). This can be attributed to the production of fatty acids and di- and/or monoglycerides accumulating on the droplet surface as well as the adsorbed bile salts (Sarkar, et al., 2018; Wilde & Chu, 2011). As can be seen in Table 6.3, 3-h intestinal digestion led to the triglyceride hydrolysis of 41.05–45.55 % and SCFA release of 40.50–42.35 %. Similar figures were also reported in Chapter 3. In a previous work (Donovan, et al., 2017), it was reported that more than 90% of TP encapsulated by WPI and gamma-cyclodextrin (GC) was digested under *in vitro*

intestinal digestion. The low degree of hydrolysis observed in our study was due to the resistance of PEC to enzymatic hydrolysis and bile-salt displacement as discussed in [Chapter 3](#).

In this study, the intestinal digesta was then collected and used for an *in vitro* fermentation with pig faecal inoculum for 38 h as described in [section 6.2.3](#). As can be seen in [Table 6.3](#), triglycerides were not detected by GC analysis. This evidence shows the complete hydrolysis of triglyceride after 38 h incubation.

### 6.3.2. *In vivo* digestion and fermentation of the PEC-based emulsion

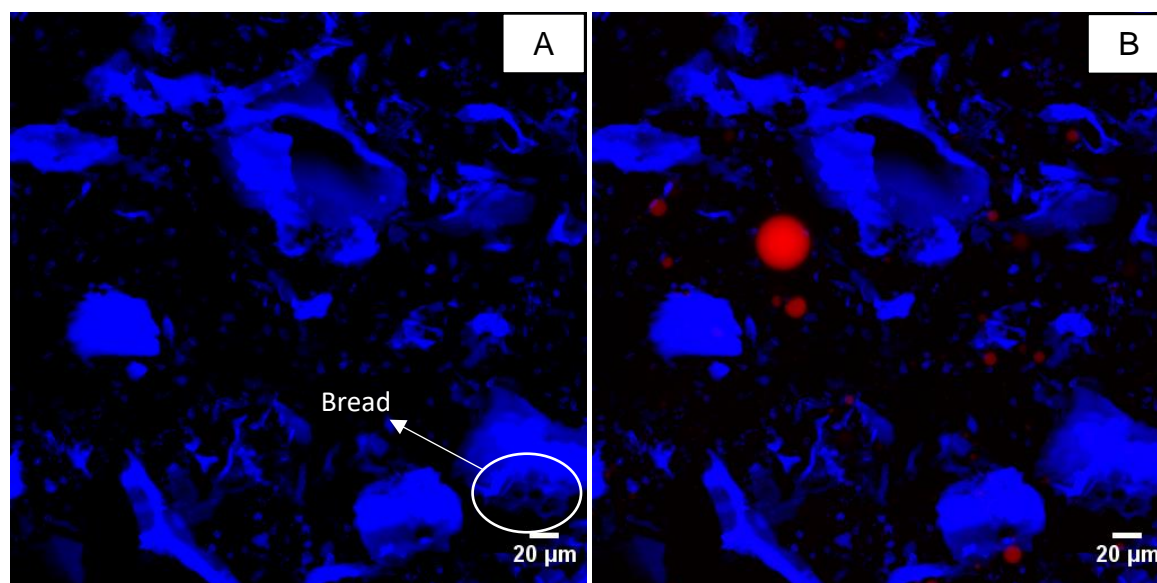


**Figure 6.5.** Confocal images of the *in vivo* intestinal digesta (A: carbohydrate channel; B: merge channel of carbohydrates and oil droplets). The digestion was collected 5 h after feeding the cannulated pigs. Blue colour represents the carbohydrates in the digesta such as cellulose, lignin, PEC, etc (stained by Calcofluor white) and red colour represents the oil phase (stained by Nile red).

In this *in vivo* study, gastric digesta was not collected. As reviewed by [Wilde, et al., \(2011\)](#), the degree of lipolysis in *in vivo* human gastric digestion is approximately 30%. [Fig. 6.5](#) shows the microscopic structure of the *in vivo* intestinal digesta from the experimental diet which was collected 5 h after feeding the pigs. [Fig. 6.5A](#) represents the Calcofluor-white channel (PEC and other carbohydrates) and [Fig. 6.5B](#) illustrates the merged channel of Calcofluor-white and Nile Red (oil droplets).

[Fig. 6.5B](#) clearly shows the presence of a low population of intact oil droplets. In the fresh diet that was used to feed the pigs, the total oil content (from basal diet and added PEC-based emulsions) was accounted for only 3.85% the whole diet. Based on the quantification of the inert marker (TiO<sub>2</sub>), the diet was diluted ~ 2.5 times upon reaching the ileum. Therefore, only a small proportion of oil droplets (~1.5%) would reach the ileum. However, the presence of oil droplets was a clear evidence of delivery of some SCFA into the colon.

It is also worth noting that adsorbed PEC at the O/W interface was not clearly seen in [Fig. 6.5B](#). Calcofluor white is not a specific dye for PEC and it could bind to  $\beta$  1-3 and  $\beta$  1-4 polysaccharides, such as found in cellulose and chitin ([Harrington & Hageage, 2003](#)). Other carbohydrates that were present in the ileal digesta, such as cellulose and starches might interfere with the PEC staining. The phenomenon was clearly seen in the [Fig. 6.5](#) with the presence of a high proportion of undigested carbohydrates (green colour). A specific microstructure of bread, which was observed in previous studies ([Kim, Morita, Sang-HanLeec, & Moon, 2003](#); [Li, Dobraszcz, & Wilde, 2004](#)) was also clearly seen in [Fig. 6.5A](#).

The results in [Table 6.4](#) show that more than half of the short-chain triglycerides were hydrolysed. This degree of hydrolysis was approximately 10% higher than that of the *in vitro* digestion. On the other hand, the amount of SCFAs quantified in the *in vivo* ileal digesta was around 15% of the maximum SCFA release, while the value for the *in vitro* digesta was around 40%. In addition, there was no significant difference between PA and BA release. A possible explanation for the difference between *in vitro* and *in vivo* digestion was the absorption of SCFA. Under the *in vitro* condition, released SCFA remained within the digesta media, i.e. either at the O/W interface or dissolved in the media ([Wilde, et al., 2011](#)). However, when the concentration of SCFA in the media reached a saturated level, newly released SCFAs would remain longer at the O/W interface and inhibit further hydrolysis, i.e. product inhibition. *In vivo*, a certain proportion of SCFAs would be absorbed through the small intestine, leading to a reduction of their concentrations in the ileal digesta. Previous work also reported a significant absorption of SCFAs within the small intestine ([Montoya, Rutherford, et al., 2016](#)). Consequently, more released SCFAs would enter the digesta media rather than remain at the O/W interface and that possibly improved further lipolysis.

SCFAs were detected even in the ileal digesta of the control group ([Table 6.3](#)), which consumed SCFA-free diet. This observation was in line with the results in previous studies on *in vivo* ileal fermentation of carbohydrate-based diet using cannulated pig model ([Hooda, et al., 2011](#); [Hu, Heyer, Wang, Zijlstra, & Gänzle, 2020](#); [Le, et al., 2017](#)). In these studies, it was reported that ileal bacteria fermented diet carbohydrates to produce SCFAs. In addition, the SCFA production yield and ratio amongst them was dependent on the diet composition and viscosity of the diet, which influenced the retention time of the diet within the small intestine ([Hooda, et al., 2011](#)). In the current

study, the production of SCFAs from the experimental diet was significantly higher than that from the control diet. In other words, the fermentation of diet carbohydrates and hydrolysis of TP and TB occurred simultaneously within the small intestine. Also, BA and PA contents in the *in vivo* ileal digesta were different. This observation was due to the fermentation of diet carbohydrates, which produced SCFAs with various levels (Tan, et al., 2014). In the present study, BA was the dominant SCFA product of the fermentation.

**Table 6.4.** TP, TB, PA and BA profiles (concentration, mg/g fresh matter; and proportions of hydrolysis/release, %) in the *in vivo* intestinal digesta and faecal samples.

	Intestinal digesta			Faeces		
	Control group	Experimental group		Control group	Experimental group	
	Concentration	Hydrolysis/release (%)		Concentration	Hydrolysis/release (%)	
TP	Not detected	0.959 ± 0.133 <sup>a</sup>	53.0 ± 7.4 <sup>a</sup>	Not detected	Not detected	100
TB	Not detected	0.994 ± 0.086 <sup>a</sup>	51.3 ± 4.9 <sup>a</sup>	Not detected	Not detected	100
PA	0.142 ± 0.050 <sup>b</sup>	0.295 ± 0.072 <sup>c</sup>	13.7 ± 6.2 <sup>b</sup>	0.565 ± 0.094 <sup>a</sup>	0.663 ± 0.133 <sup>a</sup>	....
BA	0.285 ± 0.047 <sup>a</sup>	0.468 ± 0.083 <sup>b</sup>	15.9 ± 5.8 <sup>b</sup>	0.800 ± 0.224 <sup>a</sup>	0.812 ± 0.084 <sup>a</sup>	....

Different superscripts (a–c) in the same column represent significant differences between different samples at the  $p < 0.05$  level.

In the faecal samples, no triglycerides were detected, showing complete hydrolysis and/or fermentation of TP and TB in the colon. Previously *Bacillus sp.* was identified as the best lipase producer amongst all lipase-producing bacteria when TB tributyrin agar medium was used as a substrate (Treichel, Oliveira, Mazutti, Luccio, & Oliveira, 2010). *Bacillus sp.* was also found abundant in pig microbiota (Schokker, et al., 2015), which might be the explanation for hydrolysis of triglycerides in the gut. Also, the retention time of the undigested diet from the distal ileum to the faecal excretion of growing pigs (BW of 30 kg) (Wilfart, Montagne, Simmins, Noblet, & Milgen, 2007) was around 3 days, which might be long enough to digest all triglycerides.

In contrast to triglycerides, SCFAs (PA and BA) were detected in the faeces with no significant difference between the control and experimental pigs (Table 6.4). The presence of SCFAs in the faeces of cannulated pigs was also reported in previous studies with various concentrations and ratios amongst them, depending on the diet compositions (Hooda, et al., 2011; Hu, et al., 2020; Le, et al., 2017). In fact, up to 95% of SCFAs produced in the colon were adsorbed by the colonocytes, while only 5% were excreted in faeces (Besten, et al., 2013). Therefore, low remaining proportions of produced SCFAs in the faeces did not result in significant difference between control and experimental pigs.

## 6.4. Conclusions

The results demonstrated successful delivery of PA and BA into the colon using an O/W emulsion stabilised by CT-HM PEC under the *in vitro* digestion and *in vivo* study with ileal-cannulated pigs. The thick layers of adsorbed PEC at the O/W interface was revealed under CLSM, which might be the main factor that delayed lipid digestion.

However, the lipolysis degree in the *in vivo* study was significantly higher than that in the *in vitro* study. Such difference was due to the absorption of SCFAs, product inhibitors of the digestion, in the small intestine of the pigs that enhanced further lipolysis. Within the colon, all short-chain triglycerides were completely hydrolysed and/or fermented and therefore, they were then not detected in the faeces. Behaviours of the delivery system under the *in vivo* study showed a strong promise in the application of this system for future human study on delivery of not only SCFAs but also other bioactive compounds.

## Chapter 7 - Key findings and future research prospects

---

### 7.1. Overall findings

- The OSA modification of IN and CNCs significantly enhanced their emulsifying abilities and improved the stability of the M-IN and MCNC-stabilised emulsions under storage at 4°C for up to 28 days.

- Amongst all carbohydrate materials, PEC demonstrated the lowest emulsifying ability but proved to be the best material to resist *in vitro* gastrointestinal digestion. As PEC stabilised the O/W emulsions mainly through steric effects, changes in pH and ionic strength did not significantly impact on the microscopic structure of the emulsions. PEC-based emulsions were resistant to gastric digestion whereas changes in the emulsion structure and the release of SCFAs were observed in the intestinal phase, in which the release profile could be modulated by the concentration of pectin. At a sufficient concentration (2.5 wt% or higher), pectin produced a thick coverage around the oil droplets, which provided strong resistance to displacement by bile salts and, as a consequence, delayed lipid digestion. On the other hand, modified starches and M-IN demonstrated weak protection against *in vitro* intestinal digestion, mainly due to enzymatic destruction of modified starches and bile-salt displacement of both modified starches and M-IN.

- Pickering O/W emulsions stabilised by MCNCs were prone to flocculation at pH < 4.0, ionic strength higher than 20 mM NaCl and under *in vitro* gastric environment. The formation of aggregates was due to a reduction in the electrostatic repulsive force between the emulsion droplets, which was induced by low pH and high ionic strength. The aggregation of the emulsion droplets under gastric conditions reduced the surface area for the intestinal lipolysis. In addition, electrostatic repulsions of MCNCs to bile salts and the high desorption energy of the MCNCs particles were responsible for the resistance to bile salt displacement, which occurred in the initial stage of the digestion process.

- For the *in vivo* study using ileal-cannulated pigs, an O/W emulsion stabilised by CT-HM-PEC was chosen. The presence of intact oil droplets in the ileal digesta suggested the delivery of some SCFAs to the colon. In addition, the degree of lipolysis in the *in vivo* study was significantly higher than that in the *in vitro* study. Also, all short-chain triglycerides were hydrolysed and/or fermented in the colon.

## 7.2. Exploring possible mechanisms

### 7.2.1. Structural changes in the double-layer emulsion system under gastrointestinal digestion

The formation of double-layer O/W emulsions is usually based on the electrostatic interaction of the first and second layers at a specific pH. In this approach, a primary emulsion is produced by using an ionic emulsifier that rapidly adsorbs to the surface of lipid droplets during homogenization, then an oppositely charged material is added to the primary emulsion. The second material adsorbs to the droplet surface and

produces secondary emulsions containing droplets coated with a two-layer interfacial membrane. Under certain environmental stresses, multilayer O/W emulsions have been found to have better stability than conventional oil-in-water emulsions with single-layered interfacial membranes. In this study, the double-layer O/W emulsion was formed by combining WPI and CS that are negatively and positively charged at pH 5.5 respectively (Fig. 7.1A). Although WPI has a good emulsifying ability, the protein is sensitive to enzymatic digestion occurring in the upper gastrointestinal tract. Therefore, CS was added as the second layer in order to protect WPI from pepsinolysis in the gastric stage and pancreatic digestion in the small intestine. However, the changes of the pH within the digestive system significantly influenced the original structure of the emulsion; and therefore, led to premature release of SCFAs. In the *in vitro* gastric stage using the INFOGEST static protocol, pH was maintained at 2.0 and that altered the surface charge of WPI from negative to positive. This pH value was no longer an ideal condition for the adsorption of CS onto the surface of WPI-stabilised droplets. As a result, WPI at the O/W interface was hydrolysed by pepsin present in the gastric phase (Fig. 7.1B). The hydrolysis of WPI in the gastric stage favoured the lipolysis in the small intestine. To summarise, although under certain circumstances, double-layer O/W emulsions have some combined advantages that single-layer systems do not, the use of double-layer emulsions formed through electrostatic interaction for delivery of bioactive compounds is not recommended based on the findings in this study.

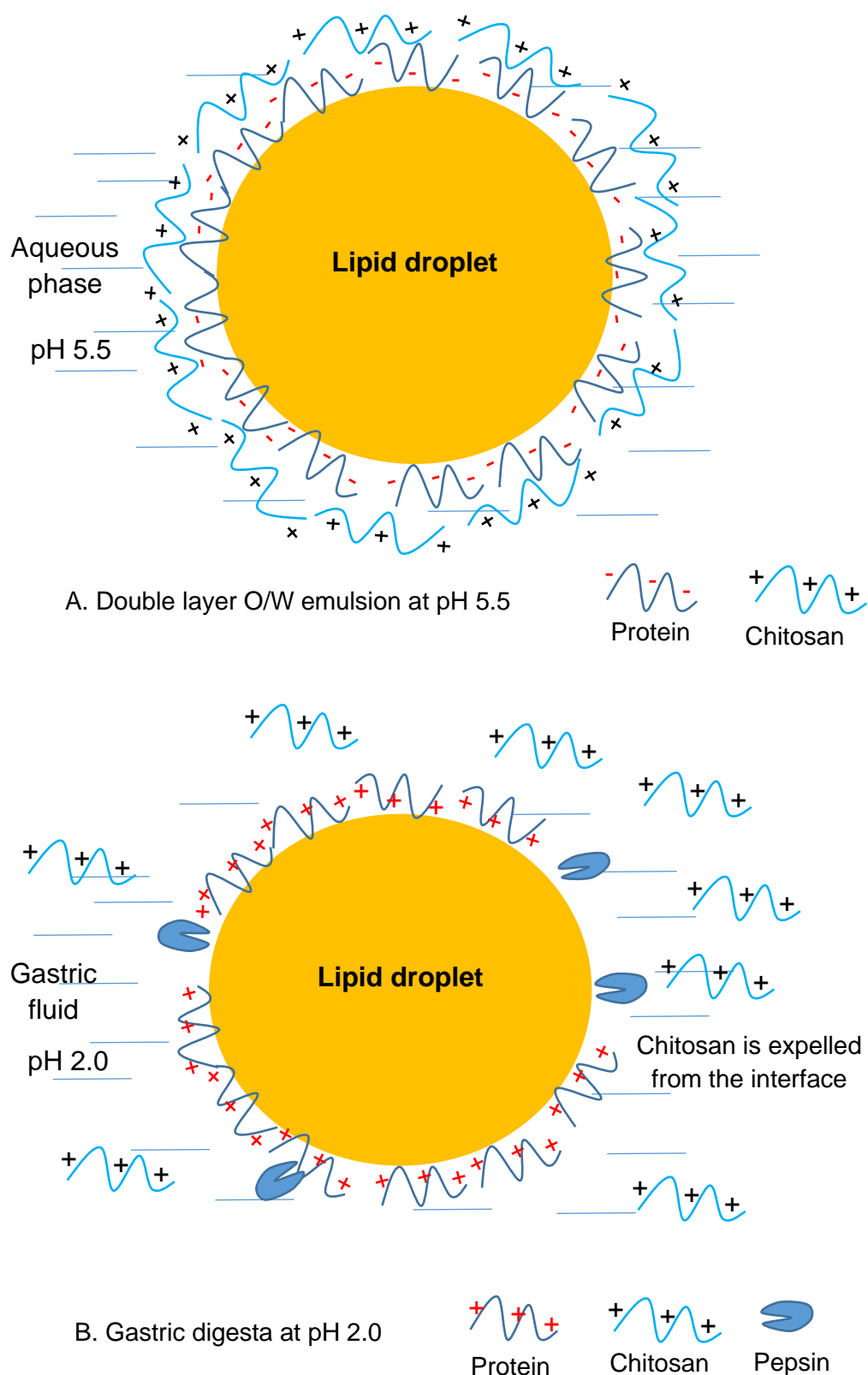


**Figure 7.1.** Structural changes of CS-WPI O/W emulsion under the *in vitro* gastric conditions

### 7.2.2. Improvement of the emulsifying ability through the OSA modification

In the design of O/W emulsions for delivery of bioactive compounds, the selection of emulsifiers is essential as it determines the stability of the emulsion systems under various environmental stresses, such as pH, ionic strengths and the presence of enzymes. Some materials that have been investigated in this study, such as WPI and modified starches, demonstrated excellent emulsifying ability but failed to protect triglycerides from gastrointestinal digestion. Other materials, such as Inulin (IN) and CNCs, are naturally undigested by human digestive enzymes. However, these materials have a high proportion of hydroxyl groups on the backbone, which limits their ability to adsorb on the hydrophobic surfaces, such as oil droplets. In other words, IN and CNCs have poor emulsifying ability that restricts their further applications. This study demonstrated that hydrophobic modification of IN and CNCs with OSA significantly improved their emulsifying ability. Under alkaline environment, hydroxyl groups reacted with OSA groups, which significantly enhanced the hydrophobic property of the materials. The diagram in [Fig. 7.2](#) illustrates the possible mechanisms of IN and CNC adsorptions on the O/W interface before and after the hydrophobic modification. The mechanism of the M-IN stabilised emulsion is related to its hydrophilic-lipophilic balance ([Fig. 7.2A](#)). Before the modification, IN is hydrophilic and therefore does not adsorb onto the oil droplet surface to stabilise the O/W emulsion. However, after the modification, non-polar groups (OSA) along the M-IN molecules submerged into the oil phase while the backbone remained at the interface. This process allowed the formation of a stable O/W emulsion. As IN has a short chain length, steric effects do not play a significant role in the stability of the emulsion. Instead, the presence of -OH groups of adsorbed M-IN on the O/W interface guaranteed a sufficient electrostatic interaction to prevent aggregation. In this study,

the emulsion stabilised by M-IN had a homogenous structure that was stable for 4 days storage at 4°C.

For M-CNCs, the emulsifying ability depends on the M-CNC wettability in the oil phase. Unmodified CNCs were highly charged with the presence of -OH and -SO<sub>4</sub> groups on the crystal surface (Fig. 7.2B). As a result, CNCs had a low wettability in the oil phase, which resulted in an unstable emulsion with high degree of coalescence. However, the partial replacement of -OH by OSA significantly increased the hydrophobicity of M-CNCs as evidenced by water contact angle as reported in Chapter 5. As a result, the wettability of M-CNCs in the oil phase was significantly enhanced, which allowed deeper adsorption of M-CNCs into the oil phase as compared to the that of unmodified CNCs. In this study, the emulsions stabilised by M-CNCs were stable against droplet coalescence for up to 4-week storage at 4°C.

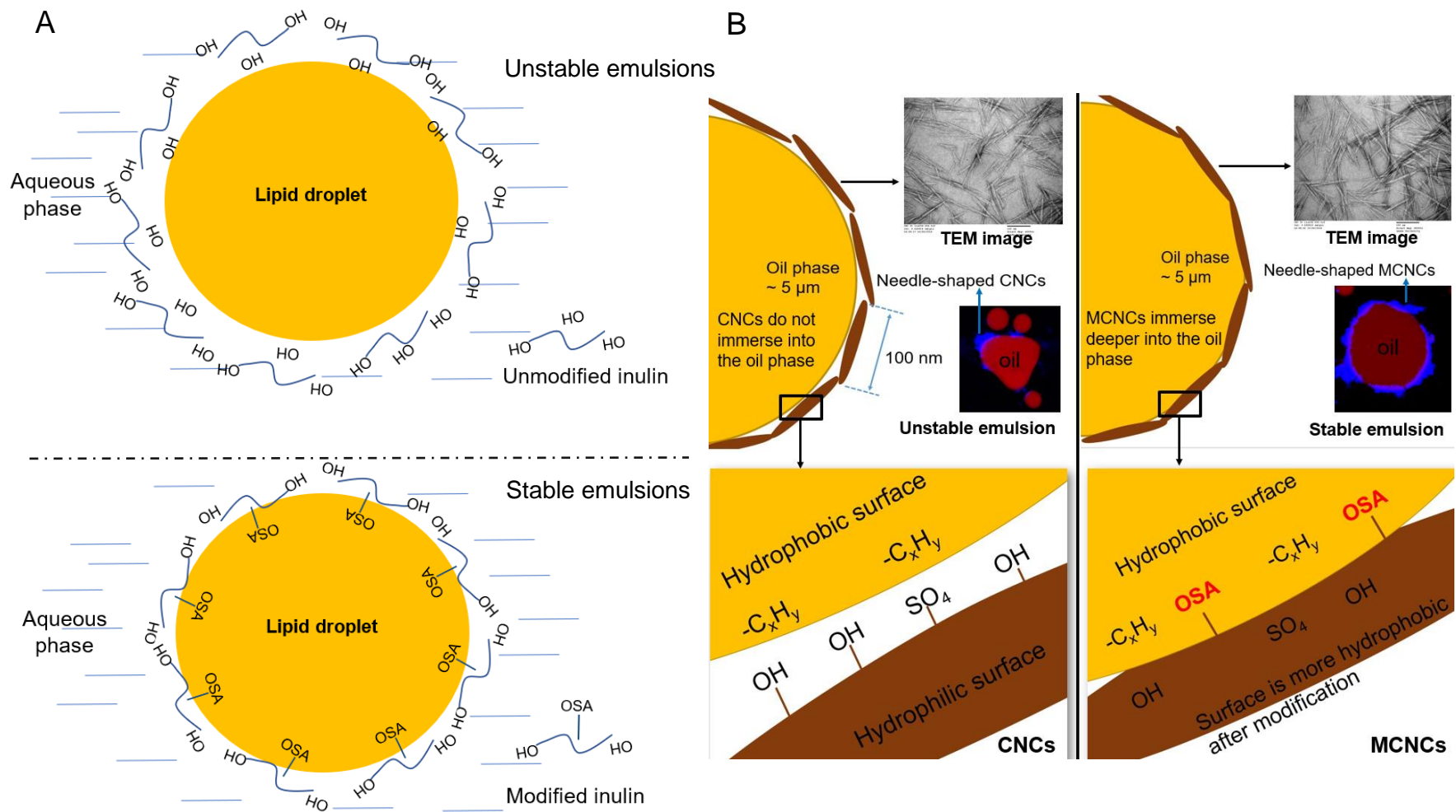


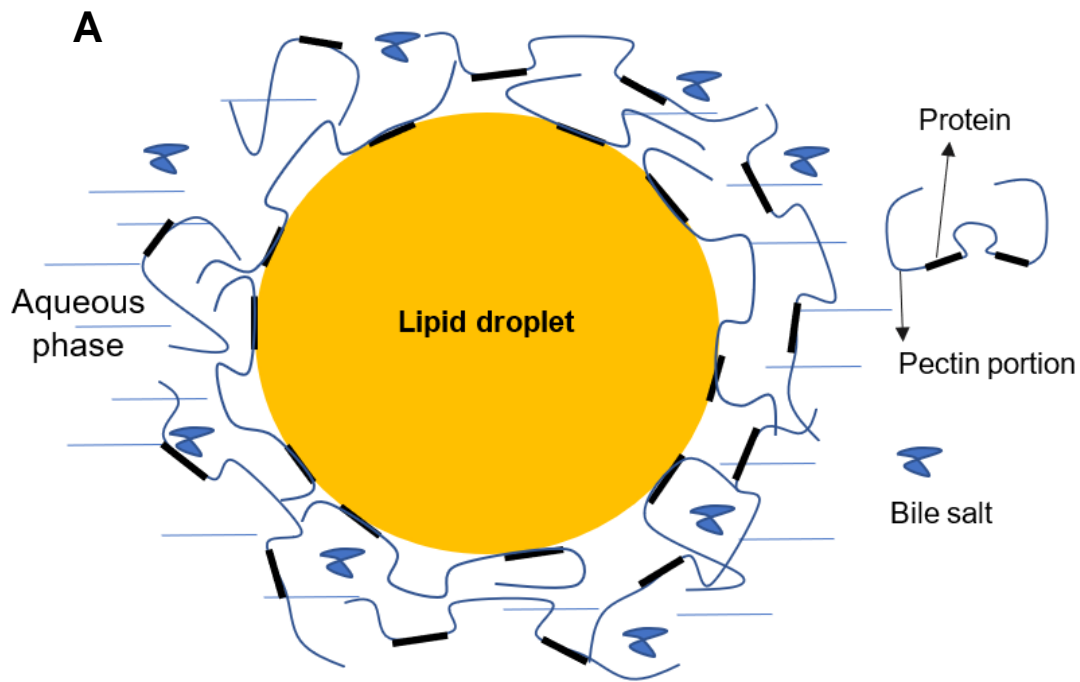
**Figure 7.2.** Effects of OSA modification on emulsifying ability of IN and CNCs

### 7.2.3. Resistance to intestinal digestion through manipulation of surface coverage

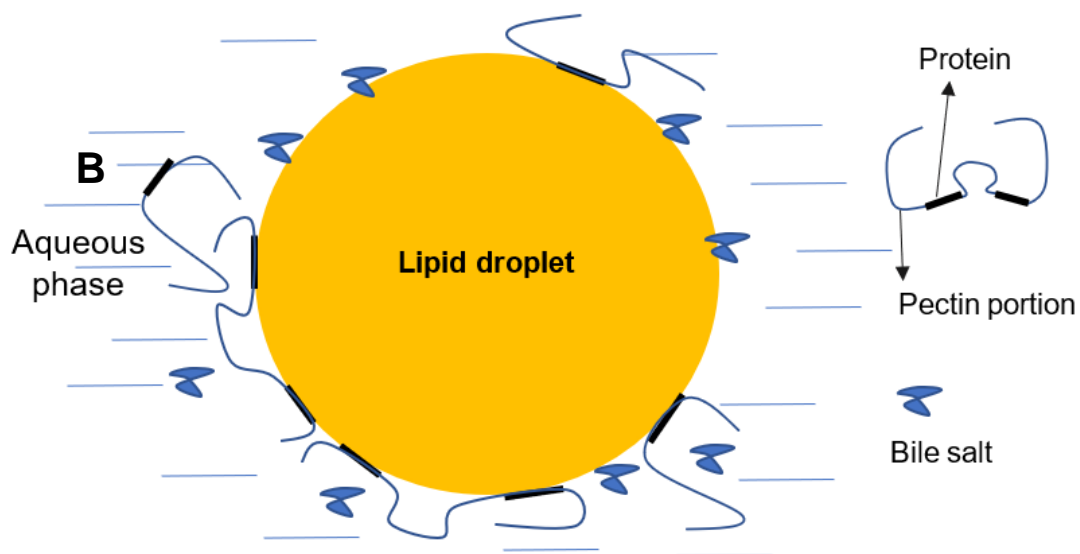
In this study, lipolysis in the intestinal stage was controlled by the design of the emulsions with thick layer of PEC adsorbed on the O/W interface. The diagram in [Fig. 7.3](#) illustrates the mechanism how PEC influences the lipid digestion in the small intestine as a function of time. The PEC-based emulsions had a thick layer that was clearly shown in the confocal images in [Chapter 6](#). Also, the PEC coverage of the emulsion stabilised by PEC 2.5 wt% was  $7.7 \text{ mg.m}^{-2}$ . Such thick PEC layer was formed by layer-by-layer of rhamnogalacturonan-I in the pectin backbones. In addition, the emulsion stability was achieved through steric effects, which was due to the long chain length of PEC.

Bile salt structure is composed of 4 rings with a side chain terminating in carboxylic acid. The ring structure and hydroxyl groups location result in a bile salt molecule with hydrophobic and hydrophilic faces. This unique structure allows bile salts to develop both hydrophobic and electrostatic interactions with adsorbed emulsifiers on the O/W interface, and subsequently displace them from the interface. This process is widely known to facilitate the adsorption of lipase onto the lipid surface to initiate the digestion. In addition, the bile salts are highly negative charged, due to the presence of a hydroxyl group (cholic acid) or a sulphite group (taurocholic acid). Therefore, emulsions that are negatively charged under intestinal conditions could resist the bile salt adsorption onto the O/W interface. In this study, PEC-based emulsion was negatively charged at pH 7.0 (the  $\zeta$ -potential of around -18 mV). This property could play a role in delaying the bile salt displacement. In addition, thick coverage and long chain of PEC adsorbed on the O/W interface produced a physical barrier that was strong enough to delay bile

salt displacement. In the first 30 min of the *in vitro* intestinal digestion, the overall structure of PEC-based emulsion appeared to be stable. In addition, a thick layer of adsorbed PEC on the O/W interface was still clearly observed in the first 30 min of the *in vitro* intestinal digestion, suggesting strong resistance of PEC against bile salt displacement (Fig. 7.3A). However, bile salts are small molecule that could penetrate through such thick adsorbed PEC layer (Fig. 7.3B). Therefore, a high proportion of adsorbed PEC was displaced after 3h. In conclusion, although the formation of thick negatively charged PEC layer at the O/W interface could delay bile salt displacement in the first 30 min of the intestinal digestion, bile salts could still penetrate through the layer to facilitate the lipolysis process.



In the first 30 min, thick layer off PEC resisted bile salt displacement



After 3 h, more bile salt penetrated through the thick layer to displace PEC

**Figure 7.3.** Influence of PEC during the *in vitro* intestinal digestion

#### 7.2.4. Resistance of M-CNC-based Pickering emulsion to the gastrointestinal digestion

The results of this study demonstrated excellent resistance of the Pickering emulsion to the intestinal lipid digestion, which was due to high desorption energy and surface charge.

The first and the most important factor was associated with the high desorption energy of the MCNC from the O/W interface. The MCNCs has a  $r \approx 20$  nm and a contact angle of  $86^\circ$  at the oil–water interface (typical value of  $\gamma_{ow} \approx 50$  mN m<sup>-1</sup>). This will have a desorption energy ( $\Delta E$ ) of nearly  $10^5 k_B T$ . Therefore, it is unlikely that bile salts displace MCNCs from the interface. Secondly, under SIF environment of pH 7.0, both the MCNCs and the bile salts have negative charges. Therefore, it is likely the adsorbed MCNCs will repel anionic bile salts from the vicinity of negatively charged emulsion droplets, which will prevent the displacement. Finally, the exposure of the Pickering emulsion to gastric fluid led to significant changes in its microscopic structure. Under low pH and high ionic strength conditions,  $\zeta$ -potential of the droplets dropped to almost 0 mV because of the charge screening associated with the cellulose molecules at the surface. This resulted in a reduction in electrostatic repulsion, leading to aggregation. Such aggregation played an important role in delaying the small intestinal digestion. For example, the droplet aggregation significantly reduced surface area for lipid digestion.

Although M-CNCs were not displaced by bile salts, the use of such Pickering emulsion did not completely prevent lipid from hydrolysis. In the present study, needle-shaped M-CNCs had width and length of around 10 and 100 nm, respectively. Therefore, it

was impossible for an emulsion stabilised by M-CNCs to stop the penetration of lipase to the droplet surface.

### **7.3. Advantages and disadvantages of this study**

In this study, the static INFOGEST digestion protocol and *in vivo* digestion with cannulated pigs were used to evaluate the delivery ability of all emulsion systems. In addition, PEC-based and M-CNC-based emulsions that were selected from the screening studies were investigated at a greater depth. Therefore, in this section, the advantages and limitations of these digestion protocols will be discussed through the findings obtained from the two selected emulsion systems.

#### **7.3.1. *In vitro* digestion**

The static *in vitro* digestion is the simplest method for simulating the *in vivo* digestion. This method is reproducible, robust, simple, relatively low cost and easy to assess each digestion phase. In this study, a screening experiment was conducted to select suitable carbohydrate materials to design delivery emulsion systems. As a wide range of carbohydrates were investigated, the use of an *in vivo* digestion model will be time consuming and costly. From that perspective, the static *in vitro* digestion is the most suitable method to minimise the use of resources before a more complex protocol is employed. However, the static digestion method has some limitations as it cannot mimic the complexity of the dynamic digestion process and the physiological interactions with the host. For example, in this study, the gastric pH was kept constantly at 2.0, gastric fluid was not gradually added and there was the lack of gastric emptying. However, in the *in vivo* condition, gastric pH changes constantly from a

value of around 2.0 due to the secretion of HCl in the stomach. In this study, the PEC-based emulsions demonstrated a good stability under pH and ionic strength changes as reported in [Chapter 4](#). The overall structure of the emulsions stabilised by citrus PEC remained stable at various pH and ionic strength conditions. In addition, PEC is an indigestible carbohydrate to human digestive enzymes. This suggested that PEC-based emulsions might behave similarly under both *in vitro* and *in vivo* conditions. However, in case of the Pickering emulsion stabilised by M-CNCs, the behaviour of the emulsion systems under *in vitro* and *in vivo* conditions might be different. The Pickering emulsion illustrated significant structural changes with the formation of aggregation when pH dropped to 4.0 or lower. With the dynamic pattern of pH within the *in vivo* gastric conditions, the Pickering emulsion might experience several structural changes during the gastric digestion. However, the *in vitro* gastric digestion did not include the ramp up and down of the pH, which might therefore not show a good correlation with the *in vivo* digestion. In conclusion, in the gastric phase, the emulsions that show a good stability under various pH and ionic strength conditions will have a better correlation in their behaviours under *in vitro* and *in vivo* digestions as compared to those that are significantly influenced by pH and/or ionic strengths.

In addition to the limitations in the gastric phase, the *in vitro* digestion also has some drawbacks in the intestinal phase. For example, the intestinal phase in this study was treated as a single phase rather than as the sequential duodenal, jejunal and ileal phases, which exhibit various dilutions, mineral content, pH and enzyme activities. In addition, the result in [Chapter 6](#) demonstrated that ileal bacteria fermented a certain degree of carbohydrate to produce SCFAs. However, ileal fermentation was not used in the *in vitro* study. While PEC was more fermentable under the ileum, M-CNCs have

a better resistance to ileal fermentation. Therefore, it may suggest that the Pickering emulsions have a good correlation between the *in vitro* and *in vivo* digestions. On the other hand, the PEC-based emulsions, which were more sensitive to ileal fermentation demonstrated a lower degree of correlation between the *in vitro* and *in vivo* digestions when the ileal fermentation was not used. Furthermore, the absorption of lipolysis products, such as SCFAs within the host, also plays a role in boosting the hydrolysis. This was not observed in the *in vitro* digestion.

### **7.3.2. *In vivo* digestion**

In this study, cannulated pigs were used as an *in vivo* model. The main strengths of this model are its similarity to human gastrointestinal digestion and the availability of cannula for ileal digesta collection that is limited in human study. However, the model has some limitations. For example, it usually takes an average three days for a diet to go through the colon of a fully-grown pig, while for an adult human it takes around one day. In addition, the ileal and gut microbiota between human and pigs are different, which might result in differences between lipolysis products and other metabolites.

## **7.4. Future research prospects**

- In this study, it was demonstrated that Inulin modified by OSA showed excellent emulsifying capacity. However, the M-IN-based emulsions failed to protect short-chain triglycerides from intestinal digestion, due to bile-salt displacement. To improve resistance to bile-salt displacement, it is proposed the use of Inulin microgel beads for producing a Pickering emulsion. Due to high desorption energy of the solid stabilisers

from the O/W interface of the Pickering emulsion, it could be hypothesised that the system could resist bile-salt displacement and delay digestion.

- Although MCNC-based emulsions showed excellent protect against *in vitro* gastrointestinal digestion, the system was not chosen for the *in vivo* study. The main reason was due to the food-grade status of the CNCs. The commercial CNCs used in this study was produced through a hydrolysis process by H<sub>2</sub>SO<sub>4</sub>, and therefore are currently not considered as safe for human consumption. However, the applications of CNCs should not be restricted within one type of commercial CNCs. CNCs produced from different resources, such as bacterial cellulose are also potential candidates for food applications. When food-grade information of CNCs is available, CNC-based emulsions could be applied for *in vivo* study with animals, such as mice and pigs.

- The *in vivo* study with cannulated pigs proved successful delivery of PA and BA into the colon with PEC-based emulsions. The *in vivo* study shows a strong promise in the use of the system for further human study. As the formulation consists of all food-grade materials, the emulsion would be safe for human consumption.

- Human studies could be carried out for the PEC-based emulsions and the production of SCFAs measured using different techniques.

## References

Alva-Murillo, N., Ochoa-Zarzosa, A., & López-Meza, J. E. (2012). Short chain fatty acids (propionic and hexanoic) decrease *Staphylococcus aureus* internalization into bovine mammary epithelial cells and modulate antimicrobial peptide expression. *Veterinary Microbiology*, 155, 324–331.

Araki, J. (2013). Electrostatic or steric? – preparations and characterizations of well-dispersed systems containing rod-like nanowhiskers of crystalline polysaccharides. *Soft matter*, 9, 4125-4141.

Armand M, Pasquier B, André M, et al. Digestion and absorption of 2 fat emulsions with different droplet sizes in the human digestive tract. *The American Journal of Clinical Nutrition*, 1999, 70, 1096–1106.

Augustina, M. A., Abeywardena, M. Y., Pattena, G., Heada, R., Locketta, T., Lucae, A. D., & Sanguansria, L. (2011). Effects of microencapsulation on the gastrointestinal transit and tissue distribution of a bioactive mixture of fish oil, tributyrin and resveratrol. *Journal of Functional Food*, 3, 25-37.

Banasiewicz, T., Krokowicz, Ł., Stojcev, Z., Kaczmarek, B. F., Kaczmarek, E., Maik, J., Marciniak, R., Krokowicz, P., Walkowiak, J., & Drews, M. (2012). Microencapsulated sodium butyrate reduces the frequency of abdominal pain in patients with irritable bowel syndrome. *Colorectal disease*, 15, 204-209.

Bergman, E. N. (1990). Energy contributions of volatile fatty acids from the gastrointestinal tract in various species. *Physiological Reviews*, 70(2), 567-590.

- Besten, G. D., Eunen, K. V., Groen, A. K., Venema, K., Reijngoud, D.-J., & Bakker, B. M. (2013). The role of short-chain fatty acids in the interplay between diet, gut microbiota, and host energy metabolism. *Journal of Lipid Research*, 54, 2325-2340.
- Bindelle, J., Pieper, R., Montoya, C. A., & Kessel, A. G. V. (2011). Nonstarch polysaccharide-degrading enzymes alter the microbial community and the fermentation patterns of barley cultivars and wheat products in an *in vitro* model of the porcine gastrointestinal tract. *FEMS Microbiology Ecology*, 76(3), 553–563.
- Boets, E., Deroover, L., Houben, E., Vermeulen, K., Gomand, S. V., Delcour, J. A., & Verbeke, K. (2015). Quantification of *in vivo* colonic short chain fatty acid production from inulin. *Nutrients*, 7, 8916–8929.
- Boffa, L. C., Vidali, G., Mann, R. S., & Allfrey, V. G. (1978). Suppression of histone deacetylation *in vivo* and *in vitro* by sodium butyrate. *The Journal of Biochemistry*, 253, 3364-3366.
- Bourlieu, C., Ménard, O., Chevasnerie, A. D. L., Sam, L., Rousseau, F., Madec, M.-N., Robert, B., Deglaire, A., Pezennec, S., Bouhallab, S., Carrière, F., & Dupontab, D. (2014). The structure of infant formulas impacts their lipolysis, proteolysis and disintegration during *in vitro* gastric digestion. *Food Chemistry*, 182, 224-235.
- Brestenský, M., Nitrayová, S., Bomba, A., Strojný, L., Patráš, P., & Heger, J. (2016). Effect of probiotics and prebiotics supplemented to the diet of growing pigs on the content of short chain fatty acids in the jejunum and cecum. *Journal of Animal Science*, 94, 219–221.

Brignot, H. and G. Feron. (2019). Oral lipolysis and its association with diet and the perception and digestion of lipids: A systematic literature review. *Archives of Oral Biology*, 108, 104550.

Cameron, D. R., Weber, M. E., Idziak, E. S., Neufeld, R. J., & Cooper, D. G. (1991). Determination of interfacial areas in emulsions using turbidimetric and droplet size data: correction of the formula for emulsifying activity index. *Journal of Agricultural and Food Chemistry*, 39, 655-659.

Capolino, P., Guérin, C., Paume, J., Giallo, J., Ballester, J.-M., Cavalier, J.-F., & Carrière, F. (2011). *In vitro* gastrointestinal lipolysis: Replacement of human digestive lipases by a combination of rabbit gastric and porcine pancreatic extracts. *Food Digestion*, 2, 43–45.

Carrière F., Barrowman J.A., Verger R. & Laugier R. Secretion and contribution to lipolysis of gastric and pancreatic lipases during a test meal in humans. *Gastroenterology*, 1993, 105, 876–888.

Chanamai, R., & McClements, D. J. (2002). Comparison of gum arabic, modified starch, and whey protein isolate as emulsifiers: Influence of pH, CaCl<sub>2</sub> and temperature. *Food Chemistry and Toxicology*, 67, 120-125.

Chahinian H., Snabe T., Attias C., Fojan P., Petersen S.B., Carriere F. How gastric lipase, an interfacial enzyme with a Ser-His-Asp catalytic triad, acts optimally at acidic pH. *Biochemistry*, 2006, 45, 993–1001.

Charoen, R., Jangchud, A., Jangchud, K., Harnsilawat, T., Naivikul, O., & McClements, D. J. (2011). Influence of Biopolymer Emulsifier Type on Formation and

---

Stability of Rice Bran Oil-in-Water Emulsions: Whey Protein, Gum Arabic, and Modified Starch. *Journal of Food Science*, 76, E165-E172.

Chen, Q.-H., Zheng, J., Xu, Y.-T., Yin, S.-W., Liu, F., & Chuan-HeTang. (2018). Surface modification improves fabrication of pickering high internal phase emulsions stabilized by cellulose nanocrystals. *Food Hydrocolloids*, 75, 125-130.

Chevalier, Y., & Bolzinger, M.-A. (2013). Emulsions stabilized with solid nanoparticles: Pickering emulsions. *Colloids and Surfaces A: Physicochemical and Engineering Aspects*, 439, 23-34.

Ciolacu, D., Ciolacu, F., & Popa, V. I. (2011). Amorphous cellulose-structure and characterization. *Cellulose chemistry and technology*, 45, 13-21.

Cohen, M., Morgan, R., & Hofmann, A. (1971). Lipolytic activity of human gastric and duodenal juice against medium and long chain triglycerides. *Gastroenterology*, 60, 1–15.

Cummings, J., Rombeau, J., & Sakata, T. (2004). *Physiological and clinical aspects of short-chain fatty acids*: Cambridge University Press, Section 31, 509-525.

Destribats, M., Rouvet, M., Gehin-Delval, C., Schmitt, C., & Binks, B. P. (2014). Emulsions stabilised by whey protein microgel particles: towards food-grade Pickering emulsions. *Soft matter*, 10, 6941-6954.

Dewulfa, E. M., Cania, P. D., Neyrincka, A. M., Possemiersb, S., Ann Van Holleb, Mucciolic, G. G., Deldicqued, L., Bindelsa, L. B., Pachikiana, B. D., Soheta, F. M., Mignolete, E., Francauxd, M., Larondellee, Y., & Delzennea, N. M. (2011). Inulin-type fructans with prebiotic properties counteract GPR43 overexpression and PPAR $\gamma$ -

related adipogenesis in the white adipose tissue of high-fat diet-fed mice. *Journal of Nutritional Biochemistry*, 22, 712–722.

Diaz, J. C. M., Cordova, J., Baratti, J., Carriere, F., & Abousalham, A. (2007). Effect of nonionic surfactants on *Rhizopus homothallicus* lipase activity. *Molecular Biotechnology*, 35, 205-214.

Dickinson, E. (2009). Hydrocolloids as emulsifiers and emulsion stabilizers. *Food Hydrocolloids*, 23, 1473-1482.

Dickinson, E. (2012). Use of nanoparticles and microparticles in the formation and stabilization of food emulsions. *Trends in Food Science & Technology*, 24, 4-12.

Donovan, J. D., Cadwallader, K. R., & Lee, Y. (2016). Volatile retention and morphological properties of microencapsulated tributyrin varied by wall material and drying method. *Journal of Food Science*, 81, E643-E650.

Donovan, J., Bauer, L., Jr, G. F., & Lee, Y. (2017). *In vitro* digestion and fermentation of microencapsulated tributyrin for the delivery of butyrate. *Journal of Food Science*, 82, 1491-1499.

Donovan, J., Cadwallader, K., & Lee, Y. (2016). Volatile retention and morphological properties of microencapsulated tributyrin varied by wall material and drying method. *Journal of Food Science*, 81, E643-E650.

Doost, A. S., Nasrabadi, M. N., Kassoziya, V., Dewettinck, K., Stevens, C., & Meeren, P. I. d. (2019). Pickering stabilization of thymol through green emulsification using soluble fraction of almond gum – Whey protein isolate nano-complexes. *Food Hydrocolloids*, 88, 218-227.

Espinal-Ruiz, M., Parada-Alfonso, F., Restrepo-Sánchez, L.-P., Narváez-Cuenca, C.-E., & McClements, D. J. (2014). Interaction of a dietary fiber (pectin) with gastrointestinal components (bile salts, calcium, and lipase): A calorimetry, electrophoresis, and turbidity study. *Journal of Agricultural and Food Chemistry*, 62, 12620-12630.

Espinal-Ruiz, M., Restrepo-Sánchez, L.-P., Narváez-Cuenca, C.-E., & McClements, D. J. (2016). Impact of pectin properties on lipid digestion under simulated gastrointestinal conditions: Comparison of citrus and banana passion fruit (*Passiflora tripartita var. mollissima*) pectins. *Food Hydrocolloids*, 52, 329-342.

Fang, S., Zhao, X., Liu, Y., Liang, X., & Yang, Y. (2019). Fabricating multilayer emulsions by using OSA starch and chitosan suitable for spray drying: Application in the encapsulation of  $\beta$ -carotene. *Food Hydrocolloids*, 93, 102-110.

Ferreira, T. M., Leonel, A. J., Melo, M. A., Santos, R. R. G., Cara, D. C., Cardoso, V. N., Correia, M. I. T. D., & Alvarez-Leite, J. I. (2012). Oral supplementation of butyrate reduces mucositis and intestinal permeability associated with 5-fluorouracil administration. *Lipids*, 47(7), 669–678.

Folter, J. W. J. d., Ruijven, M. W. M. v., & Velikov, K. P. (2012). Oil-in-water Pickering emulsions stabilized by colloidal particles from the water-insoluble protein zein. *Soft matter*, 8, 6807-6815.

Funami, T., Nakaum, M., Ishihara, S., Tanaka, R., Inoue, T., & Phillips, G. O. (2011). Structural modifications of sugar beet pectin and the relationship of structure to functionality. *Food Hydrocolloids*, 25, 221–229.

Funamia, T., Zhang, G., Hiroe, M., Noda, S., Nakauma, M., Asai, I., Cowman, M. K., Al-Assaf, S., & Phillips, G. O. (2007). Effects of the proteinaceous moiety on the emulsifying properties of sugar beet pectin. *Food Hydrocolloids*, 21, 1319–1329.

Fushimi, T., Suruga, K., Oshima, Y., Fukiharu, M., Tsukamoto, Y., & Goda, T. (2006). Dietary acetic acid reduces serum cholesterol and triacylglycerols in rats fed a cholesterol-rich diet. *British Journal of Nutrition*, 95, 916–924.

Gong, X., Wang, Y., & Chen, L. (2017). Enhanced emulsifying properties of wood-based cellulose nanocrystals as Pickering emulsion stabilizer. *Carbohydrate Polymers*, 169, 295-303.

Gupta, N., Martin, P. M., Prasad, P. D., & Ganapathy, V. (2006). SLC5A8 (SMCT1)-mediated transport of butyrate forms the basis for the tumor suppressive function of the transporter. *Life Sciences*, 78, 2419–2425.

Gurav, A., Sivaprakasam, S., Bhutia, Y. D., Boettger, T., Singh, N., & Ganapathy, V. (2015). Slc5a8, a Na<sup>+</sup>-coupled high-affinity transporter for short-chain fatty acids, is a conditional tumour suppressor in colon that protects against colitis and colon cancer under low-fibre dietary conditions. *Biochemistry Journal*, 469, 267–278.

Han, L., Ratcliffe, I., & Williams, P. A. (2015). Self-assembly and emulsification properties of hydrophobically modified inulin. *Journal of Agriculture and Food Chemistry*, 63, 3709–3715.

Harrington, B. J., & Hageage, G. J. (2003). Calcofluor white: A review of its uses and applications in clinical mycology and parasitology. *Laboratory Medicine*, 34, 361–367.

Hinnebusch, B. F., Meng, S., Wu, J. T., Archer, S. Y., & Hodin, R. A. (2002). The effects of short-chain fatty acids on human colon cancer cell phenotype are associated with histone hyperacetylation. *Nutrition and Cancer*, 132, 1012-1017.

Hooda, S., Metzler-Zebeli, B. U., Vasanthan, T., & Zijlstra, R. T. (2011). Effects of viscosity and fermentability of dietary fibre on nutrient digestibility and digesta characteristics in ileal-cannulated grower pigs. *British Journal of Nutrition*, 106, 664-674.

Hu, B., Zhang, L., Liang, R., Chen, F., He, L., Hua, B., & Zeng, X. (2015). Cross-linking of interfacial casein layer with genipin prevented pH-induced structural instability and lipase digestibility of the fat droplets. *Journal of Agricultural and Food Chemistry*, 63, 2033–2040.

Hu, Y., Heyer, C. M. E., Wang, W., Zijlstra, R. T., & Gänzle, M. G. (2020). Digestibility of branched and linear  $\alpha$ -gluco-oligosaccharides *in vitro* and in ileal-cannulated pigs. *Food Research International*, 127, 108726.

Hu, Y., Yin, S., Zhu, J., Qi, J., Guo, J., Wu, L., Tang, C., & Yang, X. (2016). Fabrication and characterization of novel Pickering emulsions and Pickering high internal emulsions stabilized by gliadin colloidal particles. *Food Hydrocolloids*, 61, 300-310.

Hu, Z., Ballinger, S., Pelton, R., & Cranston, E. (2015). Surfactant-enhanced cellulose nanocrystal Pickering emulsions. *Journal of Colloid and Interface Science*, 439, 139-148.

Huuskonen, J., Suuronen, T., Nuutinen, T., Kyrylenko, S., & Salminen, A. (2004). Regulation of microglial inflammatory response by sodium butyrate and short-chain fatty acids. *British Journal of Pharmacology*, 141, 874–880.

- Jaina, S., Winuprasith, T., & Suphantharika, M. (2019). Design and synthesis of modified and resistant starch-based oil-in-water emulsions. *Food Hydrocolloids*, 2019, 153-162.
- Kaiko G.E., Ryu S.H., Koues O.I., Collins P.L., Solnica-Krezel L., Pearce E.J., et al. The colonic crypt protects stem cells from microbiota-derived metabolites. *Cell*. (2016) 165, 1708–1720.
- Kean, T. J., & Thanou, M. (2010). Biodegradation, biodistribution and toxicity of chitosan. *Advanced Drug Delivery Reviews*, 62, 3-11.
- Kilner, J., Waby, J. S., Chowdry, J., Khan, A. Q., Noirel, J., Wright, P. C., Corfe, B. M., & Evans, C. A. (2012). A proteomic analysis of differential cellular responses to the short-chain fatty acids butyrate, valerate and propionate in colon epithelial cancer cells. *Molecular BioSystems*, 8, 1146–1156.
- Kim, H.-J., Morita, N., Sang-HanLeec, & Moon, K.-D. (2003). Scanning electron microscopic observations of dough and bread supplemented with *Gastrodia elata* Blume powder. *Food Research International*, 36, 387-397.
- Kim, Y., Faqih, M. N., & Wang, S. S. (2001). Factors affecting gel formation of inulin. *Carbohydrate Polymers*, 46, 135-145.
- Kintner, P. k., & buren, J. p. V. (1982). Carbohydrate interference and its correction in pectin analysis using the m-hydroxydiphenyl method. *Journal of Food Science*, 47, 756-759.
- Knudsen, K. E. B., Jørgensena, H., & Theil, P. K. (2016). Changes in short-chain fatty acid plasma profile incurred by dietary fiber composition. *Journal of Animal Science*, 94, 476–479.

Kokubun, S., Ratcliffe, I., & Williams, P. A. (2013). Synthesis, characterization and self-assembly of biosurfactants based on hydrophobically modified inulins. *BioMacromolecules*, 14, 2830–2836.

Kokubun, S., Ratcliffe, I., & Williams, P. A. (2015). The emulsification properties of octenyl- and dodecenyl- succinylated inulins. *Food Hydrocolloids*, 50, 145-149.

Kokubun, S., Ratcliffe, I., & Williams, P. A. (2018). The interfacial, emulsification and encapsulation properties of hydrophobically modified inulin. *Carbohydrate Polymers*, 194, 18-23.

Kondo, T., Kishi, M., Fushimi, T., Jin, S. U., & Kaga, T. (2009). Vinegar intake reduces body weight, body fat mass, and serum triglyceride levels in obese Japanese subjects. *Bioscience, Biotechnology, and Biochemistry*, 73, 1837–1843.

Kumar, A., & Chauhan, G. (2010). Extraction and characterization of pectin from apple pomace and its evaluation as lipase (steapsin) inhibitor. *Carbohydrate Polymers*, 82(2), 454-459.

Le, M. H. A., Buchet, A. D. G., Beltranena, E., Gerrits, W. J. J., & Zijlstra, R. T. (2017). Digestibility and intestinal fermentability of canola meal from *Brassica juncea* and *Brassica napus* fed to ileal-cannulated grower pigs. *Animal Feed Science and Technology*, 234, 43-53.

Lee, K.-Y., Quero, F., Blaker, J. J., Hill, C. A. S., Eichhorn, S. J., & Bismarck, A. (2011). Surface only modification of bacterial cellulose nanofibres with organic acids. *Cellulose*, 18(3), 595–605.

- Lee, L. W., Liu, X., Wong, W. S. E., & Liu, S. Q. (2017). Effects of sucrose monopalmitate (P90), Tween 80 and modified starch on coffee aroma retention and release in coffee oil-based emulsions. *Food Hydrocolloids*, 66, 128-135.
- Lett, A. M., Yeomans, M. R., Nortona, I. T., & Norton, J. E. (2016). Enhancing expected food intake behaviour, hedonics and sensory characteristics of oil-in-water emulsion systems through microstructural properties, oil droplet size and flavour. *Food Quality and Preference*, 47, 148-155.
- Levy, A. W., Kessler, J. W., Fuller, L., Williams, S., Mathis, G. F., Lumpkins, B., & Valdez, F. (2015). Effect of feeding an encapsulated source of butyric acid (ButiPEARL) on the performance of male Cobb broilers reared to 42 d of age. *Poultry Science*, 94, 1864–1870.
- Li, J., Hwang, C., Chen, X., & Park, H. J. (2016). Effects of chitosan coating on curcumin loaded nano-emulsion: Study on stability and *in vitro* digestibility. *Food Hydrocolloids*, 60, 138-147.
- Li, W., Dobraszczyk, B. J., & Wilde, P. (2004). Surface properties and locations of gluten proteins and lipids revealed using confocal scanning laser microscopy in bread dough. *Journal of Cereal Science*, 39, 403-411.
- Li, X., Li, J., Gong, J., Kuang, Y., Mo, L., & Songa, T. (2018). Cellulose nanocrystals (CNCs) with different crystalline allomorph for oil in water Pickering emulsions. *Carbohydrate Polymers*, 183, 303–310.
- Li, X., Xie, Q., Zhu, J., Pan, Y., Meng, R., Zhang, B., Chen, H., & Jin, Z. (2019). Chitosan hydrochloride/carboxymethyl starch complex nanogels as novel Pickering

stabilizers: Physical stability and rheological properties. *Food Hydrocolloids*, 93, 215-225.

Li, Y., & McClements, D. J. (2010). New mathematical model for interpreting pH-stat digestion profiles: Impact of lipid droplet characteristics on *in vitro* digestibility. *Journal of Agricultural and Food Chemistry*, 58, 8085–8092.

Li, Y., Maux, S. L., Xiao, H., & McClements, D. J. (2009). Emulsion-based delivery systems for tributyrin, a potential colon cancer preventative agent *Journal of Agricultural and Food Chemistry*, 57, 9243–9249.

Liang, R., Jiang, Y., Yokoyama, W., Yanga, C., Cao, G., & Zhong, F. (2016). Preparation of Pickering emulsions with short, medium and long chain triacylglycerols stabilized by starch nanocrystals and their *in vitro* digestion properties. *RSC Advances*, 6, 99496-99508.

Liick, E., & Jager, M. (1997b). Propionic acid. In *Antimicrobial food additives* (pp. 145-150). New York: Springer-Verlag Berlin Heidelberg GmbH.

Lin, Q., Liang, R., Zhong, F., Ye, A., & Singh, H. (2018a). Interactions between octenylsuccinic-anhydride-modified starches and calcium in oil-in-water emulsions. *Food Hydrocolloids*, 77, 30-39.

Lin, Q., Liang, R., Zhong, F., Ye, A., & Singh, H. (2018b). Physical properties and biological fate of OSA-modified-starch-stabilized emulsions containing  $\beta$ -carotene: Effect of calcium and pH. *Food Hydrocolloids*, 77, 549-556.

Liu, C., Sun, R., Zhang, A., Ren, J., & Geng, Z. (2006). Structural and thermal characterization of sugarcane bagasse cellulose succinates prepared in ionic liquid. *Polymer Degradation and Stability*, 9, 3040e3047.

Liu, X., Huang, Y., Chen, X., Deng, Z., & Yang, X. (2019). Whole cereal protein-based Pickering emulsions prepared by zein-gliadin complex particles. *Journal of Cereal Science*, 87, 46-51.

Mackie, A., Gourcy, S., Rigby, N., Moffat, J., Capron, I., & Bajka, B. (2019). The fate of cellulose nanocrystal stabilised emulsions after simulated gastrointestinal digestion and exposure to intestinal mucosa. *Nanoscale*, 11, 2991-2998.

Mallo, J. J., Balfagón, A., Gracia, M. I., Honrubia, P., & Puyalto, M. (2012). Evaluation of different protections of butyric acid aiming for release in the last part of the gastrointestinal tract of piglets. *Journal of Animal Science*, 90, 227–229.

Marefati, A., Matos, M., Wiege, B., Haase, N. U., & Rayner, M. (2018). Pickering emulsifiers based on hydrophobically modified small granular starches Part II – Effects of modification on emulsifying capacity. *Carbohydrate Polymers*, 201, 416-424.

Masina, N., E.Choonara, Y., Kumar, P., Toit, L. C. d., Govender, M., Indermun, S., & Pillay, V. (2017). A review of the chemical modification techniques of starch. *Carbohydrate Polymers*, 157, 1226-1236.

McClements, D. J. (2013). Edible lipid nanoparticles: digestion, absorption, and potential toxicity. *Progress in Lipid Research*, 52 409–423.

McClements, D. J. (2008). The biophysics of digestion: lipids. *Current Opinion in Food Science*, 2018, 1–6.

McClements, D. J., Decker, E. A., Park, Y., & Weiss, J. (2008). Designing food structure to control stability, digestion, release and absorption of lipophilic food components. *Food Biophysics*, 3, 219–228.

Miao, C., Tayebi, M., & Hamad, W. Y. (2017). Investigation of the formation mechanisms in high internal phase Pickering emulsions stabilized by cellulose nanocrystals. *Philosophical transactions of the royal society A*, 376, 1-13.

Mikulcov, V., Bordes, R., Minarik, A., & Kasparkov, V. (2018). Pickering oil-in-water emulsions stabilized by carboxylated cellulose nanocrystals: Effect of the pH. *Food Hydrocolloids*, 80 60-67.

Minekus, M., Alming, M., Alvito, P., Ballance, S., Bohn, T., Bourlieu, C., Carrière, F., Boutrou, R., Corredig, M., Dupont, D., Dufour, C., Egge, L., Golding, M., Karakay, S., Kirkhus, B., Feunteun, S. L., Lesmes, U., Macierzanka, A., Mackie, A., Marze, S., McClements, D. J., Ménard, O., Recio, I., Santo, C. N., Singh, R. P., Vegarud, G. E., Wickham, M. S. J., Weitschies, W., & Brodkorb, A. (2014). A standardised static *in vitro* digestion method suitable for food – an international consensus. *Food & Function*, 5, 1113–1124.

Montoya, C. A., Rutherford, S. M., & Moughan, P. J. (2016). Kiwifruit fibre level influences the predicted production and absorption of SCFA in the hindgut of growing pigs using a combined *in vivo*–*in vitro* digestion methodology. *British Journal of Nutrition*, 115, 1317-1324.

Montoya, C. A., Saigeman, S., Rutherford, S. M., & Moughan, P. J. (2016). The digestion of kiwifruit (*Actinidia deliciosa*) fibre and the effect of kiwifruit on the digestibility of other dietary nutrients. *Food Chemistry*, 197, 539–545.

Morroso, J., Leveckeb, B., & Infantea, M. R. (2011). Hydrophobically modified inulin from alkenyl succinic anhydride in aqueous media. *Carbohydrate Polymers*, 84, 1110–1116.

- Mortensen, P. B., & Clausen, M. R. (1996). Short-chain fatty acids in the human colon: relation to gastrointestinal health and disease. *Scandinavian Journal of Gastroenterology*, 31, 132-148.
- Moughan, P. J., Rutherfurd, S. M., & Bala, P. (2013). Kiwifruit, mucins, and the gut barrier. *Advances in Food and Nutrition Research*, 68, 169-185.
- Mudgil, D., & Barak, S. (2013). Composition, properties and health benefits of indigestible carbohydrate polymers as dietary fiber: A review. *International Journal of Biological Macromolecules*, 61, 1-6.
- Mun, S., Decker, E. A., Park, Y., Weiss, J., & McClements, D. J. (2006). Influence of interfacial composition on *in vitro* digestibility of emulsified lipids: Potential mechanism for chitosan's ability to inhibit fat digestion. *Food Biophysics*, 1(1), 21–29.
- Narayanan, A., Baskaran, S. A., Amalaradjo, M. A. R., & Venkitanarayanan, K. (2015). Anticarcinogenic properties of medium chain fatty acids on human colorectal, skin and breast cancer cells *in vitro*. *International Journal of Molecular Sciences*, 16, 5014-5027.
- Ngouémazong, E. D., Christiaens, S., Shpigelman, A., Loey, A. V., & Hendrickx, M. (2015). The emulsifying and emulsion-stabilizing properties of pectin: A review. *Comprehensive Reviews in Food Science and Food Safety*, 14, 705–718.
- Ni, Y.-F., Wang, J., Yan, X.-L., Tian, F., Zhao, J.-B., Wang, Y.-J., & Jiang, T. (2010). Histone deacetylase inhibitor, butyrate, attenuates lipopolysaccharide-induced acute lung injury in mice. *Respiratory Research*, 11, 33-40.

Nilsson, L., & Bergenståhl, B. (2007). Adsorption of hydrophobically modified anionic starch at oppositely charged oil/water interfaces. *Journal of Colloid and Interface Science*, 308, 508-513.

Nini, L., Sarda, L., Comeau, L.-C., Boitard, E., Dubèsc, J.-P., & Chahinian, H. (2001). Lipase-catalysed hydrolysis of short-chain substrates in solution and in emulsion: a kinetic study. *Biochimica et Biophysica Acta (BBA) - Molecular and Cell Biology of Lipids*, 1534, 34-44.

P.Binks, B. (2002). Particles as surfactants—similarities and differences. *Current Opinion in Colloid & Interface Science*, 7, 21-41.

Pafumi, Y., Lairon, D., Porte, P. L. d. I., Juhel, C., Storch, J., Hamosh, M., & Armand, M. (2002). Mechanisms of inhibition of triacylglycerol hydrolysis by human gastric lipase. *The Journal Of Biological Chemistry*, 277, 28070–28079.

Parker, R., Rigby, N. M., Ridout, M. J., Gunning, A. P., & Wilde, P. J. (2018). The adsorption–desorption behaviour and structure function relationships of bile salts. *Soft Matter*, 10, 6457–6466.

Pedersen, A., Bardow, A., Jensen, S. B., & Nauntofte, B. (2002). Saliva and gastrointestinal functions of taste, mastication, swallowing and digestion. *Oral Diseases*, 8, 117–129.

Popat, A., Liu, J., Lu, G. Q. M., & Qiao, S. Z. (2012). A pH-responsive drug delivery system based on chitosan coated mesoporous silica nanoparticles. *Journal of Material Chemistry*, 22, 11173-11178.

Poul, E. L., Loison, C., Struyl, S., Springael, J.-Y., Lannoy, V., Decobecq, M.-E., Brezillon, S. p., Dupriez, V., Vassart, G., Damme, J. V., Parmentier, M., & Detheux,

- M. (2003). Functional characterization of human receptors for short chain fatty acids and their role in polymorphonuclear cell activation. *The Journal Of Biological Chemistry*, 278, 5481–25489.
- Ridel, L., Bolzinger, M.-A., Gilon-Delepine, N., Dugas, P.-Y., & Chevalier, Y. (2016). Pickering emulsions stabilized by charged nanoparticles. *Soft matter*, 12, 7564-7576.
- Rinaudo, M. (2006). Chitin and chitosan: Properties and applications. *Progress in Polymer Science*, 31, 603-632.
- Roberfroid, M. B. (2005). Introducing inulin-type fructans. *British Journal of Nutrition*, 93(S1), S13-S25.
- Roediger, W. E. W. (1982). Utilization of nutrients by isolated epithelial cells of the rat colon. *Gastroenterology*, 83, 424–429.
- Sandra, S., Decker, E. A., & McClements, D. J. (2008). Effect of interfacial protein cross-linking on the *in vitro* digestibility of emulsified corn oil by pancreatic lipase. *Journal of Agricultural and Food Chemistry*, 56, 7488–7494.
- Sanguansri, L., Day, L., Shen, Z., Fagan, P., Weerakkody, R., Cheng, L. J., Rusli, J., & Augustin, M. A. (2013). Encapsulation of mixtures of tuna oil, tributyrin and resveratrol in a spray dried powder formulation. *Food & Function*, 4, 1794–1802.
- Sarkar, A., Ademuyiwa, V., Stublely, S., Esa, N. H., M.Goycoolea, F., Qin, X., Gonzalez, F., & Olvera, C. (2018). Pickering emulsions co-stabilized by composite protein/ polysaccharide particle-particle interfaces: Impact on *in vitro* gastric stability. *Food Hydrocolloids*, 282-291.

Sarkar, A., Goh, K. K. T., Singh, R. P., & Singh, H. (2009). Behaviour of an oil-in-water emulsion stabilized by  $\beta$ -lactoglobulin in an *in vitro* gastric model. *Food Hydrocolloids*, 23, 1563-1569.

Sarkar, A., Li, H., Cray, D., & Boxall, S. (2018). Composite whey protein-cellulose nanocrystals at oil-water interface: Towards delaying lipid digestion. *Food Hydrocolloids*, 77, 436-444.

Sarkar, A., Murray, B., Holmes, M., Ettelaie, R., Abdalla, A., & Yang, X. (2016). *In vitro* digestion of Pickering emulsions stabilized by soft whey protein microgel particles: influence of thermal treatment. *Soft Matter*, 12, 3558-3569.

Sarkar, A., Ye, A., & Singh, H. (2016). On the role of bile salts in the digestion of emulsified lipids. *Food Hydrocolloids*, 60, 77-84.

Sarkar, A., Zhang, S., Holmes, M., & Ettelaie, R. (2019). Colloidal aspects of digestion of Pickering emulsions: Experiments and theoretical models of lipid digestion kinetics. *Advances in Colloid and Interface Science*, 263, 195-211.

Sarkar, A., Zhang, S., Murray, B., Russell, J., & Boxal, S. (2017). Modulating *in vitro* gastric digestion of emulsions using composite whey protein-cellulose nanocrystal interfaces. *Colloids and Surfaces B: Biointerfaces*, 158, 137-146.

Sassene, P. J., Fanø, M., Mu, H., Rades, T., Aquistapace, S., Schmitt, B., Cruz-Hernandez, C., Wooster, T. J., & Müllertz, A. (2016). Comparison of lipases for *in vitro* models of gastric digestion: lipolysis using two infant formulas as model substrates. *Food & Function*, 7, 3989-3998.

Scarpellini, E., Lauritano, E. C., Lupascu, A., Petruzzellis, C., Novi, M., Roccarina, D., Gabrielli, M., Serricchio, M., Gasbarrini, G. B., & Gasbarrini, A. (2007). Efficacy of

butyrate in the treatment of diarrhoea-predominant irritable bowel syndrome. *Digestive and Liver Disease Supplements*, 1, 19-22.

Schaaf, U. v. d., Schütz, L., & Karbstein, H. P. (2017). Interfacial and emulsifying properties of citrus pectin: Interaction of pH, ionic strength and degree of esterification. *Food Hydrocolloids*, 62, 288-298.

Scheppach, W. (1995). Effects of short chain fatty acids on gut morphology and function. *Gut*, 1, S35-S38.

Schokker, D., Zhang, J., Vastenhouw, S. A., Heilig, H. G. H. J., Smidt, H., Rebel, J. M. J., & Smits, M. A. (2015). Long-lasting effects of early-life antibiotic treatment and routine animal handling on gut microbiota composition and immune system in pigs. *Plos one*, 1-18.

Schulz, P. C., Rodríguez, M. S., Blanco, L. F. D., Pistonesi, M., & Agulló, E. (1988). Emulsification properties of chitosan. *Colloids and Polymer Science*, 276, 1159–1165.

Sealy, L., & Chalkley, R. (1978). The effect of sodium butyrate on histone modification. *Cell*, 14, 115-121.

Short, F. J., Gorton, P. G., Wiseman, J. W., & Boorman, K. N. (1996). Determination of titanium dioxide added as an inert marker in chicken digestibility studies. *Animal Feed Science and Technology*, 59, 215-221.

Siew, C. K., Williams, P., Cui, S., & Wang, Q. (2008). Characterization of the surface-active components of sugar beet pectin and the hydrodynamic thickness of the adsorbed pectin layer. *Journal of Agricultural and Food Chemistry*, 56, 8111–8120.

Silva, F. C. D., Fonseca, C. R. D., Alencar, S. M. D., Thomazini, M., Balieiro, J. C. d. C., Pittia, P., & Fávoro-Trindade, C. S. (2013). Assessment of production efficiency, physicochemical properties and storage stability of spray-dried propolis, a natural food additive, using gum Arabic and OSA starch-based carrier systems. *Food and Bioproducts Processing*, 91, 28-36.

Singh, S. P., Jadaun, J. S., Narnoliya, L. K., & Pandey, A. (2017). Prebiotic oligosaccharides: Special focus on fructooligosaccharides, its biosynthesis and bioactivity. *Applied Biochemistry and Biotechnology*, 183(2), 613–635.

Sobczak, A., & Kozłowski, K. (2016). Effect of dietary supplementation with butyric acid or sodium butyrate on egg production and physiological parameters in laying hens. *European Poultry Science*, 80, 1-14.

Tadrosa, T. F., Vandamme, A., Booten, K., Leveck, B., & Stevens, C. V. (2004). Stabilisation of emulsions using hydrophobically modified inulin (polyfructose). *Colloids and Surfaces A: Physicochemical and Engineering Aspects*, 250, 133–140.

Tan, J., McKenzie, C., Potamitis, M., Thorburn, A. N., Mackay, C. R., & Macia, L. (2014). The role of short-chain fatty acids in health and disease. *Advances in Immunology*, 121, 91-119.

Torres, O., S.Murray, B., & Sarkar, A. (2019). Overcoming *in vitro* gastric destabilisation of emulsion droplets using emulsion microgel particles for targeted intestinal release of fatty acids. *Food Hydrocolloids*, 89, 523-533.

Treichel, H., Oliveira, D. d., Mazutti, M. A., Luccio, M. D., & Oliveira, J. V. (2010). A Review on Microbial Lipases Production. *Food and Bioprocess Technology*, 3, 182–196.

Tzoumaki, M., Moschakis, T., Kiosseoglou, V., & Biliaderis, C. (2011). Oil-in-water emulsions stabilized by chitin nanocrystal particles. *Food Hydrocolloids*, 25, 1521-1529.

Venegas, D. P., Fuente, M. K. D. I., Landskron, G., González, M. J., Quera, R., Dijkstra, G., Harmsen, H. J. M., Faber, K. N., & Hermoso, M. A. (2019). Short chain fatty acids (SCFAs)-mediated gut epithelial and immune regulation and its relevance for inflammatory bowel diseases. *Frontiers in Immunology*, 10, 00277.

Verkempinck, S. H. E., Salvia-Trujillo, L., Denis, S., Loey, A. M. V., Hendrickx, M. E., & Grauwet, T. (2018). Pectin influences the kinetics of *in vitro* lipid digestion in oil-in-water emulsions. *Food Chemistry*, 262, 150–161.

Verrijssen, T. A. J., Christiaens, S., Verkempinck, S. H. E., Boeve, J., Grauwet, T., Loey, A. M. V., Salvia-Trujillo, L., & Hendrickx, M. E. (2016). *In vitro*  $\beta$ -carotene bioaccessibility and lipid digestion in emulsions: influence of pectin type and degree of methyl-esterification. *Journal of Food Science*, 81, C2327 - C2336.

Verrijssen, T. A. J., Verkempinck, S. H. E., Christiaens, S., Loey, A. M. V., & Hendrickx, M. E. (2015). The effect of pectin on *in vitro*  $\beta$ -carotene bioaccessibility and lipid digestion in low fat emulsions. *Food Hydrocolloids*, 49, 73 - 81.

Voltolini, C., Battersby, S., Etherington, S. L., Petraglia, F., Norman, J. E., & Jabbour, H. N. (2012). A novel antiinflammatory role for the short-chain fatty acids in human labor. *Endocrinology*, 153, 395–403.

Waldecker, M., Kautenburger, T., Daumann, H., Busch, C., & Schrenk, D. (2008). Inhibition of histone-deacetylase activity by short-chain fatty acids and some

polyphenol metabolites formed in the colon. *Journal of Nutritional Biochemistry*, 19, 587–593.

Wang, L., Hu, L., Yan, S., Jiang, T., Fang, S., Wang, G., Zhao, J., Zhang, H., & Chen, W. (2017). Effects of different oligosaccharides at various dosages on the composition of gut microbiota and short-chain fatty acids in mice with constipation. *Food & Function*, 8, 1966–1978.

Wang, L., Hu, L., Yan, S., Jiang, T., Fang, S., Wang, G., Zhao, J., Zhang, H., & Chen, W. (2017). Effects of different oligosaccharides at various dosages on the composition of gut microbiota and short-chain fatty acids in mice with constipation. *Food & Function*, 8, 1966–1978.

Wilde, P. J., & Chu, B. S. (2011). Interfacial & colloidal aspects of lipid digestion. *Advances in Colloid and Interface Science*, 165, 14-22.

Wilfart, A., Montagne, L., Simmins, H. H., Noblet, J., & Milgen, J. v. (2007). Effect of fibre content in the diet on the mean retention time in different segments of the digestive tract in growing pigs. *Livestock Science*, 109, 27-29.

Wong, J. M., de Souza, R., Kendall, C.W., Emam, A., & Jenkins, D. J. (2006). Colonic health: Fermentation and short chain fatty acids. *Journal of Clinical Gastroenterology*, 40, 235.

Yan, H., Chen, X., Song, H., Li, J., Feng, Y., Shi, Z., Wang, X., & Lin, Q. (2017). Synthesis of bacterial cellulose and bacterial cellulose nanocrystals for their applications in the stabilization of olive oil pickering emulsion. *Food Hydrocolloids*, 72, 127-135.

Yusoff, A., & Murray, B. S. (2011). Modified starch granules as particle-stabilizers of oil-in-water emulsions. *Food Hydrocolloids*, 25, 42-55.

Zembyla, M., Murray, B. S., & Sarkar, A. (2018). Water-In-Oil Pickering Emulsions Stabilized by Water-Insoluble Polyphenol Crystals. *Langmuir*, 34, 10001–10011.

## Appendixes

### Chapter 3 - *In vitro* digestion of SCFA-supplemented emulsions

#### using various carbohydrate surfactants: a screening study

#### 3.1. Effects of WPI concentrations and TP:SO weight ratios on particle size and $\zeta$ -potential (mV) of the emulsions

**Table 3A.1.** Average sizes ( $d_{32}$  and  $d_{43}$ ,  $\mu\text{m}$ ) and  $\zeta$ -potential (mV) of different WPI-stabilised emulsions at various WPI concentrations and TP:SO weight ratios

WPI concentration	TP:SO	$d_{32}$	$d_{43}$	$\zeta$ -potential
0.5 wt%	1:0	$7.3 \pm 6.2^a$	$58 \pm 55^a$	$-20.6 \pm 3.4^a$
	1:1	$0.297 \pm 0.001^b$	$0.458 \pm 0.003^b$	$-9.1 \pm 0.5^c$
	1:2	$0.197 \pm 0.015^c$	$0.316 \pm 0.016^c$	$-11.1 \pm 0.4^b$
1.0 wt%	1:0	$29.5 \pm 16.5^a$	$215 \pm 252^a$	$-21.8 \pm 5.0^a$
	1:1	$0.166 \pm 0.004^d$	$0.280 \pm 0.005^d$	$-10.3 \pm 1.0^{bc}$
	1:2	$0.142 \pm 0.001^f$	$0.224 \pm 0.001^f$	$-12.1 \pm 1.0^b$
1.5 wt%	1:0	$18.9 \pm 10.0^a$	$107 \pm 138^a$	$-20.8 \pm 5.6^a$
	1:1	$0.152 \pm 0.001^e$	$0.249 \pm 0.001^e$	$-12.3 \pm 1.3^b$
	1:2	$0.128 \pm 0.001^h$	$0.193 \pm 0.001^h$	$-13.5 \pm 1.1^b$
2.0 wt%	1:0	$13.5 \pm 1.6^a$	$29.7 \pm 1.0^a$	$-23.4 \pm 4.0^a$
	1:1	$0.139 \pm 0.001^f$	$0.222 \pm 0.002^f$	$-12.0 \pm 2.1^b$
	1:2	$0.127 \pm 0.001^h$	$0.181 \pm 0.001^i$	$-14.4 \pm 1.1^b$
2.5 wt%	1:0	$15.2 \pm 7.2^a$	$99.5 \pm 90.5^a$	$-20.8 \pm 4.8^a$
	1:1	$0.133 \pm 0.001^g$	$0.210 \pm 0.001^g$	$-13.0 \pm 2.0^b$
	1:2	$0.121 \pm 0.001^i$	$0.168 \pm 0.001^i$	$-13.5 \pm 1.1^b$

<sup>a</sup> Samples within the same column with the same superscript letters are not different from one another ( $p \leq 0.05$ )

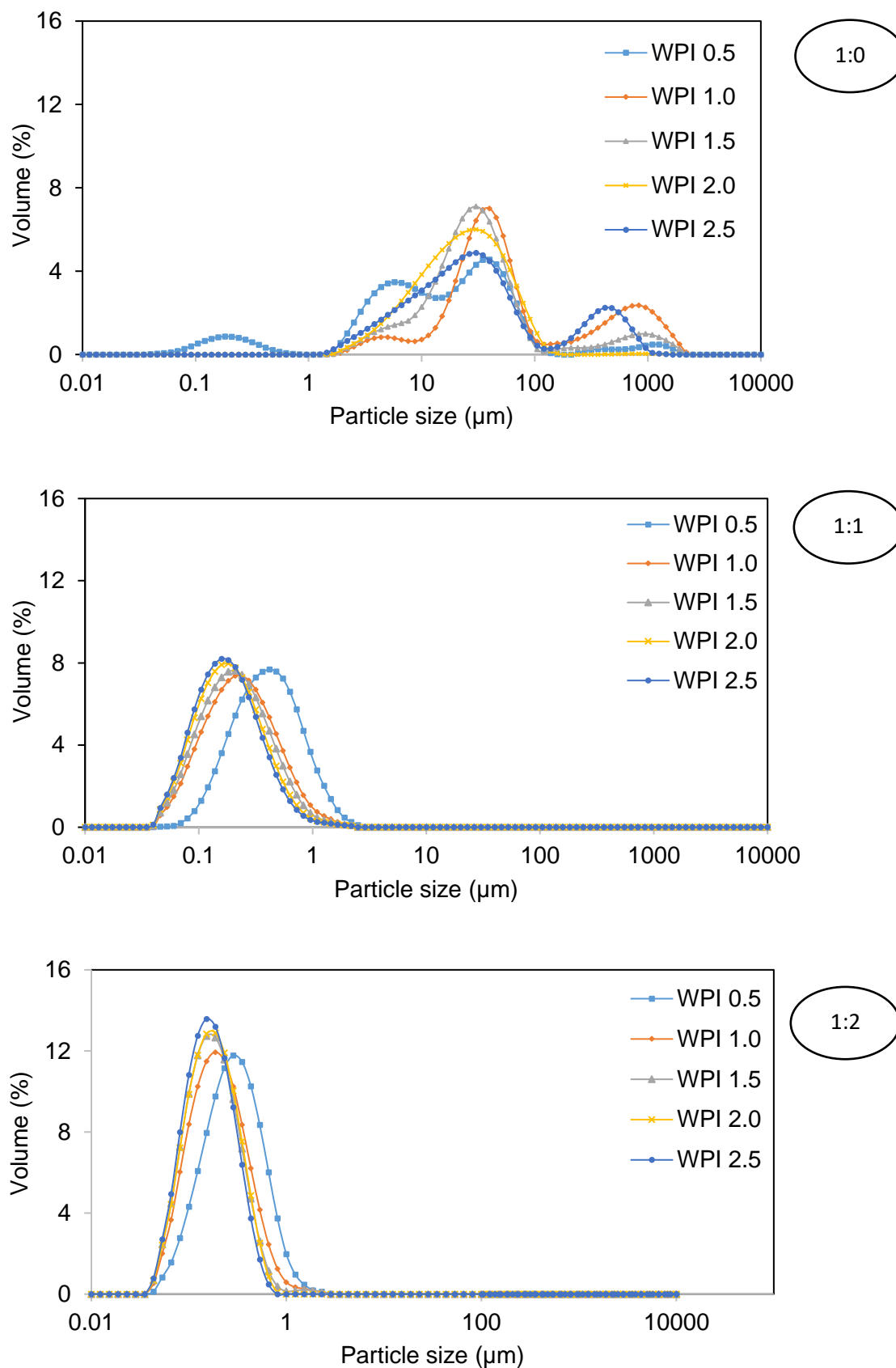


**Figure A3.1.** Size distributions of particles in various emulsions at different TP:SO weight ratio (1:0, 1:1 and 1:2) and WPI concentrations (wt%)

**Table 3A.2.** Changes of average sizes ( $\mu\text{m}$ ) of TP:SO (1:1) emulsions at different WPI concentrations for 4 days storage at 4°C

WPI concentration		$d_{32}$	$d_{43}$
0.5 wt%	0h	0.297 ± 0.001 <sup>a</sup>	0.458 ± 0.003 <sup>b</sup>
	2 days	0.285 ± 0.014 <sup>a</sup>	0.520 ± 0.059 <sup>ab</sup>
	4 days	0.307 ± 0.012 <sup>a</sup>	0.579 ± 0.006 <sup>a</sup>
1.0 wt%	0h	0.166 ± 0.004 <sup>b</sup>	0.280 ± 0.005 <sup>c</sup>
	2 days	0.173 ± 0.006 <sup>b</sup>	0.289 ± 0.009 <sup>c</sup>
	4 days	0.168 ± 0.001 <sup>b</sup>	0.279 ± 0.002 <sup>c</sup>
2.5 wt%	0h	0.152 ± 0.001 <sup>c</sup>	0.249 ± 0.001 <sup>d</sup>
	2 days	0.150 ± 0.001 <sup>c</sup>	0.245 ± 0.001 <sup>d</sup>
	4 days	0.151 ± 0.001 <sup>c</sup>	0.244 ± 0.001 <sup>d</sup>
2.0 wt%	0h	0.139 ± 0.001 <sup>d</sup>	0.222 ± 0.002 <sup>e</sup>
	2 days	0.139 ± 0.001 <sup>d</sup>	0.221 ± 0.001 <sup>e</sup>
	4 days	0.139 ± 0.01 <sup>d</sup>	0.217 ± 0.003 <sup>e</sup>
2.5 wt%	0h	0.133 ± 0.001 <sup>e</sup>	0.210 ± 0.007 <sup>f</sup>
	2 days	0.130 ± 0.002 <sup>e</sup>	0.202 ± 0.003 <sup>f</sup>
	4 days	0.133 ± 0.001 <sup>e</sup>	0.206 ± 0.001 <sup>f</sup>

<sup>a</sup> Samples within the same column with the same superscript letters are not different from one another ( $p \leq 0.05$ )

### 3.2. Effects of modified starch (GUM 2000) concentrations on particle sizes and $\zeta$ -potential (mV) of the emulsions (TP:SO ratio was 1:1)

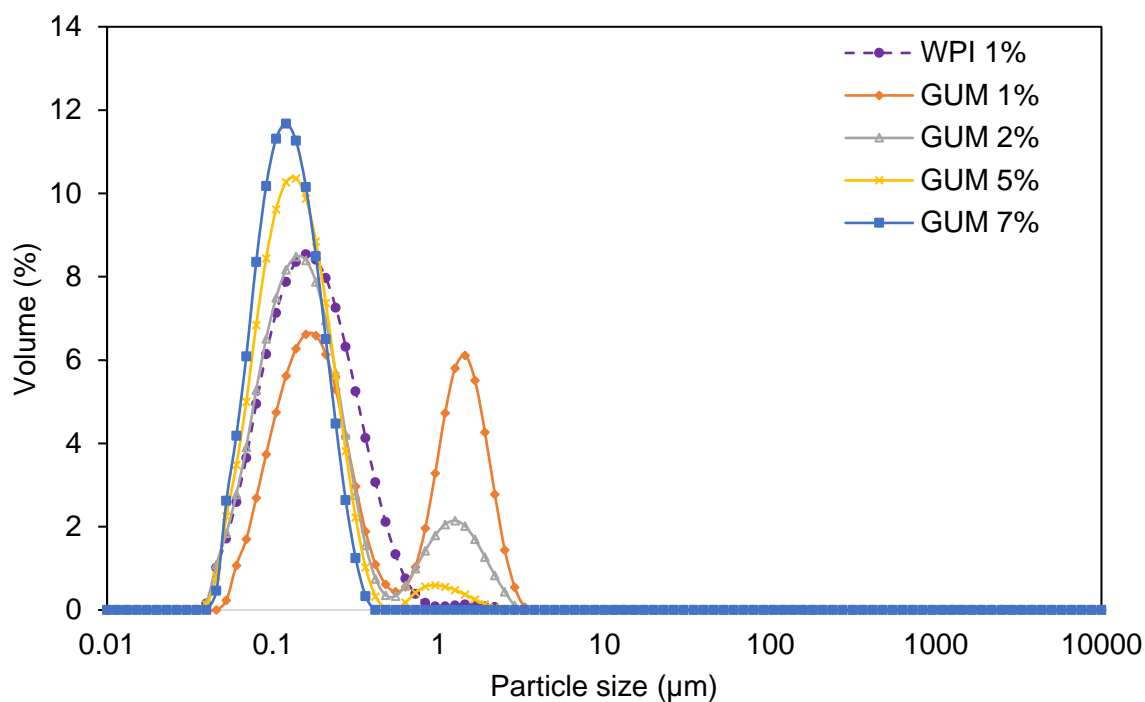


**Figure A3.2.** Particle size distribution of WPI-stabilised and various GUM-stabilised emulsions

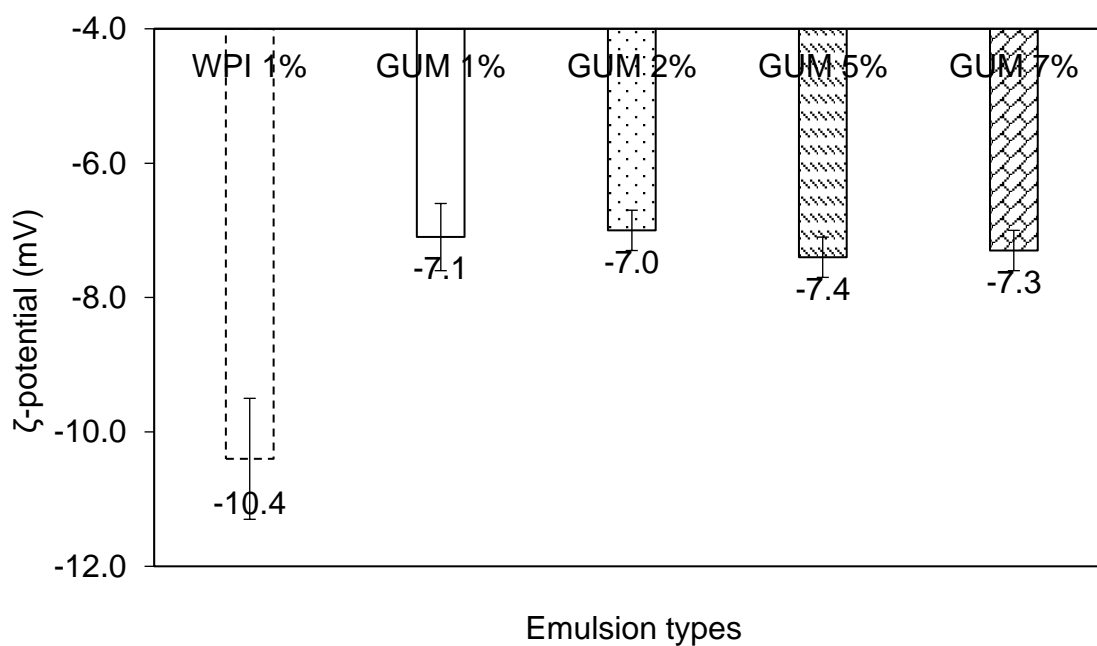


**Figure A3.3.**  $\zeta$ -potential (mV) of various carbohydrate-based emulsions

### 3.3. Effects of different pectin concentrations on particle sizes and $\zeta$ -potential (mV) of the emulsions (TP:SO ratio was 1:1)

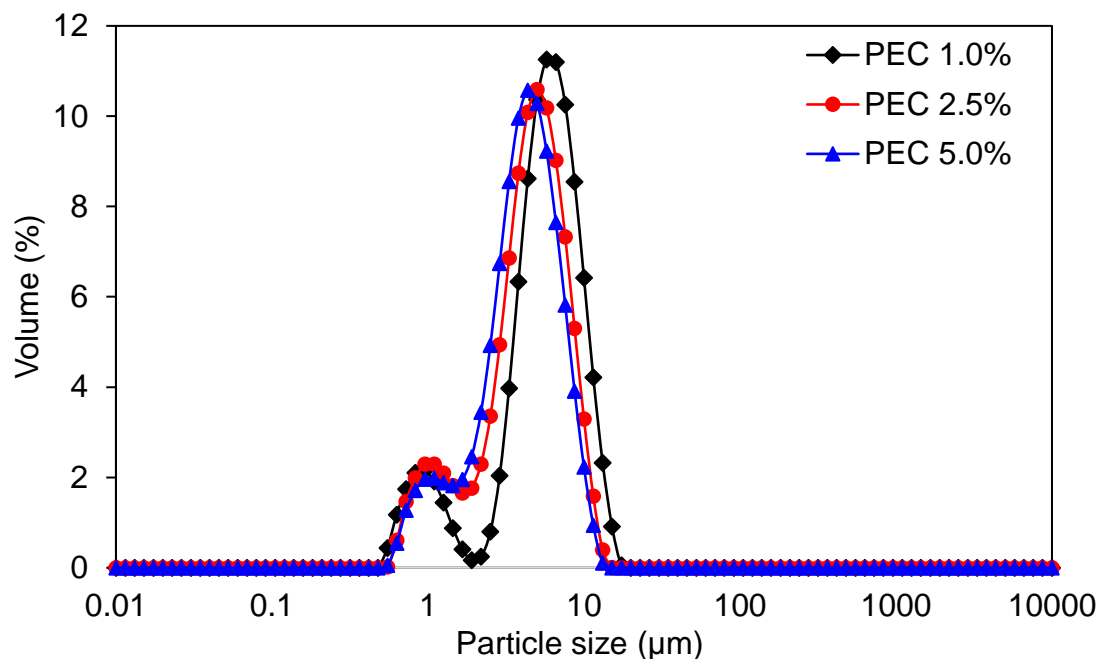


**Figure A3.4.** Effects of pectin concentration (1.0–5.0 wt%) on particle size distributions

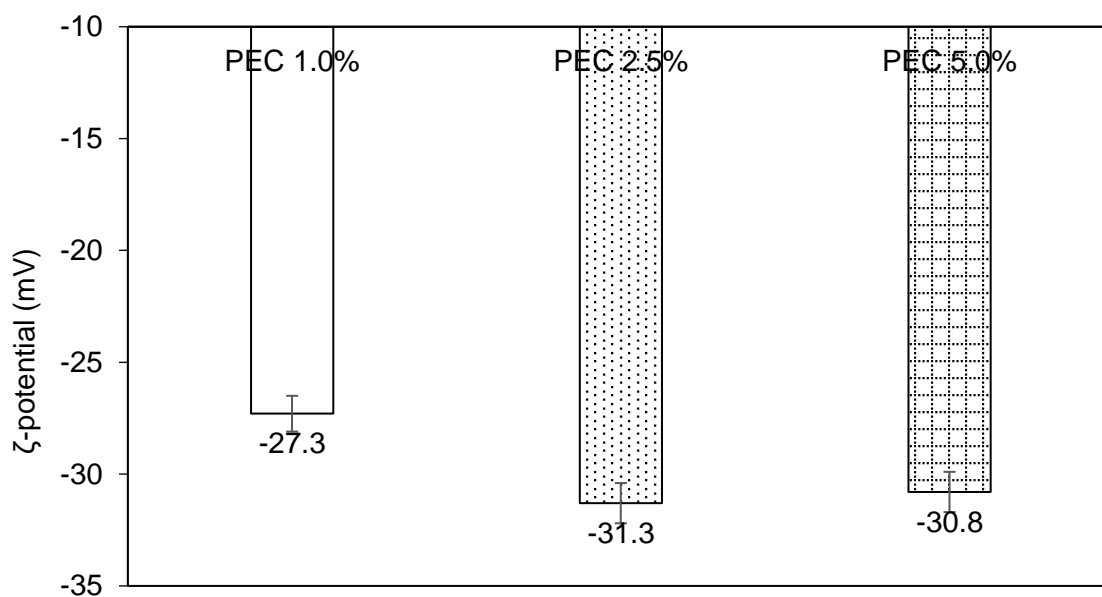


**Figure A3.5.** Effects of pectin concentration (1.0–5.0 wt%) on  $\zeta$ -potential (mV)

### 3.4. Standard curve for quantification of TP and corresponding spectrum

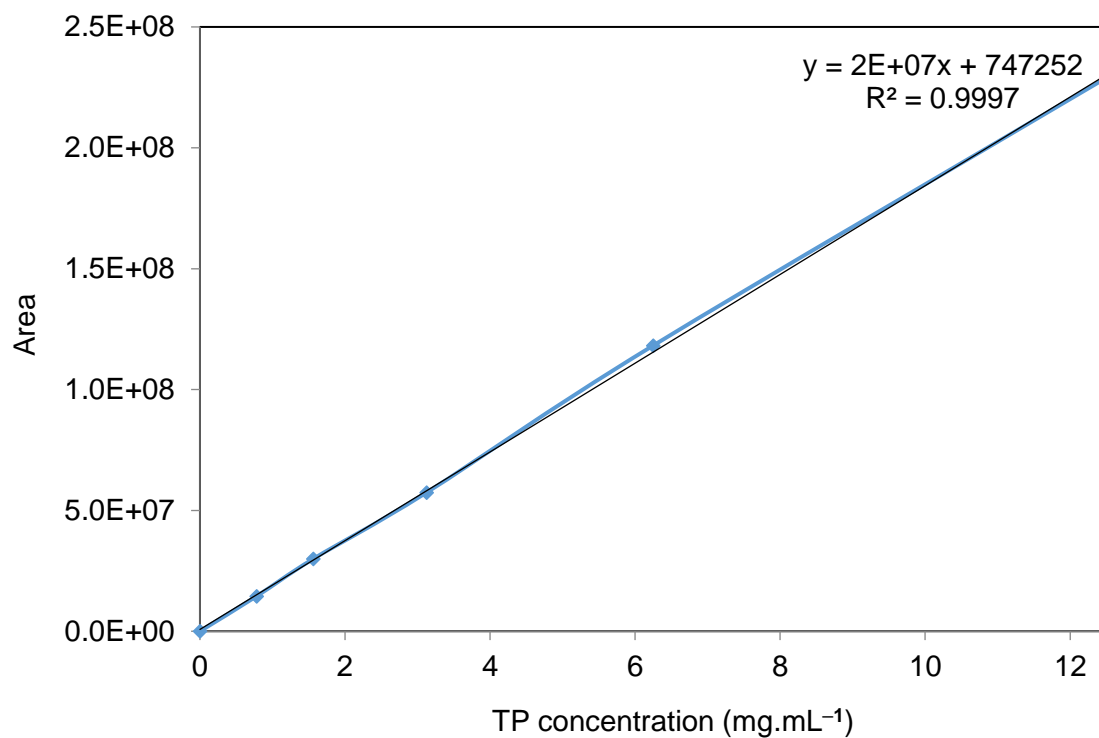


**Figure A3.6.** Standard curve for analysis of TP

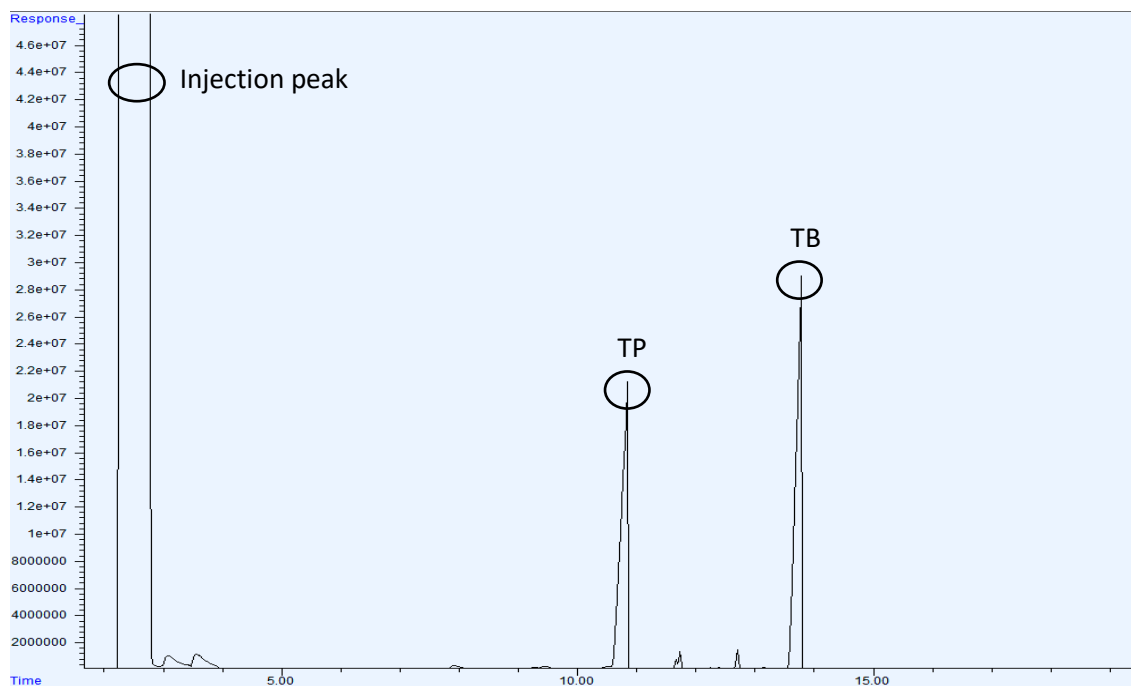


**Figure A3.7.** GC spectrum of standard TP (6 mg.mL<sup>-1</sup>) and internal standard TB

### 3.5. Standard curve for quantification of PA and corresponding GC spectrum

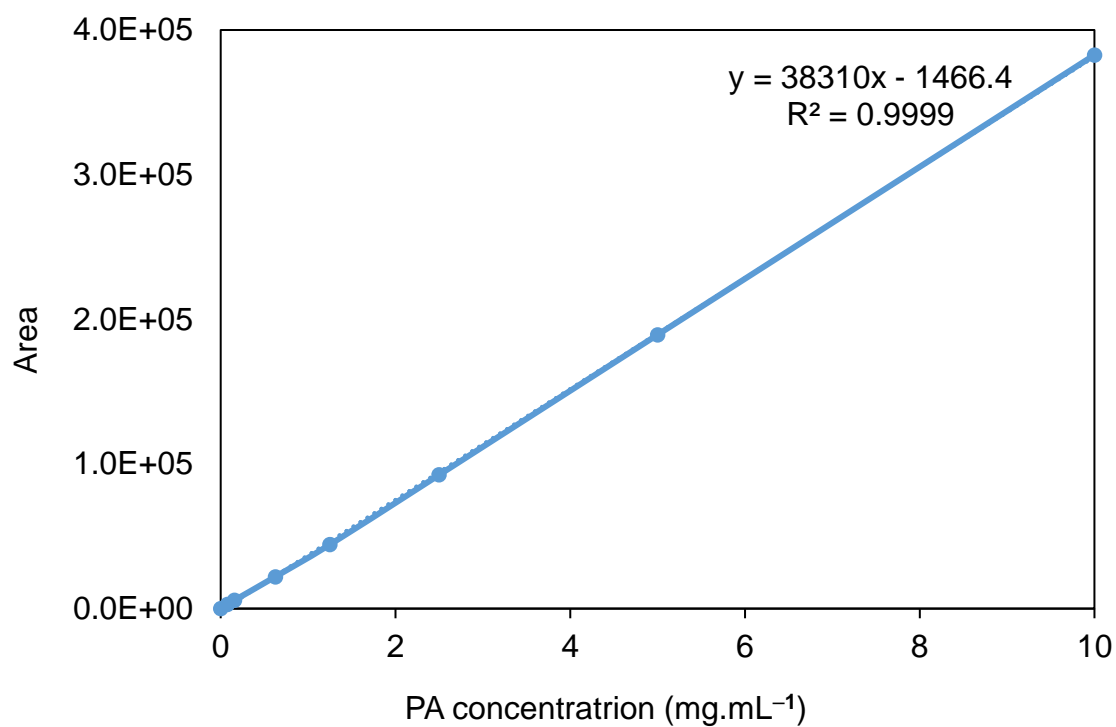


Figure A3.8. Standard curve for quantification of PA

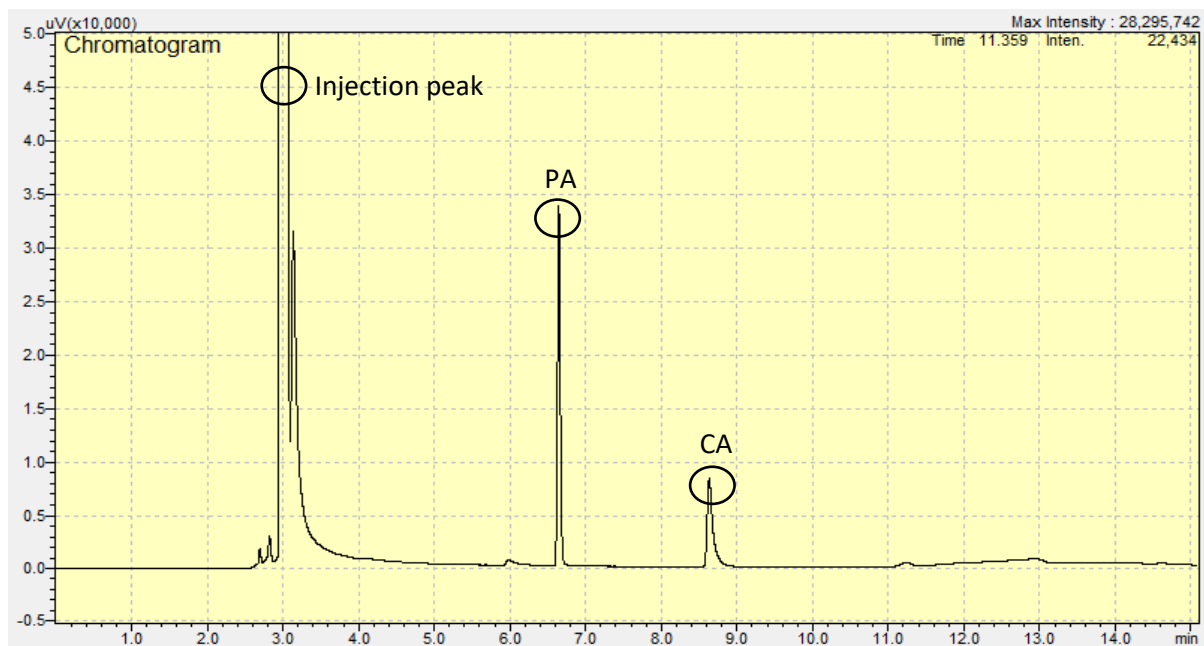
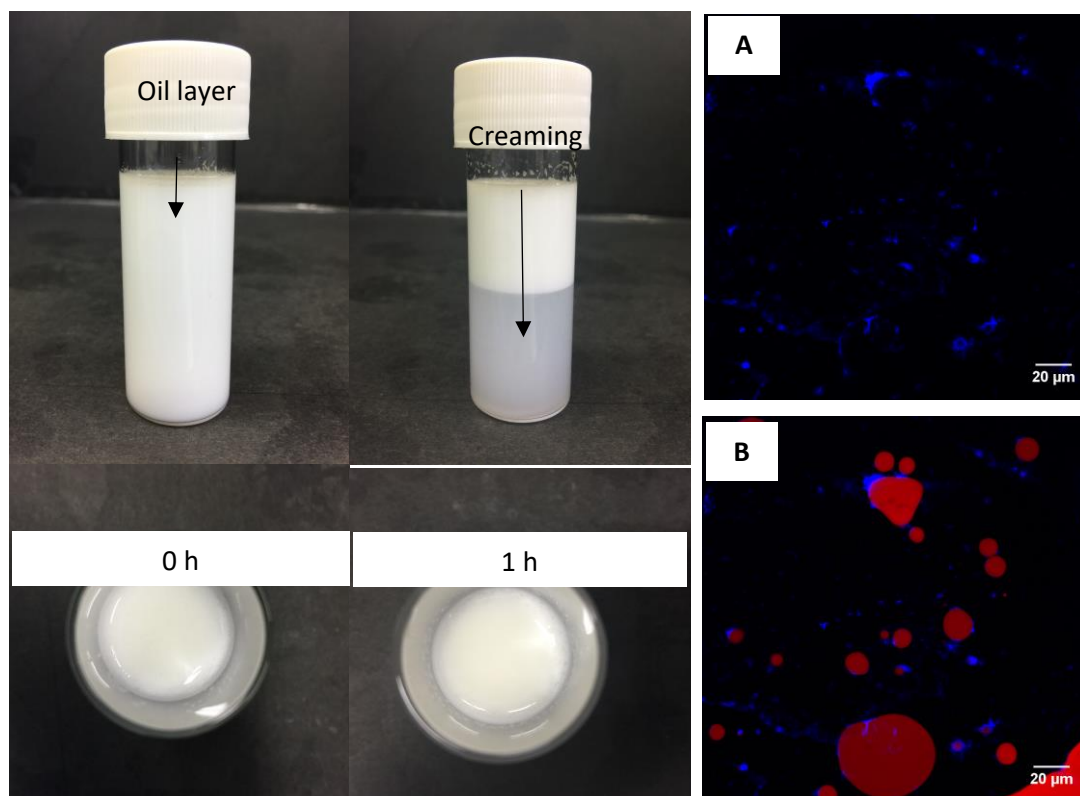


Figure A3.9. GC spectrum of standard PA (6 mg.mL<sup>-1</sup>) and internal standard CA

**Table 3A.3.**  $\zeta$ -potential (mV) of various gastric digesta

<b>Gastric digesta</b>	WPI	GUM	M-IN	PEC	WIP-CS
$\zeta$ -potential	$5.2 \pm 0.1$	$-1.2 \pm 0.1$	$-10.3 \pm 1.5$	$-1.6 \pm 0.2$	Phase separation

## Chapter 5 - *In vitro* digestion of SCFA-supplemented Pickering emulsions using hydrophobically modified CNCs



**Figure A5.1.** Visual images of creaming stability of freshly prepared emulsions stabilised by 1.00 wt% CNCs and after 1 h of storage at 4 °C, and confocal images of the freshly prepared emulsion (A: CNC channel; B: merge channel of CNCs and oil droplets); the red colour represents the oil phase (stained by Nile Red); the blue colour represents the CNCs (stained by Calcofluor-white).

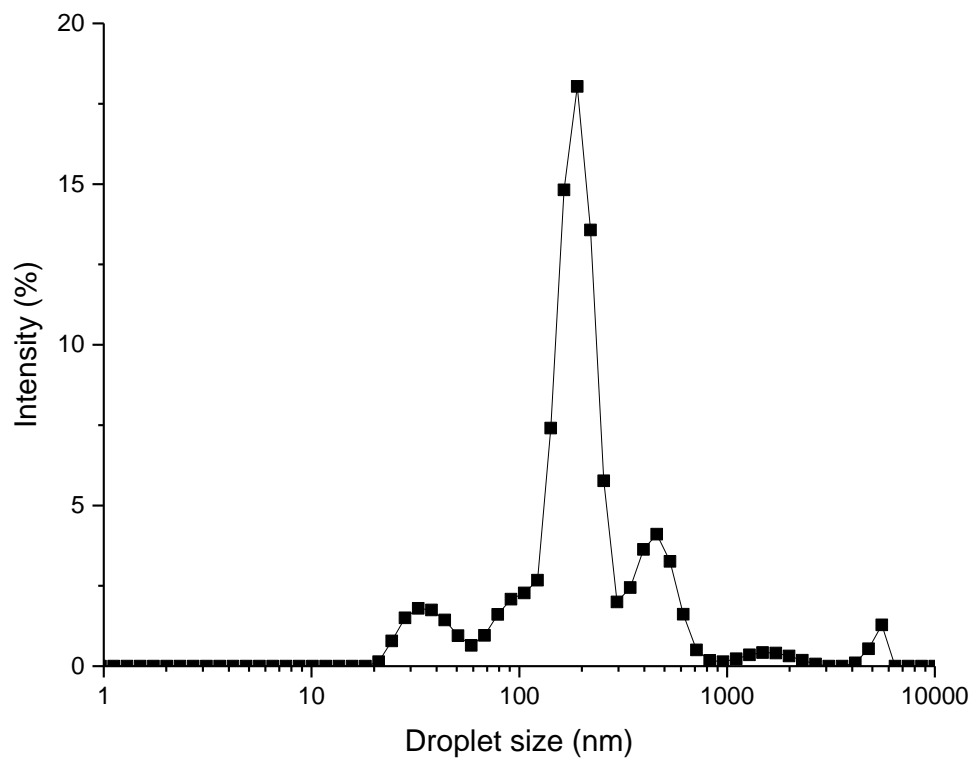


**Figure A5.2.** Particle size distribution of 1.00 wt% MCNC dispersion measured by a zetasizer (ZS Nano, Malvern Instruments Ltd, UK).

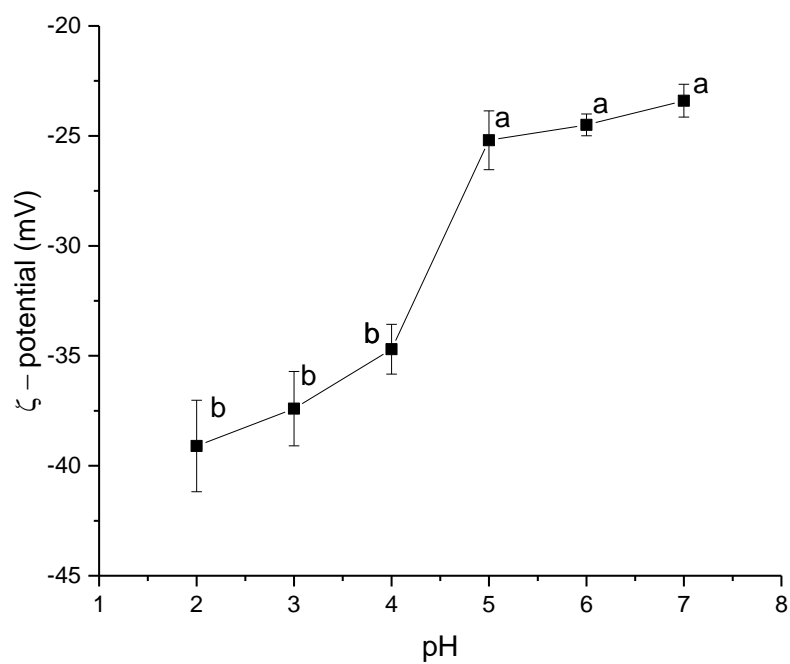


**Figure A5.3.** Mean  $\zeta$ -potential values of a 1.00 wt% MCNC dispersion as a function of pH. Error bars represent standard deviations. Different superscripts (a–b) in the curve represent significant differences at different pHs at the  $p < 0.05$  level.

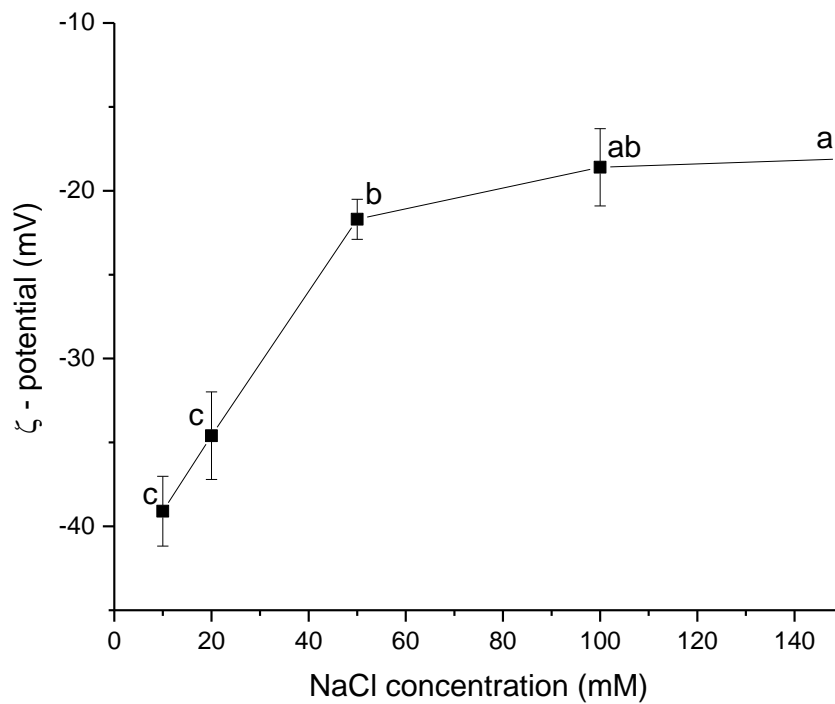


**Figure A5.4.** Mean  $\zeta$ -potential values of a 1.00 wt% MCNC dispersion as a function of ionic strength. Error bars represent standard deviations. Different superscripts (a–c) in the curve represent significant differences at different ionic strengths at the  $p < 0.05$  level.

**Table A5.1.** Mean droplet sizes of various freshly prepared emulsions, where only population in the first peak has been taken into account, latter representing the sizes of the unadsorbed cellulose nanocrystals. The values are the mean and standard deviation of at least three measurements on triplicate samples ( $n = 3 \times 3$ ).

Emulsions	$d_{32}$ (nm)	$d_{43}$ (nm)
E0.05	$38 \pm 02^a$	$86 \pm 12^a$
E0.10	$36 \pm 02^a$	$69 \pm 06^{ab}$
E0.20	$36 \pm 00^a$	$66 \pm 02^b$
E0.50	$36 \pm 00^a$	$64 \pm 01^b$
E1.00	$33 \pm 00^b$	$58 \pm 01^c$

Different superscripts (a–c) in the same column represent significant differences between different samples at the  $p < 0.05$  level.

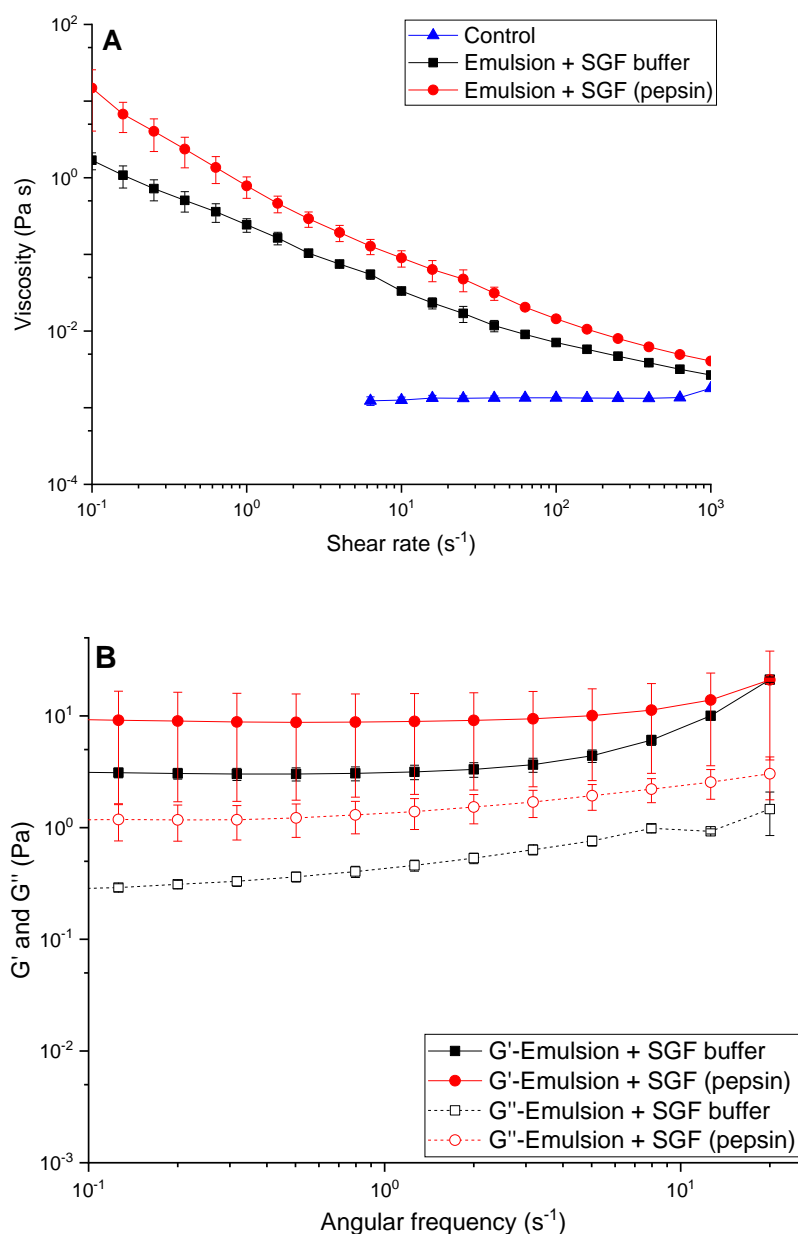


**Figure A5.5.** (A) Apparent viscosities of control (diluted freshly prepared emulsion, i.e. 10 wt% oil) and mixtures of the freshly prepared emulsion with SGF buffer without added pepsin (Emulsion + SGF buffer) and with added pepsin [Emulsion + SGF (pepsin)] at shear rates ranging from 0 to 1000  $s^{-1}$ . (B) Storage modulus ( $G'$ ) and viscous modulus ( $G''$ ) of the two systems [Emulsion + SGF buffer and Emulsion + SGF (pepsin)] at angular frequencies ranging from 0.1 to 20  $s^{-1}$ . The plotted values are the average of at least three measurements on triplicate samples ( $n = 3 \times 3$ ).

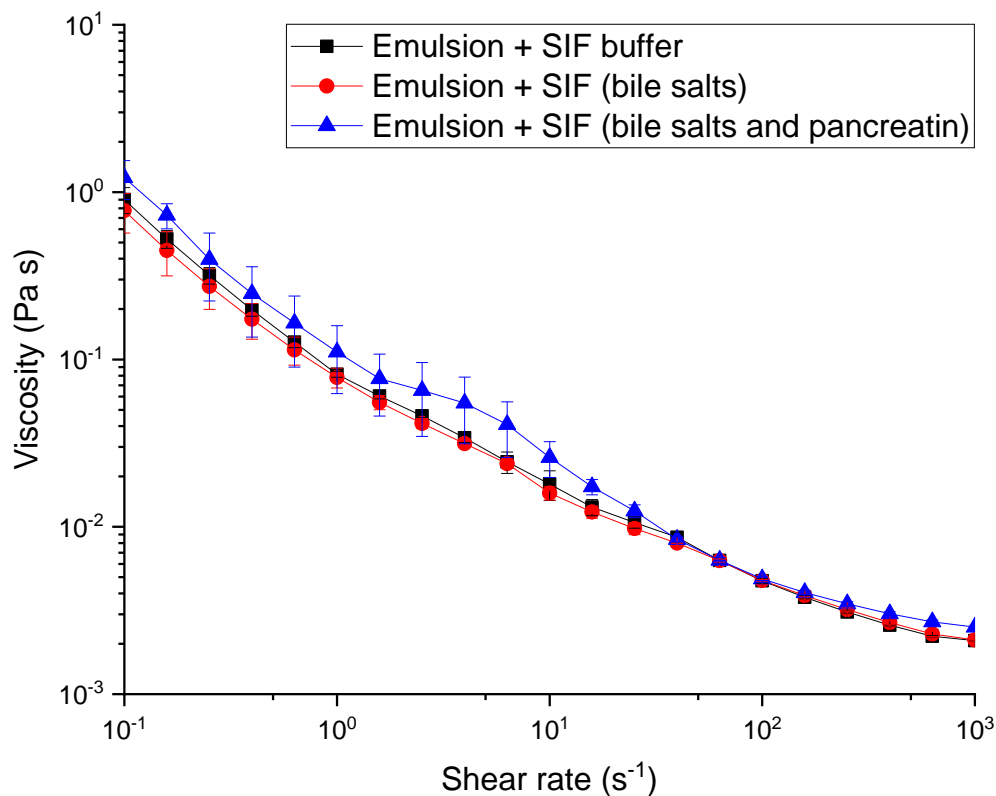


**Figure A5.6.** Apparent viscosities of the intestinal–digested samples from freshly prepared emulsions: (1) emulsion with SIF buffer; (2) emulsion with SIF buffer containing bile salts; (3) emulsion with SIF buffer containing bile salts and pancreatin after 3 h of digestion at 37 °C at shear rates ranging from 0 to 1000 s<sup>-1</sup>. The plotted values are the average of at least three measurements on triplicate samples ( $n = 3 \times 3$ ).

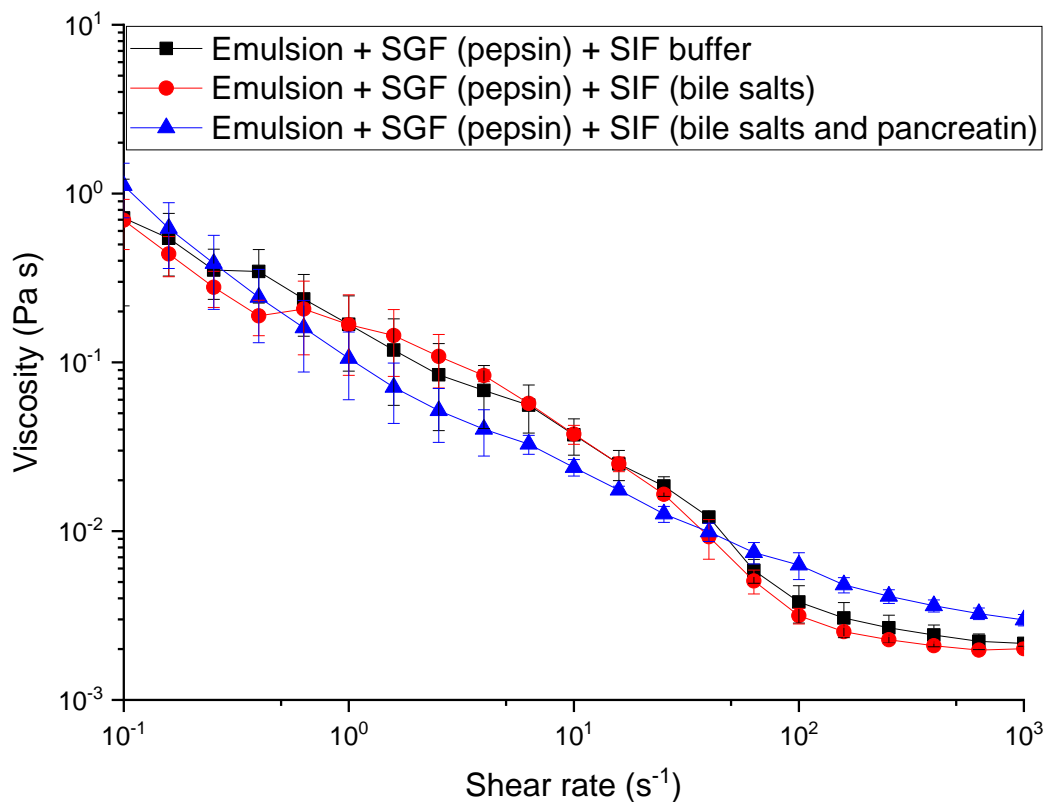


**Figure A5.7.** Apparent viscosities of the sequential gastrointestinal-digested samples: (1) emulsion + SGF (pepsin) with SIF buffer; (2) emulsion + SGF (pepsin) with SIF buffer containing bile salts; (3) emulsion + SGF (pepsin) with SIF buffer containing bile salts and pancreatin after 3 h of digestion at 37 °C at shear rates ranging from 0 to 1000 s<sup>-1</sup>. The plotted values are the average of at least three measurements on triplicate samples ( $n = 3 \times 3$ ).

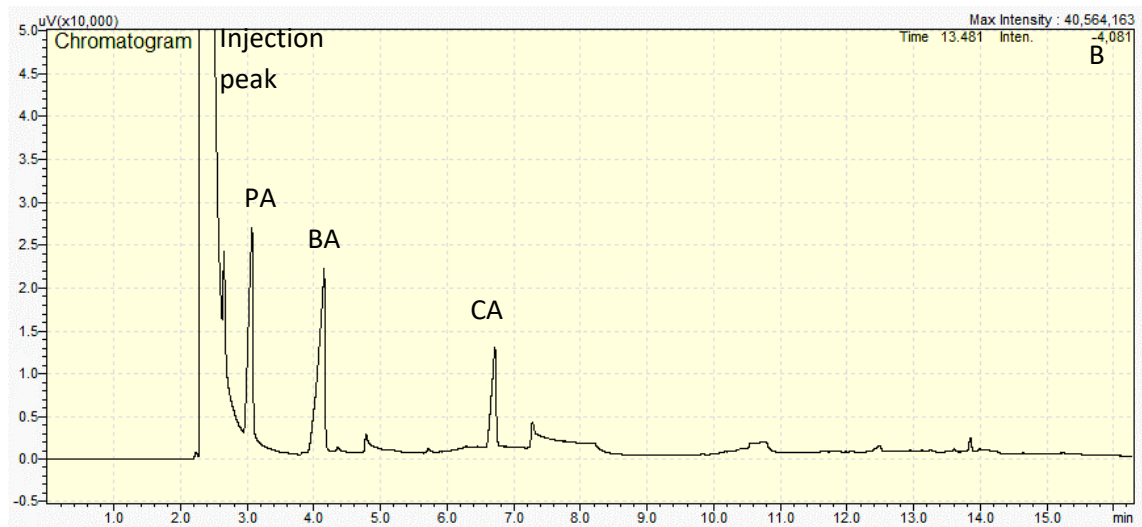
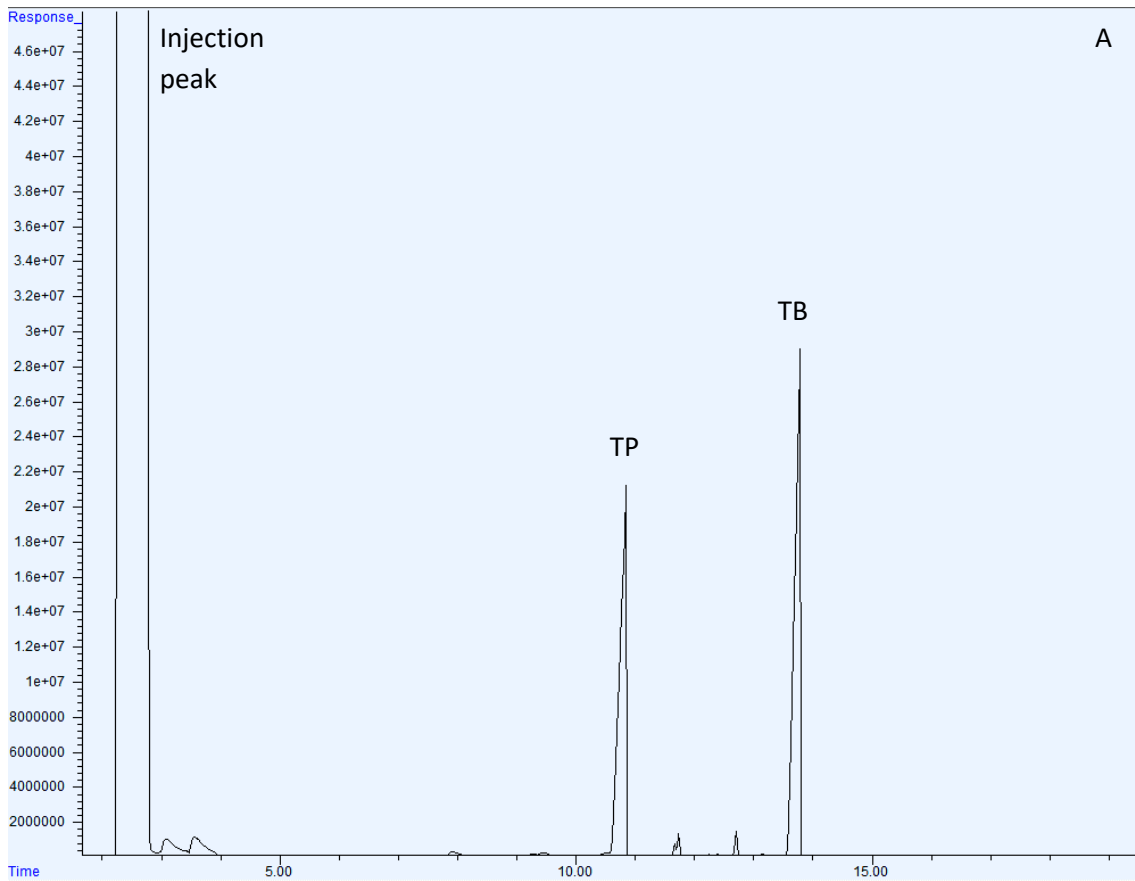


**Figure A5.8.** GC profiles of (A) short-chain triglycerides and (B) SCFAs of the sequential gastrointestinal-digested sample after 10 min of digestion.



GRADUATE  
RESEARCH  
SCHOOL

### STATEMENT OF CONTRIBUTION DOCTORATE WITH PUBLICATIONS/MANUSCRIPTS

We, the candidate and the candidate's Primary Supervisor, certify that all co-authors have consented to their work being included in the thesis and they have accepted the candidate's contribution as indicated below in the *Statement of Originality*.

Name of candidate:	Hoang Du Le
Name/title of Primary Supervisor:	Harjinder Singh
In which chapter is the manuscript /published work:	4
Please select one of the following three options:	
<input checked="" type="radio"/> The manuscript/published work is published or in press <ul style="list-style-type: none"> <li>• Please provide the full reference of the Research Output: Le, H. D., M.Loveday, S., Nowak, E., Niu, Z., &amp; Singh, H. (2020). Pectin emulsions for colon-targeted release of propionic acid. <i>Food Hydrocolloids</i>, 103, 105623. <a href="https://doi.org/10.1016/j.foodhyd.2019.105623">https://doi.org/10.1016/j.foodhyd.2019.105623</a></li> </ul>	
<input type="radio"/> The manuscript is currently under review for publication – please indicate: <ul style="list-style-type: none"> <li>• The name of the journal:</li> <li>• The percentage of the manuscript/published work that was contributed by the candidate:</li> <li>• Describe the contribution that the candidate has made to the manuscript/published work:</li> </ul>	
<input type="radio"/> It is intended that the manuscript will be published, but it has not yet been submitted to a journal	
Candidate's Signature:	
Date:	18-Feb-2021
Primary Supervisor's Signature:	
Date:	22 Feb 2021

This form should appear at the end of each thesis chapter/section/appendix submitted as a manuscript/publication or collected as an appendix at the end of the thesis.



GRADUATE  
RESEARCH  
SCHOOL

## STATEMENT OF CONTRIBUTION DOCTORATE WITH PUBLICATIONS/MANUSCRIPTS

We, the candidate and the candidate's Primary Supervisor, certify that all co-authors have consented to their work being included in the thesis and they have accepted the candidate's contribution as indicated below in the *Statement of Originality*.

Name of candidate:	Hoang Du Le
Name/title of Primary Supervisor:	Harjinder Singh
In which chapter is the manuscript /published work:	5
<p>Please select one of the following three options:</p> <p><input checked="" type="radio"/> The manuscript/published work is published or in press</p> <ul style="list-style-type: none"> <li>• Please provide the full reference of the Research Output: Le, H. D., M.Loveday, S., Singh, H., &amp; Sarkar, A. (2020). Gastrointestinal digestion of Pickering emulsions stabilised by hydrophobically modified cellulose nanocrystals: release of short-chain fatty acids. <i>Food Chemistry</i>, 320, 126650. <a href="https://doi.org/10.1016/j.foodchem.2020.126650">https://doi.org/10.1016/j.foodchem.2020.126650</a></li> </ul> <p><input type="radio"/> The manuscript is currently under review for publication – please indicate:</p> <ul style="list-style-type: none"> <li>• The name of the journal:</li>   <li>• The percentage of the manuscript/published work that was contributed by the candidate:</li>   <li>• Describe the contribution that the candidate has made to the manuscript/published work:</li> </ul> <p><input type="radio"/> It is intended that the manuscript will be published, but it has not yet been submitted to a journal</p>	
Candidate's Signature:	
Date:	18-Feb-2021
Primary Supervisor's Signature:	
Date:	22-Feb-2021

This form should appear at the end of each thesis chapter/section/appendix submitted as a manuscript/ publication or collected as an appendix at the end of the thesis.



GRADUATE  
RESEARCH  
SCHOOL

## STATEMENT OF CONTRIBUTION DOCTORATE WITH PUBLICATIONS/MANUSCRIPTS

We, the candidate and the candidate's Primary Supervisor, certify that all co-authors have consented to their work being included in the thesis and they have accepted the candidate's contribution as indicated below in the *Statement of Originality*.

Name of candidate:	Hoang Du Le
Name/title of Primary Supervisor:	Harjinder Singh
In which chapter is the manuscript /published work:	5
Please select one of the following three options:	
<input checked="" type="radio"/> The manuscript/published work is published or in press <ul style="list-style-type: none"> <li>• Please provide the full reference of the Research Output: Le, H. D., M.Loveday, S., Singh, H., &amp; Sarkar, A. (2020). Pickering emulsions stabilised by hydrophobically modified cellulose nanocrystals: Responsiveness to pH and ionic strength. <i>Food Hydrocolloids</i>, 99, 105344. <a href="https://doi.org/10.1016/j.foodhyd.2019.105344">https://doi.org/10.1016/j.foodhyd.2019.105344</a></li> </ul>	
<input type="radio"/> The manuscript is currently under review for publication – please indicate: <ul style="list-style-type: none"> <li>• The name of the journal:</li> <li>• The percentage of the manuscript/published work that was contributed by the candidate:</li> <li>• Describe the contribution that the candidate has made to the manuscript/published work:</li> </ul>	
<input type="radio"/> It is intended that the manuscript will be published, but it has not yet been submitted to a journal	
Candidate's Signature:	<i>Hoang Du Le</i>
Date:	18-Feb-2021
Primary Supervisor's Signature:	<i>Harjinder Singh</i>
Date:	22 Feb 2021

This form should appear at the end of each thesis chapter/section/appendix submitted as a manuscript/publication or collected as an appendix at the end of the thesis.